TOTAL LUMINESCENCE SPECTROSCOPY FOR SELECTIVITY ENHANCEMENT IN MULTICOMPONENT ANALYSIS

BY

EUGENE LEE INMAN, JR.

A DISSERTATION PRESENTED TO THE GRADUATE COUNCIL
OF THE UNIVERSITY OF FLORIDA IN
PARTIAL FULFILLMENT OF THE REQUIREMENTS
FOR THE DEGREE OF DOCTOR OF PHILOSOPHY

UNIVERSITY OF FLORIDA
1982

This dissertation is dedicated to the two most important people in my life. My wife and companion, Wanda, has been a continuous source of encouragement, love, and understanding throughout my educational career. My son, Joshua, has added challenge to my life, and has taught me numerous principles over the past year. His continuous curiosity and effort to explore and understand epitomizes the need for individual intellectual improvement and personal growth.

Wanda and Joshua have helped to place my scientific efforts into perspective both in this life, and the life to come.

The mind of the intelligent seeks knowledge, but the mouth of fools feeds on folly.

Proverbs 15:14

ACKNOWLEDGEMENTS

The author would like to thank Dr. James D. Winefordner for his guidance, encouragement, support, and friendship throughout this research effort. His example of scientific and individual stature has been a model for emulation. The JDW research group, both as a whole and as individual members, has been a continuous source of friendship and daily challenge. The author would like to especially thank Dr. Edward Voigtman for scientific exchange and thought-provoking discussions, many of which resulted in total disagreement. He would also like to thank his wife, Wanda, for her assistance in putting this work in its present form. Finally, the author would like to thank the faculty members who have served on his advisory committee for their help and interest throughout this educational process.

TABLE OF CONTENTS

CHAPTER		PAGE
	ACKNOWLEDGEMENTS	iv
	ABSTRACT	vii
1	INTRODUCTION TO MOLECULAR LUMINESCENCE SPECTROSCOPY	1
	Energy Model	1
	Stokes Shift	6
	Advantages of Molecular Luminescence Spectroscopy	7
	Spectral Overlap	11
	Note	22
2	TOTAL LUMINESCENCE SPECTROSCOPY	23
	Theory	23
	Instrumentation	25
	Fluorimeter	28
	Computer Hardware	37
	Computer Software	37
	Spectral Features	46
	Conclusions	62
3	SYNCHRONOUS LUMINESCENCE SPECTROSCOPY	67
	Theory	67
	Instrumentation	75
	Constant Energy Synchronous Fluorescence Spectroscopy	76
	Background	76
	Raman Scatter Reduction	80
	Introduction	80
	Instrumentation	89
	Results and Discussion	89
	Conclusions	106
	PAH Analysis	106
	Introduction	106
	Ternary Mixture	121
	Complex Mixture	134
	Synchronous Profiles	155
	Conclusions	160

4 LOW TEMPERATURE LUMINESCENCE SPECTROSCOPY 165

Introduction 165
Instrumentation 170
Results and Discussion 175
Phosphorescence Spectroscopy 211
Synchronous Profiles 215
Conclusions 220

5 MATHEMATICAL AND STATISTICAL METHODS 221

Introduction 221
Basic Matrix Principles 222
Data Smoothing 225
Multiple Linear Regression 226
Factor Analysis 232
Spectral Ratioing 235
Correlation Methods 238
Introduction 238
Experimental 239
Background 239
Results and Discussion 240
Conclusions 257

6 APPLICATIONS IN OIL ANALYSIS 258

Introduction 258
Total Luminescence Spectroscopy 259
Synchronous Luminescence Spectroscopy 260
Low Temperature Fluorescence Spectroscopy 274
Phosphorescence Spectroscopy 274
Conclusions 275

7 CONCLUSIONS AND FUTURE WORK 276

APPENDICES

1 CHEMICALS AND THEIR SOURCES USED IN THIS RESEARCH 281

2 BANDWIDTH REDUCTION AND PEAK LOCATION IN CESL 283

Geometric Model for Bandwidth Reduction 283
Algebraic Model for Bandwidth Reduction 286
Peak Location for the General CESL Scan 288
Bandwidth Reduction for the General CESL Scan 290

3 SOFTWARE FOR LTCESL 292

Memory Allocation 292
BASIC Program -- ENERGY 292
Assembly Routines 294

REFERENCES 298

BIOGRAPHICAL SKETCH 307

Abstract of Dissertation Presented to the Graduate
Council of the University of Florida in Partial
Fulfillment of the Requirements for the Degree
of Doctor of Philosophy

TOTAL LUMINESCENCE SPECTROSCOPY FOR SELECTIVITY ENHANCEMENT IN MULTICOMPONENT ANALYSIS

By

Eugene Lee Inman, Jr.

May, 1982

Chairman: J. D. Winefordner
Major Department: Chemistry

Total Luminescence Spectroscopy (TLS) involves the measurement of the luminescence emission spectrum over a range of excitation wavelengths, providing fingerprinting capabilities for many organic compounds. A TLS spectrometer was built to collect data under computer control, sequentially scanning through the wavelength regions of interest. TLS spectra contain large quantities of information, useful for analyte characterization. Instrumental and mathematical methods were developed to optimize the interpretation of the information contained in these spectra.

Synchronous Luminescence Spectroscopy (SLS) is a subset of TLS, where a single scan is made through the TLS spectrum. By studying TLS spectral relationships, SLS improvements are described, resulting in the development of Constant Energy Synchronous Luminescence Spectroscopy (CESL). By maintaining a constant energy difference between the monochromators, Raman interference is reduced and vibrational

relationships in the spectra of polynuclear aromatic hydrocarbons are used for analyte identification.

Low Temperature Constant Energy Synchronous Luminescence Spectroscopy (LTCESL) supports the results of room temperature analyses. Selectivity is enhanced by narrowing luminescence bands, making multi-component analysis practical. By relating these results back to luminescence theory, parameter optimization is achieved by evaluating characteristic spectral relationships. A model was developed to explain the resultant spectra.

Several mathematical and statistical methods are described for TLS data evaluation. Using basic linear algebra concepts, spectra evaluation is described for cases with extensive overlap. Cross-correlation methods have direct apolication to TLS data, confirming the conclusions drawn for CESL.

Finally, an evaluation of the applicability of these techniques to oil samples is described briefly. Historically, these techniques have been extensively used in oil analysis, based on empirical, rather than theoretical, considerations. By building on luminescence theory, several improvements are described for these techniques. These improvements result in selectivity enhancement in multicomponent analysis.

CHAPTER 1
INTRODUCTION TO MOLECULAR LUMINESCENCE SPECTROSCOPY

Energy Model

Molecular luminescence spectroscopy concerns the measurement of emission accompanying the deexcitation of a molecule from an excited electronic state, where the molecule had been previously excited by the absorption of a photon of light. The intensity, frequency distribution, and temporal characteristics of the emitted radiation have been used extensively for the identification and quantitation of a wide variety of molecular species. Numerous analytical techniques and instruments have been developed utilizing these molecular luminescence characteristics. Effective application of luminescence techniques requires an understanding of luminescence theory.

Many molecular spectroscopic techniques are envisioned utilizing a molecular potential energy diagram, as shown in Figure 1. The absorption of light by molecules at room temperature or below generally occurs from the lowest vibrational levels of the ground singlet state to a number of vibrational levels in one or more excited singlet states. Whether this transition is labeled as $\pi \rightarrow \pi^*$ or $n \rightarrow \pi^*$, electronic absorption processes generally occur in the ultraviolet to visible region of the spectrum. Once in an excited state, various deexcitation mechanisms are available with charateristic rates and therefore, probabilities for occurrence. Luminescence spectroscopy encompasses those processes resulting in radiative deexcitation.

Figure 1. Potential energy diagram of the luminescence processes for an organic molecule.

A = absorption
F = fluorescence
P = phosphorescence
IC = internal conversion
ISC = intersystem crossing
VR = vibrational relaxation
S = singlet
T = triplet

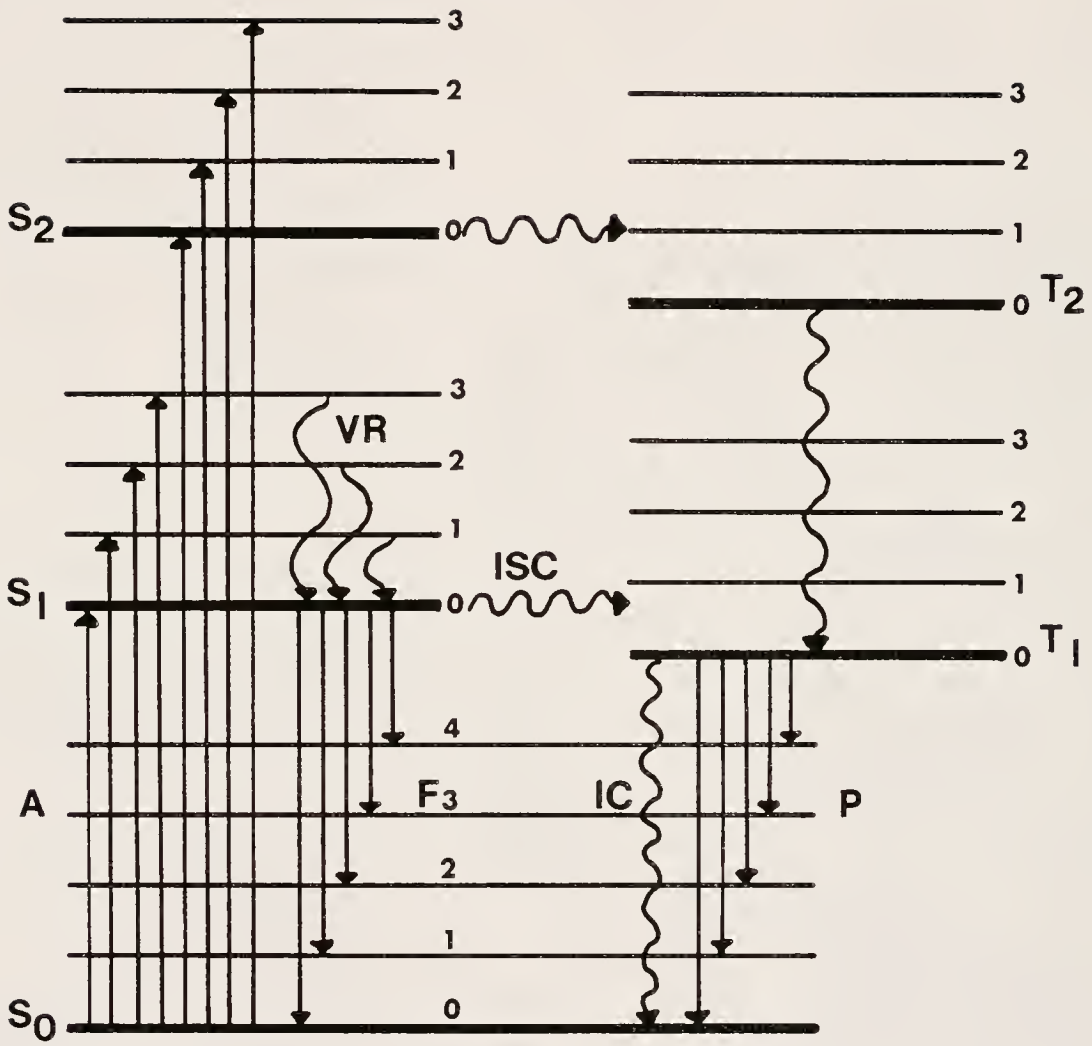
3
2
1
S2
0
3
VR
2
1
S1
0
ISC
4
A
F3
IC
P
2
1
S0
0
3
2
1
0 T2
3
2
1
0 T1

Luminescence generally accompanies a transition from the lowest vibrational state within the excited electronic energy manifold. Once excited, rapid radiationless deexcitation places the molecule in the lowest vibrational state within the first excited singlet state, S_1. If a molecule then returns to the ground electronic state, S_0, emitting a photon, this radiation is referred to as fluorescence. If, however, intersystem crossing occurs and emitted radiation accompanies a transition originating in the lowest vibrational state of the first excited triplet, the radiation is referred to as phosphorescence. Both fluorescence and phosphorescence processes are included in subsequent discussions of luminescence.

Assuming monochromatic excitation, the measured fluorescence from a sample containing a single fluorescing compound can be mathematically described as

$$M_{ij} = I_o(\lambda_i)\phi_f(1-e^{-2.3\varepsilon(\lambda_i)bc})\gamma_f(\lambda_j)\kappa(\lambda_j) \qquad (1)$$

where M_{ij} is the measured relative intensity at excitation wavelength λ_i and emission wavelength λ_j, ϕ_f is the fluorescence quantum efficiency (a fraction), $1-e^{-2.3\varepsilon(\lambda_i)bc}$ is the optical density with $\varepsilon(\lambda_i)$ the molar absorptivity of the compound (L $mol^{-1}m^{-1}$), b the path length (m), and c the sample concentration (mol L^{-1}), $I_o(\lambda_i)$ is the relative intensity of the incident radiation on the sample, $\gamma_f(\lambda_j)$ is the fraction of the total fluorescence emitted at wavelength λ_j, and $\kappa(\lambda_j)$ is the detection system relative response function. Several assumptions are necessary for this relationship to be strictly valid. First, no pre-filter, post-filter, or self-absorption effects are present. Second, the excitation source is monochromatic or $\varepsilon(\lambda_i)$ is constant over the bandpass of the excitation radiation. Also, exact

background correction is possible. These conditions are met for dilute solutions of simple mixtures. Using conventional instrumentation, fluorescence emission is not measured at a single wavelength, but is integrated over the spectral bandpass of the emission monochromator. This instrumental limitation is included in $\gamma_f(\lambda_j)$. For low concentrations of luminescing species, Equation (1) reduces to

$$M_{ij} = 2.3I_o(\lambda_i)\phi_f\varepsilon(\lambda_i)bc\gamma_f(\lambda_j)\kappa(\lambda_j) \quad (2)$$

An analogous equation can be written for phosphorescence,

$$M_{ij} = 2.3I_o(\lambda_i)\phi_{ISC}\phi_p\varepsilon(\lambda_i)bc\gamma_p(\lambda_j)\kappa(\lambda_j) \quad (3)$$

In this case, ϕ_{ISC} is the intersystem crossing quantum efficiency, ϕ_p is the phosphorescence quantum efficiency, and $\gamma_p(\lambda_j)$ is the fraction of the total phosphorescence emitted at λ_j. For simplicity, Equation (2) can be written in a shortened form, with the phosphorescence equation simplification following similarly. The terms α, x_i, and y_j are defined as

$$\alpha = 2.3\phi_f bc \quad (4)$$

$$x_i = I_o(\lambda_i)\varepsilon(\lambda_i) \quad (5)$$

$$y_j = \gamma_f(\lambda_j)\kappa(\lambda_j) \quad (6)$$

In this way, α is the product of wavelength independent terms, x_i is the product of excitation wavelength dependent terms, and y_j is the product of emission wavelength dependent terms. Equation (2) is then written as

$$M_{ij} = \alpha x_i y_j \quad (7)$$

for a single fluorescing compound.

Many of the spectral features observed in absorption and luminescence spectra can be easily explained by the corresponding processes depicted in the energy level diagram. For example, fluorescence excitation and emission spectra are approximately mirror

images of each other. The distribution of vibrational levels within the first excited singlet and ground singlet energy manifolds determines the structure with each respective spectrum. Often these manifolds are similarly spaced, resulting in mirror image spectra. This symmetry is centered around the resonant 0-0 excitation/emission transitions with excitation occurring at shorter wavelengths (higher energy) and fluorescence occurring at longer wavelengths (lower energy). This characteristic was observed as early as 1949 with respect to the 1400 K vibrational spacing[1] observed in the fluorescence spectra of many polynuclear aromatic hydrocarbons (1) and has been of considerable interest in the literature (2,3). Changes in spectral features due to temperature reduction or fluorescence quenching can also be explained by processes within the energy diagram model.

Stokes Shift

One spectral feature often observed in fluorescence spectra obtained at room temperature is the Stokes Shift. The Stokes Shift corresponds to the difference between the wavelength of excitation corresponding to a transition from the lowest vibrational state of the ground singlet state to the lowest vibrational state of the first excited singlet state, and the wavelength of emission corresponding to a transition between these same two energy levels. This difference occurs because of an energy change that occurs between the time a photon is absorbed and the time a photon is emitted, approximately 10^{-9} s. During this time, the solvent cage around the newly excited molecule has time to rearrange itself to a state of lower potential energy. The magnitude of the Stokes Shift can be calculated from

$$\bar{\upsilon}_x - \bar{\upsilon}_m = (2/hc\varepsilon_o)((m^u_{oo} - m^u_{ii})^2/a^3)((D-1)/(D+2) - (n_o^2-1)/(n_o^2+1)) + (2/hc\varepsilon_o)((\alpha^u_o - \alpha^u_i)* (3(m^u_{oo})^2 - 5(m^u_{ii})^2 + (m^u_{oo})(m^u_{ii}))/a^6)* ((D-1)/(D+2) - (n_o^2-1)/(n_o^2+1))^2 \quad (8)$$

where $\bar{\upsilon}_x$ is the frequency of the absorbed radiation (K), $\bar{\upsilon}_m$ is the frequency of the emitted radiation (K), h is Planck's constant (Js), c is the speed of light (ms^{-1}), m^u_{oo} is the dipole moment of the solute in the ground state (Cm), m^u_{ii} is the dipole moment of the solute in the excited state (Cm), a is the effective cavity radius of the solvent (m), D is the static dielectric constant of the solvent, n_o is the solvent refractive index at zero frequency, α^u_o is the polarizability of the solute in the ground state (m^3), α^u_i is the polarizability of the solute in the excited state (m^3), and ε_o is 8.857×10^{-12} C^2N^{-1} m^{-2}, the permittivity of vacuum. This solvent reorientation occurs more slowly than the 10^{-15} s absorption process. Therefore the energy levels of excitation and emission do not exactly coincide. The Stokes Shift commonly observed is on the order of a few hundred K.

Advantages of Molecular Luminescence Spectroscopy

Molecular luminescence spectroscopy has been used extensively in a wide variety of applications and has proven to be a powerful analytical tool. Its widespread importance is evidenced by the numerous luminescence books describing its theory and practice (2,4-9). Luminescence techniques are routinely used in clinical chemistry, pharmacology, forensic chemistry, pesticide analysis, environmental monitoring, and hydrology utilizing fluorescent tracers.

Many of the characteristics of luminescence measurement make it an excellent analytical tool for the analysis of molecules in solution.

The major advantages are often listed as 1. high sensitivity and detection power, 2. high selectivity, and 3. wide linear dynamic range. High sensitivity and detection power are obtained due to the basic measurement process relative to absorption measurement. Instead of measuring differences between two large signals, luminescence signals are essentially measured against zero background. In this way, luminescence detection limits are commonly three orders of magnitude better than absorption detection limits. High selectivity results from two sources. First, more compounds absorb ultraviolet-visible radiation than fluoresce or phosphoresce. The second selectivity advantage is the dependence upon two independent wavelengths, the excitation and emission wavelengths. The luminescence measurements yield three spectra for identification: excitation, fluorescence, and phosphorescence spectra. The wide linear dynamic range is due to the low detection limits and makes luminescence techniques effective over a concentration range up to five orders of magnitude.

The sensitivity of luminescence techniques has attracted a great amount of research interest (10). The past decade has seen a continuous push toward lower and lower detection limits (11,12). Recent work has shown that using conventional fluorescence instrumentation, detection limits in the pg/mL range are achieved for many polynuclear aromatic hydrocarbons (PAHs) (13). These detection limits extend below those needed for routine analysis in many areas. Scientific speculation has been used to determine the theoretical lower limit to experimentally attainable detection limits (14).

Equation (2) indicates the direct relationship between the measured fluorescence intensity and the intensity of radiation incident on the

sample. With the introduction of lasers as excitation sources, incident radiation can be increased by several orders of magnitude (15-18). While some work has demonstrated modest detection limit improvements with laser excitation (19-22), more powerful lasers generally do not yield substantially lower detection limits. This is due to the limiting noise or background in fluorescence measurements. Luminescence detection limits are generally limited by spectral interferences due to the blank. Blank spectral interferences result from two broad classes of effects. First are those features not associated with fluorescence and phosphorescence. Included in this group are Rayleigh and Raman scatter. The second group includes the luminescence properties of compounds found in the blank. Often this luminescence overlaps the luminescence of the compound of interest. Because of this, the implementation of laser excitation sources must take advantage of laser temporal, spectral, and spatial characteristics rather than high intensity alone.

Variation of the excitation wavelength in luminescence analysis improves selectivity by utilizing the method of selective excitation. Selective excitation optimizes the selected excitation wavelength by matching this wavelength with a spectral region with an absorption band of the compound of interest. The excitation wavelength is selected to excite preferentially only one species independently of all others that may be present. In this way, each compound is excited independently and its fluorescence measured. For a mixture of six components, six excitation wavelengths are selected. This technique requires one to locate spectral regions characteristic of each analyte.

Selective excitation requires familiarity with the compounds of interest, their luminescence characteristics, and potential spectral

interferences. However, this may be difficult or even unnecessary in cases where a large number of compounds are present, and complete identification and quantitation of each compound are unnecessary. For example, the analysis of polynuclear aromatic compounds in oil samples represents this situation. Oil identification has made extensive use of luminescence techniques to characterize these samples by their temporal and spectral characteristics. In cases such as this, one is generally more interested in locating spectral characteristics common to broad categories of compounds. This is especially true for samples where the chemical composition is unknown. For elemental analysis, it may be possible to document all potential elemental spectral interferences. This task for molecular interferences becomes formidable. Because of this, selective excitation often becomes "hit and miss" analysis.

Development of luminescence spectroscopy has focused on the analysis of a single component in a pure solvent. This represents the simplest case for an analytical technique. Attempts to apply many luminescence techniques to mixtures, as in real samples, have proven that many of these techniques have limited potential. Thus, the present research emphasis is on the development of techniques capable of analyzing compounds in real sample matrices. In applications where luminescence is commonly used, sensitivity is often not the limiting factor, but rather, selectivity.

Theoretically, only a single measurement value is needed for quantitation of a single component if that point is unique. But for identification, a spectrum is required due to the vast number of potentially luminescing compounds. Spectroscopists are accustomed

to using spectral maxima only, not fully using the vast amount of information available. In many cases, the maximum may be a poor choice and inadequate for multicomponent analysis. With computers readily available, there is an increasing ability to more effectively utilize the available data, taking full advantage of its information content. This is the primary objective of this research.

Spectral Overlap

If the luminescence spectra of several components in a mixture overlap extensively, identification and quantitation become difficult. There are two broad means of resolving the spectrum for each compound. The first group of methods are mathematical and statistical manipulations. Multiple linear regression and factor analysis are important techniques in this area. The alternate group falls under the category of instrumental developments, including band narrowing methods and temporal resolution. The principle underlying this group is that if the spectral features are narrowed and the spectral range spanned by each component is reduced, the probability of overlap is reduced and chances are greater that there exists a region of the spectrum unique to each component in the mixture. Examples of band narrowing techniques are the use of low temperature and of Shpol'skii solvent spectroscopy. Both of these broad groups of techniques will be evaluated with respect to their utility in Total Luminescence Spectroscopy and Synchronous Luminescence Spectroscopy.

To introduce the extent of spectral overlap routinely observed in conventional fluorimetry at room temperature, a set of 24 polynuclear aromatic hydrocarbons (PAHs) were selected as a model set. PAHS are an analytically important class of compounds because many

compounds in this class demonstrate varied degrees of mutagenicity and carcinogenicity and are seemingly ubiquitous. A brief perusal of any major analytical journal demonstrates the challenge they present to analytical chemists. In luminescence spectroscopy, PAHs are especially important because many of these compounds demonstrate ideal luminescence qualities. Technique development often begins with PAH analysis before further applications to other classes of compounds.

The 24 PAHs used throughout this research are listed in Table 1. Compounds selected are the more important PAHs from a biological position, include a number of similar compounds and isomers, represent a wide range of luminescence characteristics, and include enough variety to allow one to draw conclusions based on trends found in the data. For the spectral overlap analysis, a database was generated for the fluorescence excitation and emission spectra for the 24 PAHs in Table 1. The instrumentation required for this is described in Chapter 2. Using spectral bandpasses of 2 nm for both the excitation and emission monochromators, excitation spectra were collected and digitally stored over the range of 220 to 420 nm in 1 nm increments, and emission spectra were collected and stored over the range of 250 to 600 nm in 1 nm increments. Because all spectra were uncorrected for instrumental response (see Chapter 2), exact numerical significance cannot be established, but rather, general characteristics can be studied.

Concentration selection was an important consideration for this analysis to prevent concentration effects, such as non-linear absorption, dimer formation, and intermolecular energy transfer, from appearing in the spectra. PAHs, as a class of compounds, have exceptionally large molar absorptivities (2) and large quantum

Table 1. Polynuclear Aromatic Hydrocarbons Selected as a Model Set for Database Generation With Corresponding RTF Concentrations

	Compound	Concentration (μg/mL)
1.	1,2-Benzopyrene	4.0
2.	Anthracene	0.10
3.	1,12-Benzoperylene	1.0
4.	Pyrene	3.0
5.	1,2-Benzofluorene	1.0
6.	2,3-Benzofluorene	0.21
7.	Perylene	0.022
8.	1,2:5,6-Dibenzanthracene	0.23
9.	3,4-Benzopyrene	0.11
10.	Chrysene	0.84
11.	Fluoranthene	0.90
12.	Phenanthrene	5.0
13.	1,2:3,4-Dibenzanthracene	0.51
14.	2-Methylanthracene	0.12
15.	9-Methylanthracene	0.10
16.	1,2-Benzanthracene	0.32
17.	1-Methylpyrene	1.1
18.	Naphthacene	0.12
19.	9,10-Diphenylanthracene	0.090
20.	Fluorene	0.30
21.	9,10-Dimethylanthracene	0.082
22.	Naphthalene	12.
23.	Acenaphthene	1.0
24.	Anthanthrene	0.014

efficiencies, resulting in intense fluorescence with detection limits often in the 10^{-12} M range. It has been shown that fairly low concentrations must be selected to remain in the linear region of the calibration curve. The concentrations selected for the 24 PAHs are also listed in Table 1. The following criteria were used in their selection. The typical dark current for the system used was 0.6 nA with peak-to-peak noise about 0.1 nA. To provide sufficient signal-to-noise, yet remaining on the linear region of the calibration curve, a concentration was selected yielding a fluorescence maximum signal between 20 and 100 nA. As a rough estimation, this corresponds to a concentration about 200 to 1000 times the detection limit of the selected compound. This proved to be quite effective. A time constant of 0.5 s was used for all measurements, with a scan rate of 40 nm/minute. The solvent for each solution was n-heptane.

The method for spectral overlap calculation used is similar to that described elsewhere (23). Each spectrum was normalized so that for an nX1 vector $\underline{V}$ and its transpose $\underline{V}^T$,

$$\underline{V}^T\underline{V} = 1 \qquad (9)$$

The overlap was calculated by multiplying the spectrum of A by the spectrum of B. The results have been tabulated in Tables 2 and 3. From the excitation spectra data in Table 2, 68.1% of the pairs have an overlap of at least 25% and 35.5% have an overlap of at least 50%. From the emission spectra data in Table 3, 54.3% of the pairs have an overlap of at least 25% and 36.6% have an overlap of at least 50%. Thus spectral overlap is considerable in the fluorescence spectra of PAHs.

The values obtained from this study cannot be directly compared to those previously presented but are similar in magnitude (23). The

Table 2. Conventional Fluorescence Excitation Relative Spectral Overlap

		COMPOUND A[a]							
		1	2	3	4	5	6	7	8
	1	1.000	0.219	0.192	0.832	0.747	0.762	0.043	0.770
	2	---	1.000	0.248	0.267	0.297	0.290	0.130	0.173
	3	---	---	1.000	0.146	0.222	0.191	0.924	0.265
	4	---	---	---	1.000	0.539	0.611	0.047	0.592
	5	---	---	---	---	1.000	0.953	0.061	0.745
	6	---	---	---	---	---	1.000	0.056	0.653
	7	---	---	---	---	---	---	1.000	0.043
C	8	---	---	---	---	---	---	---	1.000
O	9	---	---	---	---	---	---	---	---
M	10	---	---	---	---	---	---	---	---
P	11	---	---	---	---	---	---	---	---
O	12	---	---	---	---	---	---	---	---
U	13	---	---	---	---	---	---	---	---
N	14	---	---	---	---	---	---	---	---
D	15	---	---	---	---	---	---	---	---
	16	---	---	---	---	---	---	---	---
B[a]	17	---	---	---	---	---	---	---	---
	18	---	---	---	---	---	---	---	---
	19	---	---	---	---	---	---	---	---
	20	---	---	---	---	---	---	---	---
	21	---	---	---	---	---	---	---	---
	22	---	---	---	---	---	---	---	---
	23	---	---	---	---	---	---	---	---
	24	---	---	---	---	---	---	---	---

Table 2-continued

		COMPOUND A[a]							
		9	10	11	12	13	14	15	16
	1	0.332	0.724	0.618	0.532	0.700	0.250	0.201	0.715
	2	0.427	0.250	0.511	0.131	0.203	0.948	0.734	0.355
	3	0.581	0.204	0.319	0.212	0.219	0.263	0.395	0.278
	4	0.232	0.567	0.581	0.276	0.478	0.275	0.197	0.538
	5	0.382	0.872	0.476	0.629	0.664	0.373	0.324	0.636
	6	0.326	0.897	0.493	0.546	0.628	0.363	0.306	0.611
	7	0.252	0.061	0.094	0.060	0.048	0.141	0.214	0.070
C	8	0.507	0.678	0.615	0.683	0.749	0.195	0.165	0.763
O	9	1.000	0.378	0.611	0.453	0.441	0.450	0.637	0.547
M	10	---	1.000	0.497	0.701	0.715	0.334	0.298	0.673
P	11	---	---	1.000	0.493	0.706	0.491	0.456	0.866
O	12	---	---	---	1.000	0.861	0.199	0.188	0.813
U	13	---	---	---	---	1.000	0.244	0.206	0.947
N	14	---	---	---	---	---	1.000	0.854	0.378
D	15	---	---	---	---	---	---	1.000	0.333
	16	---	---	---	---	---	---	---	1.000
B[a]	17	---	---	---	---	---	---	---	---
	18	---	---	---	---	---	---	---	---
	19	---	---	---	---	---	---	---	---
	20	---	---	---	---	---	---	---	---
	21	---	---	---	---	---	---	---	---
	22	---	---	---	---	---	---	---	---
	23	---	---	---	---	---	---	---	---
	24	---	---	---	---	---	---	---	---

Table 2-continued

		COMPOUND A[a]							
		17	18	19	20	21	22	23	24
	1	0.627	0.279	0.170	0.432	0.144	0.505	0.619	0.267
	2	0.340	0.036	0.565	0.225	0.522	0.161	0.071	0.133
	3	0.163	0.286	0.485	0.209	0.405	0.189	0.226	0.763
	4	0.727	0.184	0.185	0.231	0.149	0.233	0.325	0.199
	5	0.406	0.311	0.302	0.709	0.378	0.623	0.755	0.360
	6	0.497	0.320	0.306	0.653	0.363	0.558	0.640	0.312
	7	0.047	0.229	0.314	0.055	0.288	0.049	0.032	0.757
C	8	0.500	0.309	0.148	0.588	0.105	0.600	0.842	0.315
O	9	0.294	0.264	0.665	0.390	0.528	0.393	0.434	0.314
M	10	0.420	0.504	0.321	0.775	0.341	0.703	0.727	0.305
P	11	0.705	0.298	0.441	0.348	0.342	0.510	0.472	0.189
O	12	0.266	0.650	0.233	0.797	0.250	0.928	0.848	0.181
U	13	0.445	0.590	0.218	0.687	0.196	0.924	0.832	0.200
N	14	0.340	0.077	0.607	0.324	0.591	0.230	0.114	0.149
D	15	0.270	0.081	0.729	0.300	0.631	0.209	0.093	0.194
	16	0.604	0.521	0.321	0.632	0.271	0.839	0.762	0.198
B[a]	17	1.000	0.197	0.224	0.199	0.174	0.217	0.233	0.136
	18	---	1.000	0.182	0.614	0.146	0.671	0.478	0.180
	19	---	---	1.000	0.332	0.878	0.235	0.100	0.298
	20	---	---	---	1.000	0.394	0.817	0.740	0.192
	21	---	---	---	---	1.000	0.255	0.096	0.297
	22	---	---	---	---	---	1.000	0.829	0.167
	23	---	---	---	---	---	---	1.000	0.305
	24	---	---	---	---	---	---	---	1.000

[a]Compound numbers match those in Table 1.

Table 3. Conventional Fluorescence Emission Relative Spectral Overlap

COMPOUND B[a]	COMPOUND A[a] 1	2	3	4	5	6	7	8
1	1.000	0.789	0.489	0.915	0.332	0.116	0.167	0.732
2	---	1.000	0.486	0.861	0.352	0.148	0.150	0.735
3	---	---	1.000	0.422	0.081	0.014	0.787	0.673
4	---	---	---	1.000	0.442	0.183	0.131	0.751
5	---	---	---	---	1.000	0.836	0.020	0.205
6	---	---	---	---	---	1.000	0.003	0.068
7	---	---	---	---	---	---	1.000	0.282
8	---	---	---	---	---	---	---	1.000
9	---	---	---	---	---	---	---	---
10	---	---	---	---	---	---	---	---
11	---	---	---	---	---	---	---	---
12	---	---	---	---	---	---	---	---
13	---	---	---	---	---	---	---	---
14	---	---	---	---	---	---	---	---
15	---	---	---	---	---	---	---	---
16	---	---	---	---	---	---	---	---
17	---	---	---	---	---	---	---	---
18	---	---	---	---	---	---	---	---
19	---	---	---	---	---	---	---	---
20	---	---	---	---	---	---	---	---
21	---	---	---	---	---	---	---	---
22	---	---	---	---	---	---	---	---
23	---	---	---	---	---	---	---	---
24	---	---	---	---	---	---	---	---

Table 3-continued

		COMPOUND A[a]							
		9	10	11	12	13	14	15	16
	1	0.634	0.689	0.253	0.451	0.910	0.895	0.914	0.921
	2	0.638	0.707	0.246	0.444	0.905	0.856	0.637	0.714
	3	0.611	0.248	0.781	0.122	0.422	0.596	0.670	0.560
	4	0.562	0.826	0.208	0.567	0.960	0.889	0.796	0.882
	5	0.139	0.692	0.037	0.938	0.431	0.323	0.236	0.291
	6	0.036	0.378	0.007	0.639	0.180	0.120	0.067	0.093
	7	0.298	0.068	0.832	0.034	0.132	0.270	0.352	0.248
C	8	0.636	0.473	0.378	0.273	0.714	0.739	0.788	0.741
O	9	1.000	0.443	0.411	0.201	0.565	0.821	0.677	0.713
M	10	---	1.000	0.122	0.789	0.785	0.739	0.546	0.664
P	11	---	---	1.000	0.057	0.206	0.375	0.396	0.322
O	12	---	---	---	1.000	0.556	0.430	0.340	0.412
U	13	---	---	---	---	1.000	0.871	0.780	0.849
N	14	---	---	---	---	---	1.000	0.853	0.929
D	15	---	---	---	---	---	---	1.000	0.933
	16	---	---	---	---	---	---	---	1.000
B[a]	17	---	---	---	---	---	---	---	---
	18	---	---	---	---	---	---	---	---
	19	---	---	---	---	---	---	---	---
	20	---	---	---	---	---	---	---	---
	21	---	---	---	---	---	---	---	---
	22	---	---	---	---	---	---	---	---
	23	---	---	---	---	---	---	---	---
	24	---	---	---	---	---	---	---	---

Table 3-continued

		COMPOUND A[a]							
		17	18	19	20	21	22	23	24
	1	0.800	0.021	0.677	0.000	0.673	0.044	0.049	0.231
	2	0.924	0.014	0.691	0.000	0.758	0.051	0.060	0.232
	3	0.351	0.275	0.872	0.013	0.802	0.042	0.016	0.619
	4	0.886	0.029	0.586	0.002	0.595	0.062	0.076	0.160
	5	0.405	0.007	0.125	0.025	0.139	0.354	0.436	0.023
	6	0.177	0.005	0.026	0.039	0.036	0.400	0.497	0.000
	7	0.089	0.443	0.514	0.009	0.431	0.031	0.004	0.571
C	8	0.688	0.073	0.786	0.013	0.754	0.050	0.047	0.296
O	9	0.459	0.034	0.867	0.000	0.856	0.027	0.015	0.511
M	10	0.720	0.006	0.391	0.001	0.411	0.121	0.151	0.112
P	11	0.155	0.625	0.598	0.014	0.560	0.036	0.005	0.586
O	12	0.514	0.009	0.183	0.073	0.195	0.309	0.364	0.042
U	13	0.952	0.015	0.596	0.001	0.611	0.060	0.077	0.182
N	14	0.768	0.060	0.814	0.012	0.812	0.054	0.052	0.379
D	15	0.645	0.052	0.791	0.001	0.704	0.035	0.031	0.363
	16	0.706	0.043	0.739	0.005	0.697	0.045	0.045	0.310
B[a]	17	1.000	0.009	0.510	0.000	0.541	0.054	0.071	0.121
	18	---	1.000	0.101	0.034	0.100	0.029	0.009	0.077
	19	---	---	1.000	0.000	0.968	0.032	0.015	0.607
	20	---	---	---	1.000	0.007	0.402	0.309	0.000
	21	---	---	---	---	1.000	0.036	0.021	0.567
	22	---	---	---	---	---	1.000	0.926	0.024
	23	---	---	---	---	---	---	1.000	0.001
	24	---	---	---	---	---	---	---	1.000

[a]Compound numbers match those in Table 1.

selection of monochromator bandpasses of 2 nm is significant for this and later studies. A major objective in selectivity enhancement is band narrowing of the fluorescence spectra. In attempting to achieve this objective in fluorescence spectroscopy, the monochromator bandpasses must not introduce significant band broadening beyond the narrowest bandwidths inherent in the fluorescence spectra. Because PAH fluorescence bands are as narrow as 4 to 10 nm at room temperature, a bandpass less than this should be selected. Therefore, monochromator bandpasses were selected to reduce instrumental broadening effects on the luminescence spectra. This significance will be important throughout this work.

A major advantage of luminescence techniques is the capability of varying two wavelengths during an analysis, as mentioned. The full potential of this advantage is usually not realized in conventional luminescence spectroscopy. Conventionally, a spectrum is obtained by maintaining one monochromator (excitation or emission) at a constant wavelength and scanning the other monochromator (emission or excitation) over a range of wavelengths. Two techniques that take advantage of this selectivity capability are Total Luminescence Spectroscopy and Synchronous Luminescence Spectroscopy. Exploitation of this capability to enhance selectivity has been the underlying determination in this research.

Chapter 1 has described the basic luminescence concepts of considerable importance in Total Luminescence Spectroscopy and Synchronous Luminescence Spectroscopy. Total Luminescence Spectroscopy is described in detail in Chapter 2, while the concepts of Synchronous Luminescence Spectroscopy are set forth in Chapter 3. Chapter 4 extends

the concepts of Synchronous Luminescence Spectroscopy to low temperature analysis. Chapter 5 includes several mathematical and statistical methods available for data evaluation from the techniques described in Chapters 2-4. The objective of the techniques in Chapters 2-5 is to enhance selectivity in multicomponent analysis using the concepts established in Chapter 1. Chapter 6 summarizes the application development of these techniques, with Chapter 7 suggesting areas for further investigation.

Note

[1]Throughout this work, energy units are expressed as kaisers, defined as cm^{-1}, and abbreviated K. The kaiser is the accepted primary unit while the wavenumber is common throughout the literature and is the accepted secondary unit. The symbol K is also used throughout this work for degrees kelvin. While both are used extensively in Chapter 4, the desired units are clear from the context.

CHAPTER 2
TOTAL LUMINESCENCE SPECTROSCOPY

Theory

Total Luminescence Spectroscopy (TLS) measures the emission spectrum of a sample over a range of excitation wavelengths. Data obtained in this manner represent variation in both the excitation and emission wavelengths, making more spectral information available for sample characterization. While an abundance of information is potentially present within the data, full understanding of data relationships over analyzed spectral regions is necessary to exploit the data to their maximal analytical potential. As the analytical chemist approaches this goal, improved selectivity in multicomponent analysis should be the natural result.

As will become obvious, TLS data encompass a broad set of closely related luminescence techniques. Therefore a thorough investigation was completed in attempting to understand TLS from an instrumental and mathematical perspective. Thus TLS bridges the gap between fundamental luminescence principles as described in Chapter 1, and the more specific techniques described in later chapters.

The mathematical description of TLS data is a natural extension of Equation (7). Now instead of measuring a single data point, groups of measurements are made. Equation (7) then becomes

$$\underline{M} = \alpha \underline{X} \underline{Y} \tag{9}$$

where $\underline{M}$ is an nXm matrix defining the TLS data plane, $\underline{X}$ is an nX1 matrix (array of length n) representing a conventional fluorescence excitation

spectrum, and $\underline{Y}$ is a 1Xm matrix representing a conventional fluorescence emission spectrum. Thus the measured quantity M_{ij} is a single point within the matrix $\underline{M}$. Each point within $\underline{M}$ represents a unique pair of experimental wavelengths. Selection of an i,j pair defines an excitation, emission wavelength pair and a corresponding fluorescence measurement.

For a single fluorescent component, the measured emission spectrum is independent of the excitation wavelength, and the measured excitation spectrum is independent of the emission wavelength. In multicomponent analysis, this is no longer true. For a solution of r fluorescing compounds, Equation (9) becomes

$$\underline{M} = \sum_{k=1}^{r} \alpha_k \underline{X}_k \underline{Y}_k \qquad (10)$$

Analytical applications of TLS directly depend on this relationship.

There are several advantages of TLS over conventional luminescence spectroscopy. Selectivity is improved by varying both the excitation and emission wavelengths, as described earlier. TLS requires minimal a priori knowledge of an unknown's luminescence characteristics. TLS has excellent potential resolvability of complex mixtures with little or no sample pretreatment. Also, TLS spectra are unique for each luminescing compound, offering fingerprinting capabilities, ideal for analyte identification (24).

The last advantage of TLS spectra suggests that because there are unique spectral characteristics for each compound, one need only identify those spectral characteristics that are specific for the analyte of interest and recognize these characteristics within the spectrum of an unknown solution. Because the TLS spectrum extends over such a large range of wavelengths, there is an excellent probability that if the

compound fluoresces, its characteristics are defined by the TLS spectrum. Thus, one need not examine several data sets, corresponding to various experimental parameters, but rather, a single data set, capable of identifying numerous compounds with minimal experimental variation of parameters.

TLS, as an analytical tool, was established in the middle 1970's with several instrumental developments, making data collection practical (25). For TLS to be a routinely used technique, data collection must be rapid and automated. To speed the data collection process, one must either scan more rapidly or make many measurements simultaneously. While the matrix format of TLS data was pointed out earlier (26), experimental realization had not taken a foothold until the late 1970's. This can be traced to two technological advances necessary for TLS instrumentation: the computer and rapid data collection devices.

Instrumentation

Instrumentation for TLS data collection has been described by several authors by interfacing the monochromator scan drives of a conventional fluorimeter to a computer (27). What would be manually difficult and time-consuming then becomes practical for routine analysis. The monochromators are sequentially scanned over the desired excitation and emission ranges. This requires excellent reproducibility in the stepping motors of the monochromators. The scan speed is determined by the mechanical limitations of the monochromators and the signal-to-noise ratio (S/N) required for the analysis. Mechanical improvements have been made with high-speed stepping motors (28,29) and galvanometrically scanned mirrors (30).

An alternate data collection system for TLS utilizes a multichannel detection system. The Videofluorometer is based on this system. The Videofluorometer was presented in 1976 (31) as a result of TLS research at the University of Washington. This instrument and its applications have been described in detail (32-35). The unique features of this instrument are the polychromatic irradiation of the sample cuvette and an SIT vidicon detector. Using a xenon arc lamp excitation source, the wavelength of excitation is a function of the physical height within the cuvette. The multichannel detector allows an entire TLS spectrum to be collected in less than 20 ms, although integration times of approximately 1 s are commonly used. As improvements are made in the sensitivity of SIT vidicon detectors, the TLS data collection efficiency using instrumentation similar to the Videofluorometer will increase (36-38).

Talmi has reviewed the status of multichannel image detectors and their utility in spectroscopy (39-41). A major direction of instrumental development has been in the application of these systems to HPLC, most commonly for spectrophotometric measurements. For this use, an entire spectrum can be obtained in approximately 1 s. With this speed, image detectors make fluorescence detectors practical for HPLC analysis (42).

The Videofluorometer suffers from several major problems. For adequate sensitivity, spectral resolution is generally around 10 nm, with additional degradation of resolution by pixel summing. With present-day image detectors, this system is less sensitive to the emission region below 360 nm. Also, its cost, on the order of $50,000, is prohibitive for routine analysis. The unique sample illumination

design makes adaptation to other luminescence techniques other than room temperature fluorescence difficult. Thus instrumental improvements are needed to overcome many of these limitations.

Baird (Baird Corp., Bedford, MA 01730) has designed a TLS system that is presently on the market. It uses photomultiplier detection with computer-controlled monochromator scanning. A PDP 11/04 computer is used for instrument control, data manipulation, and contour plotting. Information on this system was obtained after most of the instrumental development for this research was completed although many similarities can be found.

For further study, a database of TLS spectra was necessary. While the research efforts of others have emphasized instrumentation, this research is more concerned with the spectra obtained and spectral relationships. Because of this, adequate instrumentation was developed with the main effort made towards software development, establishment of a database, and evaluation of data. The following criteria were established to direct instrument development (43):

- -adequate resolution (varies with process measured)
- -broad spectral range (220-650 nm)
- -on-line computer for
    - -data acquisition
    - -data display
    - -data analysis
    - -plotting
    - -complete instrument control
    - -spectra library organization

Implementation of these requirements suggests three areas of instrument development: the fluorimeter, computer hardware, and computer software.

Fluorimeter

Previous research has proven that room temperature fluorescence spectroscopy (RTF) is the best starting point due to its relative simplicity in instrumentation and data interpretation. A fluorimeter was constructed as shown in Figure 2, with individual components and their sources listed in Table 4. Each component was selected to provide sufficient versatility to expand as research needs dictated. The components of the fluorimeter correspond to what is commonly found in commercial instruments. The secondary goal of this development was to keep instrumental costs low for practical reasons.

The xenon arc lamp is the most commonly used source of excitation in luminescence spectroscopy. It provides sufficient intensity over a broad spectral region, and its output is more continuous than the sharp-spiked output characterisitc of medium-pressure mercury lamps. Various optical arrangements and reflector descriptions have been described to improve upon the standard arrangement of xenon arc lamp use.

The monochromators were selected because of their versatility, compactness, and ease of automation. Both monochromators and scan controls are identical except for the grating blaze wavelength. These monochromators are f/3.5 and have a reciprocal linear dispersion of 8 nm/mm. With 2 nm bandpasses, sufficient throughput is achieved for the RTF studies. The excitation monochromator has a blaze wavelength of 250 nm and the emission monochromator has a blaze wavelength of 450 nm. These are optimal for PAH analysis. Wavelength calibration of these monochromators using a low-pressure mercury lamp (Oriel Corp.,

Figure 2. Block diagram of Total Luminescence Spectrometer.

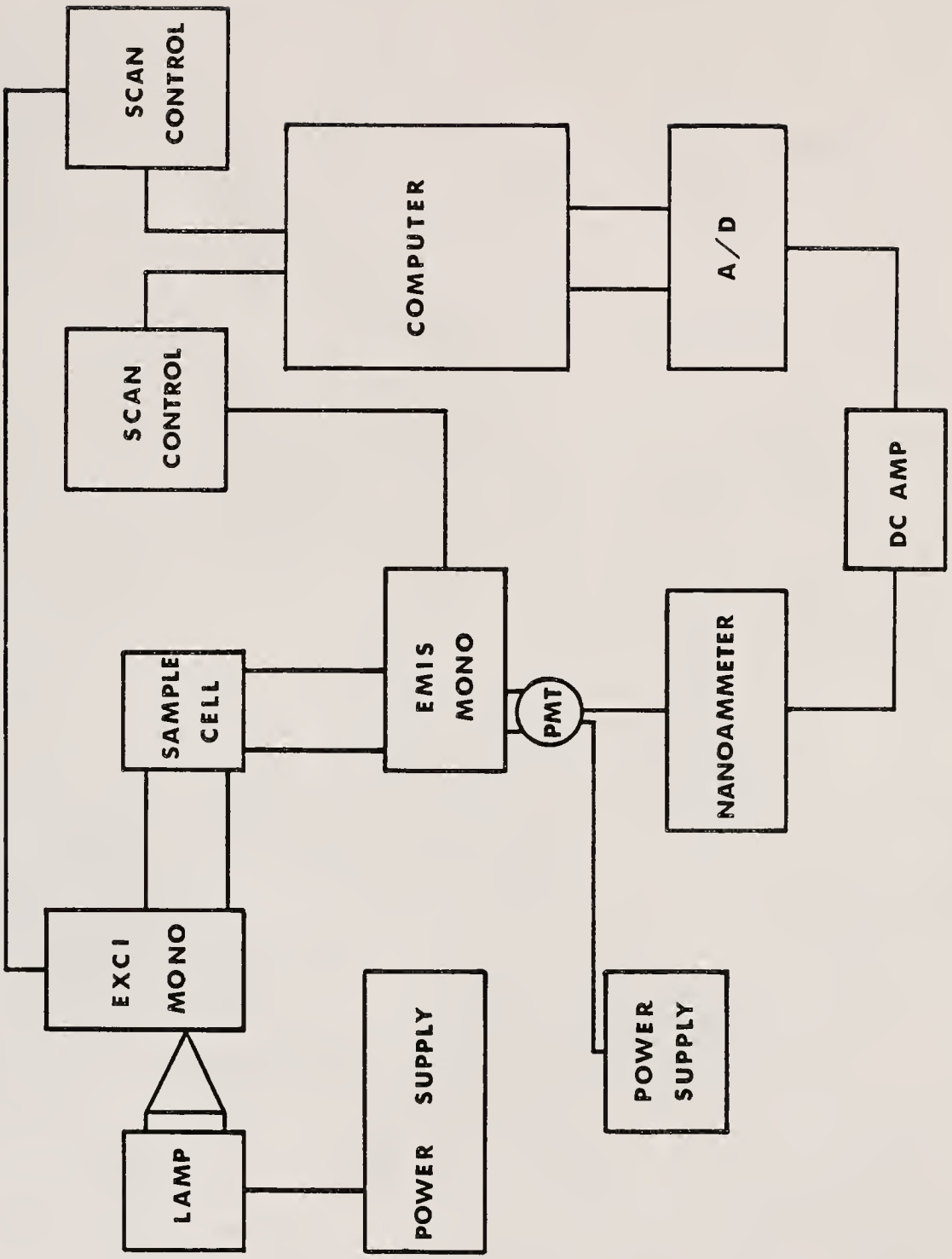
SCAN CONTROL
COMPUTER
A/D
SCAN CONTROL
DC AMP
EMIS MONO
SAMPLE CELL
PMT
NANOAMMETER
EXCI MONO
POWER SUPPLY
POWER SUPPLY
LAMP

Table 4. Experimental Equipment Used in Total Luminescence Spectroscopy

Item	Model	Source
Eimac Xenon Arc Lamp 150 W	VL-150-2	Eimac, Division of Varian San Carlos, CA 94070
Eimac Illuminator Power Supply operated at 12 A	P250S-2	Eimac, Division of Varian San Carlos, CA 94070
Excitation Monochromator f/3.5, holographic grating 1200 grooves/nm	H-10UV	American ISA, Inc. Metuchen, NJ 08840
Sample Housing		American Instrument Co. Silver Spring, MD 20910
Emission Monochromator f/3.5 holographic grating 1200 grooves/nm	H-10V	American ISA, Inc. Metuchen, NJ 08840
Photomultiplier Tube	1P928	Hammamatsu Waltham, MA 02154
High Voltage Power Supply operated at -1000 V	EU-42A	Heath Co. Benton Harbor, MI 49022
Nanoammeter		Laboratory Constructed[a]
DC Amplifier		Laboratory Constructed
Monochromator Scan Controls	1020-SS	American ISA, Inc. Metuchen, NJ 08840
Minicomputer	PDP 11/34	Digital Equipment Corp. Maynard, MA 01754
Analog-to-Digital Converter	Laboratory Peripheral System (LPS-11)	DEC Maynard, MA 01754
Digital Plotter	HIPLOT DMP-4	Houston Instrument Division of Bausch & Lomb Austin, TX 78753

[a]Reference 44

Stamford, CT 06902) demonstrated accuracy of ±0.2 nm over the entire spectral region.

The 1P928 photomultiplier tube was specifically selected for its wide spectral response range, extending well into the near infrared region. Other work with this PMT has shown excellent sensitivity out to 1050 nm. This is especially important for PAH analysis as the phosphorescence of many PAHs extends from 600 to 800 nm.

In all these studies, the spectra are uncorrected for instrumental response and excitation source output. Ideally, all spectra should be corrected to provide information that is specific-instrument independent. While this instrument is capable of correcting spectra digitally, this feature was not used in this work. Even without corrected spectra, one should be aware of the spectral limitations of the instrument for proper data interpretation. As a result, the instrument response functions were obtained for the excitation and emission arms of the fluorimeter.

Several procedures have been described for the correction of luminescence spectra (45). To obtain the spectral response functions for this instrument, a 1000 W quartz-halogen tungsten coiled-coil filament lamp was used for reference (Optronic Laboratories, Inc., Silver Spring, MD 20910). Although absolute irradiance data are available for this lamp, only relative measurements were made. This lamp is recommended by the National Bureau of Standards as a spectral irradiance calibration standard (46). The lamp was operated at 8.00 ± 0.008 A dc using a Model 83 Precision DC Current Source (Optronic Laboratories, Inc., Silver Spring, MD 20910).

The procedure used for calibration required two sets of measurements. The sample cell was modified to allow direct illumination by the lamp

through the sample cell into the measurement arm of the fluorimeter. A bandpass of 2 nm was used on the emission monochromator. The emission spectral response function was obtained by dividing the measured spectrum by the published spectral irradiance of the lamp. The lamp was then removed and a quartz cuvette wall was placed in the sample cell to scatter the xenon arc lamp output directly into the measurement system. A bandpass of 2 nm was also used on the excitation monochromator. The total instrument response function was obtained by scanning the emission monochromator to the selected wavelength, scanning the excitation monochromator through the same spectral region, and recording the maximum signal obtained. This compensated for imperfect placement of the quartz plate in the sample cell. The excitation spectral response function was then obtained by dividing the total response function by the emission response function. Each of these is displayed in Figure 3. The general shapes of these functions agree with what has been reported (47). Each function defines the relative instrumental response per nm, measured at each wavelength interval. The xenon arc lamp suffers from low relative intensity below 300 nm, with a peak intensity around 800 nm.

A decision was made to leave spectra uncorrected to eliminate the artificial distortion imposed by digital correction. Although the emission response functions shows several minor spectral features, correction for emission response causes few changes in the spectra obtained from this system. The excitation output of this system, however, involves substantial change over the commonly used wavelength range. Thus when correcting spectra, the region below 300 nm is multiplied by fairly large factors. With noise present, the S/N becomes grossly distorted with noise peaks almost as large as strong signals

Figure 3. Relative spectral response functions for TLS instrument.

A. Excitation

B. Emission

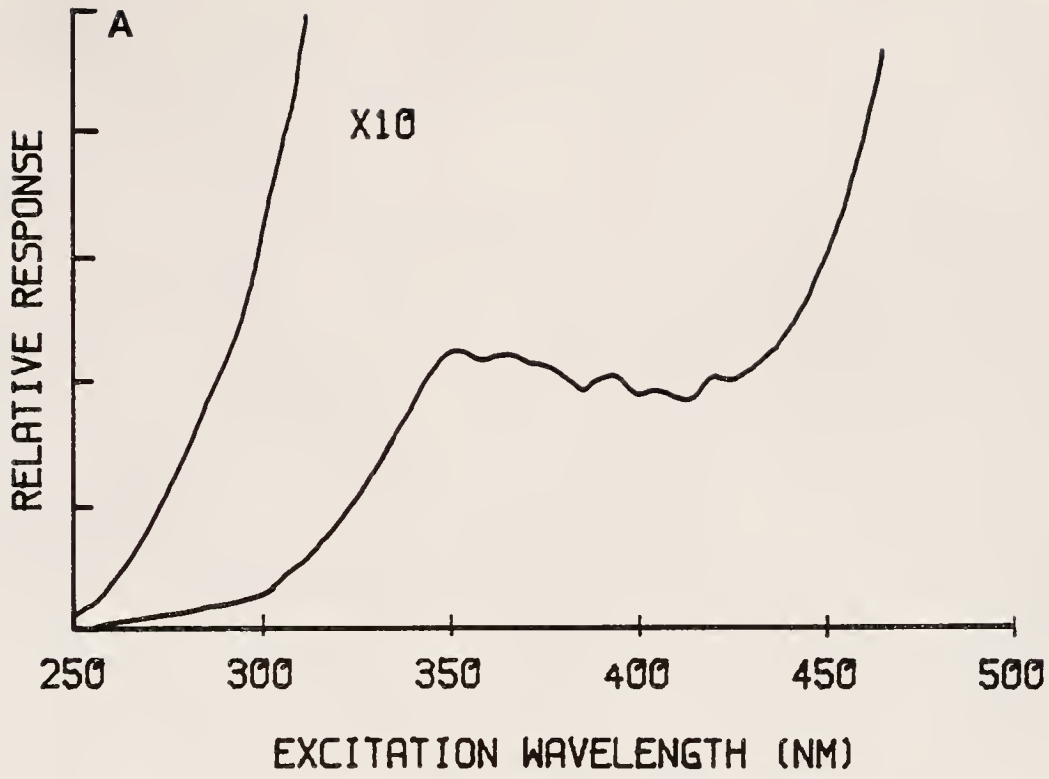
A
X10
RELATIVE RESPONSE
250
300
350
400
450
500
EXCITATION WAVELENGTH (NM)

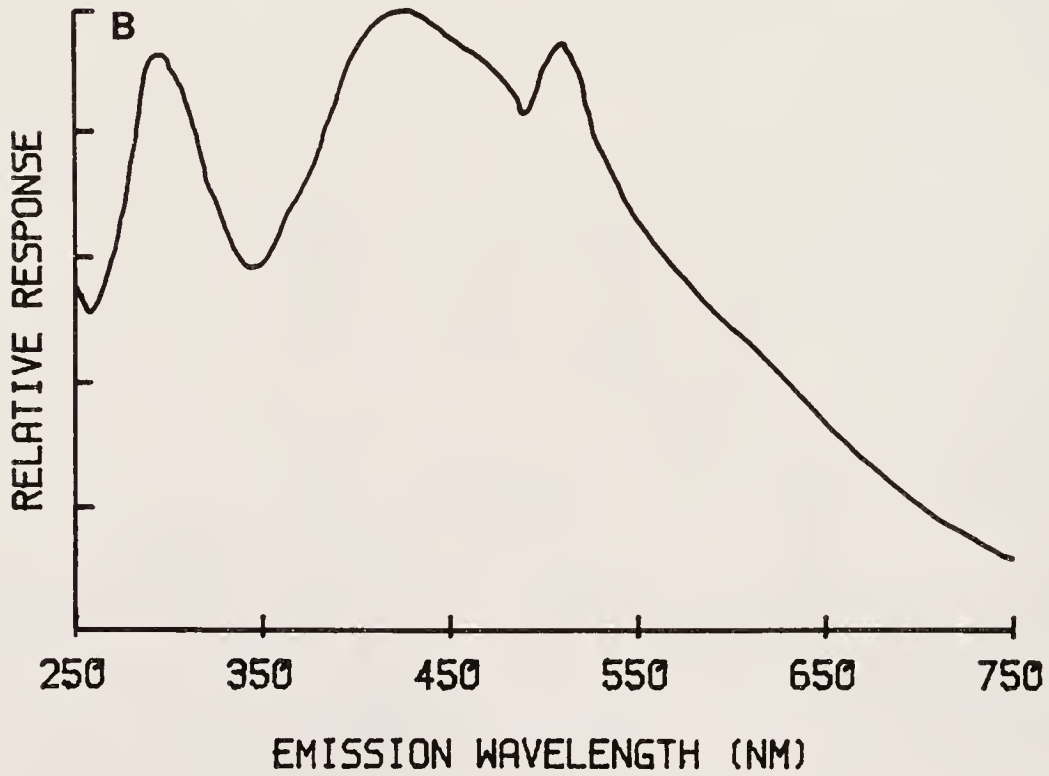
B
RELATIVE RESPONSE
250
350
450
550
650
750
EMISSION WAVELENGTH (NM)

towards the red region of the spectrum. An excellent example of this distortion is given in Reference 48.

Because of the common use of xenon arc lamps in luminescence spectroscopy, most instruments have similar response functions. While corrected spectra are important in absolute measurements and quantitative data, the conclusions drawn and principles set forth in this work are in no way altered by the lack of instrumental independence. Of more concern in the present research is the temporal output fluctuation of the excitation source. The radiant flux from a xenon arc lamp is generally noisy, drifts over time, and is interrupted by occasional spikes. To stabilize the lamp output, a closed loop feedback system has been described in the literature (49).

Deoxygenation of solutions has been suggested as a method to increase fluorescence sensitivity. By bubbling nitrogen through the solution, oxygen quenching is decreased with a resultant increase in fluorescence signal. An apparatus was designed to provide deoxygenation of solutions for the TLS system. A teflon cap is fitted over the cuvette with a stainless steel needle extending to the bottom of the cuvette along the back corner. House nitrogen is bubbled through the solution for 5 minutes and then blown over the solution during the analysis using a three-way stopcock to direct the nitrogen flow to another stainless steel needle extending to just above the surface of the solution. To prevent solvent evaporation, the nitrogen is saturated with solvent. While some researchers suggest that deoxygenation is always necessary (50), it proved to be of limited utility in routine analysis. Although analyte fluorescence signals increase by a modest factor of two or three, oxygen-free nitrogen is not practical for

routine use. Also spectra are generally unchanged by deoxygenation, making it unnecessary for the study at hand.

Computer Hardware

The PDP 11/34 with 32 K words RAM was selected for instrumental control and proved to be more than sufficient for all computing requirements. A parallel digital interface to the PDP 11/34 was connected to the monochromator scan controls requiring three lines for each scan control: ground, direction selection, and scan speed control. Data collection is through the analog-to-digital converter of the LPS-11. With this available, little hardware development was necessary.

Computer Software

The RSX-11M operating system was used for all software development and corresponding instrumental control throughout this work. Software development comprised a major effort in successful completion of this research. Rather than a collection of independent programs, a rather extensive network of files, programs, and directories was necessary to meet all the requirements placed on the computer for the TLS system. The chart in Figure 4 illustrates the overall philosophy in the software development. Two analogous sets of programs are available for Total Luminescence Spectroscopy and Synchronous Luminescence Spectroscopy experimentation, with several peripheral programs. Each of the six main programs shares a set of about 25 library subroutines, performing a wide variety of operations. The network of programs and subroutines and their functions are listed in Tables 5 and 6.

Data are organized into four types of data files, identified by the three letter extension after the file name. DAT identifies a TLS spectrum of raw data as collected, BKD files have been background

Figure 4. Organization of TLS software and data files.

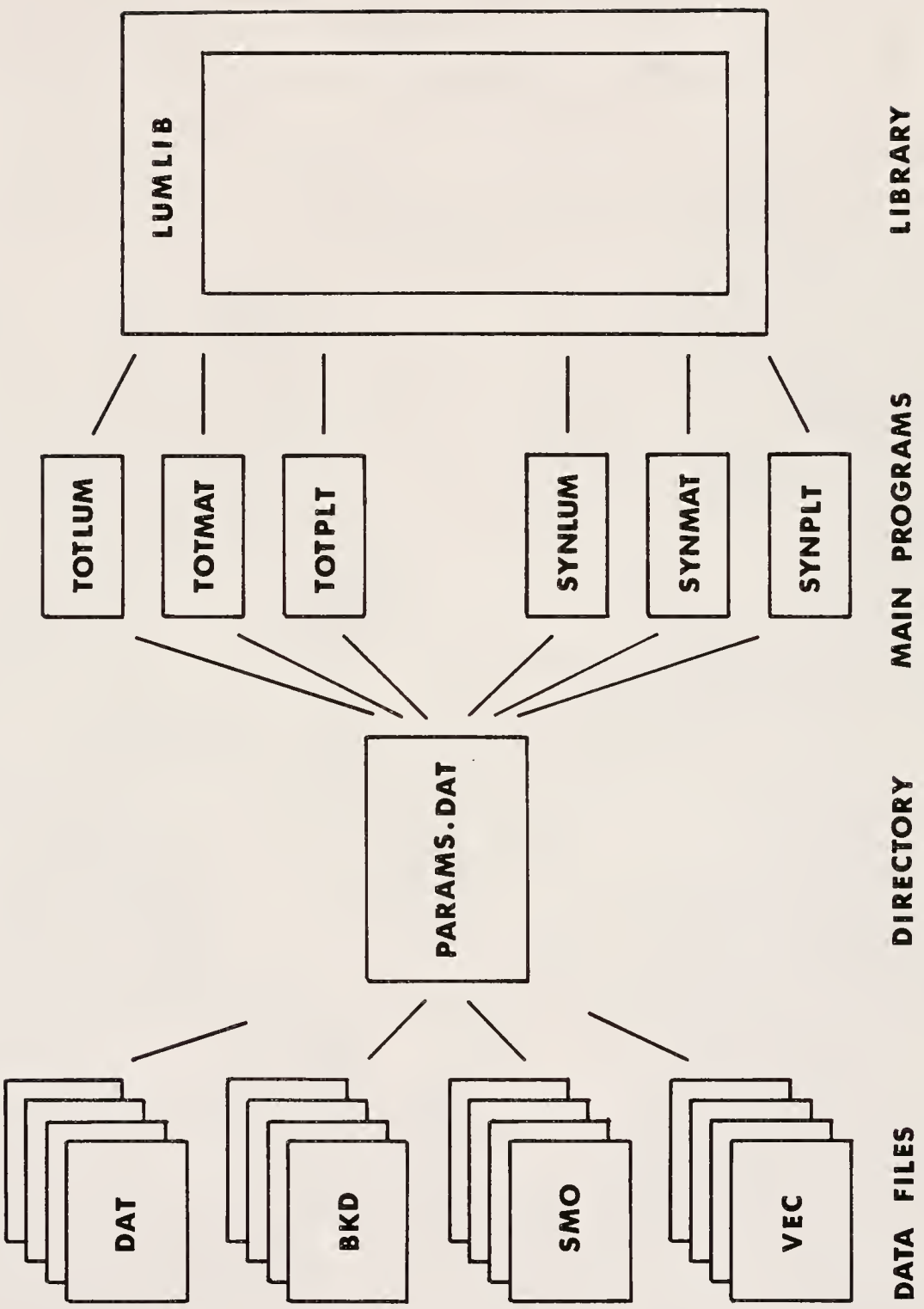
LUMLIB
TOTLUM
TOTMAT
TOTPLT
SYNLUM
SYNMAT
SYNPLT
PARAMS.DAT
DAT
BKD
SMO
VEC
LIBRARY
MAIN PROGRAMS
DIRECTORY
DATA FILES

Table 5. FORTRAN Programs Developed for TLS System

Program Name	Function
BANDPS	- to convert a spectrum with bandpass 1 to spectrum with bandpass 2
ENERGY	- to convert a spectrum as a function of wavelength to one that is a function of energy
MAINFL	- to maintain TLS data files and PARAMS.DAT
MIXTUR	- to simulate TLS mixtures
NRNBR	- to perform a nearest neighbor smooth on a TLS data file
OPT	- to calculate synchronous optimization parameters
OVRLAP	- to calculate extensive synchronous optimization parameters
PEAKS	- to determine wavelength position of spectral features in vectors files
SCATT	- to remove Rayleigh scatter from vector files in LTF
TSTART	- to initialize PARAMS.DAT
UNIQUE	- to calculate spectral overlap between luminescence spectra
VECFRM	- to create vector files directly
VECPLT	- to plot vector files

Table 6. Library Subroutines Developed for TLS System

Subroutine Name	Function
AXES2D	- to draw axes in two-dimensional plots
AXES3D	- to draw axes in three-dimensional plots
AXLB2D	- to label axes in two-dimensional plots
AXLB3D	- to label axes in three-dimensional plots
DISPLA	- to display TLS data file
FIND	- to locate file parameters in PARAMS.DAT
FLIST	- to list file parameters in PARAMS.DAT
INIT	- to initialize the digital plotter
LOCMAX	- to locate the local maximum in a TLS data file
MAXFND	- to locate the maximum in a TLS data file
MONO	- to scan monochromators to their desired locations
NEWFIL	- to initialize parameters for a new data file
OLDFIL	- to locate file parameters for an existing data file
SCAN	- to scan monochromators
SMOOTH	- to perform a nearest neighbor smooth on a TLS data file
SMTH	- to smooth a TLS data file using basis vectors
SPECTR	- to plot an array of data
STAND	- to generate a standard synchronous spectrum
SUBBLK	- to blank subtract a TLS data file
SYNLUM	- to control synchronous instrumentation
SYNMAT	- to perform mathematical operations on synchronous data files
TOTLUM	- to control TLS instrumentation

Table 6-continued

Subroutine Name		Function
TOTMAT	-	to perform mathematical operations on TLS data file
TOTPLT	-	to plot TLS data files
VECTOR	-	to create a vector file from a TLS data file

subtracted with the appropriate TLS blank spectrum, while SMO files have been digitally smoothed. The VEC file contains two records; the first is the luminescence excitation spectrum and the second is the luminescence emission spectrum. VEC files are obtained by one of two possible routes. Both spectra can be obtained by directly scanning the desired spectrum with the other monochromator at the peak maximum, or the spectra can be obtained by selecting the most intense column and row of the TLS data matrix after proper background subtraction. Because of the mathematical relationship described by Equation (9), a TLS data file can be generated from the VEC file. Therefore, in the generation of a database, the data are more compactly stored using a VEC file with a resulting storage savings of a factor of 30 to 50 for each file. For TLS reference spectra of single component solutions, the data file is generated from a VEC file as needed.

Access to any data file is through the file PARAMS.DAT. This file contains a directory defining the parameters under which each data file was collected, along with identifying information. Each data file is named as X##LLL.EXT, where ## corresponds to an identification number for each compound (01-24 were used for the compounds in Table 1). LLL is a group of three letters identifying the luminescence method used to collect the data, such as, RTF for room temperature fluorescence and LTP for low temperature phosphorescence, and EXT corresponds to one of the four file extensions. Thus, each compound-method pair has four extension possibilities and four corresponding data files. PARAMS.DAT records which files have been created and are available for evaluation and which files have been deleted.

TOTLUM and SYNLUM are used for data collection and instrumental control. The TLS data are collected using a rapid scan procedure.

From its initial wavelength settings, the emission monochromator is scanned forward to the terminal wavelength, the excitation wavelength is advanced, and the emission monochromator is scanned in reverse. Each emission scan is stored as a separate data record upon completion of the scan. Scan rates, wavelength intervals and ranges, and amplifier gain are variable and selected by the user. All software was written in FORTRAN with A/D control and signals sent via the parallel interface for monochromator scan control using a set of FORTRAN-callable assembly language routines obtained from DEC. With this software, a 1700 points/s data collection rate is achievable.

Due to the vast amount of data that is collected for a TLS experiment, effective visualization becomes a challenge. If one cannot visualize the data and understand their relationships, full utility of their informational content is generally not realized. Attempts were made to locate a plotting package at a moderate cost that was compatible with the PDP 11/34 system. After several unsuccessful attempts, a plotting package was written for the specific needs of this work. Three plotting modes were needed: two-dimensional plots, three-dimensional isometric projections, and contour plots. This work is certainly not unique and comprehensive, but it fulfills the current needs and will be described briefly.

Several textbooks have described considerations in plotting software development (51,52). The steps involved in the plotting routines for the TLS system include initializing the plotter, establishing a point of reference, defining a data window, drawing axes, labeling axes, plotting the spectrum, and terminating plotting operations. All plots are produced on a digital x-y recorder. Two-

dimensional plotting is fairly routine with the spectrum scaled to its maximum or to any selected size. The three-dimensional plotting routines required substantially more effort to develop.

Isometric projection plots depend on hidden line calculations, rapid enough to be practical. Because TLS spectra include such a large number of data points, the calculations must be simple, not having large memory requirements. Isometric projection plots display the emission wavelength along the x axis, the excitation wavelength along the z axis, and the relative intensity along the y axis. The x,y,z position is first determined for each point and its projection onto the x-y plane defined by the paper is calculated. If this projection is below a previously plotted surface, the line from the previous point to the current point is hidden.

Implementation of this hidden line concept is straight forward. The data file is plotted horizontally an emission row at a time at whatever selected excitation resolution. For any scanned row, only two records are needed in memory at one time, the current data row and the previously plotted row. For each new row, an array is created from the data record, linearly interpolated to fit the plot size. This new array fits each point to a single position on the plotter, providing maximum resolution. The projection of this array onto the x-y surface is then calculated and plotted. As the array is plotted, each point is compared to the corresponding point of the previously plotted array. A pen up or pen down command is generated as needed for hidden lines. When completed, the plotted array is then stored as the previously plotted array. This cycle is then repeated for the entire plot. A typical plot requires about 10 to 15 minutes to complete. The viewpoint for the plot is

determined by the definition of the z axis location. That is, an x,y point is selected by the user as the terminal point for the z axis. This point then defines the angles of projection for an x,y,z point onto the x-y plane. In this way, one has 90° of freedom in viewing the TLS data.

Contour plotting is generally implemented using triangularization (53). For this work, a simple contour concept was used, similar to that described for isometric projection plotting. Again, only the previously plotted record and the current record are kept in memory. A data array is generated that is a linear interpolation between the two data records to the desired resolution. This current array is plotted with a pen up or pen down command sent to the plotter each time a contour boundary is crossed. When completed, contour regions are represented by alternating regions of black and white.

To illustrate the spectra obtained using these three plotting routines, a dilute solution of quinine sulfate in 0.01 N sulfuric acid was analyzed. Figure 5 shows the conventional fluorescence excitation and emission spectra for this solution. Figure 6 is the isometric projection of the TLS data file, while Figure 7 is the contour plot for the same solution. Both the isometric projection and contour plots have advantages and disadvantages, so each is used as necessary. For complete visualization, both plots are needed.

Spectral Features

Once TLS data are obtained, interpretation of these data is necessary to identify the compound of interest. To do so, the unique spectral features for that compound must be determined. Several methods have been tried to highlight these features. One method that has been

Figure 5. Conventional fluorescence excitation (left) and emission (right) spectra of quinine bisulfate.

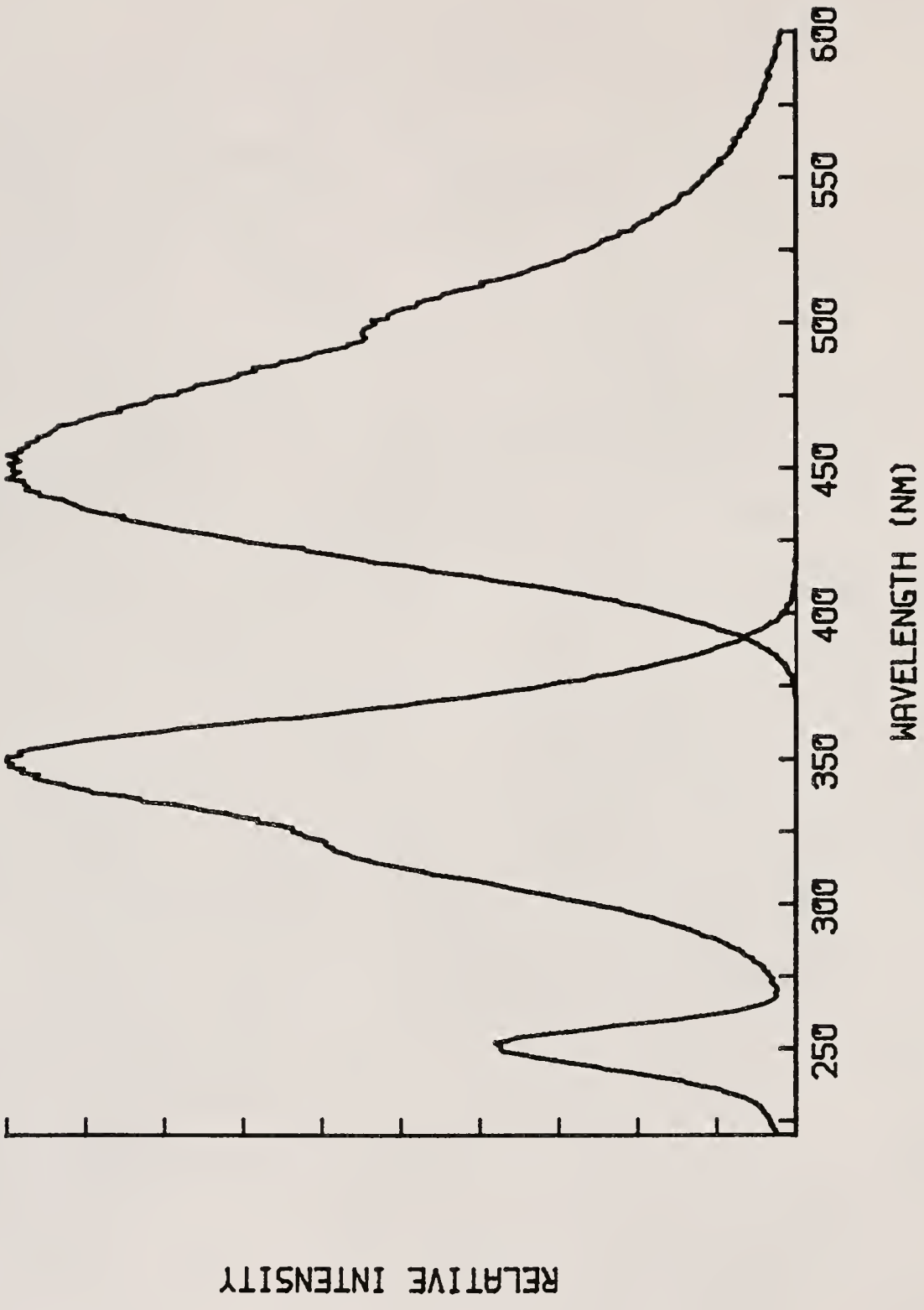
RELATIVE INTENSITY
250
300
350
400
450
500
550
600
WAVELENGTH (NM)

Figure 6. TLS isometric projection of quinine bisulfate.

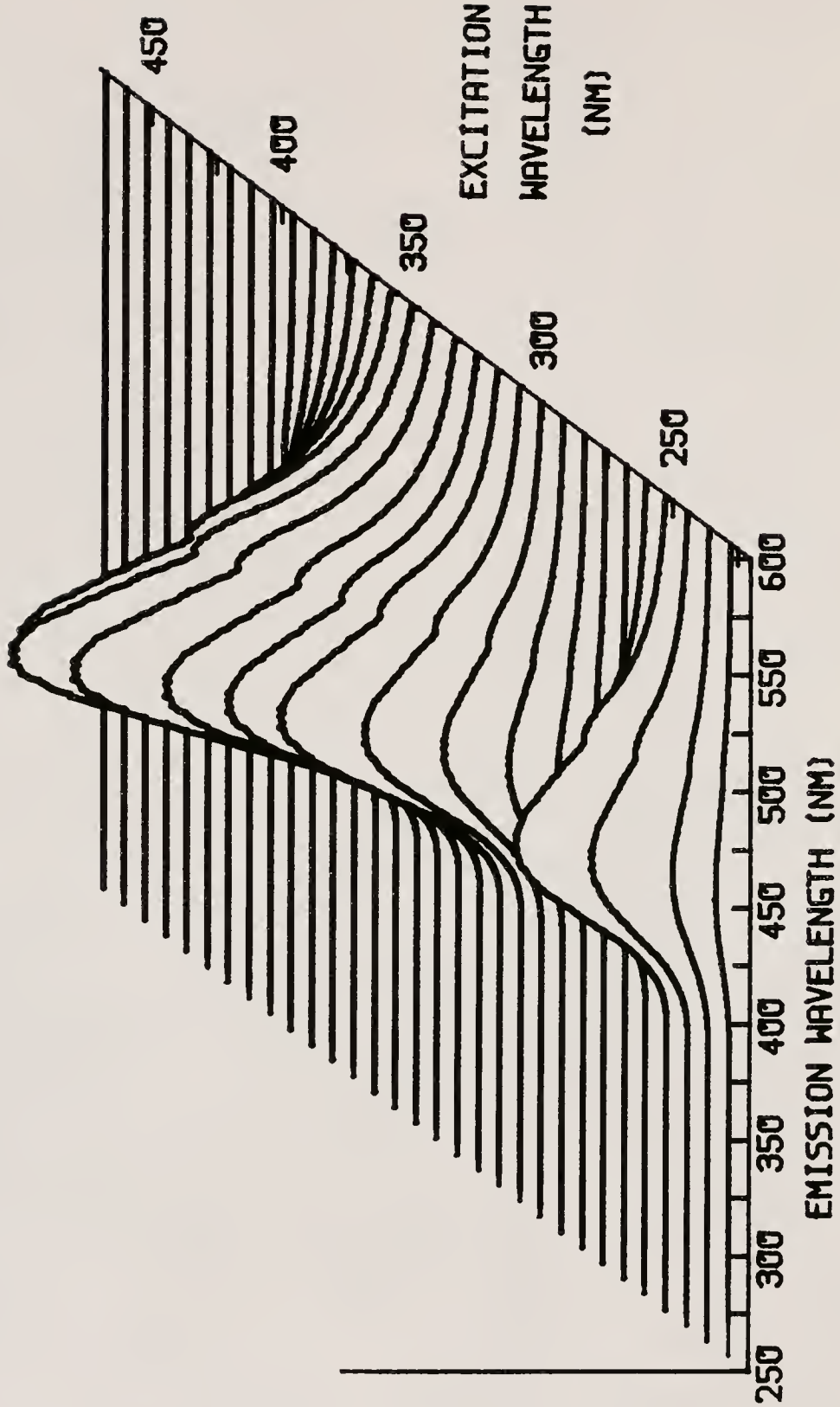
450
400
350
300
250
EXCITATION
WAVELENGTH
(NM)
250 300 350 400 450 500 550 600
EMISSION WAVELENGTH (NM)

Figure 7. TLS contour plot of quinine bisulfate.

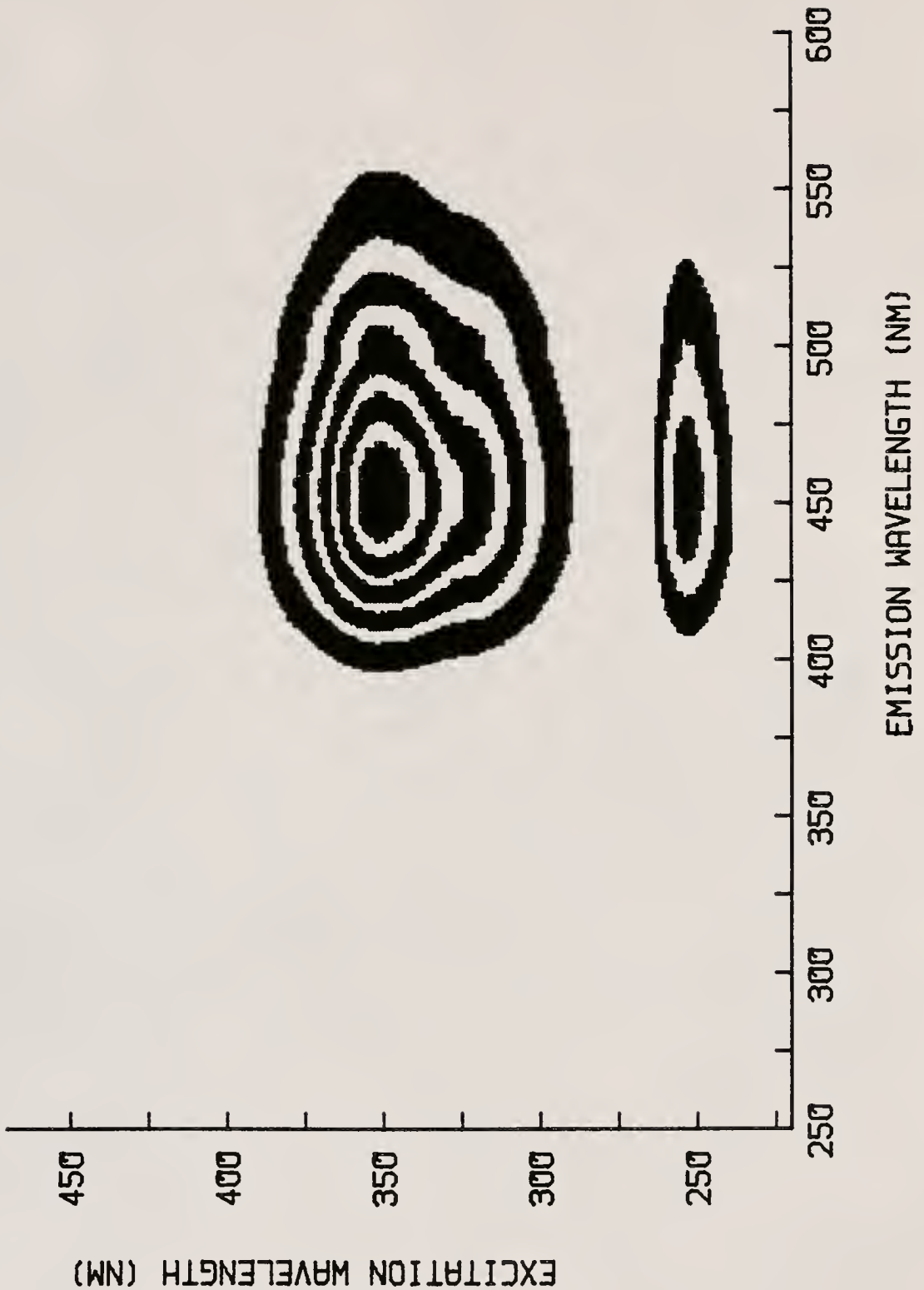
EXCITATION WAVELENGTH (NM)
450
400
350
300
250
EMISSION WAVELENGTH (NM)
250
300
350
400
450
500
550
600

successful in simple mixture analysis and in oil sample screening is the generation of difference spectra (48). The TLS spectrum of a spectrally interfering compound can be subtracted from the TLS spectrum of the analyte to reveal characteristic spectral regions. To illustrate, Figure 8A is the TLS spectrum of 1-methylpyrene and Figure 8B is the TLS spectrum of pyrene. When the difference spectrum is plotted, shown in Figure 9, unique regions are readily identifiable for 1-methylpyrene. The excitation region between 340 and 350 nm appears to be the region of choice in this situation.

Another suggestion to enhance key spectral features is the use of log plots. That is, log relative intensity is plotted on the y axis. This tends to enhance regions of low intensity and suppress regions of high intensity. While perhaps useful in limited cases, multicomponent analysis still remains difficult. Both of these methods are empirical in nature and do not rely on theoretical considerations.

To fully exploit TLS data, spectral features must be interpretted relative to luminescence theory. The TLS spectrum of a ternary mixture of PAHs, anthracene, perylene, and naphthacene, reveals that the spectra of PAH mixtures become complicated rapidly, as in Figure 10. Yet this spectrum suggests an inherent symmetry, perhaps useful in further analysis.

When solutions of low fluorescence intensity are analyzed, their TLS spectra contain several readily identifiable spectral features. Three such features are Rayleigh (elastic) scatter, Raman scatter, and second order Rayleigh scatter, as shown in Figure 11. Rayleigh scatter, the redirection of the incident photons by atoms and molecules within the solution, appears along a 45° line through the plot where the excitation

Figure 8. TLS contour plot of:

A. 1-methylpyrene

B. pyrene

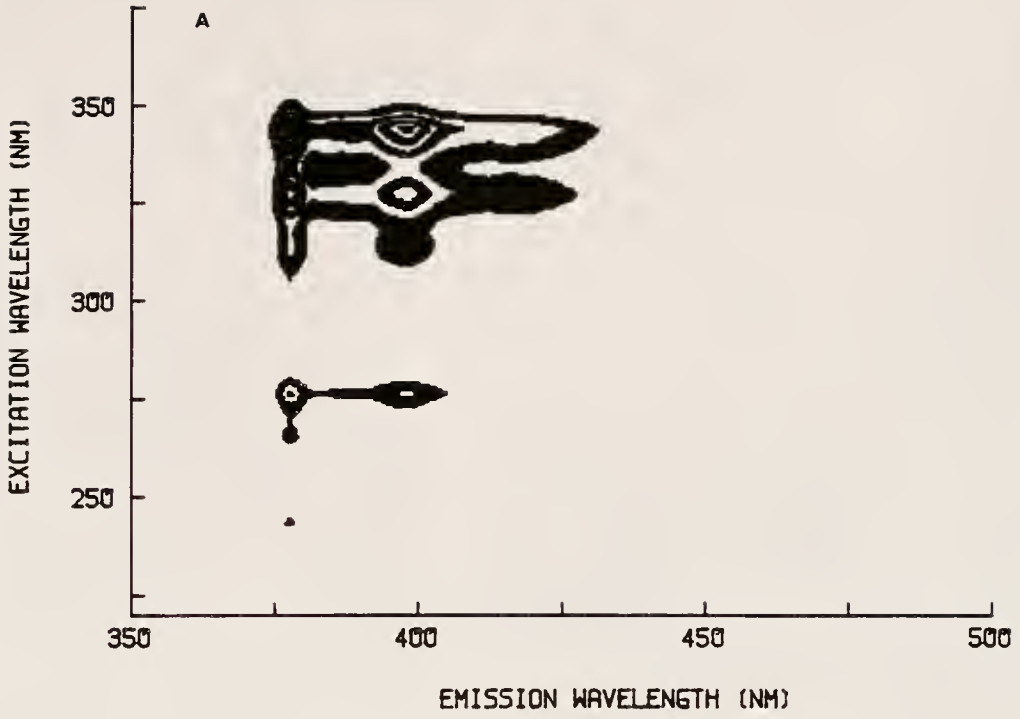
A
EXCITATION WAVELENGTH (NM)
350
300
250
350
400
450
500
EMISSION WAVELENGTH (NM)

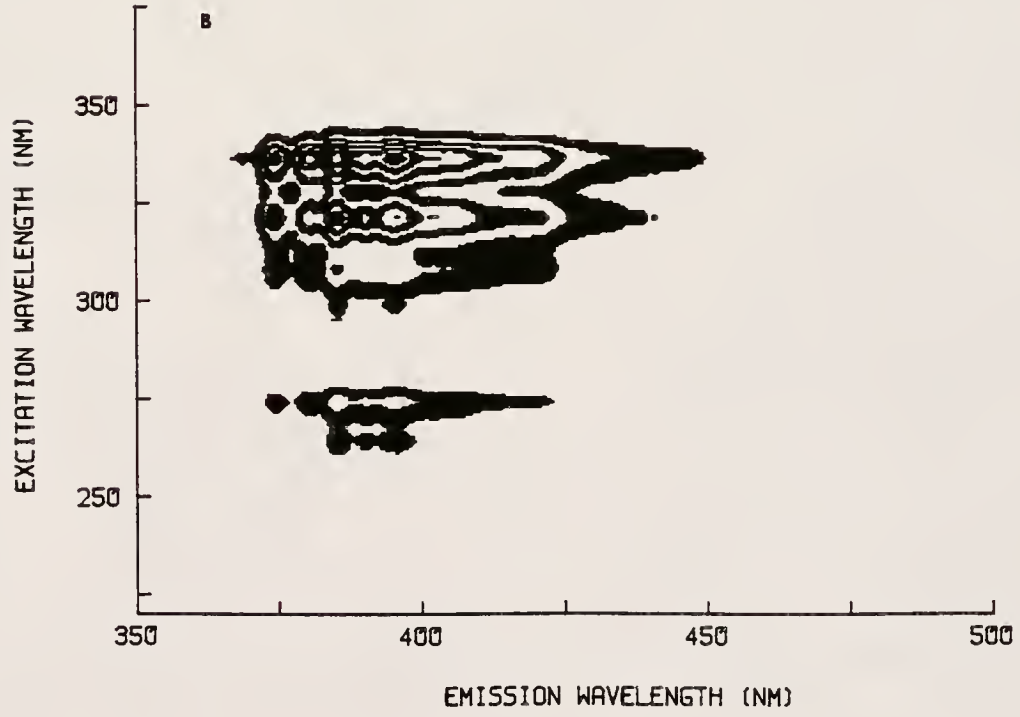
B
EXCITATION WAVELENGTH (NM)
350
300
250
350
400
450
500
EMISSION WAVELENGTH (NM)

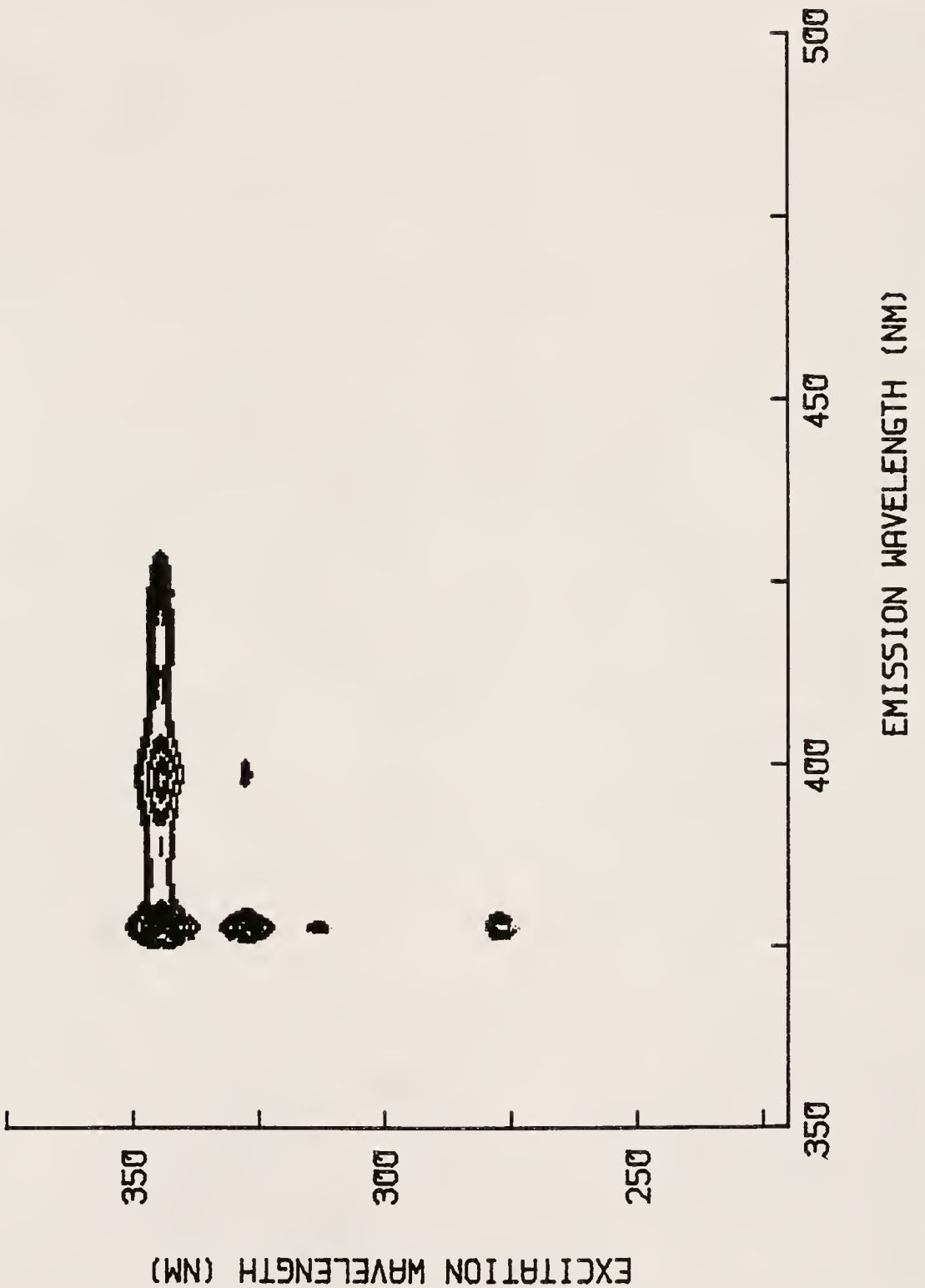
EXCITATION WAVELENGTH (NM)
350
300
250
EMISSION WAVELENGTH (NM)
350
400
450
500

Figure 10. TLS spectrum for a mixture of anthracene, perylene, and naphthacene.

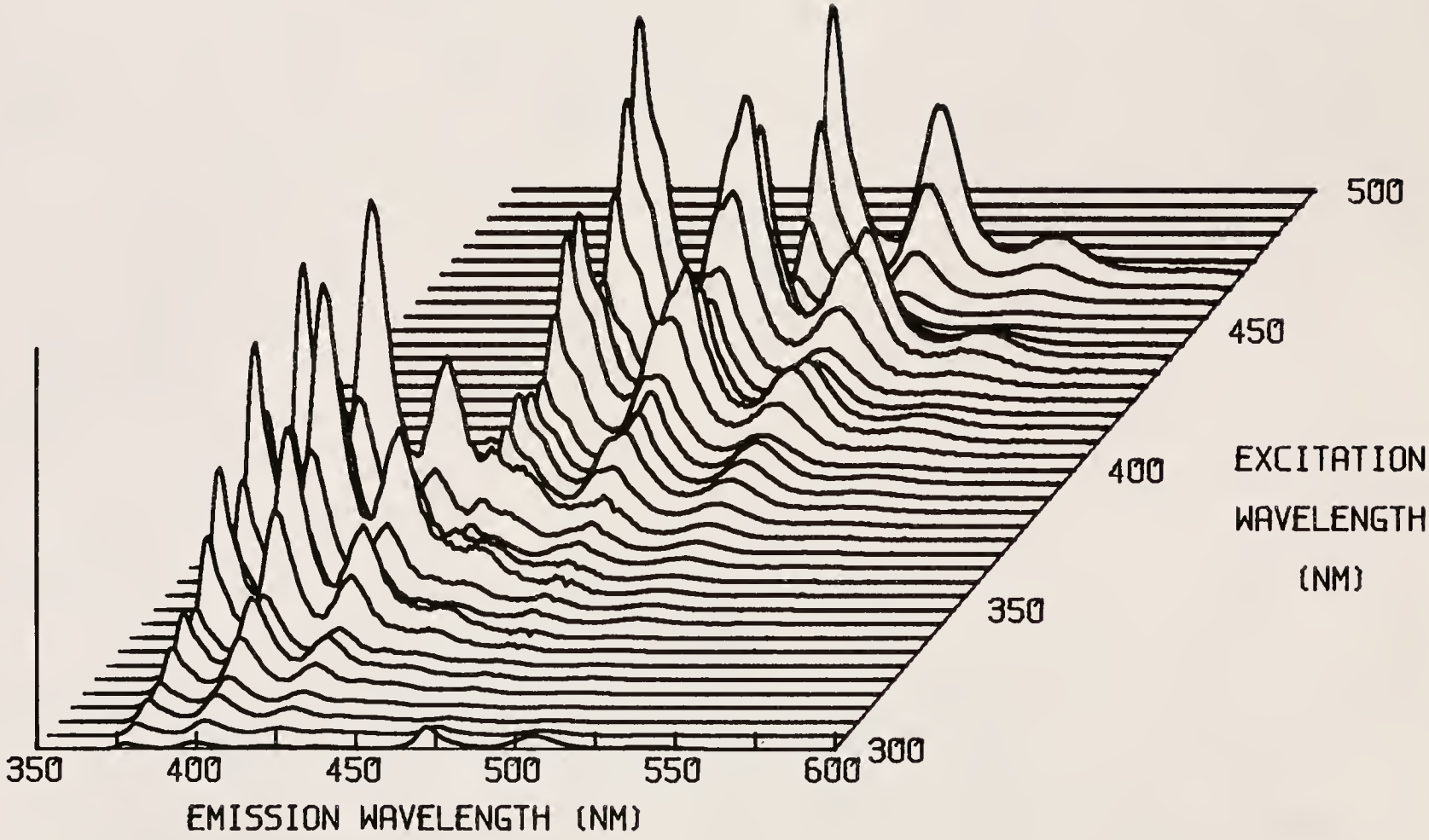
500
450
400
350
300
EXCITATION
WAVELENGTH
(NM)
350
400
450
500
550
600
EMISSION WAVELENGTH (NM)

Figure 11. TLS spectrum of ethanol blank to illustrate the positions of common spectral features.

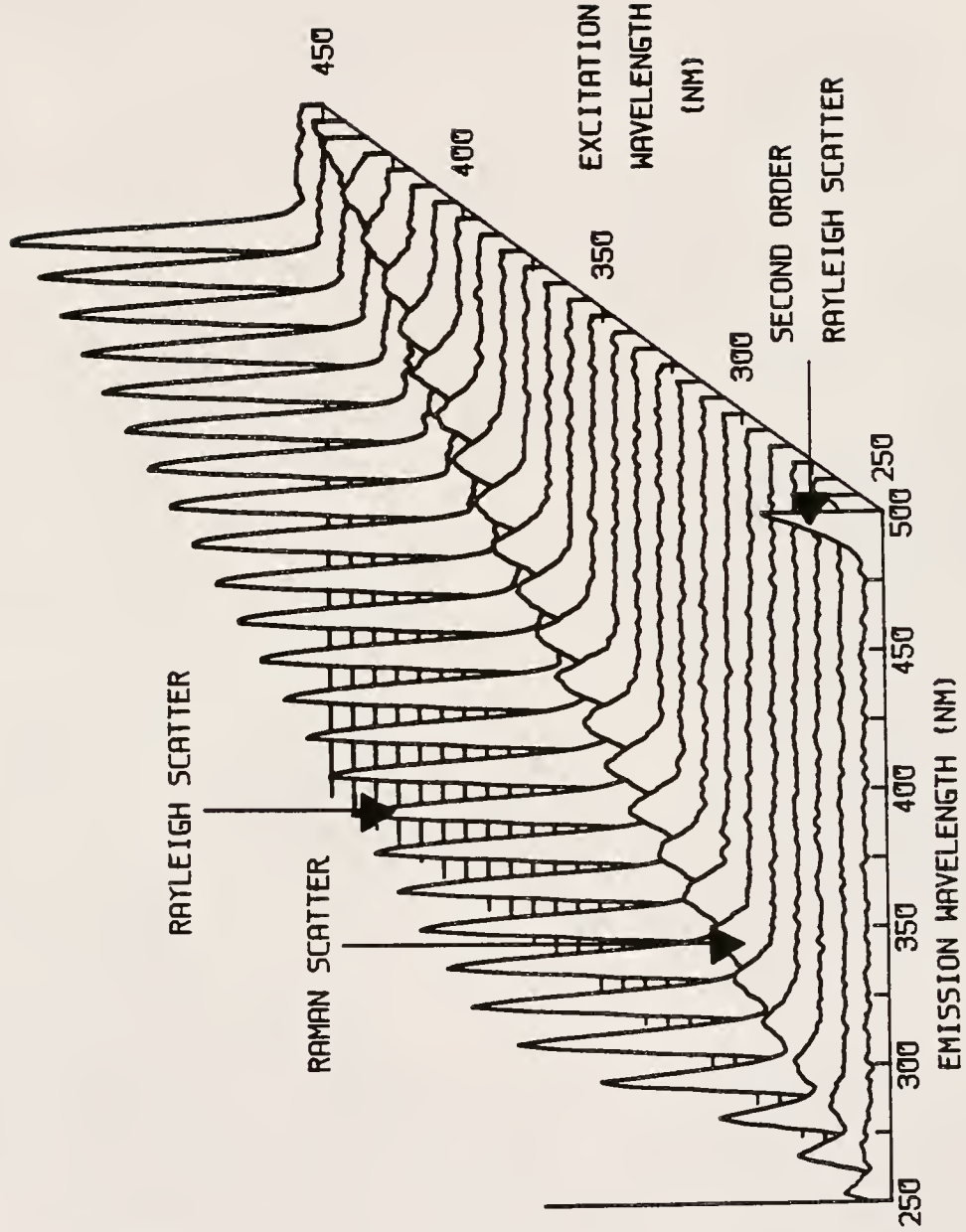
RAYLEIGH SCATTER
RAMAN SCATTER
450
400
350
300
EXCITATION WAVELENGTH (NM)
SECOND ORDER RAYLEIGH SCATTER
250
300
350
400
450
500
250
EMISSION WAVELENGTH (NM)

wavelength and the emission wavelength are equivalent. Raman scatter also appears along a curved path through the TLS spectrum that is characteristic of the solvent used. This is generally of low intensity. Second order Rayleigh scatter occurs where the emission wavelength is twice the excitation wavelength. This appears because of the dispersive (interference) characteristics of the grating within the monochromator.

The upper triangle in the TLS data matrix corresponding to the region where the excitation wavelength is greater than the emission wavelength is of little analytical utility. Stokes Law states that the emission wavelength must be greater than or equal to the excitation wavelength. While luminescence has been observed in the region where λ_i is greater than λ_j, it is generally of low intensity and is not useful in trace analysis. Two instrumental modifications were made to exploit this feature. In obtaining TLS spectra, this region is scanned around to save time, and the matrix is zero-filled in this region. The time savings varies but can extend up to 50%. Secondly, this region is placed in the rear of the TLS isometric projection plot, providing as broad a view as possible of spectral regions with analyte luminescence.

Conclusions

Many of the assumptions made for TLS analysis must correspond to those that are made in conventional luminescence spectroscopy. These assumptions will be basic to all luminescence theory and discussions described for these studies. They include: 1. The excitation and emission processes are completely independent. That is, the shape of the emission spectrum is independent of the wavelength selected to excite the sample. 2. No appreciable electronic energy transfer occurs between species. 3. Absorbance is low and the optical density

is less than 0.01. Other luminescence principles of conventional luminescence apply in the areas of filter and quenching effects. These assumptions are usually met when working with dilute solutions. For PAHs, concentrations less than 10 μg/mL are sufficient to meet these requirements.

TLS as an analytical technique suggests several basic disadvantages. Generally, large amounts of data are generated. For example, in the PAH TLS spectra used throughout this study, there are more than 35,000 data points in each data file. This number can be reduced substantially by reducing the spectral range or by increasing the sampling interval, and therefore, reducing spectral resolution. Also a much more elaborate experimental and data handling system is required over conventional luminescence instrumentation, especially if an image detector is used. Often this makes its cost prohibitive for routine use. Within the TLS data matrix, there is extensive data redundancy. Later, this redundancy will be utilized for statistical analysis of the data set. Finally, data collection and evaluation are more time-consuming. Some of these difficulties are instrumental in nature and improvements will inevitably come. However, some of these difficulties are inherent in TLS.

Thus, it appears that while extensive work has been done to allow for more data to be generated at increasingly faster rates, that is, instrumental improvements have been made, one is still faced with the need to interpret these data, whether manually or by computer assistance. The problem of data redundancy and the generation of voluminous amounts of data is shared by other analytical techniques.

> For example, during the course of a capillary GC-MS experiment, it is easily possible to obtain over 7000 mass spectra per hour. There is every indication that the development of liquid chromatographic-mass spectrometer (LC-MS) systems will follow the same course. While LC-MS may not require the fast scan times of GC-MS, each LC-MS experiment on a complex mixture will generate a tremendous amount of mass spectral data. The analyst is often only interested in some small subset of these data; and it is becoming increasingly necessary to utilize the speed of computers to search through the spectra obtained and screen for compounds of interest in the particular analysis. (54)

As improvements are made in multichannel detectors, TLS spectra can be collected more rapidly, more reliably, and with greater sensitivity. These developments are extending the utility of TLS as detection systems in HPLC and TLC.

To the analytical chemist, TLS is more than the generation of large amounts of data. TLS data are a superset of the data from other luminescence techniques. Figure 12 depicts the relationship between TLS and luminescence techniques such as Synchronous Luminescence Spectroscopy (SLS). Perhaps by studying TLS spectra, SLS will be better understood, making optimization more systematic. Instrumental and mathematical similarities make the study of SLS a natural extension of the principles set forth in TLS.

Figure 12. Scan paths for other luminescence techniques relative to the TLS spectrum.

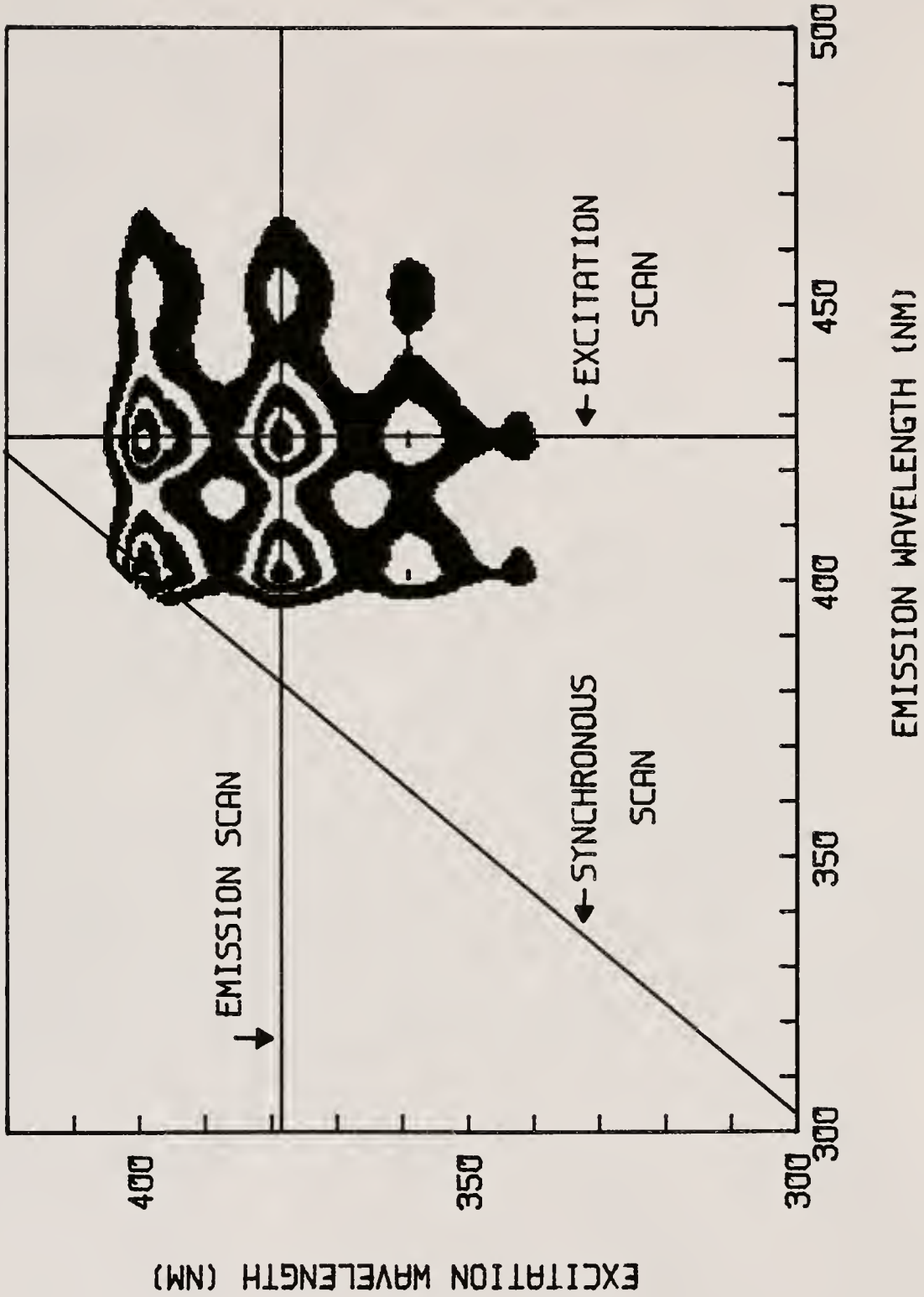
EXCITATION WAVELENGTH (NM)
400
350
300
300
350
400
450
500
EMISSION WAVELENGTH (NM)
EMISSION SCAN
SYNCHRONOUS SCAN
EXCITATION SCAN

CHAPTER 3
SYNCHRONOUS LUMINESCENCE SPECTROSCOPY

Theory

In the analysis of samples with completely unknown luminescence characteristics, TLS appears to have many desirable qualities. However, in many analyses, the luminescence characteristics of the sample are approximately known, as in the search for an impurity in a product, or where slight changes in spectral characteristics provide the desired information. In these cases, TLS generates more data than is necessary. If one has catalogued the spectral regions characterizing the compound of interest, the focus of the analysis should be on this spectral region. That is, previous information about the sample's characteristics should be used to limit the analysis to those spectral regions providing the greatest amount of information for analyte identification and quantitation. Synchronous Luminescence Spectroscopy (SLS) offers an alternate solution to this problem.

SLS requires the simultaneous scan of both the excitation and emission monochromators, synchronized so that a well-defined relationship is maintained between the wavelengths. Conventionally, this relationship is a constant wavelength difference. Mathematically, SLS data closely resemble TLS data. Equation (7) also defines each SLS data point in a single component sample with one added restriction. That is,

$$\lambda_j - \lambda_i = \Delta\lambda \tag{11}$$

where $\Delta\lambda$ is the wavelength difference between the excitation and

emission monochromators. With this added condition, SLS becomes a subset of TLS data. The synchronous scan path can be envisioned as a line through the TLS plane. In this way, one can again take advantage of the selectivity capability of molecular luminescence spectroscopy by varying both the excitation and emission wavelengths during analysis.

SLS, as an analytical technique, depends not only on the compound's luminescence excitation characteristics or the luminescence emission characteristics, but on both, and especially the relationship between the two. From the perspective of the energy level model from Chapter 1, the analyst is not interested in a single process, but rather, the relationship between two processes. Proper application of SLS techniques to multicomponent samples requires an understanding of the luminescence principles in Chapter 1 and the relationship they hold to TLS theory.

There are several advantages of SLS over conventional luminescence techniques that make it a technique for consideration in multicomponent analysis (55). The spectra obtained in SLS are reduced in complexity. Another selectivity advantage is the reduction of spectral bandwidths because of the scan process employed. A practical improvement is a reduction in the effect of Rayleigh scatter on the data. This technique can be combined with several conventional luminescence measurement systems. The instrumentation of SLS, as well as data handling requirements, is significantly simpler than in TLS. The analysis focuses on the key spectral regions of known analytes, making SLS useful for qualitative and quantitative mixture analysis. Perhaps a more thorough discussion of each of these characteristics will reveal some of the analytical potential of this technique.

The reduction in spectral complexity is best demonstrated with an example. Figure 13A shows the conventional fluorescence spectra for a solution of anthracene in n-heptane. The SLS spectrum for this same solution using a $\Delta\lambda$ of 3 nm is shown in Figure 13B. As will become clear, the selection of $\Delta\lambda$ determines the complexity of the spectrum obtained. The objective is to provide sufficient complexity for analyte identification, yet maintaining enough simplicity to make multicomponent analysis practical.

All SLS spectra are plotted as a function of emission wavelength, as shown in Figure 13B. Given the position along the emission wavelength axis, the excitation wavelength can be easily calculated using the conditions described to obtain the spectrum, such as a constant wavelength difference. Thus, the SLS spectrum is plotted as a projection of the data array onto the emission wavelength axis.

An improvement in selectivity is difficult to quantitate. A clear demonstration of this improvement is the band narrowing capabilities of SLS. This advantage has been stated by proponents of this technique but has not been quantitatively evaluated. One published quantitation of this improvement by Andre et al. (56) states that

$$\delta\lambda_s \simeq \delta\lambda_x+\delta\lambda_m-(\delta\lambda_x^2+\delta\lambda_m^2)^{1/2} \qquad (12)$$

where $\delta\lambda_s$ is the effective synchronous bandwidth (nm), $\delta\lambda_x$ is the luminescence excitation bandwidth (nm), and $\delta\lambda_m$ is the luminescence emission bandwidth (nm). This, once again, demonstrates the dependence of SLS characteristics on the characterisitics of both the excitation and emission spectra. While this equation seems to yield approximate results for limiting cases, no derivation of this equation is available in the literature.

Figure 13. A. Conventional RTF excitation and emission spectra of anthracene in n-heptane.

B. SLS spectrum of anthracene in n-heptane using a $\Delta\lambda$ of 3 nm.

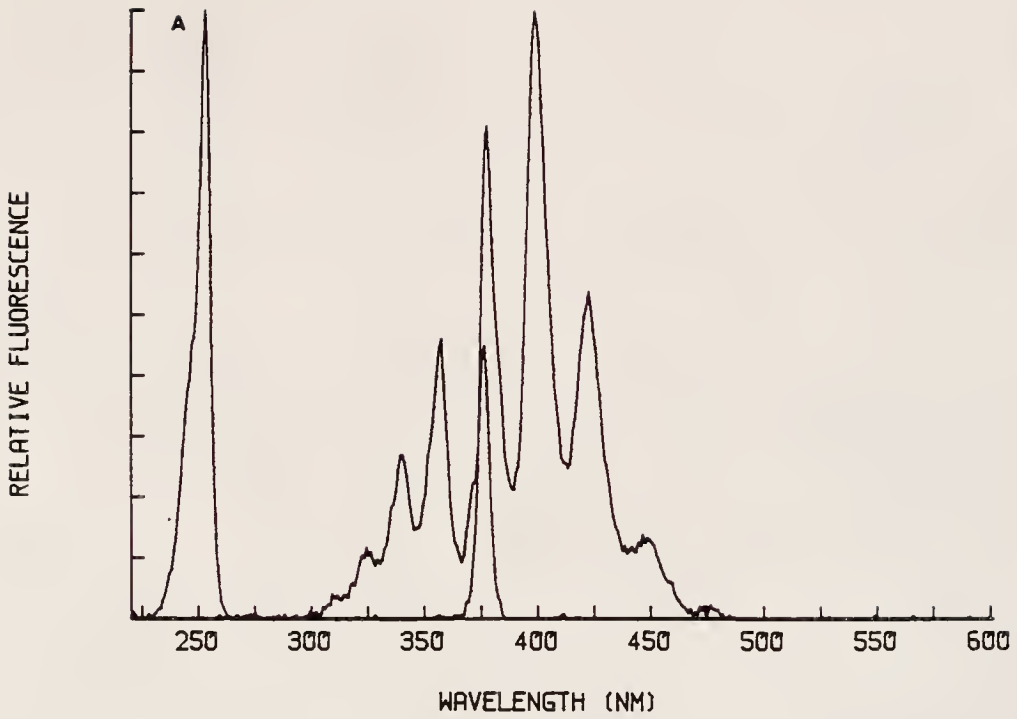
A
RELATIVE FLUORESCENCE
250
300
350
400
450
500
550
600
WAVELENGTH (NM)

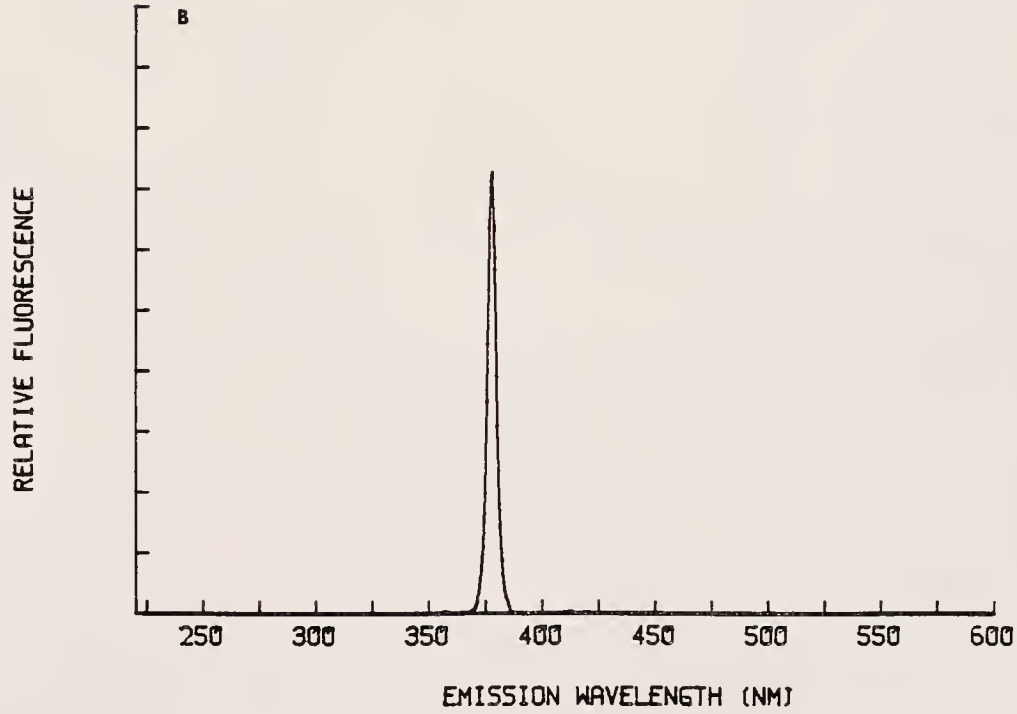
B
RELATIVE FLUORESCENCE
250
300
350
400
450
500
550
600
EMISSION WAVELENGTH (NM)

To gain an understanding of the quantitation of this effect, a geometric model and an algebraic model were designed. A basic assumption was made that the luminescence band can be described as a Gaussian function on both the excitation and emission axes and that the synchronous scan path passes directly over the center of the band. If the bandwidth is defined as the full-width-half-maximum, the bandwidth of the entire band defines an ellipse. Using the simple relationships shown in Appendix 2, the relationship

$$\delta\lambda_s = \delta\lambda_x\delta\lambda_m/(\delta\lambda_x^2+\delta\lambda_m^2)^{1/2} \quad (13)$$

is obtained. Three cases are of special interest. If the excitation and emission bandwidths are approximately equal, the bandwidth defines a circle and the band is completely symmetrical around the band maximum. For this case, Equation (13) reduces to

$$\delta\lambda_s = \delta\lambda_x/\sqrt{2} = \delta\lambda_m/\sqrt{2} \quad (14)$$

This is envisioned by realizing that although the scan path passes over the same band size, the SLS spectrum is plotted as a projection onto the emission wavelength axis. In room temperature fluorescence spectroscopy, this case has significance for many compounds. While a $\sqrt{2}$ reduction seems modest at best, it is substantial under these conditions. For example, a spectrum with a bandwidth of 30 nm is reduced to 21 nm, important for a technique that is limited by extensive band overlap. Two other limiting cases are also of special interest. If the excitation bandpass is much greater than the emission bandpass so that $\delta\lambda_x >> \delta\lambda_m$, Equation (13) reduces to

$$\delta\lambda_s = \delta\lambda_m \quad (15)$$

Analogously, if the reverse is true, $\delta\lambda_m >> \delta\lambda_x$, and

$$\delta\lambda_s = \delta\lambda_x \quad (16)$$

This confirms the characteristic of SLS spectra that its features follow most closely the features of the excitation or emission spectrum with the narrowest features. For some compounds, the emission spectrum is more structured than the excitation spectrum, while for other compounds, this condition is reversed. In SLS, only one of the two conventional spectra needs to contain sharp spectral features for the SLS spectrum to also be well-structured, a natural consequence of the multiplication effect describing this technique.

To model luminescence data more closely, luminescence bands are more effectively described in energy-related terms. Wavelength units are approximations and are limited to special cases. Appendix 2 gives the conversion of these equations to energy units. For the following discussion, energy terms are used.

Algebraically, similar results are obtained. For the previous assumption of Gaussian intensity functions, x_i and y_j are defined as

$$x_i = x_{i_o} \exp(-(\bar{\upsilon}_i-\bar{\upsilon}_{i_o})^2/(2\sigma_i^2)) \tag{17}$$

and

$$y_j = y_{j_o} \exp(-(\bar{\upsilon}_j-\bar{\upsilon}_{j_o})^2/(2\sigma_j^2)) \tag{18}$$

where x_i and y_j are intensities at wavelengths λ_i and λ_j, x_{i_o} and y_{j_o} are intensities at the peak wavelengths λ_{i_o} and λ_{j_o}, $\bar{\upsilon}_i$, $\bar{\upsilon}_{i_o}$, $\bar{\upsilon}_j$, and $\bar{\upsilon}_{j_o}$ are the energy values corresponding to the respective wavelength terms, and σ_i and σ_j are the standard deviations of the Gaussian bands, given in K. If $\delta\bar{\upsilon}_i$ and $\delta\bar{\upsilon}_j$ are the energy equivalents of $\delta\lambda_i$ and $\delta\lambda_j$, and $\delta\bar{\upsilon}_x/\bar{\upsilon}_{i_o}$ and $\delta\bar{\upsilon}_m/\bar{\upsilon}_{j_o}$ are less than 0.05, then σ_i and σ_j are proportional to $\delta\bar{\upsilon}_x$ and $\delta\bar{\upsilon}_m$. The exact relationship is given by

$$\sigma_i = ((1+(\delta\bar{\upsilon}_x/\bar{\upsilon}_{i_o})^2)^{1/2}-1)((10^7\delta\bar{\upsilon}_x/\bar{\upsilon}_{i_o})(2\ln 2)^{1/2})^{-1} \tag{19}$$

with an analogous equation for σ_j (57). With the details given in

Appendix 2, the synchronous bandwidth again reduces to Equation (13). Using energy units for these calculations provides a more realistic model than the wavelength approximation. In SLS, the scan paths need not pass exactly over the excitation and emission maxima. This presents a more difficult situation. A more general equation can be given for $\delta\bar{\upsilon}_s$. Equation (13) is a limited case of the expression

$$\delta\bar{\upsilon}_s = (\delta\bar{\upsilon}_x\delta\bar{\upsilon}_m/(\delta\bar{\upsilon}_x^{-2}+\delta\bar{\upsilon}_m^{-2})^{1/2})(\delta\bar{\upsilon}_x^{-2}+\delta\bar{\upsilon}_m^{-2}-(\bar{\upsilon}_{j_o}-\Delta\bar{\upsilon}-\bar{\upsilon}_{i_o})^2)^{1/2} \qquad (20)$$

where $\Delta\bar{\upsilon}$ is the energy equivalent of $\Delta\lambda$.

The reduction in Rayleigh scatter is a major consideration in SLS. This characteristic is explained by examination of the relationship between TLS and SLS, pictured in Figure 12. Rayleigh scatter is observed when the bandpasses of the excitation monochromator and the emission monochromator overlap, reaching a maximum along the line where λ_i and λ_j are equal. The Rayleigh scatter line can be thought of as an SLS scan with a $\Delta\lambda$ of 0 nm. That is, the SLS scan path runs parallel to the Rayleigh scatter ridge. Proper selection of $\Delta\lambda$ and the bandpasses eliminates this scatter.

TLS and SLS can be used under a variety of sample conditions. Fluorescence or phosphorescence can be measured at room temperature or at low temperatures. Implementation of SLS requires only the instrumentation required for the conventional luminescence technique. SLS data requirements are much less than those for TLS, reducing the computational and data storage needs.

SLS has had limited success since its introduction by Lloyd in 1971 (58-61). This group was the only one to publish in this area until the work of Andre and Vo-Dinh. Lloyd's work has focused on oil sample screening, with empirical rather than theoretical developments. The

work of Andre extended the application of SLS to drug samples (56) and fluorescence tracers in hydrology (62), again with little theoretical backing. The work of Vo-Dinh, and especially his paper in 1978 (63), was the first to attempt to force development along a path backed by luminescence theory. The same year saw a question raised as to the practical potential of SLS (64). Recently, Vo-Dinh has presented a review of SLS principles and applications (55). Significant improvements are necessary to make SLS more than a curiosity in the analytical literature.

Instrumentation

Thus, the stage was set for the current investigation of SLS and its potential in multicomponent analysis. The same experimental system that was described in Chapter 2 was used for this work. Additional software was written as needed to fit the overall software philosophy. Several software developments are worthy of mention. With a database of TLS spectra on file, standard SLS spectra can be obtained from either the TLS data files, using the appropriate extension, or generated from the excitation and emission spectra in the VEC files. A thorough investigation demonstrated that the generated spectra and instrumentally obtained SLS spectra agree very closely. Thus, to obtain an SLS spectrum using a different $\Delta\lambda$, the generation parameters need only be changed accordingly. Thus a new experiment is not necessary for each desired spectrum. Seemingly trivial, without this ability, this entire project would be prohibitively time-consuming. The database requirements for TLS data files complement those of SLS, again providing considerable data storage savings.

Bandpass selection influences experimentally obtained SLS spectra and should also be reflected in the standard spectrum generation program.

That is, a separate database for each bandpass is undesirable. Fortunately, a similar problem has been studied in conventional luminescence spectroscopy. For this system, a triangular function is used as the transfer function of the monochromator and the spectrum is corrected accordingly. The new spectrum is determined in the following manner. If $\delta\lambda_1$ is the desired effective bandpass and $\delta\lambda_0$ is the bandpass used to generate the database spectra then

$$F_w = \sum_{k=l_1}^{l_2} s_k S_{k+w} \tag{21}$$

where F_w is the corrected relative intensity at wavelength λ_w, S_{k+w} is the intensity in the original spectrum at wavelength λ_{k+w}, s_k is the scaling factor, l_1 is the lower wavelength limit, and l_2 is the upper wavelength limit. Generally l_1 and l_2 are set equal to $-\delta\lambda_1$ and $\delta\lambda_1$, respectively, and s_k is defined as

$$s_k = 1-|k|/\delta\lambda_1 \tag{22}$$

Several examples using this triangular approximation resulted in an average 3.2% error for assumed Gaussian peaks. Thus, the bandpass effects can be quantitatively predicted.

One limitation is imposed on the above bandpass correction; $\delta\lambda_0$ must be smaller than $\delta\lambda_1$. Because of this, database spectra were obtained with 2 nm bandpasses, the smallest practical value for RTF using this system. This correction procedure is more properly labeled a bandpass degradation calculation.

Constant Energy Synchronous Fluorescence Spectroscopy

Background

Once the instrumentation development was completed, a comprehensive evaluation of SLS was begun. Several major disadvantages became obvious,

perhaps limiting its practical application. Problems included the requirement for more a priori knowledge about the sample of interest before analysis, the observation that improper instrumental parameter selection may not detect all the luminescing compounds present, that is, "special blindness," and the key spectral regions must be well characterized prior to analysis. Essentially, these are all directly related to parameter selection. More specifically, the selection of $\Delta\lambda$ is critical.

Stated by one author,

> the value selected for the step ($\Delta\lambda$) is arbitrary, but maximum sensitivity is obviously obtained when the value corresponds to the separation between the maxima of the excitation and emission spectra.(56)

In a previous evaluation of SLS by the Winefordner group, $\Delta\lambda$ selection seemed to be fortuitous (64-66). The recommended $\Delta\lambda$ is one that results in the best resolved and simplest spectral features. If the maxima separation rule is used, n values for $\Delta\lambda$ must be selected for the n components present. This is similar to selective excitation. In previous theoretical discussions of SLS, the simplest case was selected to demonstrate the technique's capabilities. That is, a $\Delta\lambda$ of 3 nm is usually used, approximately equal to the Stokes Shift for many PAHs in n-alkane solvents (63,67). Then by selecting carefully chosen compounds, synthetic mixtures are resolvable (68). However, theory breaks down for the remaining non-ideal compounds. A major group of compounds causing difficulty are those molecules with a weak S_1 0-0 absorption. Examples of this are pyrene, 1,2-benzopyrene, 1-methylpyrene, and 3,4-benzopyrene, which are analytically significant compounds.

What has been obviously lacking in SLS is a strong theoretical foundation, one that can be traced to invariant photophysical properties of the analyte. Luminescence theory has been building over the past 30 years, so a vast storehouse of information is available for consideration. If, as I. M. Kolthoff said, "Theory guides, experiment decides," proper guidance is needed.

In 1978, Weiner (69) suggested the use of Total Luminescence Spectroscopy to optimize the selection of $\Delta\lambda$ in SLS. He noted that the main difficulty in SLS is in finding the best value for $\Delta\lambda$. In fact, he described the selection of a range of $\Delta\lambda$'s with the SLS spectra combined to reconstruct the TLS spectrum. This short note appeared fairly trivial, but contained a concept that has been consistently overlooked by SLS users. In the past, the development of SLS and TLS has been completely independent, with the suggestion that the techniques are competitive rather than complementary.

By using SLS, the data generated are substantially less than those in TLS. But to be effective in multicomponent analysis, the data selected must retain as much information as possible. The analytical value of a subset of TLS data, such as an SLS scan, varies considerably, depending on the parameters of subset selection. Based on TLS theory as outlined in Chapter 2, a natural suggestion is to use a different subset of the TLS spectrum, one that more clearly identifies characteristic spectral regions. Experimental implementation of this change translates to selecting a different scan route. Mathematically, this corresponds to changing the restriction imposed by Equation (11).

Due to the nature of the scan process in conventional SLS, it can be best described as Constant Wavelength Synchronous Luminescence

Spectroscopy (CWSL), to contrast it with other scan modes. Identified as Variable Wavelength Synchronous Fluorescence Spectroscopy, the first suggestion was to scan the two monochromators at different rates. By scanning both monochromators at constant rates, with the emission monochromator scanned faster than the excitation monochromator, a scan path is traced through the TLS plane defining a line similar to CWSL, not on a 45° line relative to the emission wavelength axis, but rather less than 45°.

The instrumentation described for SLS was designed for a Variable Wavelength Synchronous Luminescence Spectroscopy (VWSL) scan, with CWSL representing a special case. The scan rates, $d\lambda_i/dt$ and $d\lambda_j/dt$, are defined as

$$d\lambda_j/dt - d\lambda_i/dt = c \tag{23}$$

where c is a constant greater than zero. In CWSL, c is set equal to zero. Again, reference spectra generation is possible using the same database.

Evaluation of VWSL indicated immediately that it is hampered by most of the same problems of CWSL. The lack of a solid theoretical foundation again makes multicomponent analysis difficult. Although there have been reports of research in this area, no publications are available. This evaluation was soon abandoned after a more favorable alternative was discovered.

The evaluation of TLS data and relationships that exist between spectral regions of PAH and pharmaceutical solutions has led to the development of the new method, Constant Energy Synchronous Luminescence (CESL), with fluorescence, Constant Energy Synchronous Fluorescence (CESF), and phosphorescence, Constant Energy Synchronous Phosphorescence (CESP), applications. This technique is performed by maintaining a

constant energy difference between the excitation and emission wavelengths. The restriction placed on the TLS data matrix is mathematically defined as

$$\Delta\bar{\upsilon} = (1/\lambda_i - 1/\lambda_j)*10^7 \qquad (24)$$

where $\Delta\bar{\upsilon}$ is the energy difference between wavelengths, in K. Evaluation of this technique was directed towards Raman scatter interference reduction in pharmaceutical analysis and information retention in the analysis of PAHs. The relative merits of this technique against conventional SLS and conventional fluorescence techniques will be presented.

Raman Scatter Reduction

Introduction. The fluorescence emission spectra of most common solvents used in RTF exhibit a strong Rayleigh scatter signal when the excitation and emission wavelengths are identical, and a weak Raman scatter signal, shifted in energy so that

$$\Delta\bar{\upsilon}_R = (1/\lambda_x - 1/\lambda_m)*10^7 \qquad (25)$$

where $\Delta\bar{\upsilon}_R$ is the energy of the active Raman transition, in K, λ_x is the excitation wavelength, in nm, and λ_m is the emission wavelength, in nm. The contribution of the solvent can become significant if the fluorescence signal is small and falls within the spectral region of the solvent Raman scatter.

The intensity and position of the Raman band is dependent upon the solvent used. However, similarities can be found among commonly used solvents. Figure 14 shows the Raman scatter for cyclohexane, n-heptane, ethanol, and water excited at 330 nm. All four were measured under the same instrumental conditions, including amplifier gain. Spectral bandpasses of 8 nm were used with each monochromator. The Raman band

Figure 14. Conventional fluorescence emission scan for four common fluorescence solvents: a. cyclohexane, b. n-hexane, c. ethanol, and d. water. The excitation wavelength was 330 nm. Ry = Rayleigh scatter, Rm = Raman scatter.

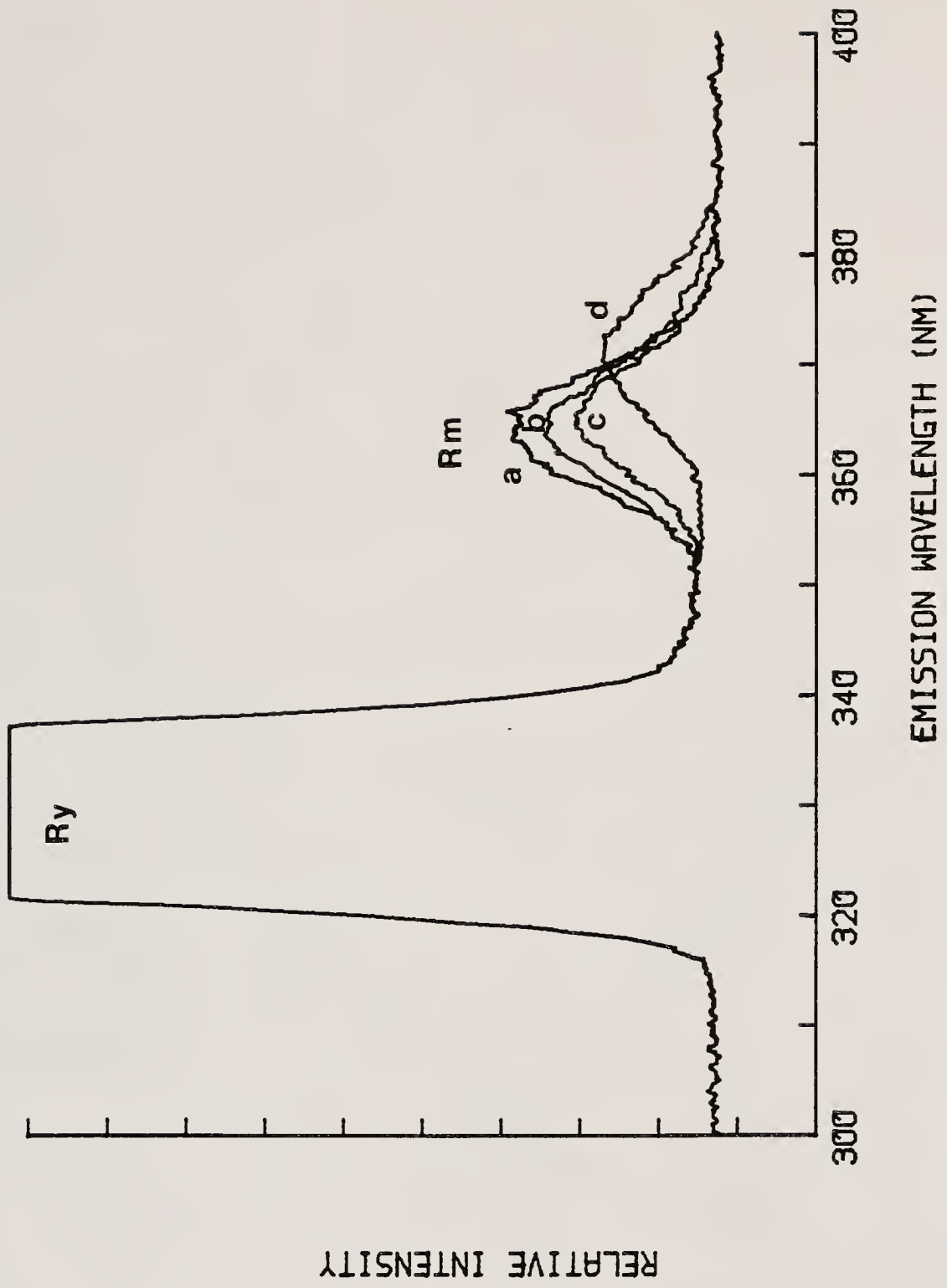
Ry
Rm
a
b
c
d
300
320
340
360
380
400
EMISSION WAVELENGTH (NM)
RELATIVE INTENSITY

positions agree with the Raman shifts reported by Parker (2) for the solvents, shown in Table 7. All solvents with a CH or OH group show a weak Raman band with an approximate 3000 K shift.

The total emission of water clearly demonstrates the spectral relationship of the Rayleigh and Raman scatter (Figure 15). The line through the Raman ridge corresponds to CWSF scans with a $\Delta\lambda$ of 32, 37, and 42 nm. Upon examination of the spectra obtained from these three scans, Figure 16, two effects are clearly noticeable. First, the Raman band becomes broadened compared to the Raman band in conventional fluorescence spectroscopy. Second, the position of the Raman band is determined by the selection of $\Delta\lambda$. The lines through the total emission spectrum run parallel to the Rayleigh scatter ridge using CWSF.

Plotted on a wavelength axis, Figure 15 shows that the Raman scatter ridge and Rayleigh scatter ridge diverge, maintaining a constant energy difference between the two. It is this basic natural relationship that forms the foundation for Constant Energy Synchronous Fluorescence (CESF). In this technique, the curve defined through the TLS spectrum runs parallel to both the Rayleigh scatter ridge and the Raman scatter ridge when plotted in energy units.

The spectral region around the Raman scatter ridge is an analytically important region. Many pharmaceuticals fluoresce in this region, as well as other aromatic compounds, such as phenol (70). Therefore, a method capable of Raman scatter reduction or elimination could provide widespread utility.

Raman scatter can generally be subtracted out with a blank measurement. Rayleigh scatter is almost impossible to subtract out and theoretically should not be the same for the sample and blank solutions.

Table 7. Raman Bands Observed in Common RTF Solvents

Solvent	Energy Shift (K)[a]
Water	3380
Ethanol	2920
	1400
Cyclohexane	2880
	1360
Chloroform	3020
	700

[a]Reference 2

Figure 15. Total fluorescence emission plot for water. The lines through the Raman scatter ridge represent conventional synchronous fluorescence scan paths. $\Delta\lambda$ = -.- 32 nm, — 37 nm, --- 42 nm.

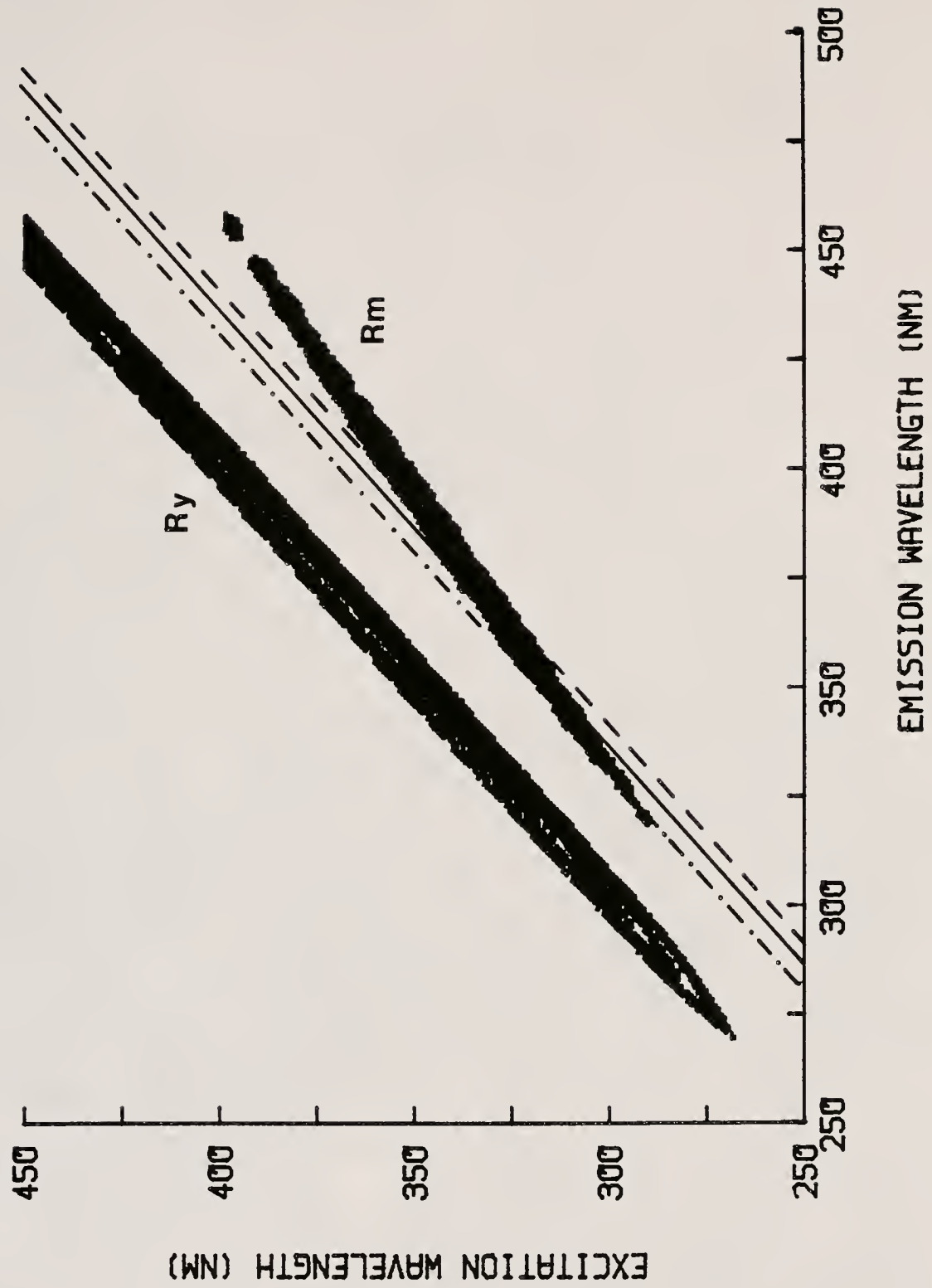
Ry
Rm
EXCITATION WAVELENGTH (NM)
EMISSION WAVELENGTH (NM)
250
300
350
400
450
500

Figure 16. Typical CWSF background spectra for water using a $\Delta\lambda$ of: a. 32 nm, b. 37 nm, and c. 42 nm.

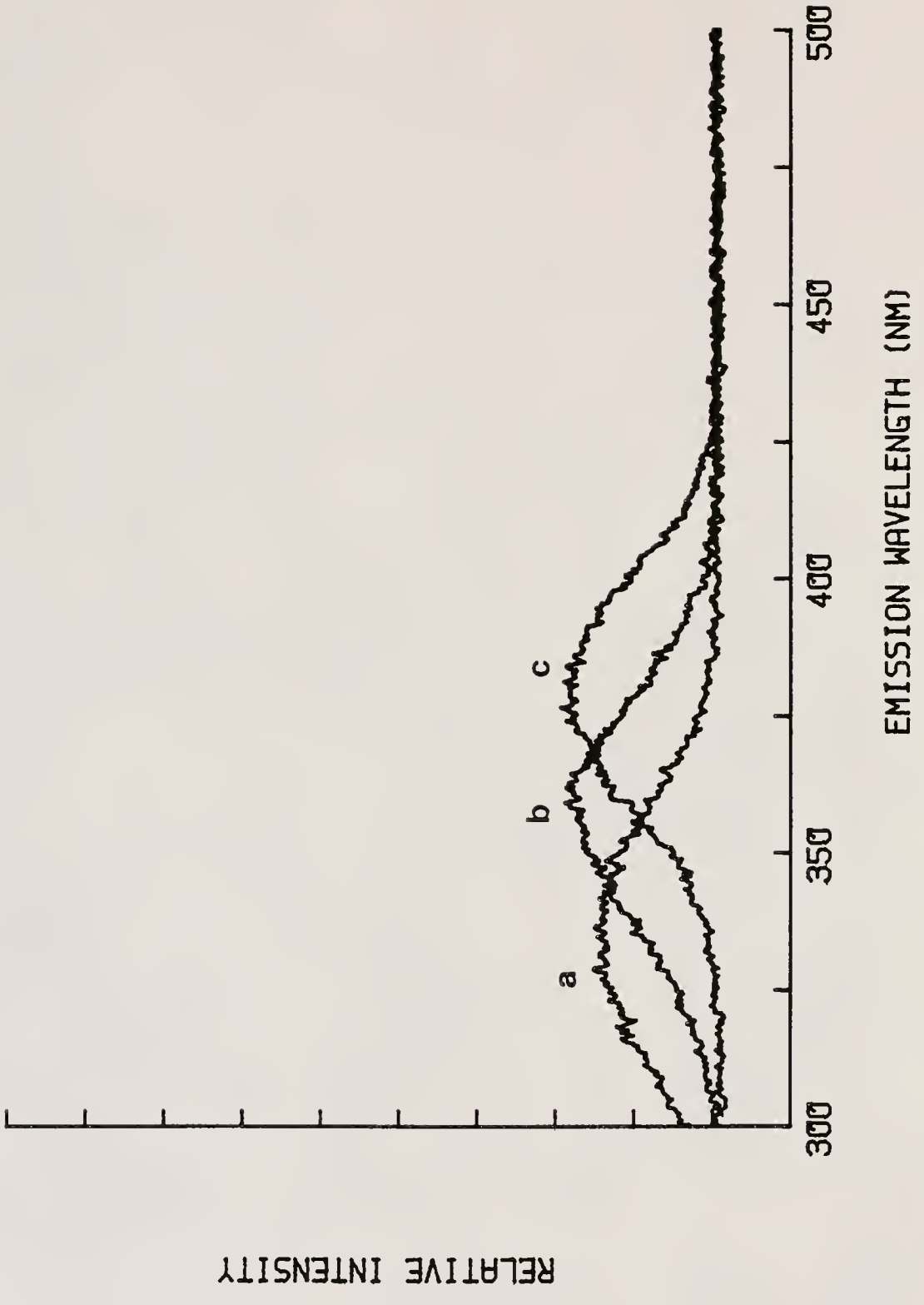
RELATIVE INTENSITY
300
350
400
450
500
EMISSION WAVELENGTH (NM)
a
b
c

Because Raman scatter is due to the solvent, its intensity is about the same from solution to solution with the same solvent. However, many situations make a blank spectrum unavailable or a truly representative blank unachievable.

Instrumentation. All CESF measurements were made on the system described in Chapter 2. In order to scan the monochromators and to maintain a constant energy difference between the two, the emission monochromator is stepped at a constant speed while the excitation monochromator speed is varied. A linear approximation is made for this, dividing the spectral range to be scanned into 1000 segments. The emission monochromator is scanned by a fixed increment, while the new position for the excitation monochromator is calculated and moved accordingly. The PMT signal is integrated over approximately 0.3 s, using an RC constant of 0.1 s. The speed of the FORTRAN calculations makes the scan essentially continuous, with the calculation time negligible. Thus a single scan requires approximately 5 minutes.

Results and Discussion. To illustrate the relationships among conventional fluorimetry, CWSF, and CESF, tripelennamine hydrochloride was selected as a model compound. Figure 17 shows the conventional fluorescence emission spectra for solutions of 0.0, 0.1, and 1.0 µg/mL tripelennamine hydrochoride in water. Note the presence of the Rayleigh scatter band and the position of the Raman scatter relative to the fluorescence. The total luminescence isometric projection of the 1.0 µg/mL solution illustrates the relative positions of the spectral features (Figure 18). The bandpass selected for both monochromators

Figure 17. Conventional fluorescence emission spectra for: a. 0.0 μg/mL, b. 0.1 μg/mL, and c. 1.0 μg/mL tripelennamine hydrochloride in water solutions.

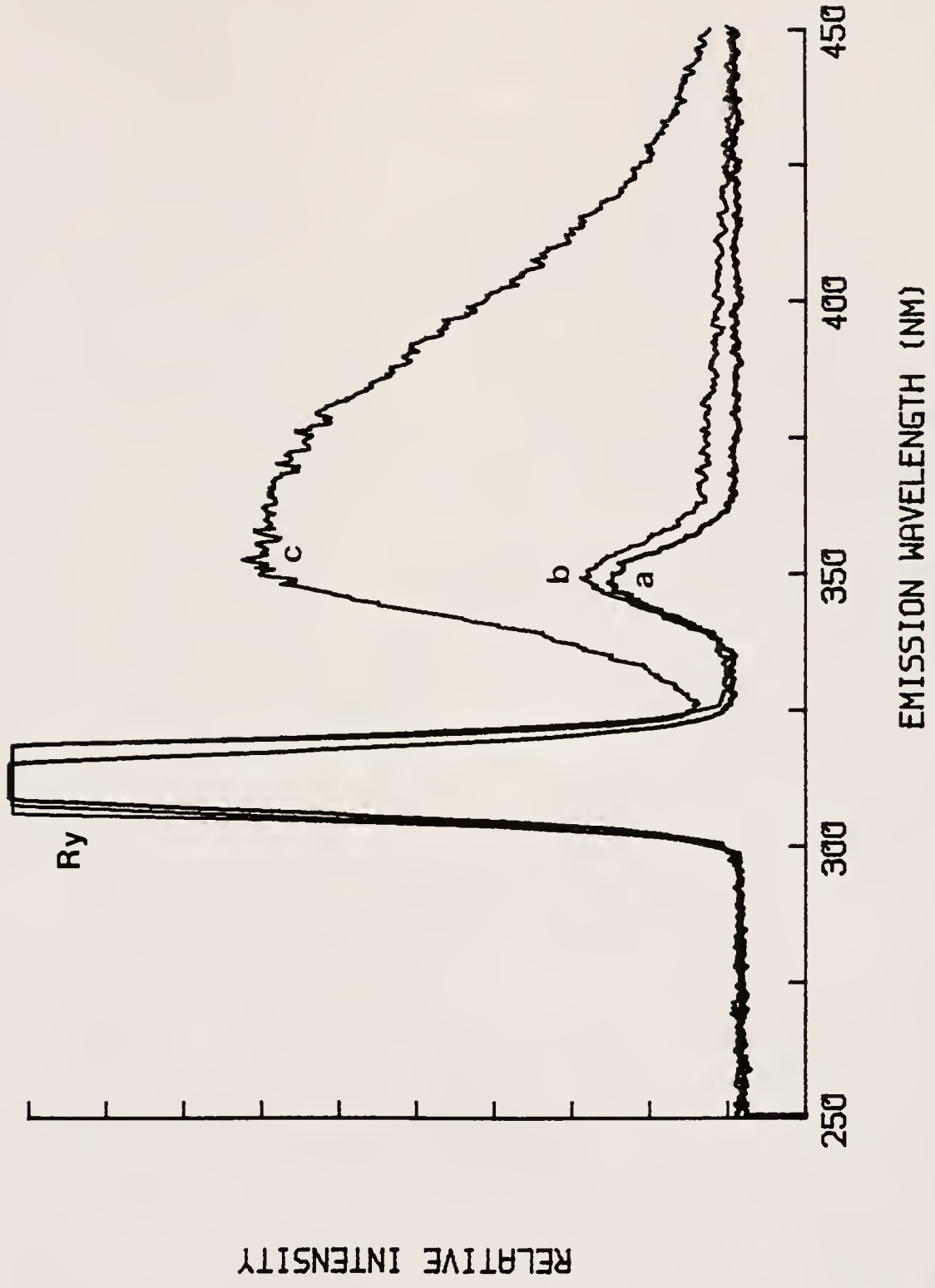
Ry
c
b
a
250
300
350
400
450
EMISSION WAVELENGTH (NM)
RELATIVE INTENSITY

Figure 18. Total fluorescence spectrum of a 1.0 μg/mL solution of tripelennamine hydrochloride in water.

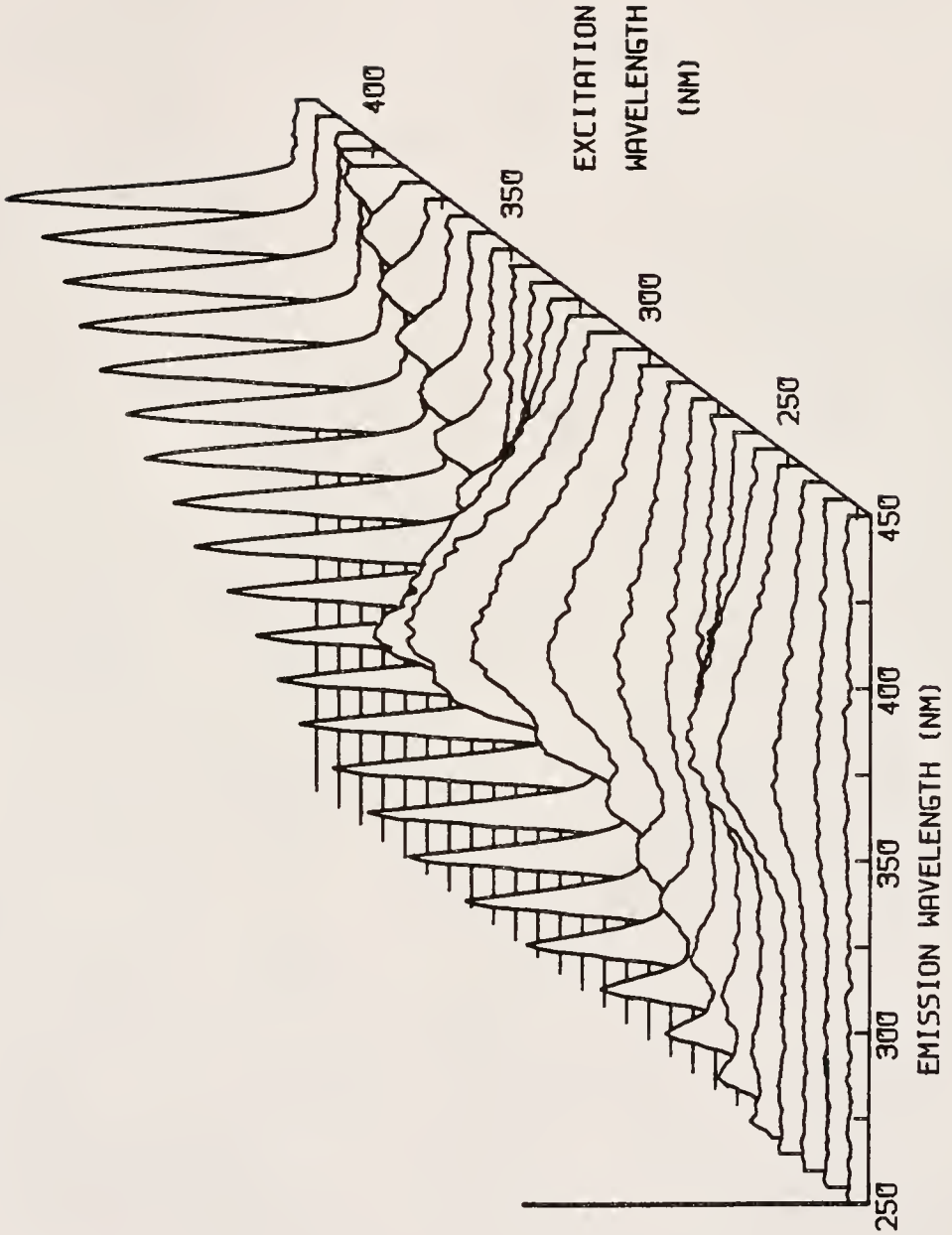
EXCITATION
WAVELENGTH
(NM)
400
350
300
250
250
300
350
400
450
EMISSION WAVELENGTH (NM)

was 8 nm, approximately that used in routine fluorimetry. The near coincidence of solvent Raman scatter and analyte fluorescence can be seen. As the concentration of the triplennamine hydrochloride is reduced, analyte fluorescence becomes increasingly more difficult to distinguish from Raman scatter.

The contour plot of the same solution in Figure 19 depicts the path traced by CWSF (solid line). In this case, $\Delta\lambda$ = 54 nm. The spectra obtained for the solutions of 0.0, 0.1, and 1.0 µg/mL tripelennamine hydrochloride in water under these conditions are shown in Figure 20A. Note that the Raman scatter band is still present. The broken line in Figure 19 depicts the path traced by a CESF scan. An energy difference, $\Delta\bar{\upsilon}$, of 4730 K was selected. The resultant spectra under these conditions for the three solutions are shown in Figure 20B. These confirm the spectral selectivity shown in the contour plots.

A second example was chosen to evaluate the selection of the proper $\Delta\bar{\upsilon}$. By scanning the spectral region beyond the Raman scatter, so that $\Delta\bar{\upsilon} > \Delta\bar{\upsilon}_R$, as in the previous example, spectral interference is reduced. However, terbutaline sulfate was studied to determine if a $\Delta\bar{\upsilon}$ selected so that $\Delta\bar{\upsilon} < \Delta\bar{\upsilon}_R$ would yield similar results. That is, the spectrum is obtained by scanning between the Rayleigh and Raman scatter ridges.

Figure 21 shows the emission spectra obtained by conventional fluorimetry for terbutaline sulfate solutions of 0.0, 0.1, 0.3, and 1.0 µg/mL, with water again the solvent. The excitation wavelength was 280 nm, the maximum for this compound. CWSF spectra are presented in Figure 22A, with a $\Delta\lambda$ of 31 nm for the same four solutions. In Figure 22B, the CESF spectra again illustrate the Raman scatter reduction capabilities of this technique, with a $\Delta\bar{\upsilon}$ of 2400 K selected.

Figure 19. Contour plot of the total fluorescence for a 1.0 μg/mL solution of tripelennamine hydrochloride in water. The solid line through the spectrum is the conventional synchronous fluorescence scan path for $\Delta\lambda$ = 54 nm. The broken line through the spectrum represents the constant energy synchronous fluorescence scan path for $\Delta\bar{\upsilon}$ = 4730 K.

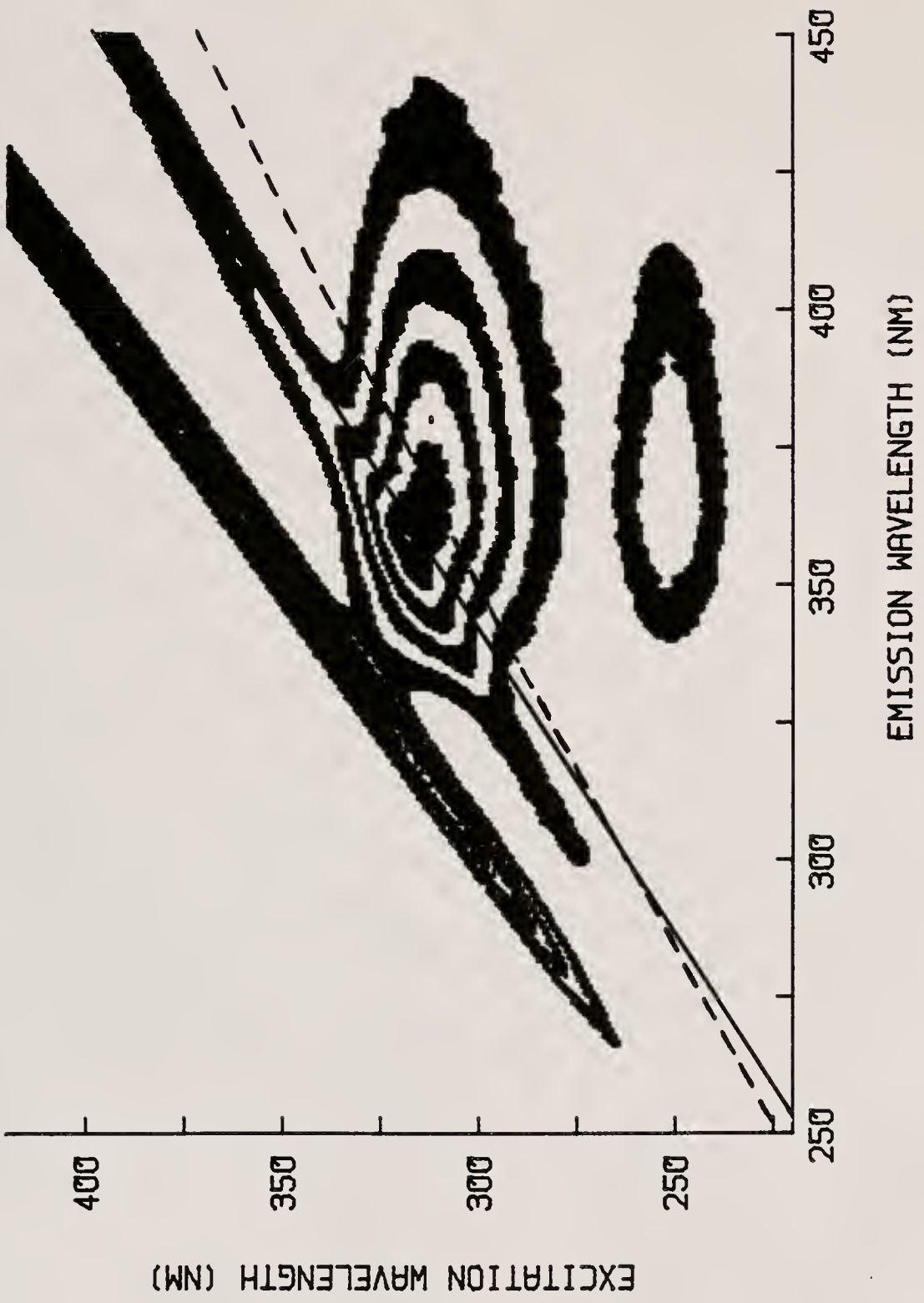
EXCITATION WAVELENGTH (NM)
400
350
300
250
250
300
350
400
450
EMISSION WAVELENGTH (NM)

Figure 20. A. Conventional synchronous fluorescence spectra for 0.0, 0.1, and 1.0 μg/mL tripelennamine hydrochloride in water. The wavelength difference was 54 nm.

B. Constant energy synchronous fluorescence spectra for 0.0, 0.1, and 1.0 μg/mL solutions of tripelennamine hydrocholoride in water. The scan interval was $\Delta\bar{\upsilon}$ = 4730 K.

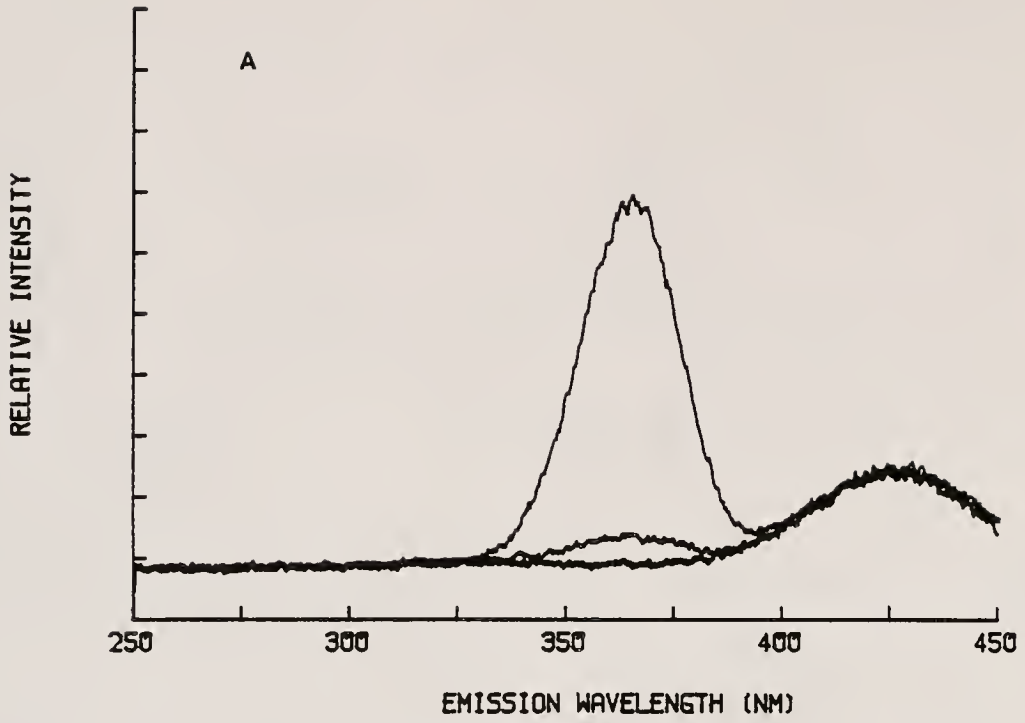
A
RELATIVE INTENSITY
250
300
350
400
450
EMISSION WAVELENGTH (NM)

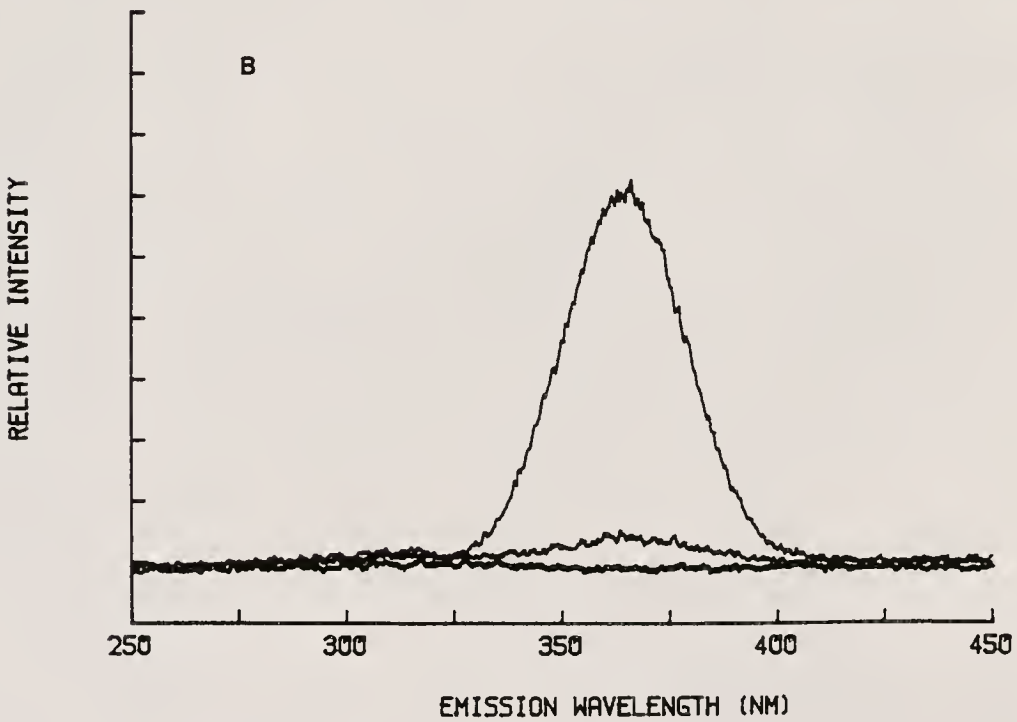
B
RELATIVE INTENSITY
250
300
350
400
450
EMISSION WAVELENGTH (NM)

Figure 21. Conventional fluorescence emission spectra for: a. 0.0, b. 0.1, c. 0.3, and d. 1.0 μg/mL terbutaline sulfate in water. The excitation wavelength was 280 nm.

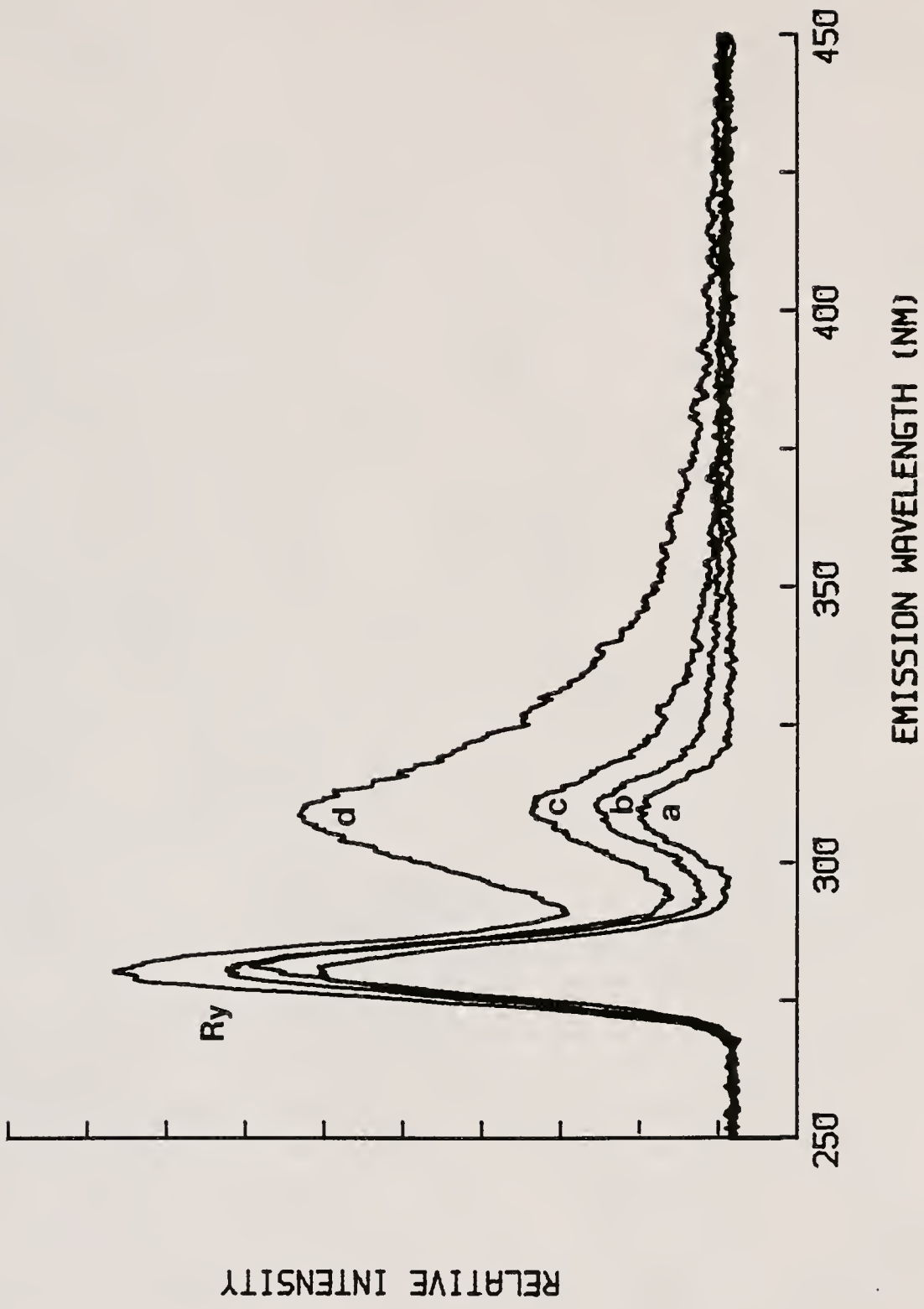
RELATIVE INTENSITY
250
300
350
400
450
EMISSION WAVELENGTH (NM)
Ry
a
b
c
d

Figure 22. A. Conventional synchronous spectra for 0.0, 0.1, 0.3, and 1.0 µg/mL terbutaline sulfate in water. The wavelength difference was 31 nm.

B. Constant energy synchronous fluorescence spectra for 0.0, 0.1, 0.3, and 1.0 µg/mL terbutaline sulfate in water. The scan interval was 2400 K.

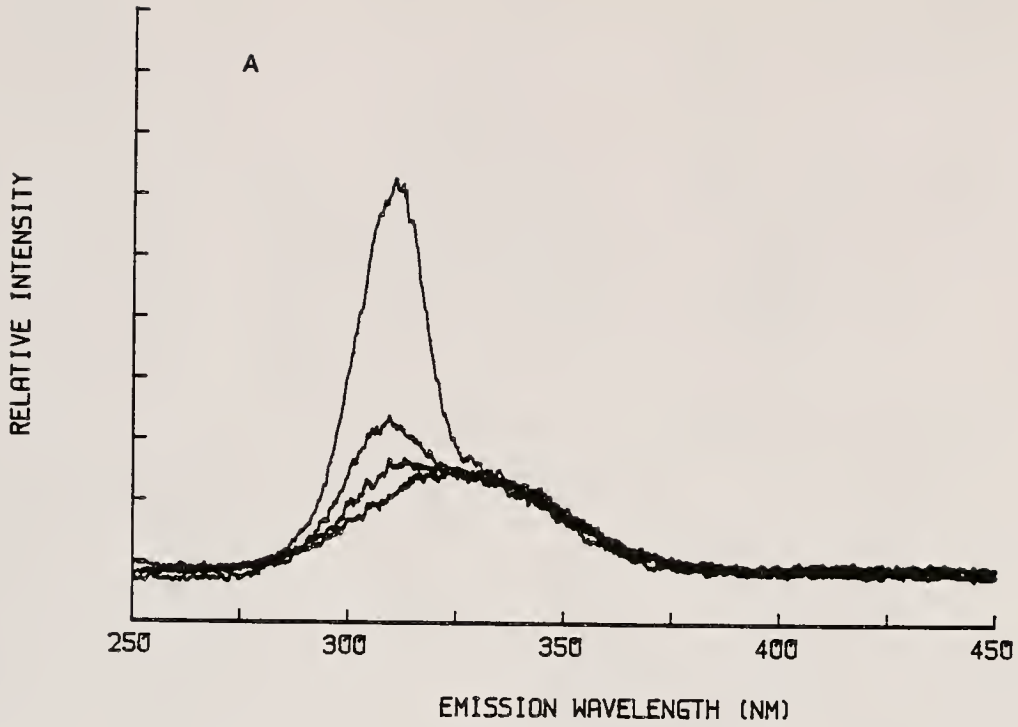
A
RELATIVE INTENSITY
250
300
350
400
450
EMISSION WAVELENGTH (NM)

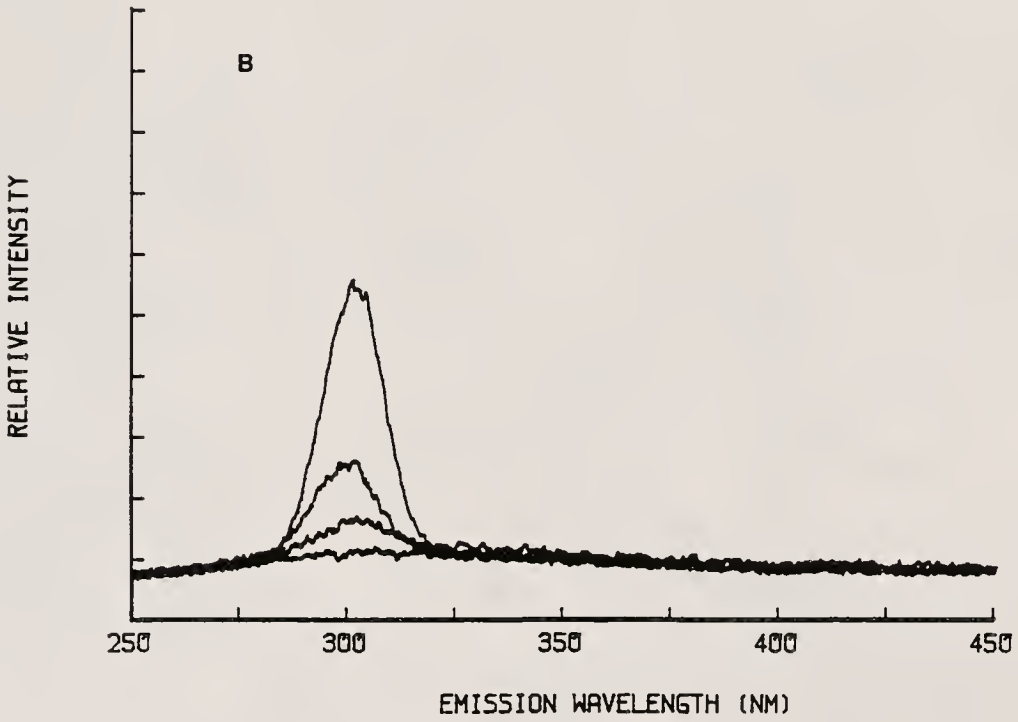
B
RELATIVE INTENSITY
250
300
350
400
450
EMISSION WAVELENGTH (NM)

Slight curvature of the blank spectrum in Figure 22B is due to the convolution of the spectral response function of the fluorimeter on the emission spectrum, as all spectra are uncorrected. Figure 23A demonstrates the effect of the emission monochromator bandpass on the blank spectrum of water obtained by CESF. An excitation monochromator bandpass of 8 nm was used with a $\Delta\bar{\upsilon}$ of 3630 K, fairly close to the Raman scatter for water at 3380 K. The upper spectrum was obtained with an emission monochromator bandpass of 8 nm, showing the convolution of the instrument response function on the $1/\lambda^4$ Raman function. This effect is reduced greatly with emission monochromator bandpasses of 4 nm and 2 nm, also plotted in Figure 23A.

Another way of reducing the Raman scatter contribution is by varying $\Delta\bar{\upsilon}$ so as not to coincide with $\Delta\bar{\upsilon}_R$. Figure 23B demonstrates the effect $\Delta\bar{\upsilon}$ has on the blank spectrum. Water was used as the blank, with bandpasses of 8 nm used for both monochromators. The top spectrum was obtained with a $\Delta\bar{\upsilon}$ equal to 3400 K, approximately equal to $\Delta\bar{\upsilon}_R$. This is the worst blank spectrum one would obtain. The middle spectrum was obtained with $\Delta\bar{\upsilon}$ equal to 4200 K, and the bottom spectrum with $\Delta\bar{\upsilon}$ equal to 5000 K. Thus, Figure 23B is best envisioned by looking at the contour plot in Figure 15. Each scan runs parallel to the Raman scatter ridge. Therefore the blank spectrum is approximately flat with a constant offset added with increasing contribution of Raman scatter in the spectral region of interest as one approaches the Raman scatter ridge.

CWSF has been used to identify impurities in spectroscopic grade solvents (71). The selection of $\Delta\lambda$ is dependent upon the solvent, the impurities, and the relative spectral positions of their emission.

Figure 23. A. Constant energy synchronous fluorescence background from water with an emission monochromator bandpass of: a. 8 nm, b. 4 nm, and c. 2 nm. The value of $\Delta\bar{\upsilon}$ used was 3630 K.

B. Constant energy synchronous fluorescence background from water as a function of $\Delta\bar{\upsilon}$. Scans correspond to: a. 3400 K, b. 4200 K, and c. 5000 K. The value of the spectral bandpass was 8 nm.

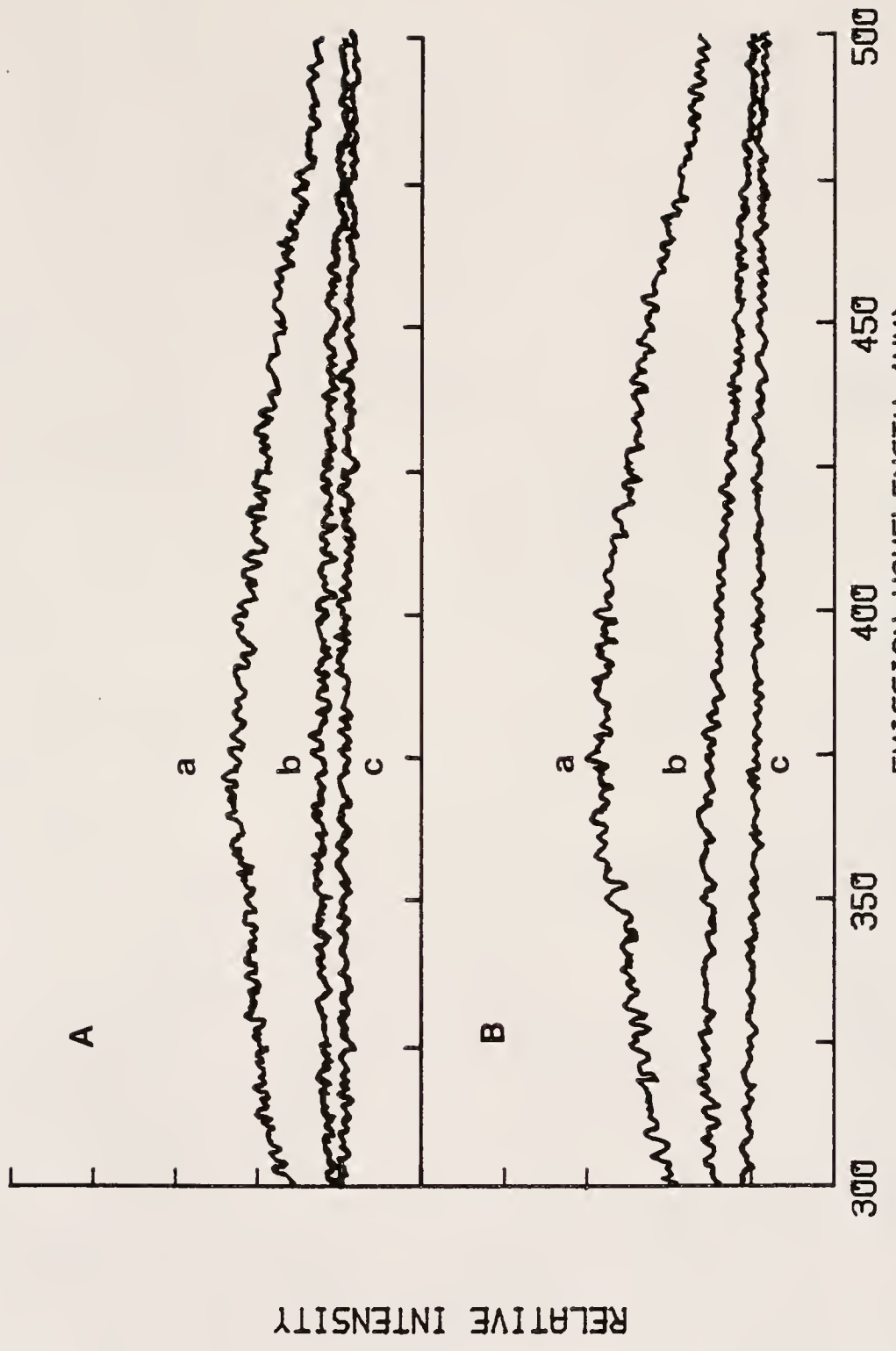
A
a
b
c
B
a
b
c
300
350
400
450
500
EMISSION WAVELENGTH (NM)
RELATIVE INTENSITY

Proper selection of $\Delta\lambda$ reduces the masking effect of the Raman scatter. CESF reduces the difficulty of parameter selection, $\Delta\bar{\upsilon}$; $\Delta\bar{\upsilon}$ is selected relative to $\Delta\bar{\upsilon}_R$, the Raman scatter due to the solvent.

Conclusions. CESF offers excellent Raman scatter interference reduction. By scanning parallel to the Raman scatter ridge, the solvent spectrum becomes featureless, reducing its contribution to the analyte fluorescence emission spectrum. This is beneficial not only for analytical determinations, but for the routine detection of solvent impurities, and the determination of the fluorescence characteristics of weakly fluorescent compounds. CESF has improved Raman scatter interference reduction in a manner similar to the improvement CWSF has made for Rayleigh scatter interference reduction. In addition, it should be stressed that the minimization of Raman scatter should also increase the linear dynamic range of calibration curves and measurement precision and therefore, reduce detection limits.

PAH Analysis

Introduction. While these results are interesting, CESL must be characterized more completely as to its application to multicomponent analysis. The same model set of PAHs used in the previous studies was investigated. The instrumentation used was the same as described, with extensive use of the database of RTF spectra. The energy concept seems logical in that most spectroscopic principles are explained in energy relationships. Wavelength approximations have provided instrumental simplification, such as the use of grating dispersing elements. Spectra plotted in energy units are theoretically more meaningful, as demonstrated in this evaluation.

Fluorescence excitation and emission spectra of PAHs are generally characterized by fairly complex vibrational features, even at room temperature. To illustrate, Figure 24A is the fluorescence excitation and emission spectra for a solution of anthracene in n-heptane. The numbers correspond to the wavelength differences between vibrational bands in nanometers, ±2 nm. If these spectra are replotted in energy units, the plots in Figure 24B are obtained. As will become apparent, energy differences between spectral features are quite important in the interpretation of synchronous spectra. The 1.4 kK (±0.2 kK) vibrational spacing is characteristic of many PAHs. The TLS spectrum of anthracene, plotted in wavelength units is shown in Figure 25. The high symmetry of this spectrum is clear. The lines drawn through the contour plot represent typical CWSF scan paths with $\Delta\lambda$'s selected to coincide with the maximum of each peak in the top row of emission peaks. The numbers at the top of the spectrum correspond to the $\Delta\lambda$'s used, in nm. Note that by optimizing each line for one peak, other peaks generally appear as weak shoulders or do not appear at all. The spectra obtained by these scans are shown in Figure 26. The main feature is a lack of spectral clarity and consistent peak separation. Replotted in energy units, the spectrum in Figure 27 represents the same anthracene solution. The lines drawn through the peaks depict the scan paths used in CESF. Note the coincidence of the lines with the peak maxima in each scan. The resultant CESF spectra are shown in Figure 28.

The values selected for the difference between monochromators, $\Delta\bar{\upsilon}$, can be traced to fluorescence theory, detailed in Chapter 1; the 0.2 kK (see Figure 27) corresponds to the approximate Stokes Shift

Figure 24. Conventional fluorescence excitation and emission spectra of 10 ng/mL anthracene in n-heptane in:

A. wavelength units, and

B. energy units,

with the numbers on the plots representing the respective differences between the vibrational bands.

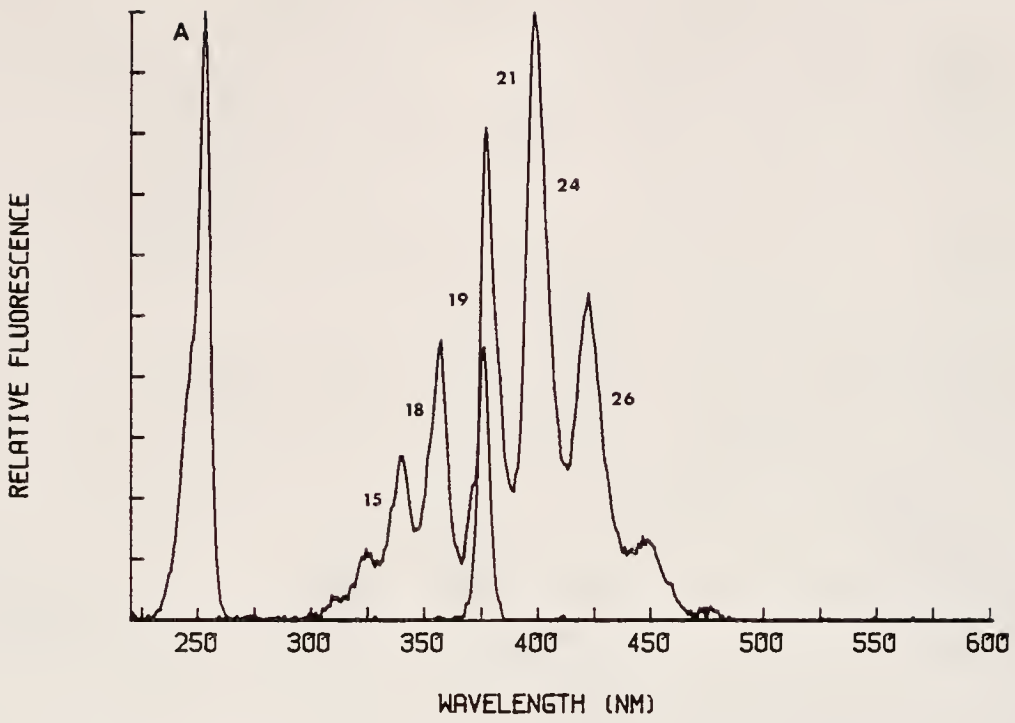
A
21
24
19
18
26
15
RELATIVE FLUORESCENCE
250
300
350
400
450
500
550
600
WAVELENGTH (NM)

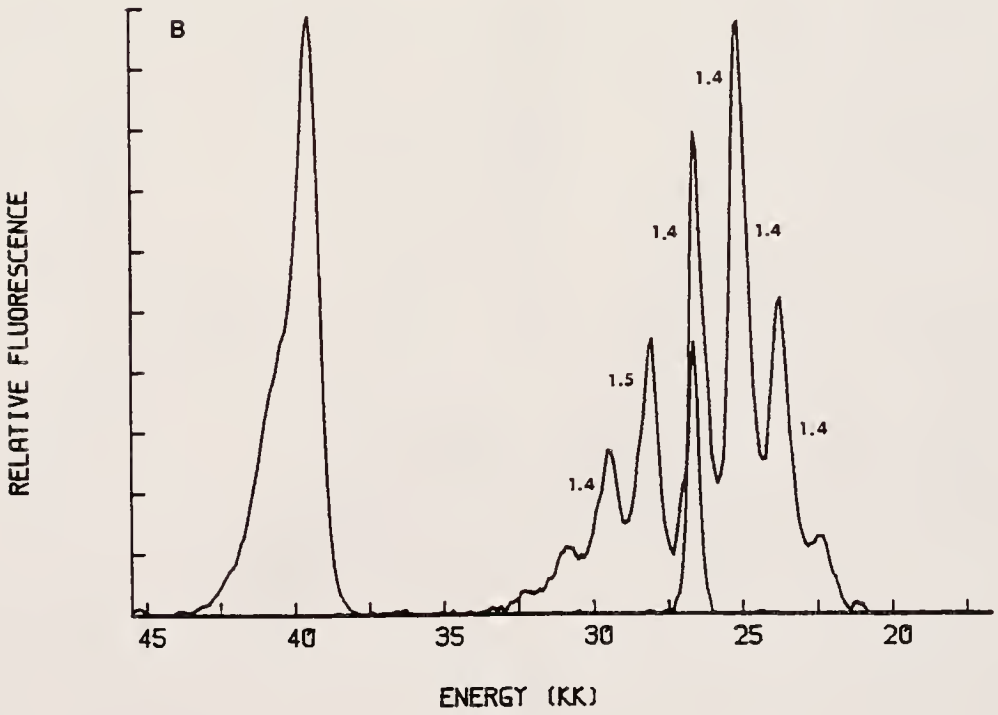
B
1.4
1.4
1.4
1.5
1.4
1.4
RELATIVE FLUORESCENCE
45
40
35
30
25
20
ENERGY (KK)

Figure 25. TLS spectrum of a 10 ng/mL anthracene in n-heptane solution. The numbers correspond to $\Delta\lambda$ values selected to obtain the scan paths drawn through the spectrum.

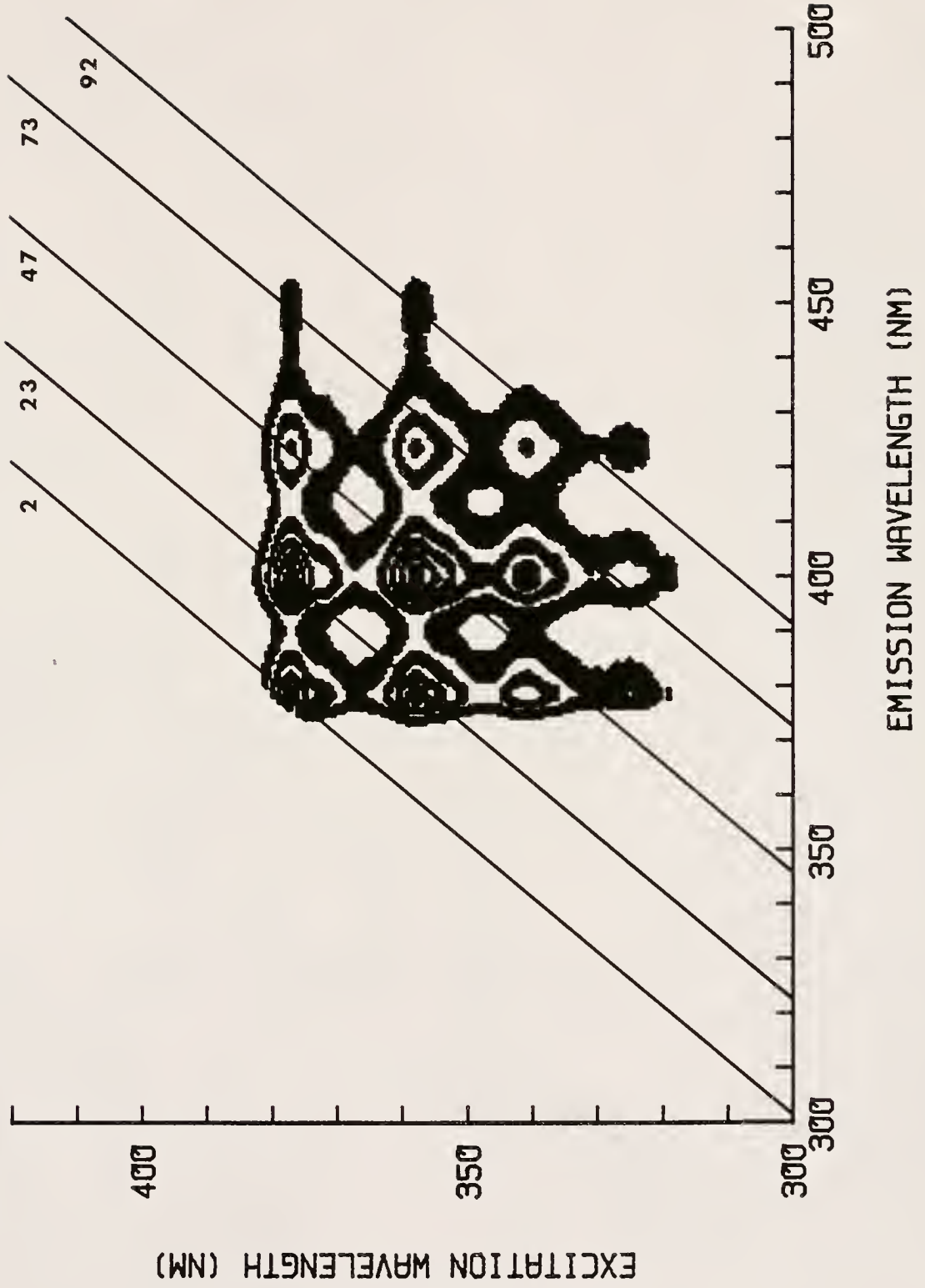
2
23
47
73
92
300
350
400
500
EMISSION WAVELENGTH (NM)
EXCITATION WAVELENGTH (NM)

Figure 26. Resultant CWSF spectra of a 10 ng/mL anthracene in n-heptane solution obtained from the scan paths depicted in Figure 25. $\Delta\lambda$ =: A. 2 nm; B. 23 nm; C. 47 nm; D. 73 nm; E. 92 nm.

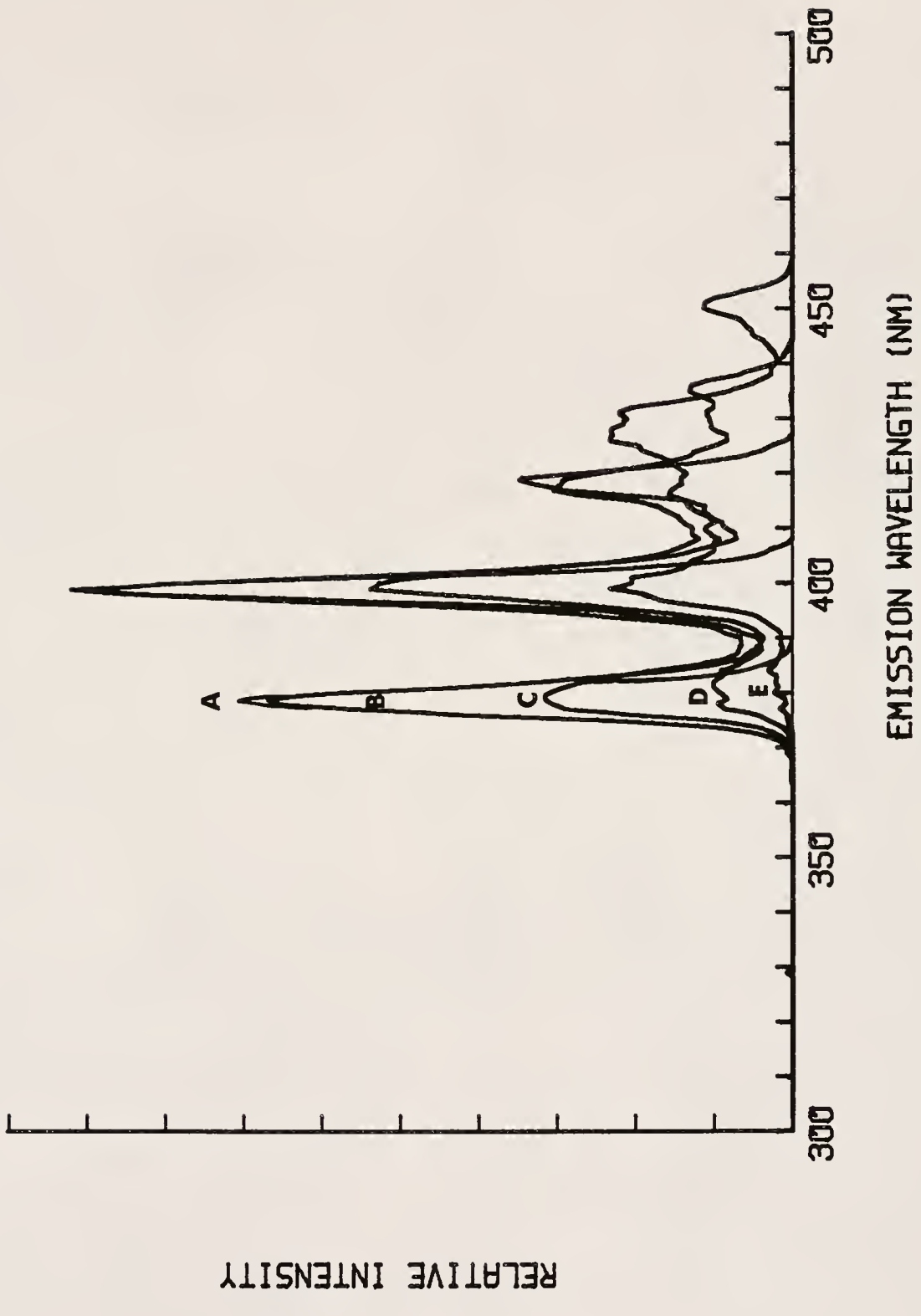
RELATIVE INTENSITY
300
350
400
450
500
EMISSION WAVELENGTH (NM)
A
B
C
D
E

Figure 27. Total fluorescence spectrum of a 10 nm/mL anthracene in n-heptane solution, plotted in energy units. The numbers correspond to $\Delta\bar{\upsilon}$ values selected to obtain the scan paths drawn through the spectrum, in kK.

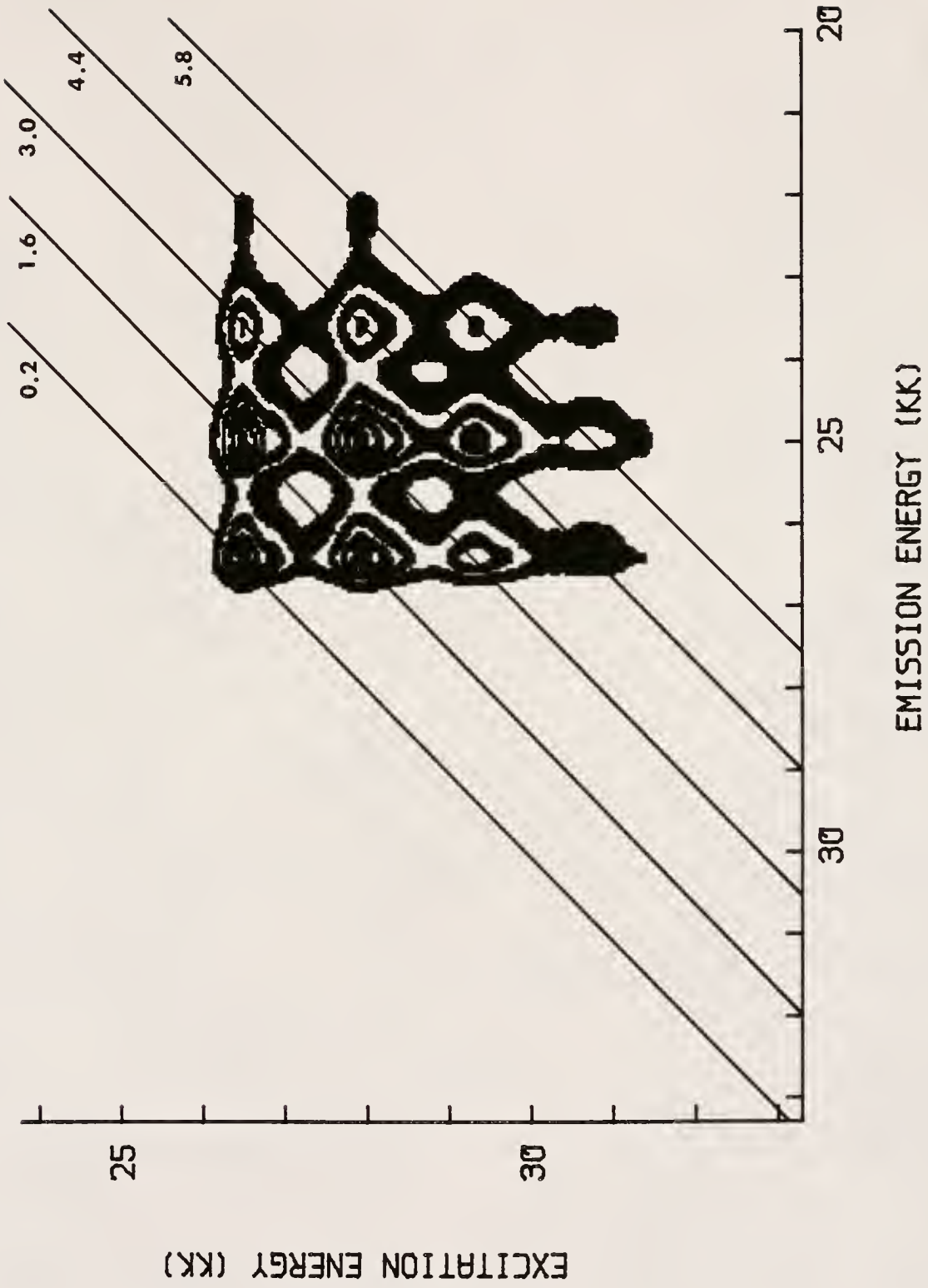
0.2
1.6
3.0
4.4
5.8
20
25
30
EMISSION ENERGY (KK)
25
30
EXCITATION ENERGY (KK)

Figure 28. Resultant CESF spectra of a 10 ng/mL anthracene in n-heptane solution obtained from the scan paths depicted in Figure 27. $\Delta\bar{\upsilon}$ =: A. 0.2 kK; B. 1.6 kK; C. 3.0 kK; D. 4.4 kK; E. 5.8 kK.

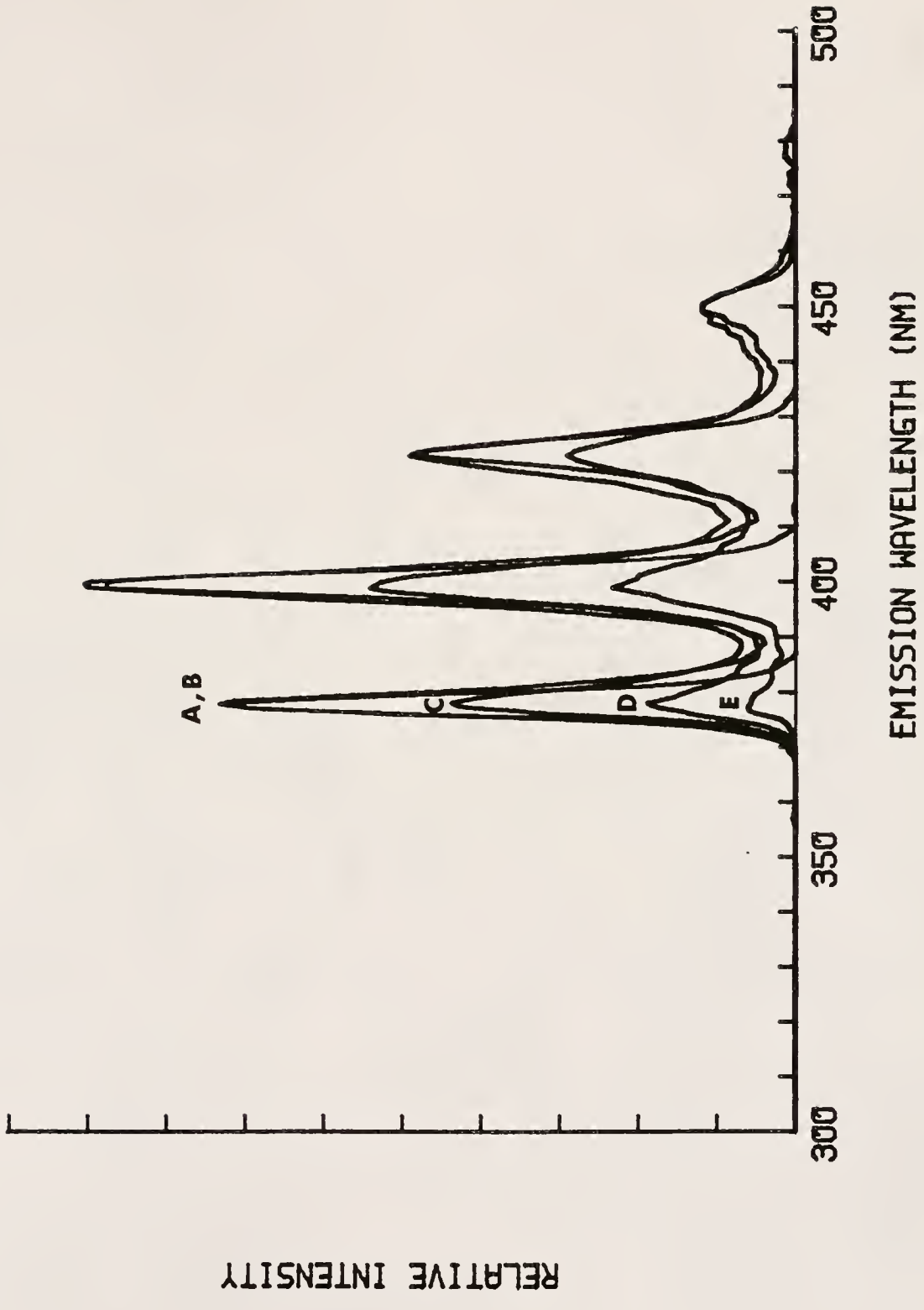
RELATIVE INTENSITY
300
350
400
450
500
EMISSION WAVELENGTH (NM)
A,B
C
D
E

observed for PAHs in n-alkane solvents, as shown in the anthracene example. The 1.4 kK separation agrees with the vibrational energy differences expected for PAHs. Using CWSF, these energy differences have been approximated by $\Delta\lambda$'s of 3, 20, and 34 nm. The selection of $\Delta\lambda$ generally involves calculating the difference between the maxima in the fluorescence excitation and emission spectra. A different $\Delta\lambda$ must be selected for each compound of interest. For molecules exhibiting a strong 0-0 excitation transition, the use of a $\Delta\lambda$ of 3 nm is a good approximation to the Stokes Shift, and multicomponent analysis is possible. However, many PAHs do not exhibit a strong 0-0 excitation transition in alkane solutions at room temperature. Thus, a $\Delta\lambda$ of 20 to 30 nm is recommended (58). Using larger $\Delta\lambda$'s makes CWSF spectra prohibitively difficult to interpret. Also the use of a small $\Delta\lambda$ can be instrumentally limited if larger bandpasses are needed for increased throughput. As the bandpasses of both monochromators increasingly overlap, Rayleigh scatter becomes a significant problem.

To extend CESF to other compounds, several PAHs were studied to optimize $\Delta\bar{\upsilon}$. Table 8 includes the results from this study. The fluorescence excitation and emission spectra from the database were used. The wavelengths listed are selected maxima corresponding to vibrational levels for $S_0 \rightarrow S_1$ absorption or for low energy $S_0 \rightarrow S_2$ absorption (see Chapter 4), and $S_1 \rightarrow S_0$ emission only. General absorption processes of $S_0 \rightarrow S_n$ will be discussed later. Each number in the table corresponds to the energy difference between each pair of wavelengths where a peak would appear in the TLS plot. Each wavelength is $\pm$1 nm and therefore, each $\Delta\bar{\upsilon}$ is $\pm$0.2 kK. It is readily

Table 8. Energy Differences Between Excitation and Emission Wavelengths, in kK, for Several PAHs in n-Heptane (± 0.2 kK)

Compound	Wavelengths (nm)	Number of Vibrational Units Between Excitation and Emission Wavelengths						
		0	1	2	3	4	5	6
Anthracene	324,339,357,376[a]	0.1	1.5	3.0	4.3			
	378,399,423,449[b]		1.6	2.9	4.4	5.7		
				3.0	4.4	5.9	7.2	
					4.4	5.8	7.2	8.6
Perylene	386,407,435	0.2	1.5	3.0				
	438,466,500		1.7	3.1	4.6			
				3.1	4.4	5.9		
Naphthacene	395,413,439,468	0.3	1.6	2.8				
	472,507,539		1.6	3.1	4.2			
				3.0	4.5	5.7		
					4.1	5.6	6.8	
9-Methyl-anthracene	332,348,365,386	0.1	1.6	3.0	4.3			
	388,411,436,463		1.6	3.1	4.5	5.8		
				3.0	4.4	5.8	7.1	
					4.3	5.8	7.2	8.5
Pyrene	309,320,335			3.1	3.8 4.5			
	374,385,395				4.5	5.3 5.9		
						5.6	6.4 7.0	
1,2-Benzo-pyrene	305,317,331				4.5	5.1 5.8		
	389,398,410					5.8	6.4 7.2	
							7.1	7.7 8.4
3,4-Benzo-pyrene	346,364,383		1.4	2.7	4.1			
	404,428,455			2.7	4.1	5.5		
					4.1	5.5	6.9	
Chrysene	294,306,320				3.7	5.1	6.4	
	363,382,403					5.1	6.5	7.9
							6.5	7.8 9.2

Table 8-continued

1-Methylpyrene	312,326,343					2.6		4.0	5.1				
	377,397,416							4.1		5.5	6.6		
										5.5		6.9	8.0
2,3-Benzo-	303,316,325,341	0.1	0.8	1.5									
fluorene	342,351,359			1.5	2.3	2.9							
					2.4	3.2	3.8						
							3.8	4.5	5.1				
Anthanthrene	383,399,405,421,	0.1		1.5		2.9							
	429		0.6		1.9		3.3						
	431,458,489			1.5		2.9		4.2					
					1.9		3.2		4.6				
						2.9		4.3		5.7			
Acenaphthene	288,300,320	0.2	0.9	1.7		3.2							
	322,329,338,356				2.3	2.9	3.7		5.2				
							3.7	4.3	5.1		6.6		
1,2-Benz-	325,340,358				2.0		3.4		4.8				
anthracene	386,408,433						3.5		4.9		6.3		
									4.9		6.3		7.7
9,10-Diphenyl-	352,373,392		0.9		2.1								
anthracene	407,428				2.2		3.4						
							3.8		5.0				

[a] $S_0 \rightarrow S_1$ or $S_0 \rightarrow S_2$ excitation wavelengths

[b] $S_1 \rightarrow S_0$ emission wavelengths

apparent that the $\Delta\bar{\upsilon}$'s fall into a small, evenly-spaced set of values. It can be noted that anthracene represents an excellent model system for CESF.

Ternary Mixture. The conclusions drawn from this table were then applied to a ternary mixture of PAHs, anthracene, perylene, and naphthacene. Figure 29 shows the TLS spectrum obtained. While this represents a simple mixture, several important observations can be made. CWSF lines are shown in Figure 29 and demonstrate the difficulty in $\Delta\lambda$ selection. The CESF scan paths are shown in Figure 30 on the same contour plot. The $\Delta\bar{\upsilon}$'s used for anthracene are also quite appropriate for perylene and naphthacene in this mixture. If a $\Delta\lambda$ of 3 nm is used in CWSF and a $\Delta\bar{\upsilon}$ of 0.2 kK is used in CESF, similar spectra are obtained. However, for those PAHs that do not exhibit a strong 0-0 absorption transition, it is necessary to increase the wavelength separation by one vibrational unit. Figure 31A shows the spectrum for each compound in the ternary mixture using CWSF at a $\Delta\lambda$ of 20 nm. Figure 31B shows the spectra for the same compounds using a $\Delta\lambda$ of 34 nm. These can be compared to the CESF spectrum using a $\Delta\bar{\upsilon}$ of 1.6 kK (Figure 32A). A $\Delta\lambda$ of 20 nm appears optimal for anthracene, while 34 nm appears optimal for perylene and naphthacene. It is apparent that 20 and 34 nm are approximations for 1.6 kK in each respective spectral region. Figure 32B shows the CESF spectra obtained for the same compounds using a $\Delta\bar{\upsilon}$ of 3.0 kK.

Comparisons of CESF spectra of 0.2, 1.6, and 3.0 kK $\Delta\bar{\upsilon}$'s also demonstrate other interesting features. 2,3-Benzofluorene will be used for illustration. Figure 33A shows the fluorescence emission spectrum for this compound. The use of $\Delta\bar{\upsilon}$'s of 0.2, 1.6, and 3.0 kK (Figures 33-

Figure 29. Total fluorescence spectrum of anthracene, perylene, and naphthacene in n-heptane. The numbers correspond to $\Delta\lambda$ values selected to obtain the CWSF scan paths drawn through the spectrum. A = Anthracene, P = Perylene, N= Naphthacene.

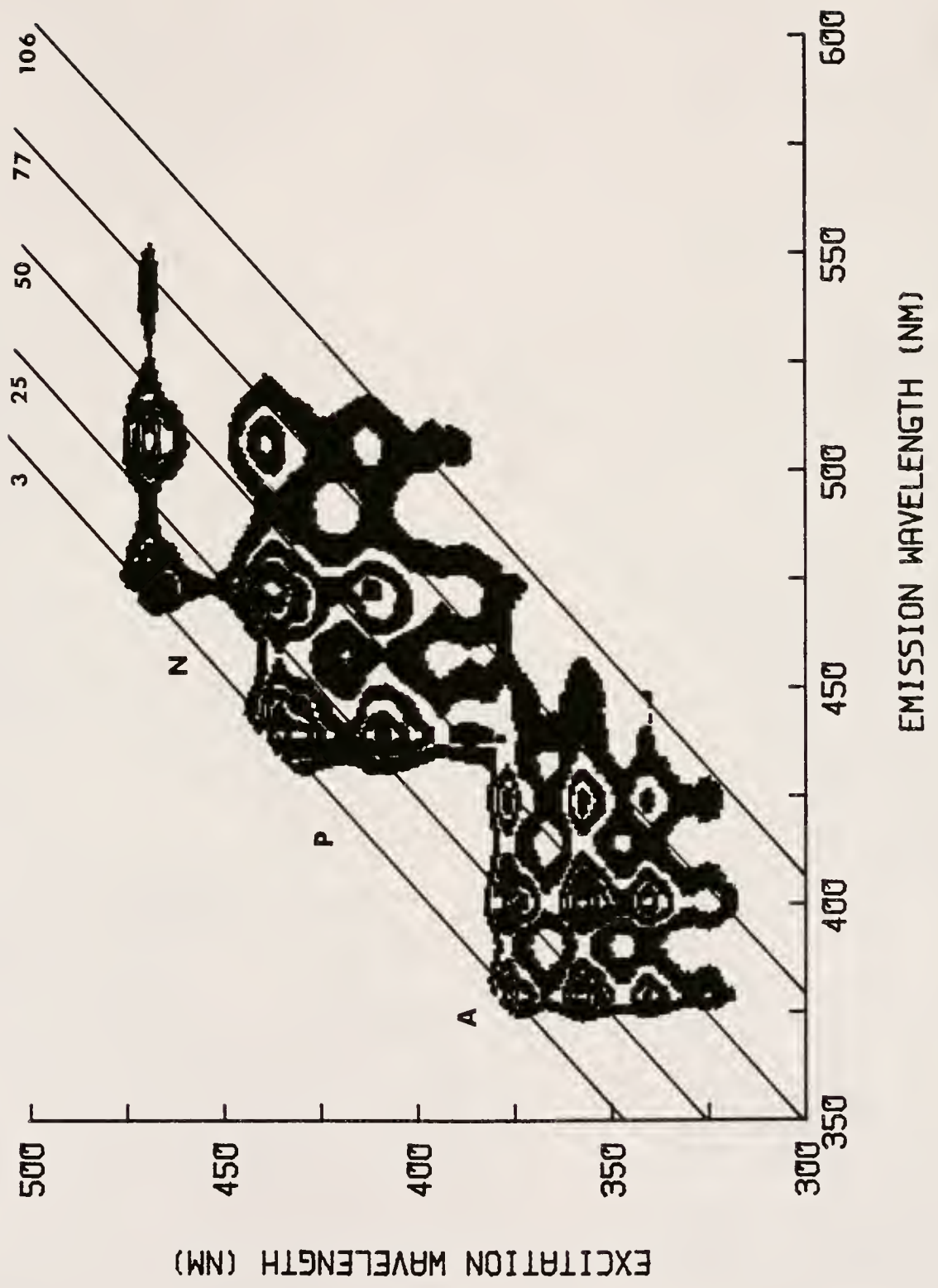
3
25
50
77
106
N
P
A
500
450
400
350
300
350
400
450
500
550
600
EXCITATION WAVELENGTH (NM)
EMISSION WAVELENGTH (NM)

Figure 30. Total fluorescence spectrum of anthracene, perylene, and napthacene in n-heptane. The numbers correspond to $\Delta\upsilon$ values selected to obtain the CESF scan paths drawn through the spectrum.

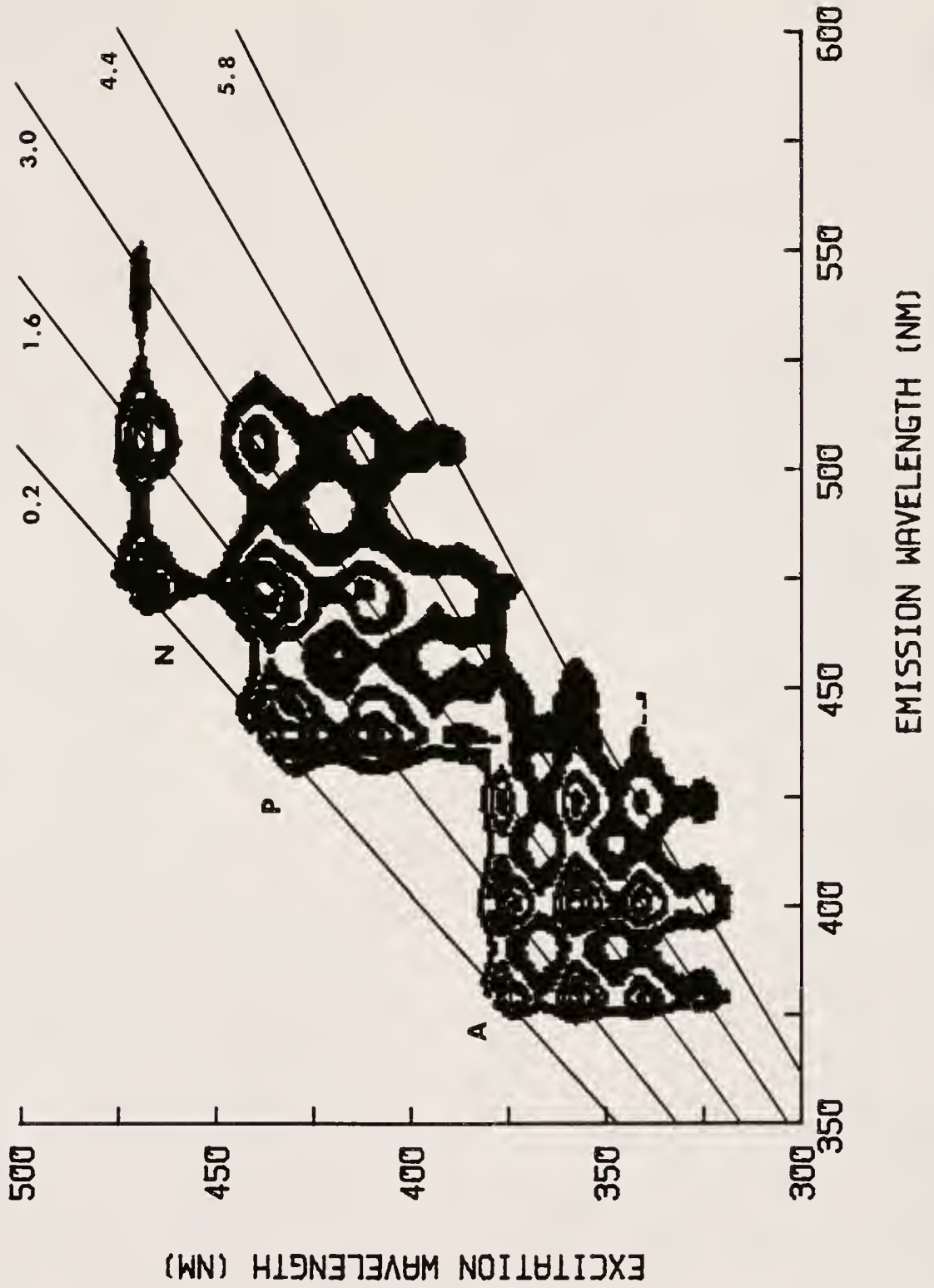
0.2
1.6
3.0
4.4
5.8
N
P
A
500
450
400
350
300
350
400
450
500
550
600
EXCITATION WAVELENGTH (NM)
EMISSION WAVELENGTH (NM)

Figure 31. A. CWSF spectra for anthracene (A), perylene (P), and naphthacene (N) using a $\Delta\lambda$ of 20 nm. The relative intensity scale represents the intensity relative to the maximum intensity in the total fluorescence spectrum for each compound, with the maximum equivalent to full-scale.

B. CWSF spectra for anthracene, perylene, and naphthacene using a $\Delta\lambda$ of 34 nm.

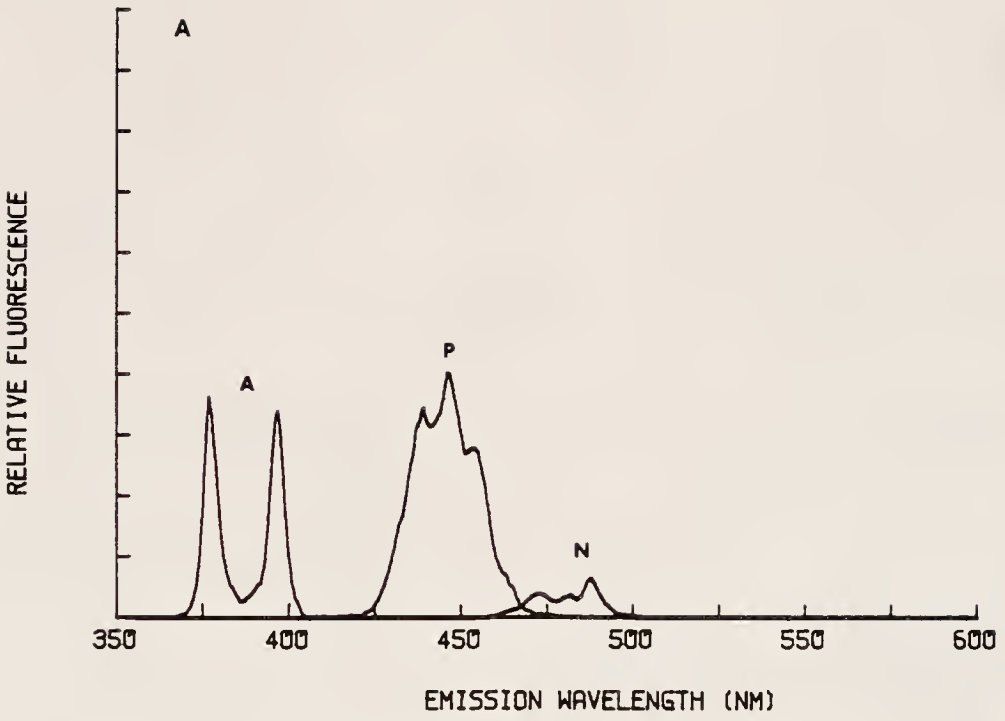
A
A
P
N
RELATIVE FLUORESCENCE
350
400
450
500
550
600
EMISSION WAVELENGTH (NM)

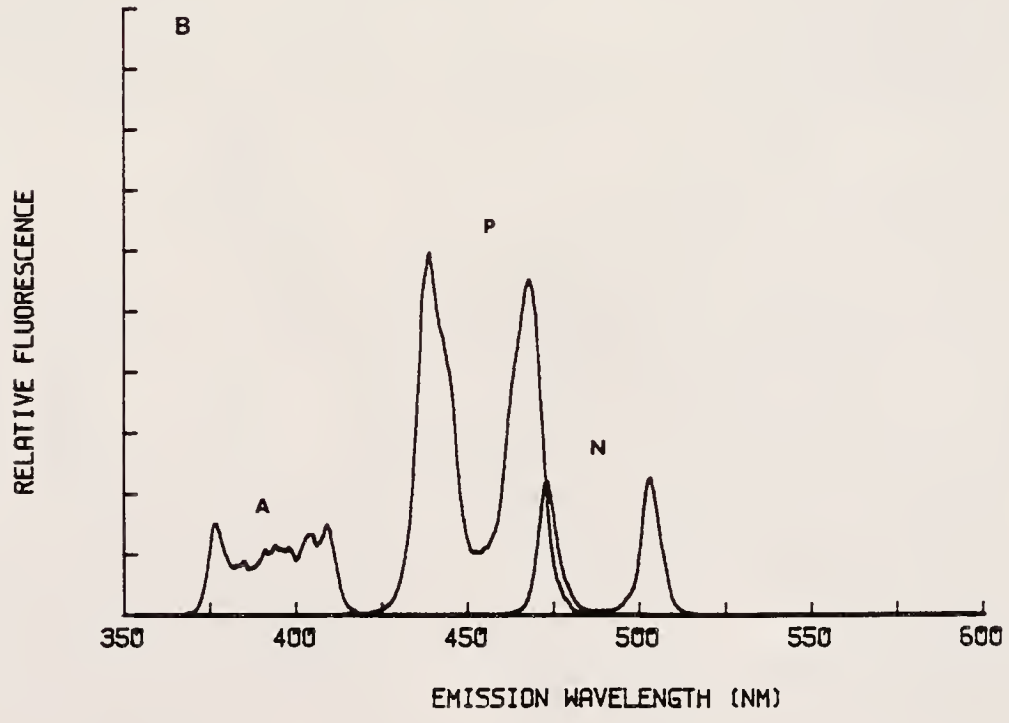
B
P
N
A
RELATIVE FLUORESCENCE
350
400
450
500
550
600
EMISSION WAVELENGTH (NM)

Figure 32. CESF spectra for anthracene, perylene, and naphthacene in n-heptane using a $\Delta\bar{\upsilon}$ of:

A. 1.6 kK

B. 3.0 kK

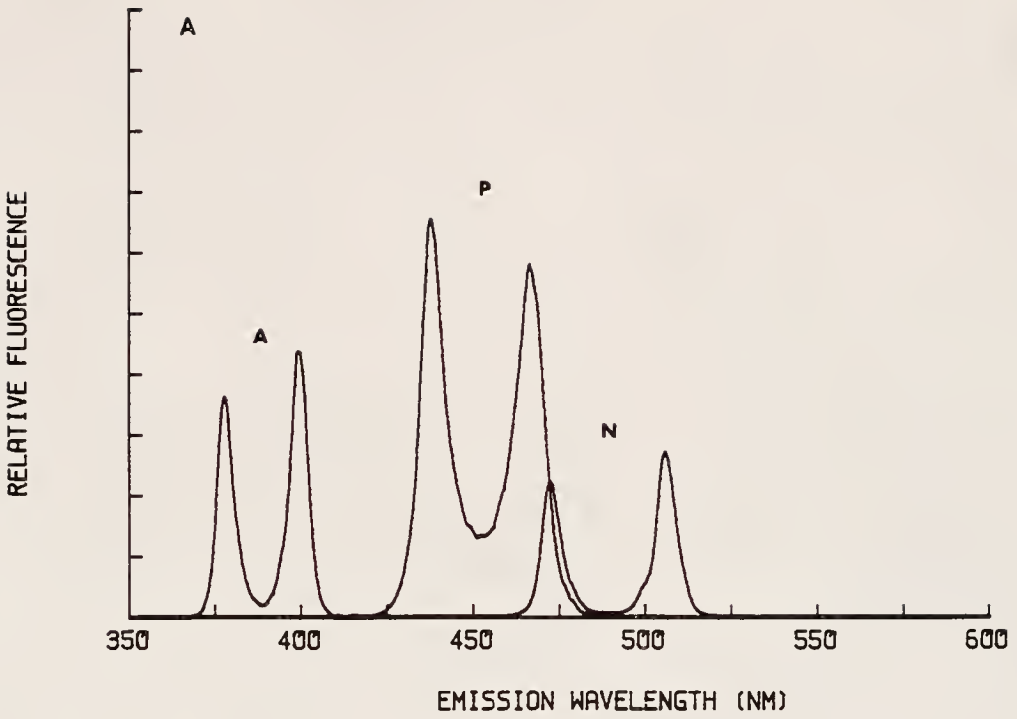
A
P
A
N
RELATIVE FLUORESCENCE
350
400
450
500
550
600
EMISSION WAVELENGTH (NM)

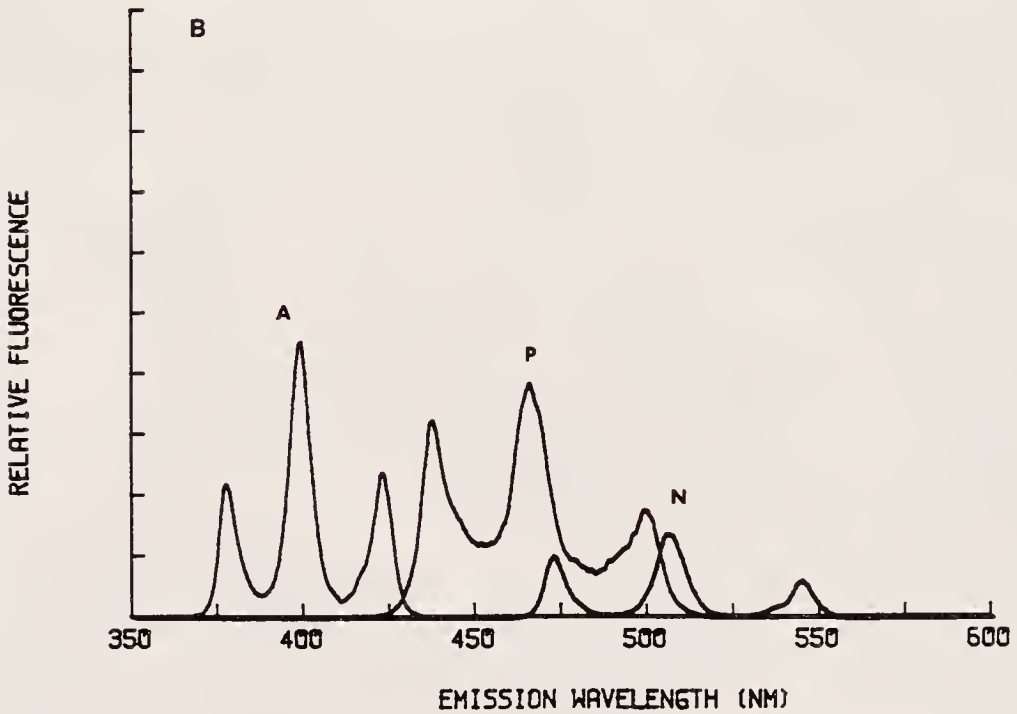
B
A
P
N
RELATIVE FLUORESCENCE
350
400
450
500
550
600
EMISSION WAVELENGTH (NM)

Figure 33. A. Conventional fluorescence emission spectrum of 2,3-benzofluerene in n-heptane.
λ_{ex} = 316 nm

B. CESF spectrum of 2,3-benzofluorene in n-heptane.
$\Delta\bar{\upsilon}$ = 0.2 kK

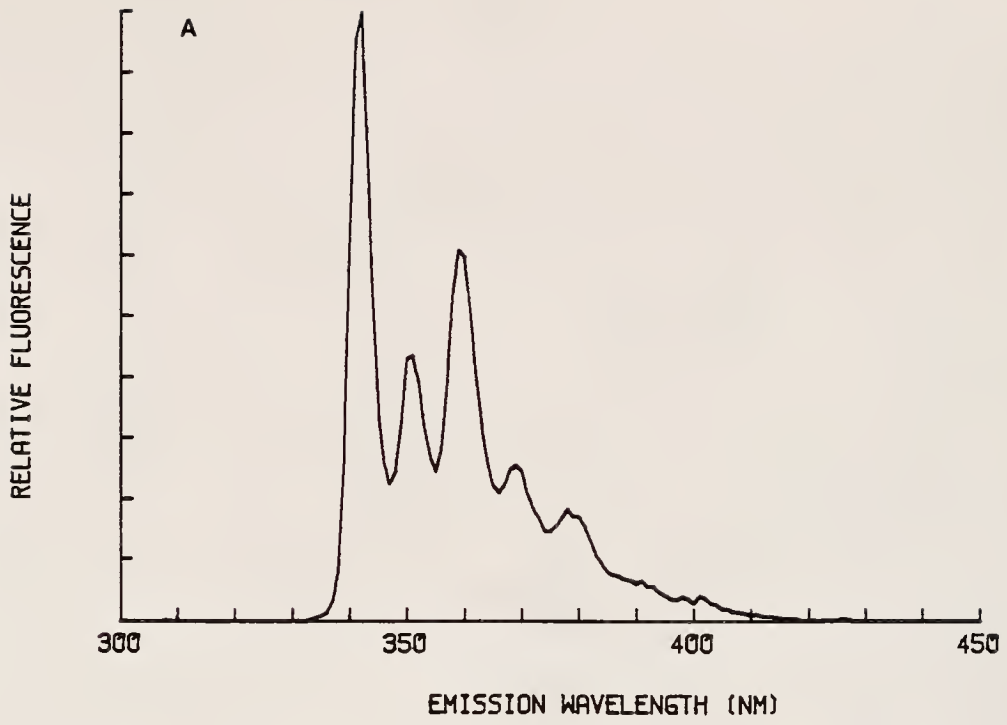
A
RELATIVE FLUORESCENCE
300
350
400
450
EMISSION WAVELENGTH (NM)

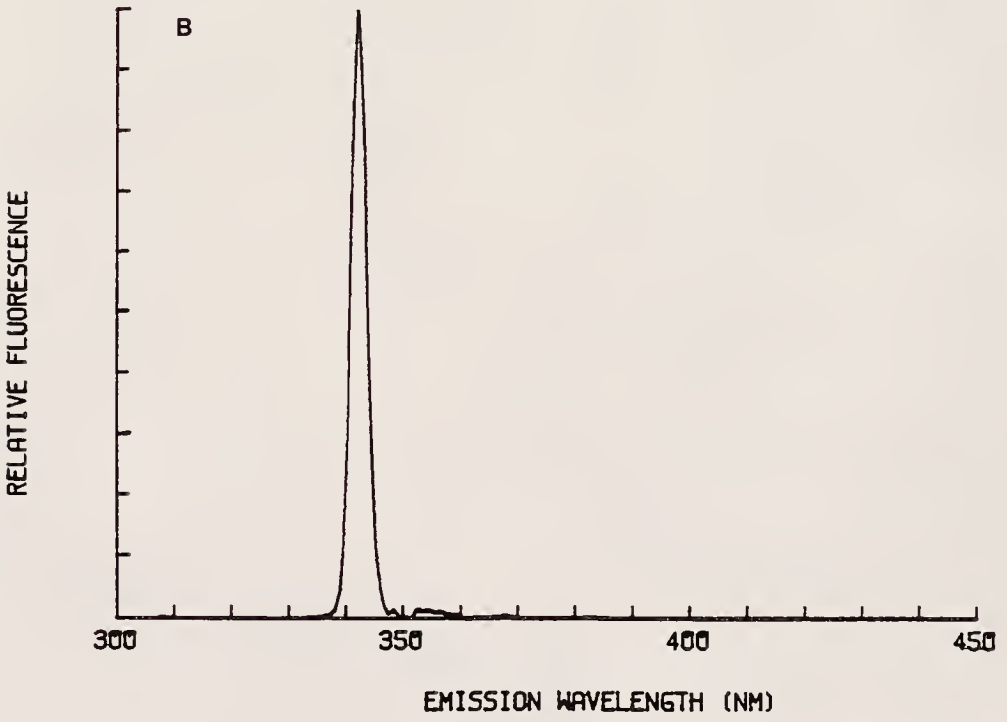
B
RELATIVE FLUORESCENCE
300
350
400
450
EMISSION WAVELENGTH (NM)

Figure 34. CESF spectrum of 2,3-benzofluorene in n-heptane for $\Delta\bar{\upsilon}$ =:

A. 1.6 kK

B. 3.0 kK

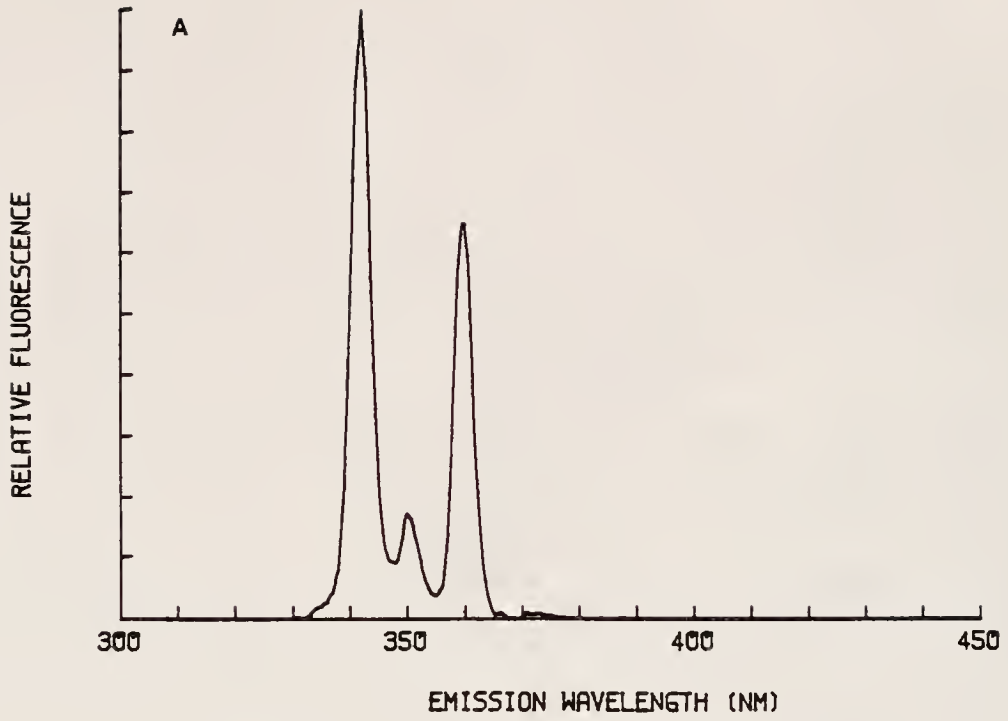
A
RELATIVE FLUORESCENCE
300
350
400
450
EMISSION WAVELENGTH (NM)

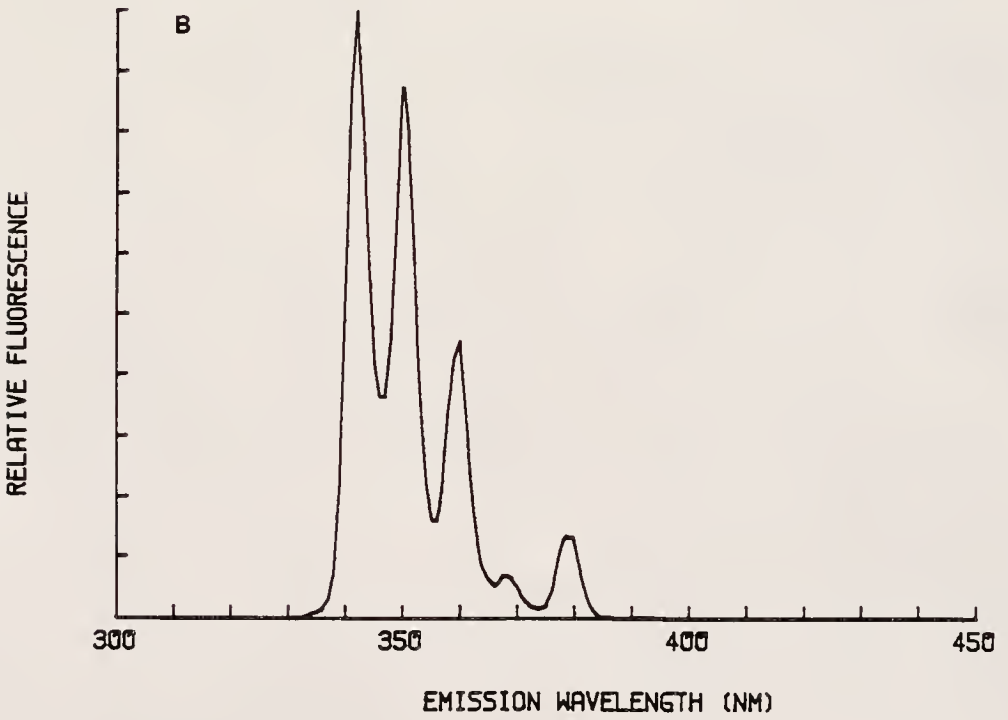
B
RELATIVE FLUORESCENCE
300
350
400
450
EMISSION WAVELENGTH (NM)

34) show increasing spectral complexity with increasing $\Delta\bar{\upsilon}$, with spectral features matching those of the fluorescence emission spectrum. Thus the degree of complexity of the CESF spectrum can be selected as necessary. Effectively, the CESF spectrum resembles a projection of the fluorescence emission spectrum onto the curved path through the TLS plane. The relative peak intensities vary, depending on the relative intensities of both the excitation and emission spectral contributions.

Complex Mixture. To evaluate the applicability of CESF to a more complex mixture, an analysis of a 20-component mixture was completed. The compounds and their concentrations are listed in Table 9. The concentrations were selected to give approximately the same signal level at the wavelength combination of most intense fluorescence for each compound. This investigation was performed in two stages. A qualitative analysis was completed using a synthetic mixture at the concentrations listed. A quantitative analysis was completed using a computer simulation of this mixture. Each was done for specific purposes and will be described in detail.

By selecting this mixture with the concentrations listed, it is not suggested that such a mixture would ever be encountered or that fluorimetry would necessarily be the technique of choice in such a case. Rather, the purpose was to evaluate the probability that sufficient signal is measurable using the instrumental parameters selected and the difficulty in discriminating between the contributions from each component. That is, even though a compound exhibits intense fluorescence at its maximum, selection of a scan mode may be spectrally blind to the contribution by this compound.

Table 9. Twenty-Component PAH Mixture Compounds and Their Concentrations

Compound	Concentration (μg/mL)
1,2-Benzopyrene	0.410
Anthracene	0.0403
Pyrene	0.406
1,2-Benzofluorene	0.414
2,3-Benzofluorene	0.0406
Perylene	0.00808
1,2:5,6-Dibenzanthracene	0.0405
3,4-Benzopyrene	0.0368
Chrysene	0.424
Phenanthrene	0.829
1,2:3,4-Dibenzanthracene	0.362
2-Methylanthracene	0.0411
9-Methylanthracene	0.0427
1,2-Benzanthracene	0.478
1-Methylpyrene	0.467
Naphthacene	0.0800
Fluorene	0.0400
9,10-Dimethylanthracene	0.0418
Acenaphthene	0.394
Anthanthrene	0.00560

The TLS spectra for this mixture are plotted in Figure 35. The top spectrum represents a 10-fold decrease in amplifier gain over the bottom spectrum. In an attempt to make this analysis as realistic as possible, no data manipulation was used and all measurements are plotted directly as the current measured from the PMT. These spectra graphically support a major premise of this work: TLS spectra contain an abundance of information, but this information is difficult to use directly without the aid of procedures to simplify and classify the data.

Using conventional fluorescence spectroscopy, four excitation wavelengths were selected for this comparison. Wavelengths of 254, 290, 340, and 375 nm were selected because of their recommended use in the literature for fluorimetric oil analysis (72). The spectra obtained are shown in Figures 36 and 37. The peaks due to Rayleigh scatter have been labeled. The CWSF spectra for $\Delta\lambda$'s of 3, 7, 20, and 34 nm are shown in Figures 38 and 39. These values were selected as previously described, with 7 nm added due to specific selection by Lloyd et al. (73). The CESF spectra for $\Delta\bar{\upsilon}$'s of 0.2, 1.6, 3.0, and 4.4 kK are shown in Figures 40 and 41.

Several comparisons can be made between the CWSF and CESF spectra. The 3 nm and 0.2 kK spectra are nearly identical. Under low resolution, small energy differences can be successfully approximated with wavelength units. An interesting comparison can be made between the 20 nm, 34 nm, and 1.6 kK spectra. The spectral features at the low end of the 1.6 kK spectrum fairly closely match those of the 20 nm spectrum over the same spectral region. Another similarity can be seen at the long wavelength end of the 1.6 kK spectrum and the 34 nm spectrum. This graphically confirms the energy-wavelength conclusions drawn from the simple ternary mixture analysis.

Figure 35. TLS spectra for 20-component PAH mixture, with the amplifier gain of B 10X the gain of A.

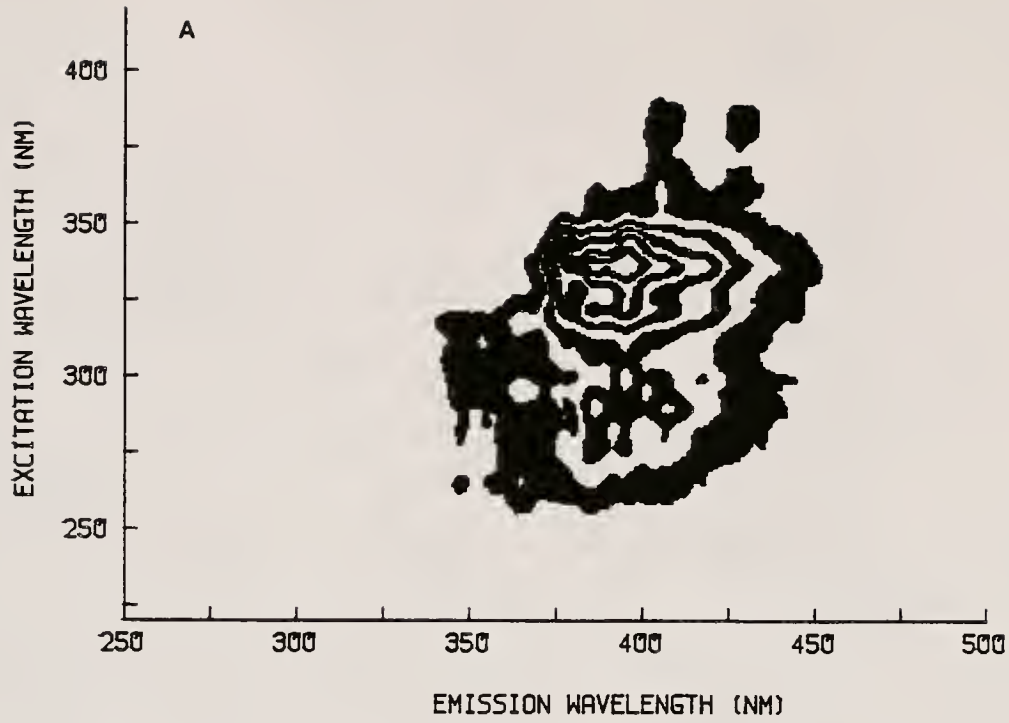
A
400
350
300
250
EXCITATION WAVELENGTH (NM)
250
300
350
400
450
500
EMISSION WAVELENGTH (NM)

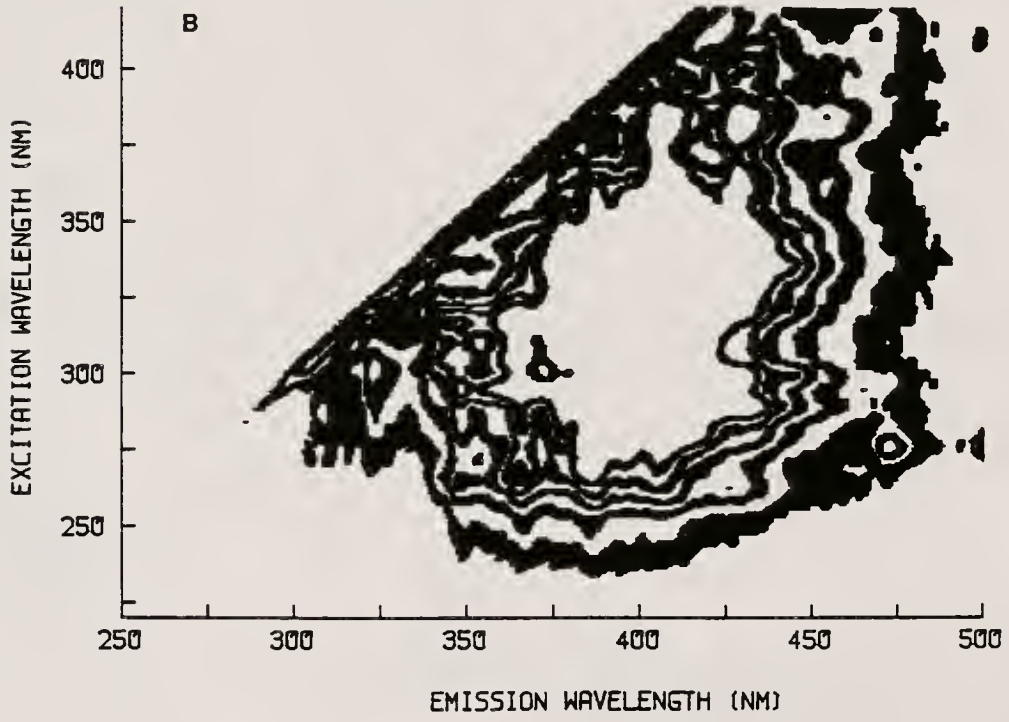
B
400
350
300
250
EXCITATION WAVELENGTH (NM)
250
300
350
400
450
500
EMISSION WAVELENGTH (NM)

Figure 36. Conventional fluorescence emission spectra of 20-component PAH mixture in n-heptane, for λ_{ex}=

A. 254 nm

B. 290 nm

Ry indicates the position of Rayleigh scatter and ÷10 indicates a tenfold reduction in amplifier gain.

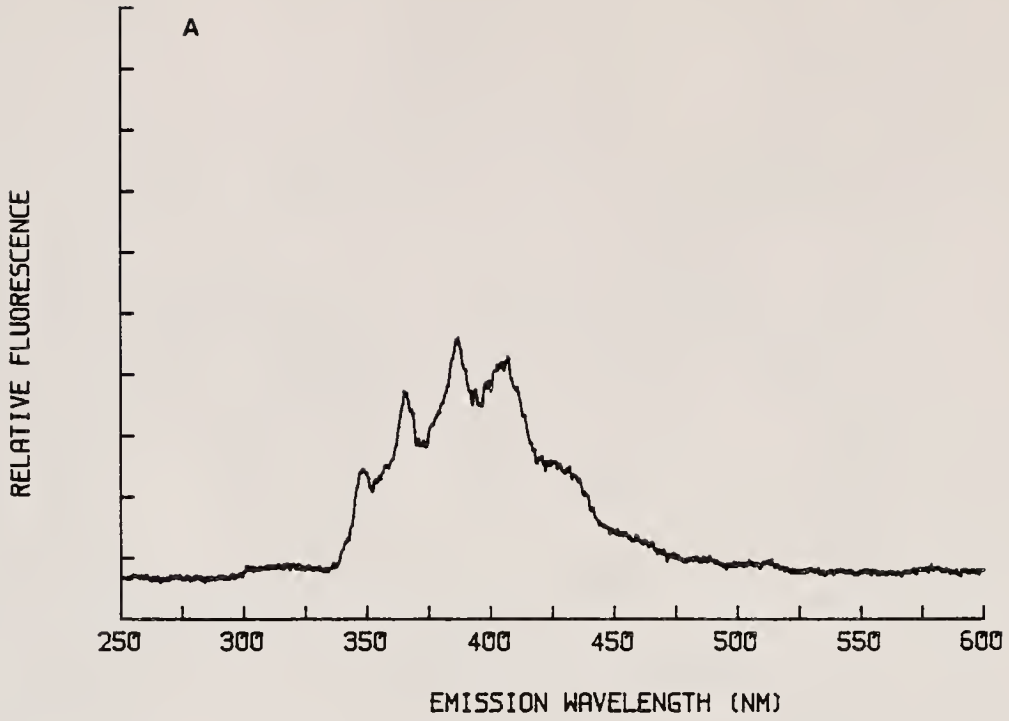
A
RELATIVE FLUORESCENCE
250
300
350
400
450
500
550
600
EMISSION WAVELENGTH (NM)

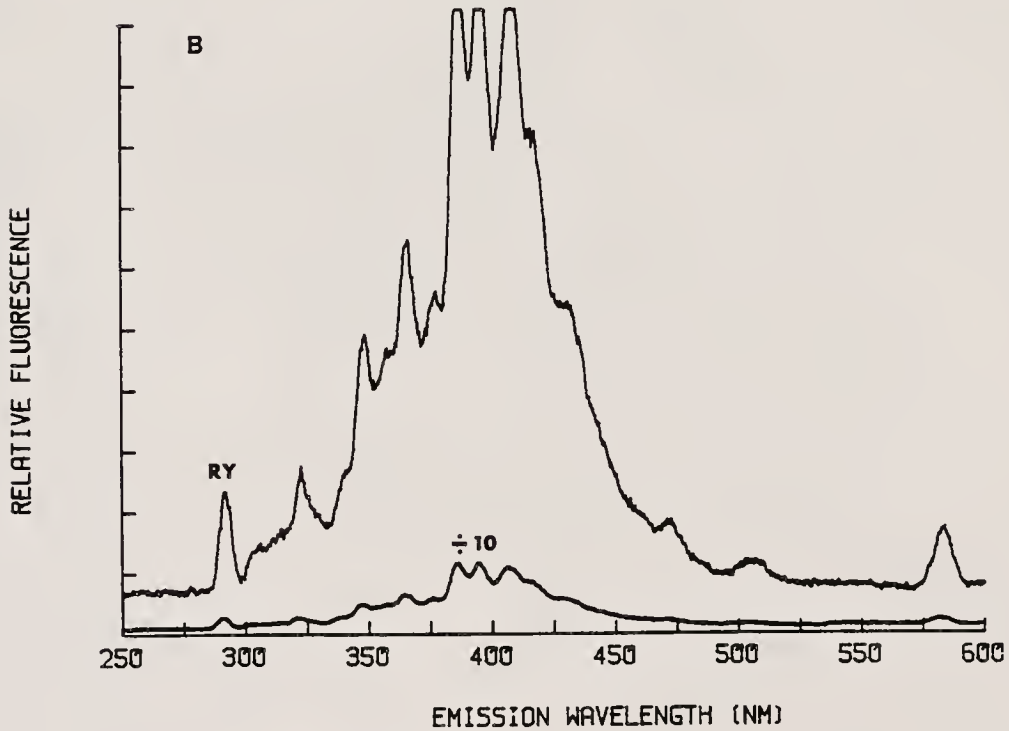
B
RY
÷10
RELATIVE FLUORESCENCE
250
300
350
400
450
500
550
600
EMISSION WAVELENGTH (NM)

Figure 37. Conventional fluorescence emission spectra of 20-component PAH mixture in n-heptane, for λ_{ex}=

A. 340 nm

B. 375 nm

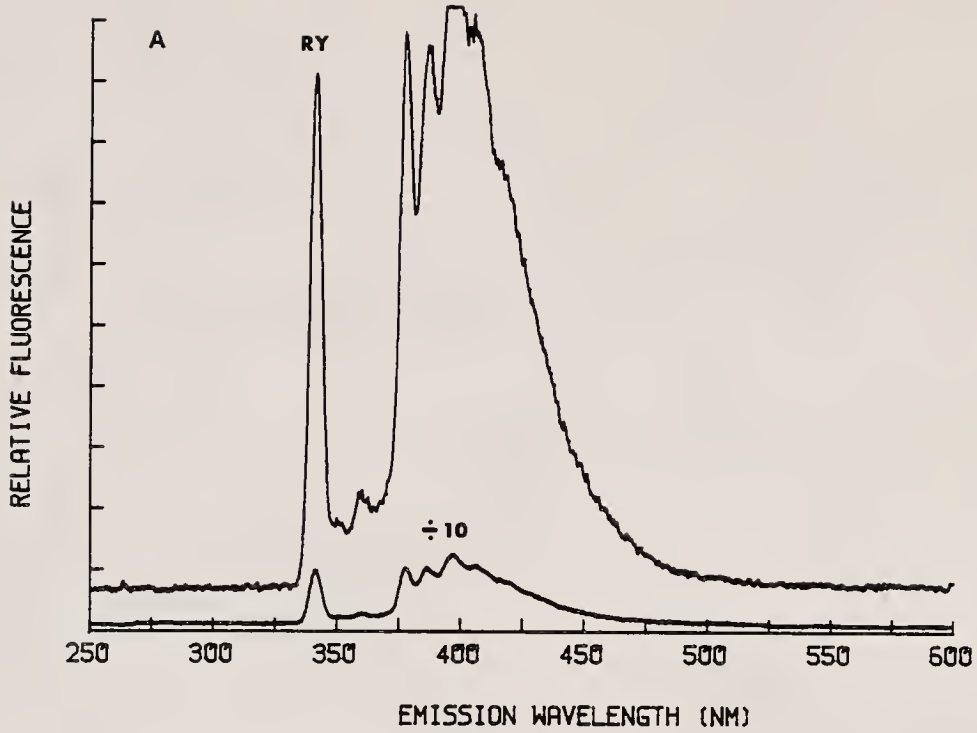
A
RY
÷10
RELATIVE FLUORESCENCE
250
300
350
400
450
500
550
600
EMISSION WAVELENGTH (NM)

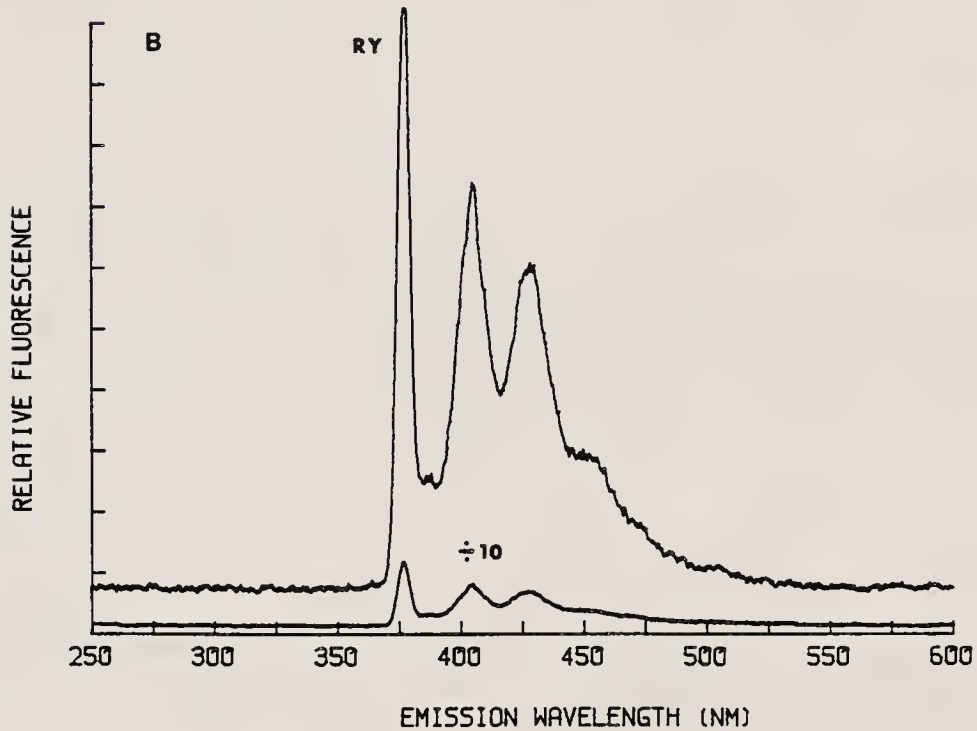
B
RY
÷10
RELATIVE FLUORESCENCE
250
300
350
400
450
500
550
600
EMISSION WAVELENGTH (NM)

Figure 38. CWSF spectra of 20-component PAH mixture in n-heptane, for $\Delta\lambda$=

A. 3 nm

B. 7 nm

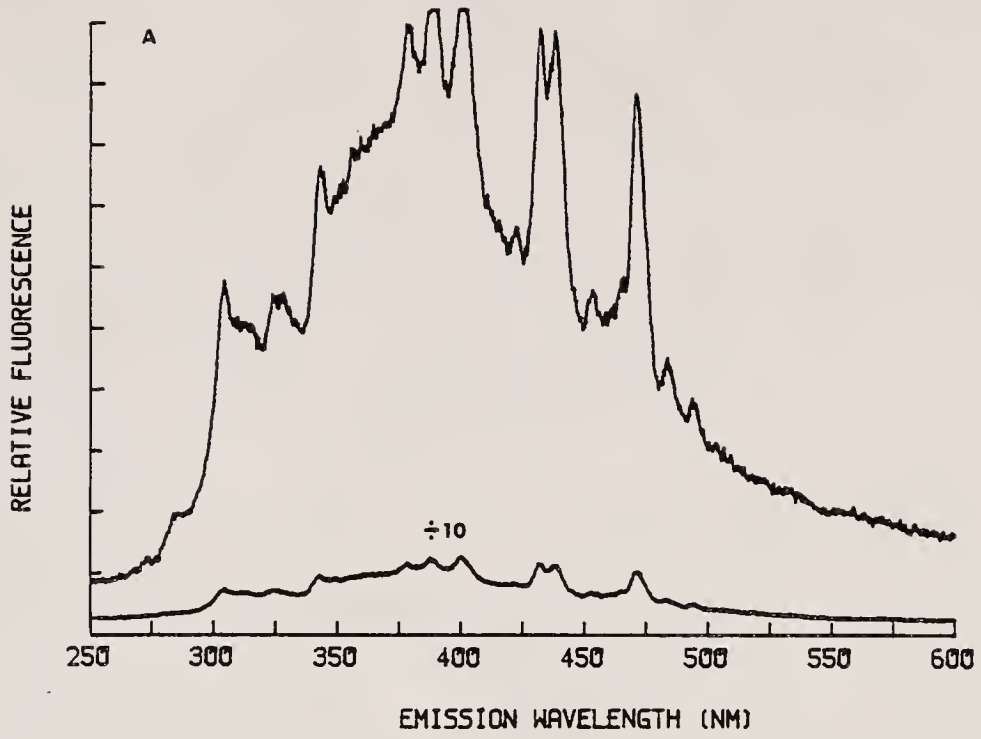
A
RELATIVE FLUORESCENCE
÷10
250
300
350
400
450
500
550
600
EMISSION WAVELENGTH (NM)

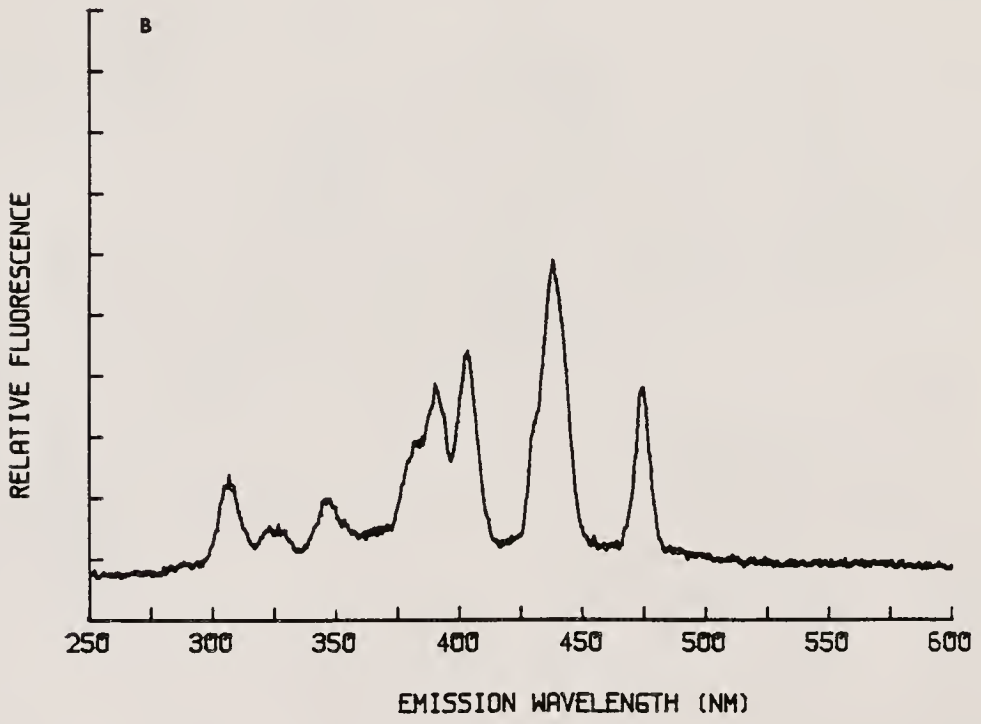
B
RELATIVE FLUORESCENCE
250
300
350
400
450
500
550
600
EMISSION WAVELENGTH (NM)

Figure 39. CWSF spectra of 20-component PAH mixture in n-heptane, for $\Delta\lambda$=

A. 20 nm

B. 34 nm

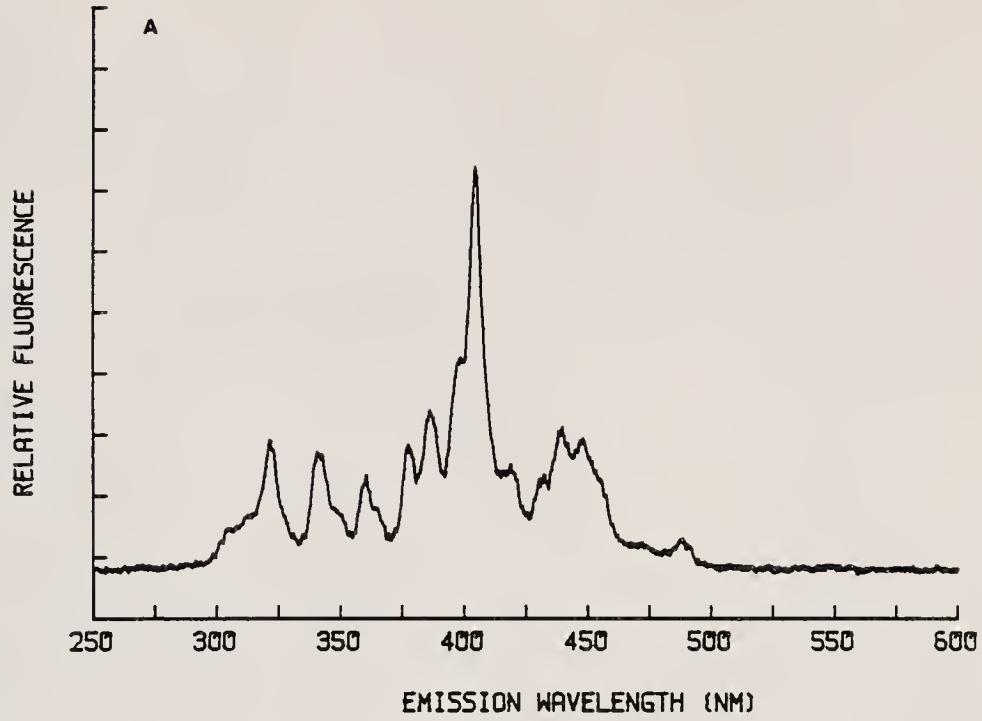
A
RELATIVE FLUORESCENCE
250
300
350
400
450
500
550
600
EMISSION WAVELENGTH (NM)

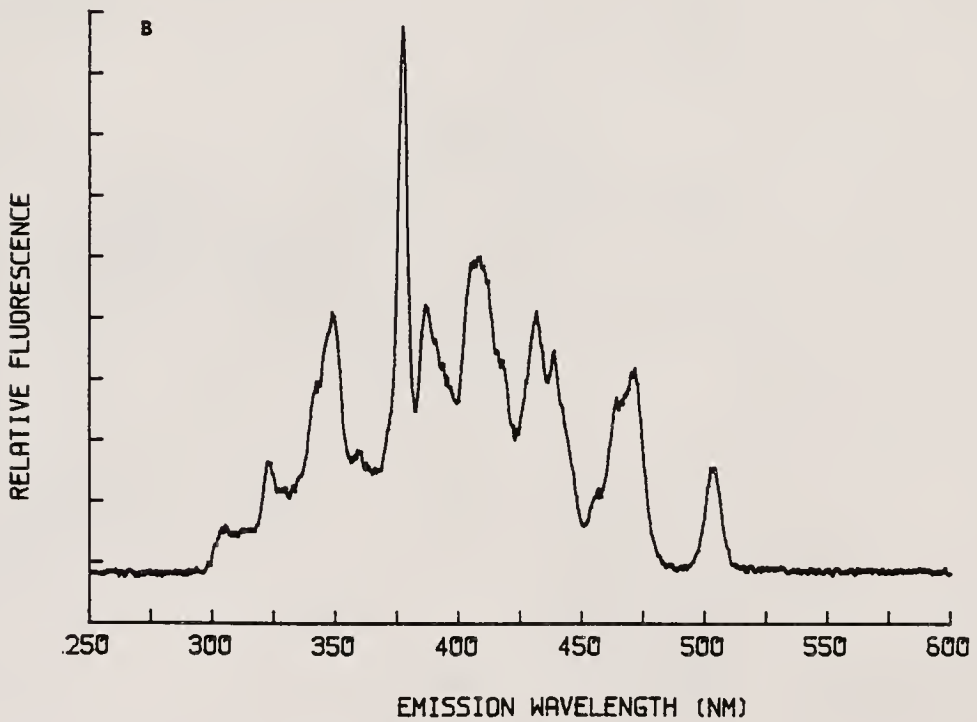
B
RELATIVE FLUORESCENCE
250
300
350
400
450
500
550
600
EMISSION WAVELENGTH (NM)

Figure 40. CESF spectra of 20-component PAH mixture in n-heptane, for $\Delta\bar{\upsilon}$=

A. 0.2 kK

B. 1.6 kK

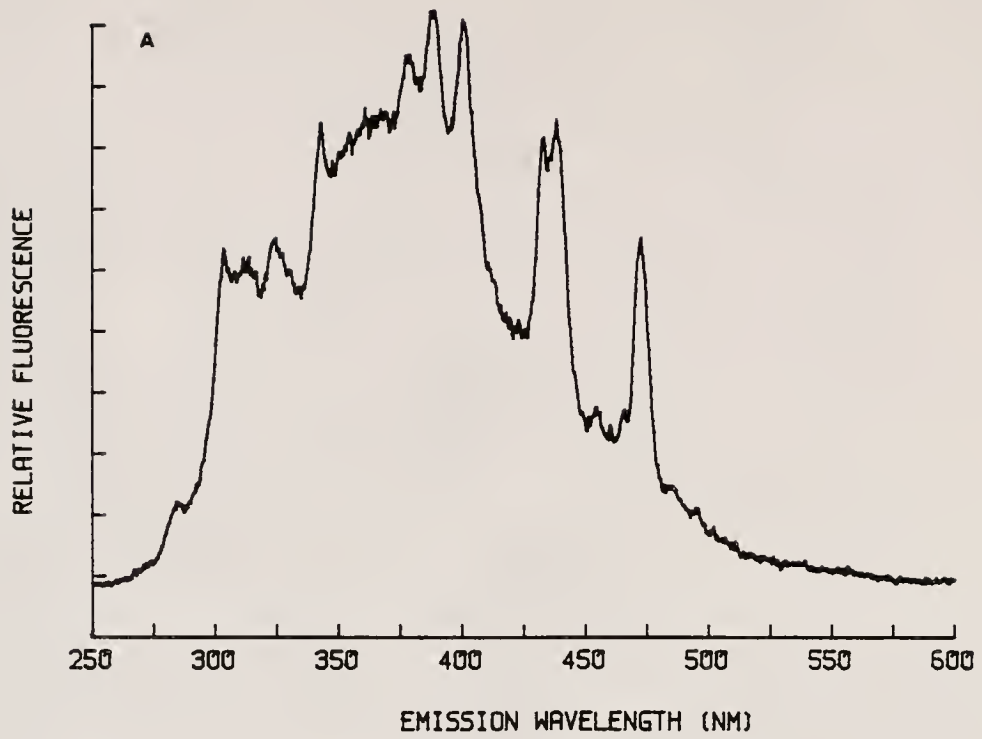
A
RELATIVE FLUORESCENCE
250
300
350
400
450
500
550
600
EMISSION WAVELENGTH (NM)

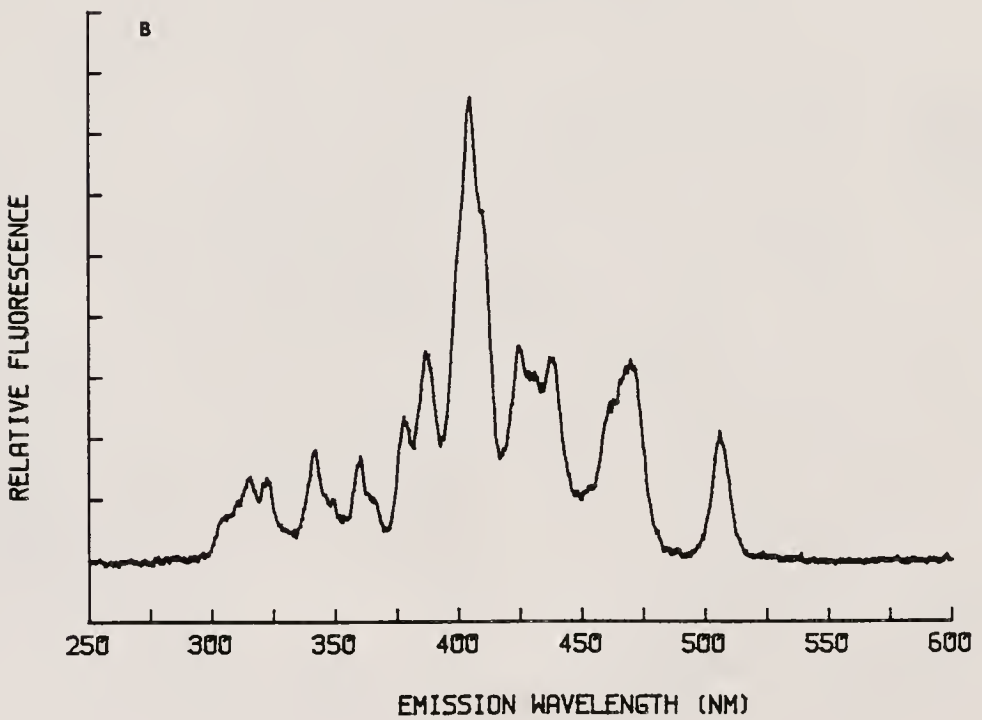
B
RELATIVE FLUORESCENCE
250
300
350
400
450
500
550
600
EMISSION WAVELENGTH (NM)

Figure 41. CESF spectra of 20-component PAH mixture in n-heptane, for $\Delta\bar{\upsilon}$=

A. 3.0 kK

B. 4.4 kK

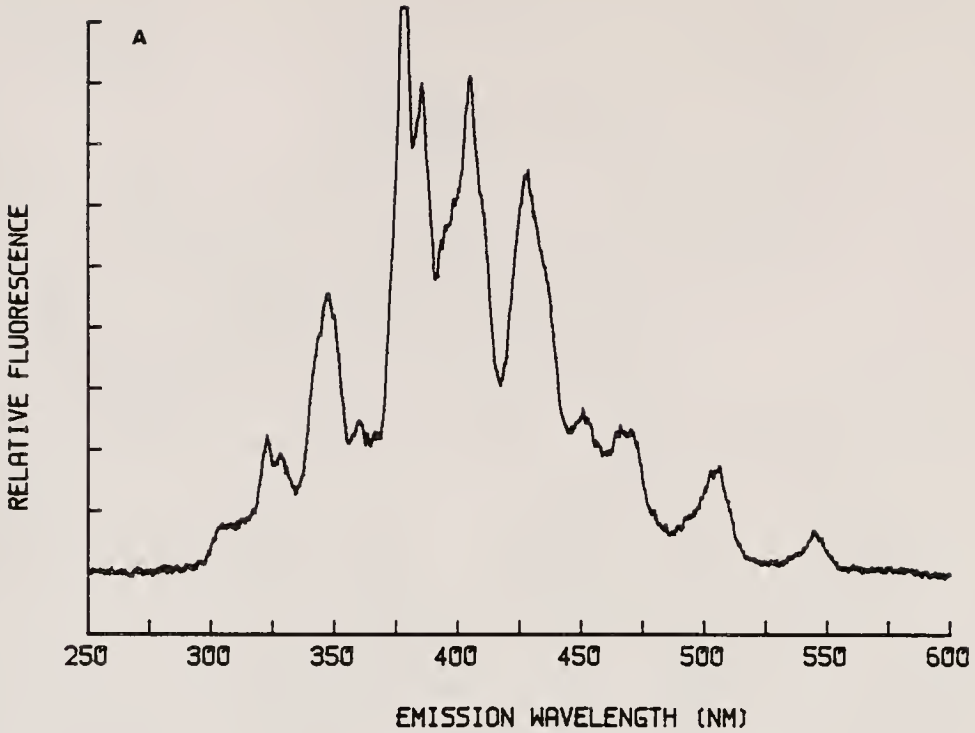
A
RELATIVE FLUORESCENCE
250
300
350
400
450
500
550
600
EMISSION WAVELENGTH (NM)

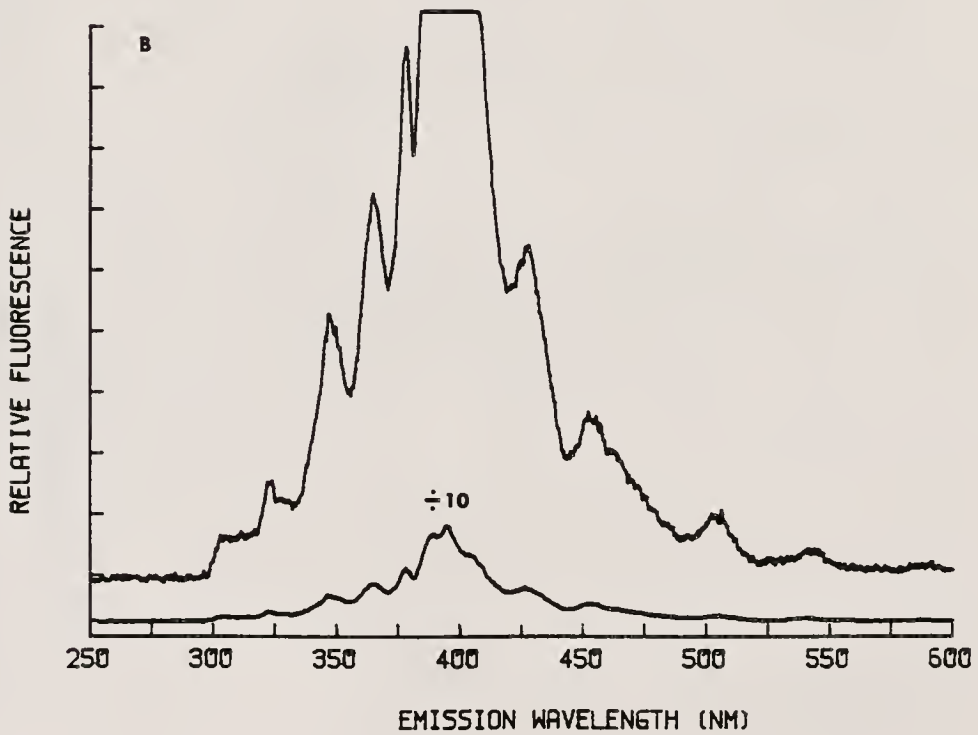
B
÷10
RELATIVE FLUORESCENCE
250
300
350
400
450
500
550
600
EMISSION WAVELENGTH (NM)

This mixture also demonstrates another characteristic of this technique. Although the spectral features contain interesting patterns, one would find quantitation quite difficult using routine methods. Peak heights are difficult to measure with such extensive peak overlap. Standard addition has been used in some SLS analyses. Current trends in analytical chemistry indicate that general statistical methods of data evaluation demonstrate great potential in spectroscopy.

A multiple linear regression analysis was performed on a simulated mixture of the 20-component solution described above. A simulation was selected to evaluate the spectral information rather than a true mixture to avoid instrumental effects, concentration distortions, and energy transfer processes. The goal was not to evaluate RTF as a whole, but rather, the relative merits of CESF within RTF. Mathematically, the matrix to be solved was created with each column corresponding to the reference spectrum of a single component thought to be present in the mixture, and the final column was formed from the simulated mixture spectrum. The concentration array was then obtained using Gauss-Jordan elimination.

The mixture spectra were generated using the 20 components listed in Table 10 with non-zero concentrations. Four compounds were also included in the data matrix to evaluate the effect of selecting compounds not present in the mixture. As mentioned, the concentrations were selected to give approximately the same signal level at the wavelength combination of most intense fluorescence for each compound. Reference spectra were generated from 300 to 540 nm in 2 nm increments under conventional fluorescence and CESF conditions.

The analysis was performed so that those compounds whose reference spectra included no fluorescence, an erroneous concentration of 0.0000

Table 10. Twenty-Component Mixture Concentrations for Fluorescence Spectra Simulation Evaluation

Compound	True Concentration (μg/mL)	Calculated Concentrations (μg/mL) / Relative Error (%)			
		Conventional Fluorescence		CESF	
		λ_{ex} = 254 nm	λ_{ex} = 340 nm	$\Delta\bar{\upsilon}$ = 3.0 kK	$\Delta\bar{\upsilon}$ = 4.4 kK
1,2-Benzopyrene	0.410	0.420 / 2	0.409 / 0	0.462 / 13	0.418 / 2
Anthracene	0.0200	0.0187 / 7	0.0168 / 16	0.0206 / 3	0.0195 / 3
1,12-Benzo-perylene	0.0000 (0.200)[a]	-0.0393 / -	-0.0220 / -	0.00078/ -	-0.0110 / -
Pyrene	0.400	0.688 / 72	0.426 / 7	0.407 / 2	0.392 / 2
1,2-Benzofluorene	0.210	0.219 / 4	0.222 / 6	0.212 / 1	0.210 / 0
2,3-Benzofluorene	0.0200	0.0199 / 1	0.0199 / 1	0.0200 / 0	0.0200 / 0
Perylene	0.00400	0.00383/ 4	0.00389/ 3	0.00394/ 2	0.00392/ 2
1,2:5,6-Dibenz-anthracene	0.200	0.236 / 18	0.203 / 2	0.214 / 7	0.215 / 8
3,4-Benzopyrene	0.0200	0.0177 / 12	0.0191 / 5	0.0201 / 1	0.0196 / 2
Chrysene	0.200	0.197 / 2	0.182 / 9	0.196 / 2	0.203 / 2
Fluoranthene	0.0000 (0.200)[a]	0.0179 / -	0.00093/ -	0.0105 / -	-0.00522/ -

Table 10-continued

Phenanthrene	2.00	1.82 / 9	1.75 / 13	1.95 / 2	1.94 / 3
1,2:3,4-Dibenz-anthracene	0.200	0.218 / 9	0.208 / 4	0.189 / 6	0.193 / 4
2-Methyl-anthracene	0.0200	0.0200 / 0	0.0201 / 1	0.0190 / 5	0.0190 / 5
9-Methyl-anthracene	0.0200	0.0192 / 4	0.0171 / 15	0.0197 / 2	0.0200 / 0
1,2-Benz-anthracene	0.200	0.180 / 10	0.194 / 3	0.203 / 2	0.205 / 3
1-Methylpyrene	0.200	0.362 / 81	0.207 / 4	0.200 / 0	0.206 / 3
Naphthacene	0.0400	0.0365 / 9	0.0000 / 100	0.0406 / 2	0.0375 / 6
9,10-Diphenyl-anthracene	0.0000 (0.0200)[a]	0.00072/ -	0.00124/ -	-0.00013/ -	0.00057/ -
Fluorene	0.0200	0.0204 / 2	0.0000 / 100	0.0198 / 1	0.0199 / 1
9,10-Dimethyl-anthracene	0.0200	0.0218 / 9	0.0247 / 24	0.0203 / 2	0.0207 / 4
Naphthalene	0.0000 (1.00)[a]	-0.0119 / -	0.0000 / -	0.0407 / -	-0.00558/ -
Acenaphthene	0.200	0.208 / 4	0.0000 / 100	0.197 / 2	0.198 / 1

Table 10-continued

Anthanthrene	0.00500	0.00568/	14	0.00619/	24	0.00532/	6	0.00437/	13

[a]Concentration needed for compound to give a peak intensity similar in magnitude to the other 20 compounds present. Comparing the measured concentrations for these compounds with zero concentration gives the reader information as to the magnitude of resulting errors.

μg/mL was obtained. Initial results gave concentrations with errors of one part in 4000, the digitization error. This indicated that the software worked properly and sufficient data were included for statistical analysis. To simulate a more realistic case, random noise was added to the mixture array. The noise was obtained from digitized data from the PMT with the shutter closed. This noise closely approximated a Gaussian distribution. The noise level added corresponded to 1% peak-to-peak noise relative to the mixture array maximum. The results of this analysis are shown in Table 10. Conventional fluorescence excitation wavelengths of 254 and 340 nm were used, as well as $\Delta\bar{\upsilon}$'s of 3.0 and 4.4 kK using CESF. The relative error for the calculated concentrations in Table 10 are fairly small except for those compounds whose spectral contributions become lost in the noise. From this, the general conclusion is that CESF yields spectra of significant magnitude for a wide range of PAHs.

Synchronous Profiles. In another attempt to understand the data relationships within the TLS spectrum, synchronous fluorescence profiles have been calculated. To obtain a synchronous fluorescence profile, synchronous fluorescence spectra are generated over a range of $\Delta\lambda$'s or $\Delta\bar{\upsilon}$'s, and the spectral intensity maxima are plotted as a function of $\Delta\lambda$ or $\Delta\bar{\upsilon}$. Effectively, this corresponds to taking an end-on view of the three-dimensional TLS spectrum, looking down each synchronous row, and plotting the profile obtained (Figure 42). To illustrate, Figures 43A and 43B show the profiles for anthracene in n-heptane using wavelength units and energy units, respectively. The position of maxima in the CESF profile take on a more fundamental relationship to the spectral features in the fluorescence excitation and

Figure 42. The generation of a spectral profile from the three-dimensional TLS spectrum.

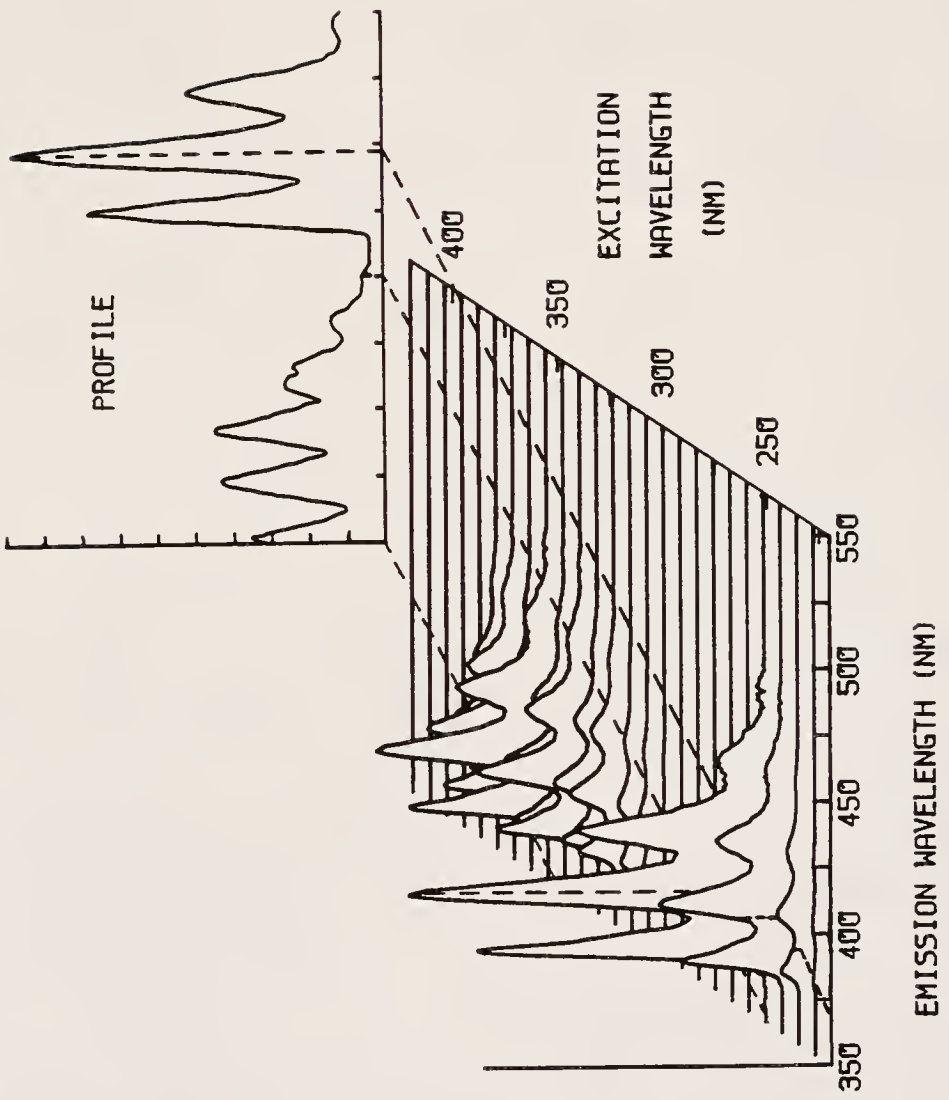
PROFILE
400
350
300
250
EXCITATION
WAVELENGTH
(NM)
350
400
450
500
550
EMISSION WAVELENGTH (NM)

Figure 43. A. CWSF profile for anthracene in n-heptane.

B. CESF profile for anthracene in n-heptane.

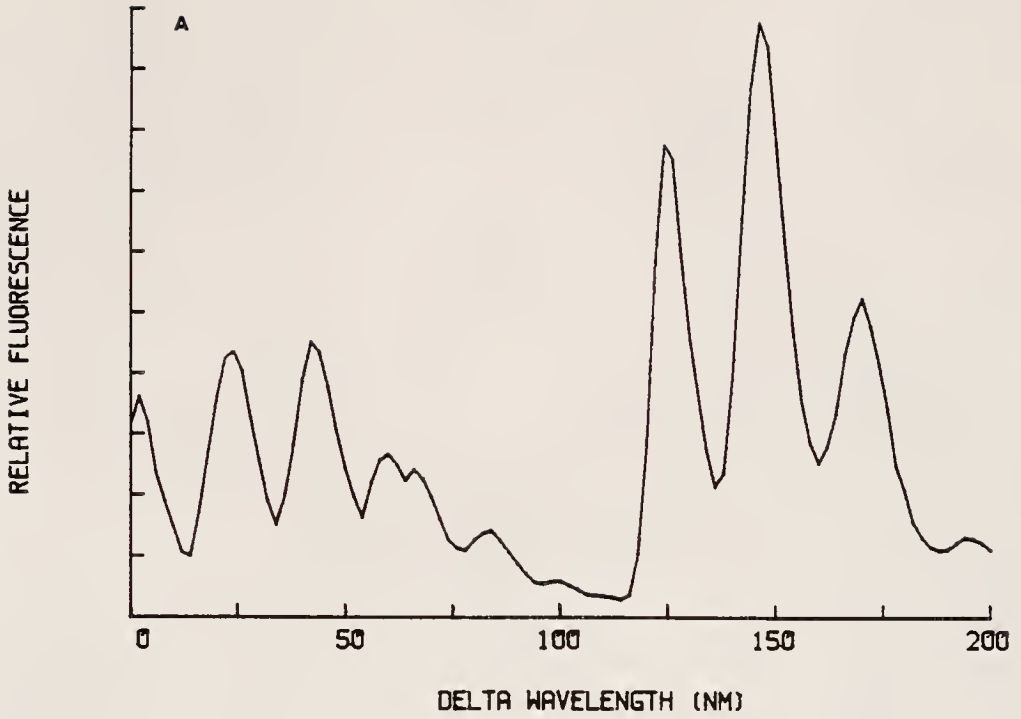
A
RELATIVE FLUORESCENCE
0
50
100
150
200
DELTA WAVELENGTH (NM)

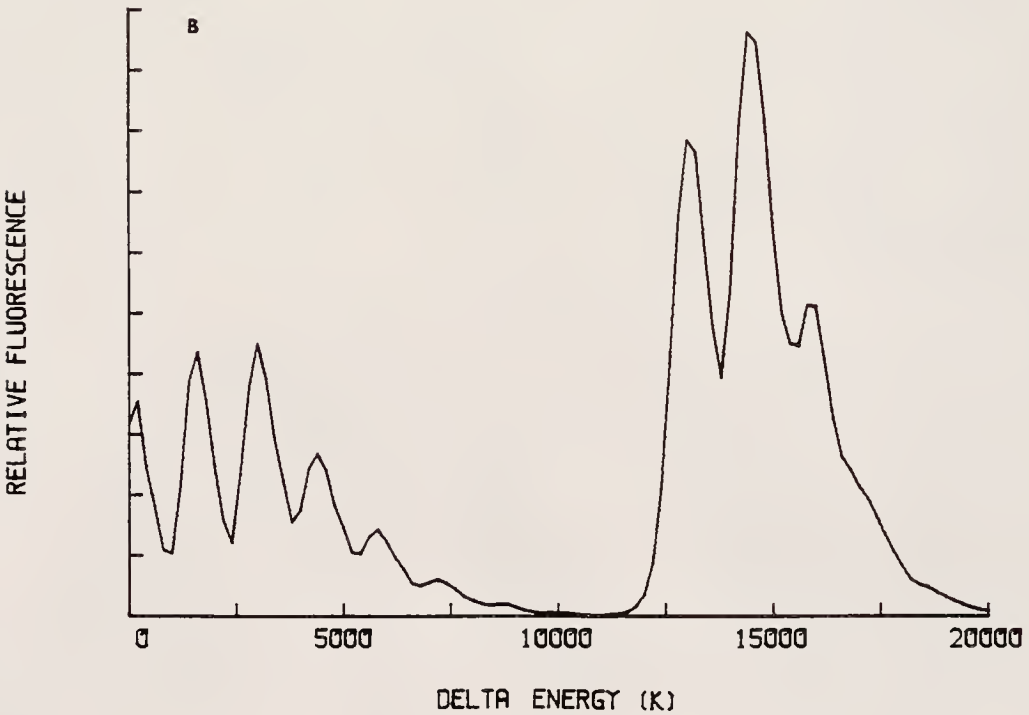
B
RELATIVE FLUORESCENCE
0
5000
10000
15000
20000
DELTA ENERGY (K)

emission spectra. Again the 1.4 kK vibrational energy difference becomes evident, as well as the 0.2 kK Stokes Shift. The details of this relationship can be demonstrated with 1,2-benzopyrene. Figure 44 shows the fluorescence excitation and emission spectra for 1,2-benzopyrene plotted in wavelength and energy units. The profiles for CWSF and CESF are shown in Figure 45. The similarity between the CESF profile and the mirror image of the fluorescence excitation spectrum is striking. This seems to be a natural conclusion from the mirror image relationship in fluorescence data known from fluorescence theory. The CWSF profile lacks this symmetrical characteristic, and appears as a poor approximation.

Conclusions

The concepts of CESF were then applied to drug analysis. In general, the problems in pharmaceutical analysis are entirely different from PAH analysis. Drugs do not yield spectra with extensive vibrational structure, but broad bands with bandwidths of 25 to 100 nm. So different approaches are necessary, perhaps even unrelated to those described for PAHs. Andre et al. have described the selection of $\Delta\lambda$ that is optimized for pharmaceutical analysis (56). Conditions are selected that match the exact requirements of the sample of interest. Thus the fluorescence characteristics of the sample must be fairly well known before analysis.

The results obtained in CESF are interesting and form a core of theoretical considerations. But, as the 20-component mixture indicates, synchronous techniques under the conditions of RTF are restricted by many of the limitations of RTF. Broad bands limit the complexity of the sample suitable for RTF analysis. In the last decade, substantial improvements in luminescence spectroscopy have been developed that can be directly applicable to SLS analysis.

Figure 44. Conventional fluorescence excitation and emission spectra of 1,2-benzopyrene in n-heptane plotted in:

A. wavelength units

B. energy units

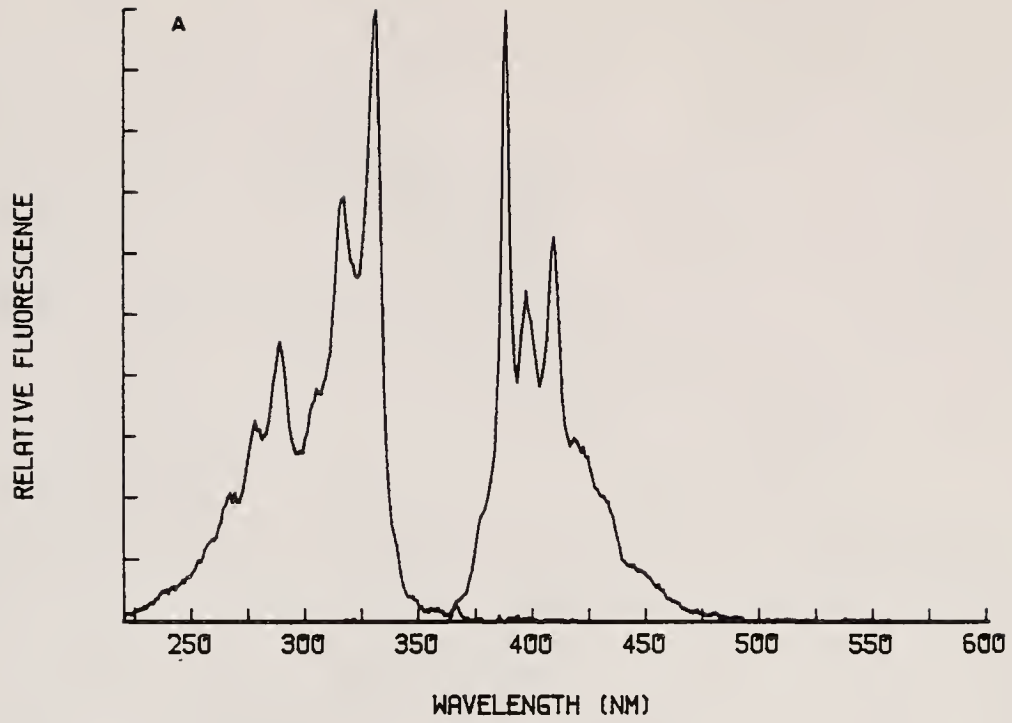
A
RELATIVE FLUORESCENCE
250
300
350
400
450
500
550
600
WAVELENGTH (NM)

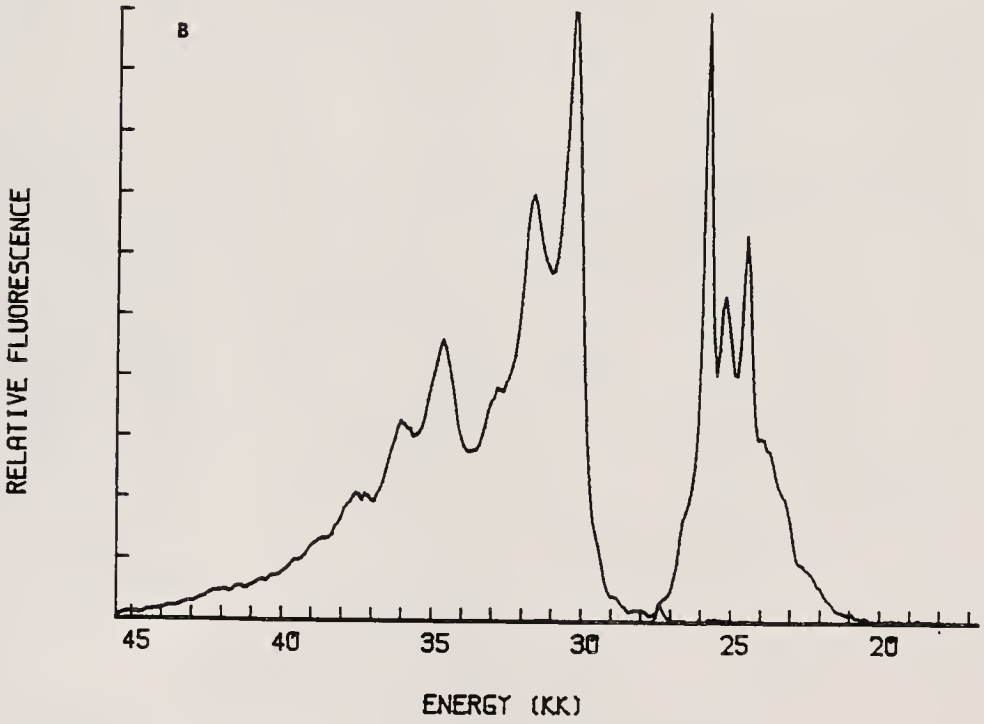
B
RELATIVE FLUORESCENCE
45
40
35
30
25
20
ENERGY (KK)

Figure 45. A. CWSF profile for 1,2-benzopyrene in n-heptane.

B. CESF profile for 1,2-benzopyrene in n-heptane.

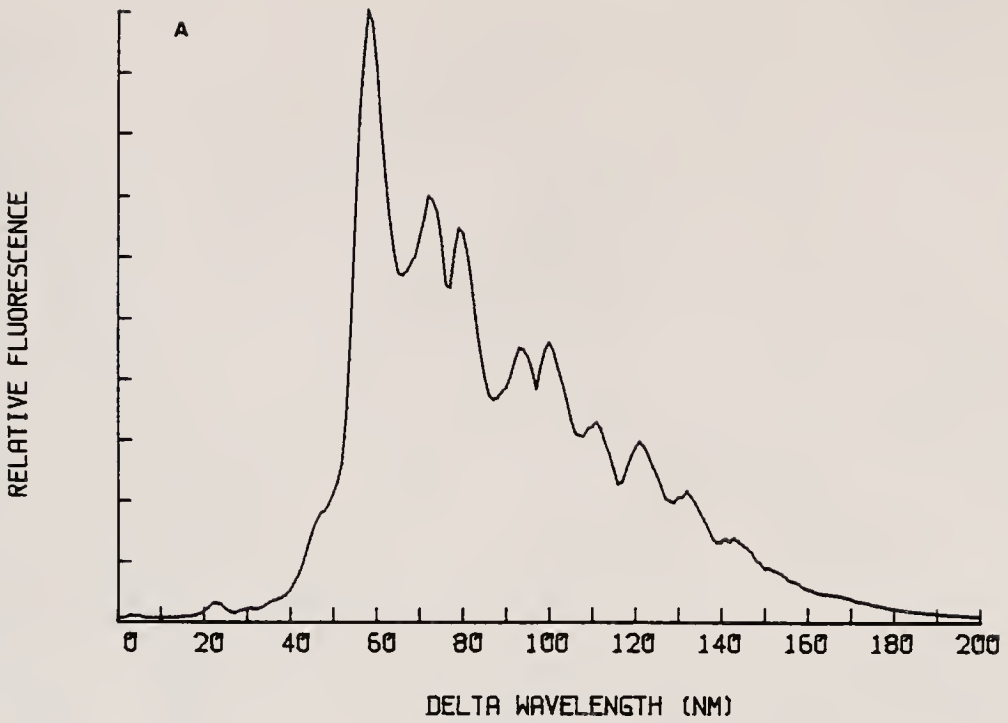
A
RELATIVE FLUORESCENCE
0
20
40
60
80
100
120
140
160
180
200
DELTA WAVELENGTH (NM)

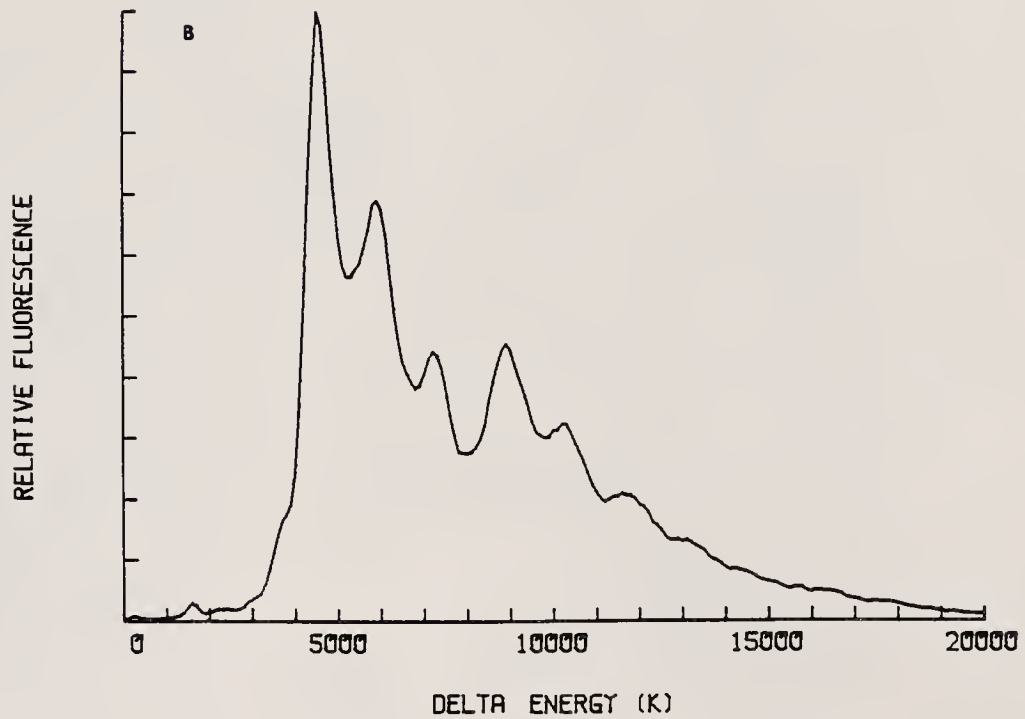
B
RELATIVE FLUORESCENCE
0
5000
10000
15000
20000
DELTA ENERGY (K)

CHAPTER 4
LOW TEMPERATURE LUMINESCENCE SPECTROSCOPY

Introduction

Broad-band emission as exhibited by the room temperature fluorescence and phosphorescence of non-PAHs make many of the apparent advantages of SLS techniques totally ineffective. This is especially true in the conversion to energy units. At room temperature, selectivity is limited by extensive spectral overlap. This overlap is reduced dramatically by reducing the sample temperature to liquid nitrogen (77 K) or liquid helium (4 K) temperatures (74,75). For PAHs analysis, this can be combined with the Shpol'skii effect by selecting an appropriate n-alkane solvent (76). This results in quasi-linear, line-rich fluorescence spectra where bands are reduced to 1 to 10 K bandwidths.

While conventional low temperature techniques use a liquid nitrogen sample environment, the current increase of low temperature research encompasses a wide variety of conditions. Liquid nitrogen is used because of the simplicity of instrumentation required. By lowering the temperature to 63 K, a significant effect can be seen from LTF spectra obtained at 77 K (77). Liquid helium has had increasing utility, but still requires expensive apparatus. Closed-cycle refrigerators are commonly used for temperatures around 10 K. The temperature becomes of considerable importance in many fluorescence techniques where band narrowing properties are observed only below 20 K.

By combining the low temperature spectral narrowing features with the unique characterisitics of a laser excitation source, several techniques have been developed for the analysis of PAHs in complex mixtures. Laser-Excited Shpol'skii Spectroscopy has been successfully used in the direct determination of liquid fuels (78,79). Fluorescence Line Narrowing takes full advantage of the narrow line properties of laser excitation to yield spectra of reduced complexity (80). Matrix Isolation Spectroscopy dilutes the vaporized sample with an inert gas and deposits it on a cryogenic surface, where quasi-linear spectra are free from original matrix effects (81,82). Each of these techniques make use of selective excitation (83,84). In selective excitation, the excitation source output, i.e. laser, is chosen to exactly coincide with the electronic absorption band of the compound of interest, exciting that compound but not exciting other compounds whose absorption bands fall outside this region. In this way, the conditions are optimized for the specific compound of interest.

Some PAHs, when dissolved in selected n-alkane solvents and then frozen to 77 K or below, produce extremely narrow, line-rich fluorescence spectra (85-87). Kirkbright and deLima (88) have reviewed the early development of Shpol'skii Spectroscopy. Much of the original work concentrated on determining the physical cause of this effect. The Shpol'skii effect is generally explained as a matching of the size of the PAH molecule and the n-alkane solvent size in the crystal lattice. Upon freezing, the n-alkane solvent forms a polycrystalline solid. The PAH molecules in the sample occupy substituent positions within the crystal, limiting their orientation to a few possible orientations. The Shpol'skii effect is noticeable at 77 K and early research combined

liquid nitrogen temperatures with relatively broad-band excitation. However, the Shpol'skii effect becomes of greatest analytical utility as the sample temperature is reduced to liquid helium temperatures. Laser excitation results in greatly improved narrowing over broad-band sources and much higher power, with an anticipated increase in research effort in this area as more reliable lasers become widespread and sample temperature reduction becomes more feasible experimentally.

The objective in Matrix Isolation Spectroscopy is to place the analyte molecule in a matrix that has no effect on the fluorescence spectrum, acting as an ideal solvent (89,90). The sample is diluted with an inert gas and deposited on a solid surface at cryogenic temperatures, usually 4 K to 10 K. Each molecule is isolated from the influence of other analyte molecules, with little analyte-solvent interaction. Wehry and Mamantov (91) have reviewed the principles of Matrix Isolation Spectroscopy, with specific application to PAH analysis.

Fluorescence Line Narrowing Spectroscopy yields fluorescence spectra of unusually narrow bands by matching the excitation wavelength as closely as possible to the 0-0 transition between the ground and first excited singlets, reducing the number of energy levels that becomes populated (92). The spectrum is simplified, with the 0-0 transition of greatest intensity. Fluorescence Line Narrowing Spectroscopy is essentially an example of Site Selection Spectroscopy (93).

The limited number of possible orientations of an analyte molecule in the solvent matrix results in another type of band broadening. Each orientation type, or site, corresponds to a transition of slightly different energy due to a difference in the environment felt by

molecules in that orientation. The energy difference between sites can extend up to 100 K. For each group of molecules within an orientation, an identical spectrum can be obtained. For the entire sample, several of these identical spectra occur, displaced by this slight energy difference, with relative intensities proportional to the number of molecules in each orientation. If the molecules in a specific orientation can be selectively excited, the fluorescence spectrum would be simplified. Site Selection Spectroscopy is a technique that preferentially excites the molecules within a specific site utilizing a narrow-line laser excitation source (94). Each multiplet in the LTF spectrum is reduced to a single band. This technique is used in combination with Shpol'skii Spectroscopy or Matrix Isolation Spectroscopy.

As the sample temperature approaches 0 K, several features of LTF spectra become more apparent. Usually the 0-0 transition is the most intense. The vibrational structure beyond the 0-0 transition is reduced to a few frequencies and combinations at 0 K. Two frequencies characteristic of PAH vibrational structure are around 1.4 kK and 0.7 to 0.9 kK (95-97). The spacings of the vibrational bands of the emission spectrum correlate well with the vibrational frequencies of the ground state that are observed in Infrared and Raman Spectroscopy. As the temperature is increased, the number of lines greatly increases. For example, 160 vibrational lines have been measured for a solution of perylene (98).

While the alkane solvent selected in Shpol'skii analysis may have an effect on the narrowing properties of the emission spectrum, solvent effects at low temperature behave similarly to the multiple site effect

on LTF spectra (99). Solvent fields affect the electronic transition, but do not significantly affect the vibrational energy level distribution. Thus the exact position of spectral features shift with solvent. For example, the LTF emission spectrum for pyrene has two peaks at 371.3 nm and 391.4 nm ($\Delta\bar{\upsilon}$ = 1.38kK) in n-pentane, at 371.6 nm and 392.0 nm ($\Delta\bar{\upsilon}$ = 1.41kK) in n-heptane (74). The similarity in vibrational spacing in fluorescence excitation and emission spectra is demonstrated by the 1.4 kK vibrational spacing for several PAHs presented by Farooq and Kirkbright (100). These characteristics are interesting in light of previous discussions of SLS at room temperature.

The application of TLS instrumentation to low temperature fluorescence spectroscopy (LTF) becomes impractical because of the resolution needed. To maintain the resolution to take full advantage of band narrowing capabilities, the number of data points required for adequate representation would be enormous. One alternative is to reduce the spectral region of interest, voiding many of the advantages of TLS. Also many of the plotting methods for three-dimensional data representation are ineffective for sharp line spectra, as all depth perspective is lost. Therefore, TLS has not been used for LTF.

SLS has had limited application to LTF analysis. In this work, an evaluation is made of combining the excellent band narrowing features of low temperature Shpol'skii matrices with SLS. From a practical viewpoint, the goal of this effort is to provide a screening technique for selective excitation techniques. From a theoretical viewpoint, the goal is to be able to trace all instrumental parameters and resultant data back to luminescence theory, as was attempted at room temperature. In doing so, a comprehensive synchronous luminescence

theory was sought. Not only is the optimization of low temperature SLS important, but an understanding is desired for the connection between room temperature and low temperature SLS.

Band narrowing is desirable in many respects, but holds special problems for CWSL techniques. With broad bands, greater probability exists for accidentally crossing an emission band even with improper parameter selection. With narrow bands, it seems quite possible to scan past desired emission bands. Spectral blindness becomes more of a problem. This results in mixed consequences for low temperature CWSL techniques. This spectral blindness can be exploited for improved spectral selectivity. However, if spectral relationships are not understood, even the fluorescence of the desired analyte may not be obtained or the spectrum may be incorrectly interpreted.

Many of the concepts of low temperature SLS should be an extension of the principles of SLS at room temperature. But this transition is not obvious. As this research progressed, it became increasingly evident that many of the problems plaguing conventional SLS are even more difficult at low temperatures. Again, a systematic selection of $\Delta\lambda$ is of utmost importance. The use of energy concepts resulted in the development of CESL for room temperature analysis. These principles were applied to low temperature analysis, resulting in the development of Low Temperature Constant Energy Synchronous Luminescence (LTCESL).

Instrumentation

Because of the need for increased resolution for the monochromators in LTCESL, a new system was designed and built for this purpose. A moderate-resolution laboratory-constructed fluorimeter was built using the components listed in Table 11, with the experimental

Table 11. Experimental Equipment Used for LTCESL Spectrometer

Item	Model	Source
Eimac Xenon Arc Lamp 300 W	R300-2	Eimac, Division of Varian San Carlos, CA 94070
Eimac Illuminator Power Supply operated at 15 A	PS 300-1	Eimac, Division of Varian San Carlos, CA 94070
Excitation Monochromator f/6.8, blaze λ= 250.0 nm 1180 lines/mm	EU-700	Heath Company Benton Harbor, MI 49022
Monochromator Scan Controls	EU-700-51	Heath Company Benton Harbor, MI 49022
Sample Housing		American Instrument Co. Silver Spring, MD 20910
Emission Monochromator f/6.8, blaze λ= 250.0 nm 1180 lines/mm	EU-700-77	GCA/McPherson Instrument Acton, MA 01720
Programmable Filter Attachment	EU-700-56	GCA/McPherson Instrument Acton, MA 01720
Photomultiplier Module	EU-700-30	Heath Company Benton Harbor, MI 49022
Photomultiplier Tube operated at -800 V	RCA 1P28	RCA Lancaster, PA 17604
Nanoammeter	---	Laboratory Constructed
Recorder	OmniScribe B5217-5I	Houston Instrument Austin, TX 78753
A/D System - Laboratory Constructed with a MDAS-8D 8 Channel Diff. 12 Bit Data Acquisition System		Datel Systems, Inc. Mansfield, MA 02048
Microcomputer	Apple II with 48 K RAM	Apple Computer, Inc. Cupertino, CA 95014

diagram given in Figure 46. Monochromator control was achieved via a parallel interference with the microcomputer, with an assembly language program utilized for timing synchronization and data collection and storage.

The Apple II microcomputer was selected because of its versatility and the limited requirements that were placed on the computer system. Complete graphics and TLS capabilities were not needed. Instead, only instrument control and data collection were implemented. A constant energy difference is maintained between the monochromators by using a linear approximation. The emission monochromator is scanned at a constant rate while the excitation monochromator is variably scanned. To implement, the emission monochromator is incremented by a constant user-selected amount, generally 0.1 nm. After each increment, the excitation monochromator is advanced the required number of steps to maintain the appropriate energy difference. The excitation steps are obtained from a look-up table, generated at the beginning of each scan. As the selected emission scan step is reduced, the scan appears continuous. The BASIC program and assembly language subroutines are included in Appendix 3.

For all the spectra obtained, an excitation monochromator bandpass of 4 nm and an emission monochromator bandpass of 0.2 nm were used. A scan rate of 0.1 nm/s was used with a 0.5 s time constant. All spectra are uncorrected for instrumental response. The xenon arc lamp output has a spectral intensity distribution similar to the lamp described in Chapter 2. The instrument response functions for this system resemble those of the TLS system with a reduction in PMT response in the red region of the spectrum. Calibration of the monochromators with a low-pressure mercury lamp resulted in an average wavelength error of $\pm$0.02 nm.

Figure 46. Block diagram of LTCESF instrumentation.

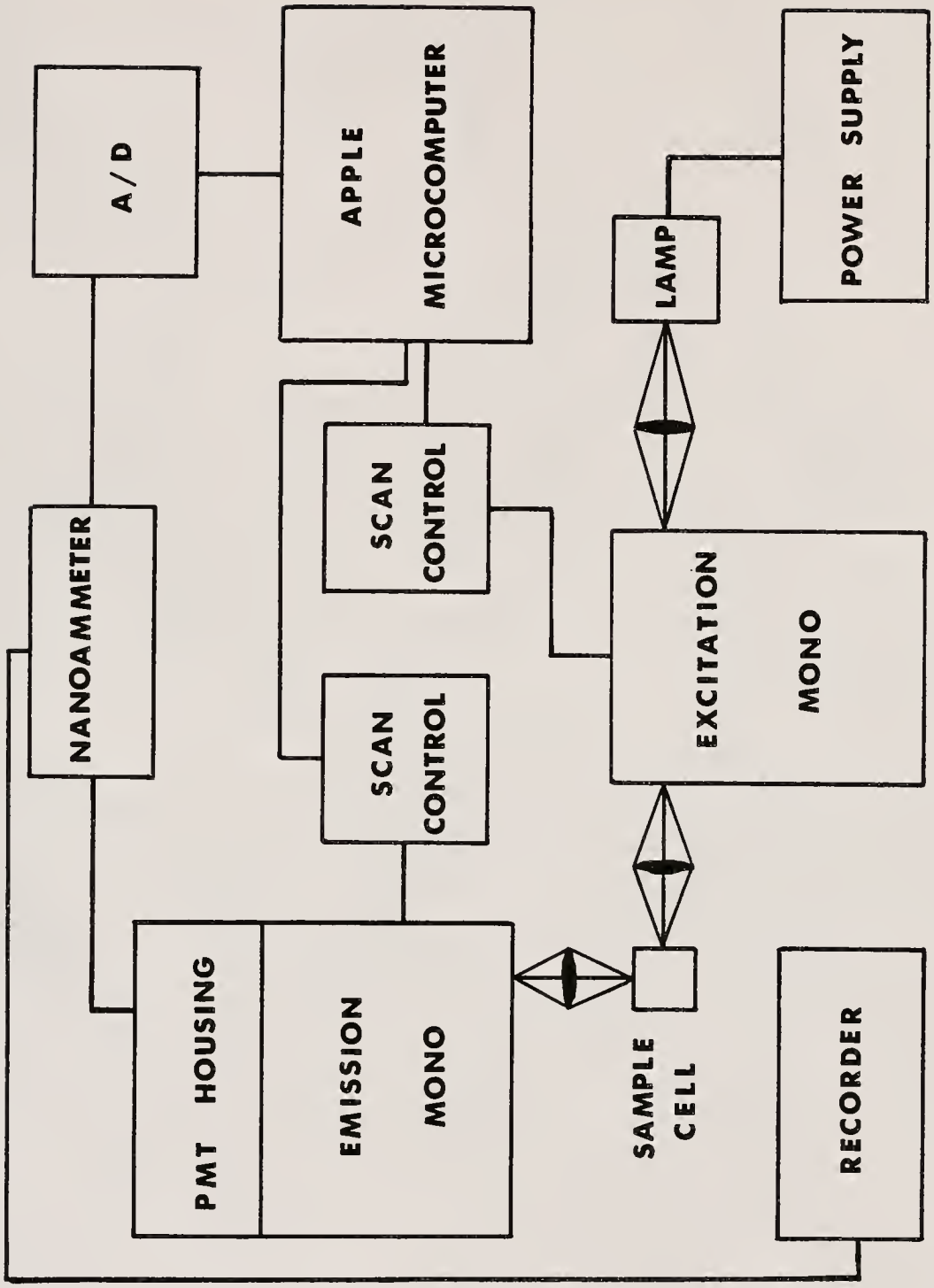
A/D
APPLE MICROCOMPUTER
POWER SUPPLY
LAMP
NANOAMMETER
SCAN CONTROL
SCAN CONTROL
EXCITATION MONO
PMT HOUSING
EMISSION MONO
SAMPLE CELL
RECORDER

Samples are placed in a precision-bore Spectrosil quartz sample tube (Thermal American Fused Quartz Co., Montville, NJ 07045), 30 cm long, with a 5 mm outer diameter and a 3 mm inner diameter, that was sealed at one end. Each tube is rapidly cooled by placing it directly in a liquid nitrogen-filled dewar to prevent inhomogeneous freezing. Throughout this work, low temperature experiments were performed at 77 K using liquid nitrogen. To avoid frost from forming on the dewar's optical tip, a gentle stream of nitrogen gas is flushed into the sample compartment.

Results and Discussion

By lowering the sample temperature to 77 K, the Stokes Shift between 0-0 excitation and emission peaks becomes small. At room temperature, PAHs in n-alkane solvents generally exhibit a 0.1 to 0.3 kK Stokes Shift. Because of this, a $\Delta\lambda$ of 3 nm is a good approximation to this difference in CWSF. This corresponds to about a 0.2 kK value for $\Delta\bar{\upsilon}$ in CESF. At reduced temperatures, however, a $\Delta\lambda$ of about 0 nm would be necessary. This is impractical due to the intense Rayleigh scatter observed under these conditions. Integral multiples of 1.4 kK for $\Delta\bar{\upsilon}$ have been effectively used at room temperature for CESF. By reducing the sample temperature, the energy difference between the lowest vibrational states of the ground and the first excited electronic singlet states is altered, but the vibrational level distribution within an electronic energy manifold is relatively unchanged. Therefore, a similar choice of $\Delta\bar{\upsilon}$ selection was used in LTCESF. For example, Figure 47 shows the LTF and RTF spectra for a solution of perylene in n-heptane. These were obtained using the TLS instrument with a 2 nm resolution. These spectra confirm the shift due to temperature and the relatively unchanged vibrational distribution.

Figure 47. Comparison of the conventional A. LTF and B. RTF low resolution spectra of perylene in n-heptane.

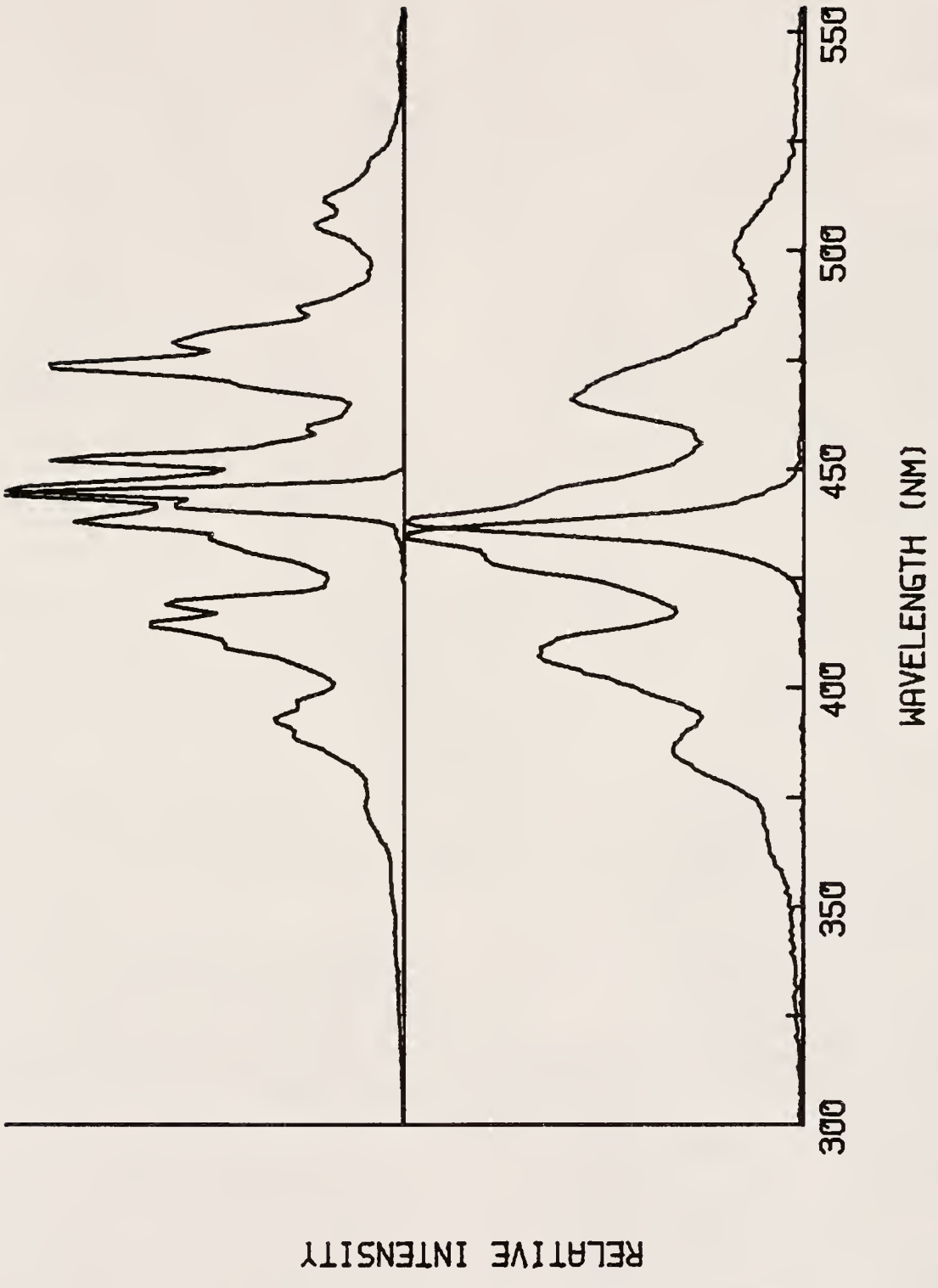
RELATIVE INTENSITY
300
350
400
450
500
550
WAVELENGTH (NM)

As shown in Chapter 3, the effective synchronous bandwidth is a function of both the excitation and emission monochromator bandpasses, mathematically expressed in Equation (20). The main interest in this work was in the narrowing characteristics in the emission spectra. Therefore, conditions were selected with $\delta\lambda_x$ about twenty times larger than $\delta\lambda_m$. Under these conditions, $\delta\lambda_s$ is approximately equal to $\delta\lambda_m$. Selecting these values for $\delta\lambda_x$ and $\delta\lambda_m$ provides sufficient source intensity for adequate sensitivity, yet retaining relatively high emission monochromator resolution. Because excitation bands are often broader than emission bands, one gains little by reducing the excitation bandpass without going to a laser excitation source. This differs substantially from room temperature considerations. Often at room temperature, the monochromator bandpasses are smaller than the bandwidths themselves. When this is so, the $\sqrt{2}$ factor for equivalent $\delta\lambda$'s is significant. At low temperatures, often the effective bandwidth is limited by the resolution and throughput of the monochromators. In this case, one sacrifices the $\sqrt{2}$ factor for increased sensitivity.

LTCESF spectra demonstrate several interesting features. Several examples illustrate these characteristics. In using integral multiples of 1.4 kK for $\Delta\bar{\upsilon}$, a 1.4 kK interval will be defined as a vibrational unit, with a $\Delta\bar{\upsilon}$ selected as a number of vibrational units from the resonant 0-0 transition. If a $\Delta\bar{\upsilon}$ of 0.0 kK is used in LTCESF, a set of peaks is expected corresponding to a 0-0 excitation and a 0-0 emission transition. If one vibrational unit is selected for $\Delta\bar{\upsilon}$, where $\Delta\bar{\upsilon}$ is equal to 1.4 kK, two sets of peaks are expected. The set lowest in wavelength in the LTCESF spectrum corresponds to a 0-1 excitation and 0-0 emission transition. The spectra in Figures 48-50 are for a

Figure 48. Low temperature fluorescence emission spectrum of anthracene in n-heptane. λ_{ex} = 248.0 nm.

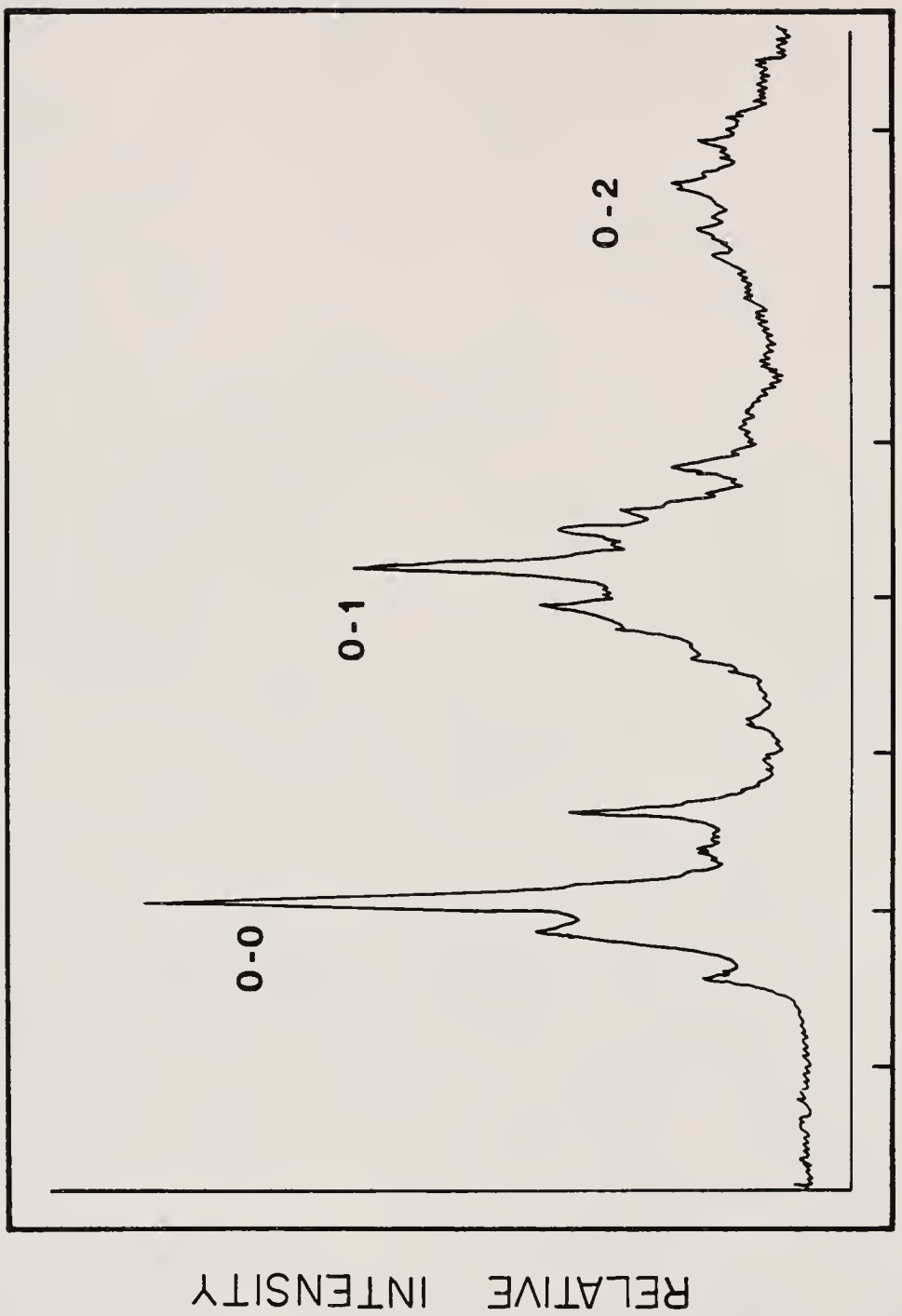
0-0
0-1
0-2
370
380
390
400
410
420
430
EMISSION WAVELENGTH (NM)
RELATIVE INTENSITY

Figure 49. LTCESF spectrum of anthracene in n-heptane.
$\Delta\bar{\upsilon}$ = 1.4 kK.

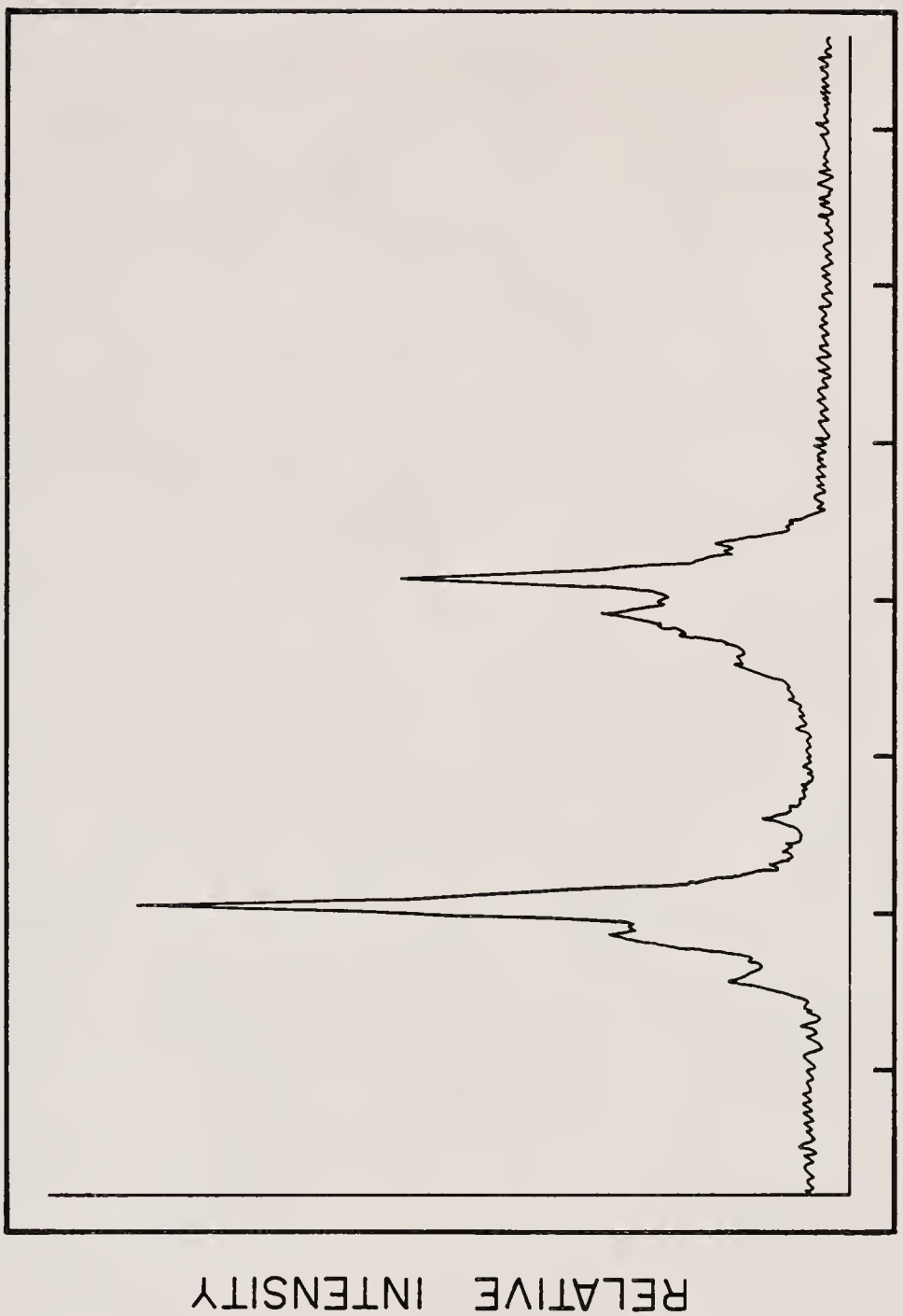
RELATIVE INTENSITY
370
380
390
400
410
420
430
EMISSION WAVELENGTH (NM)

Figure 50. LTCESF spectrum of anthracene in n-heptane. $\Delta\bar{\upsilon}$ = 2.8 kK.

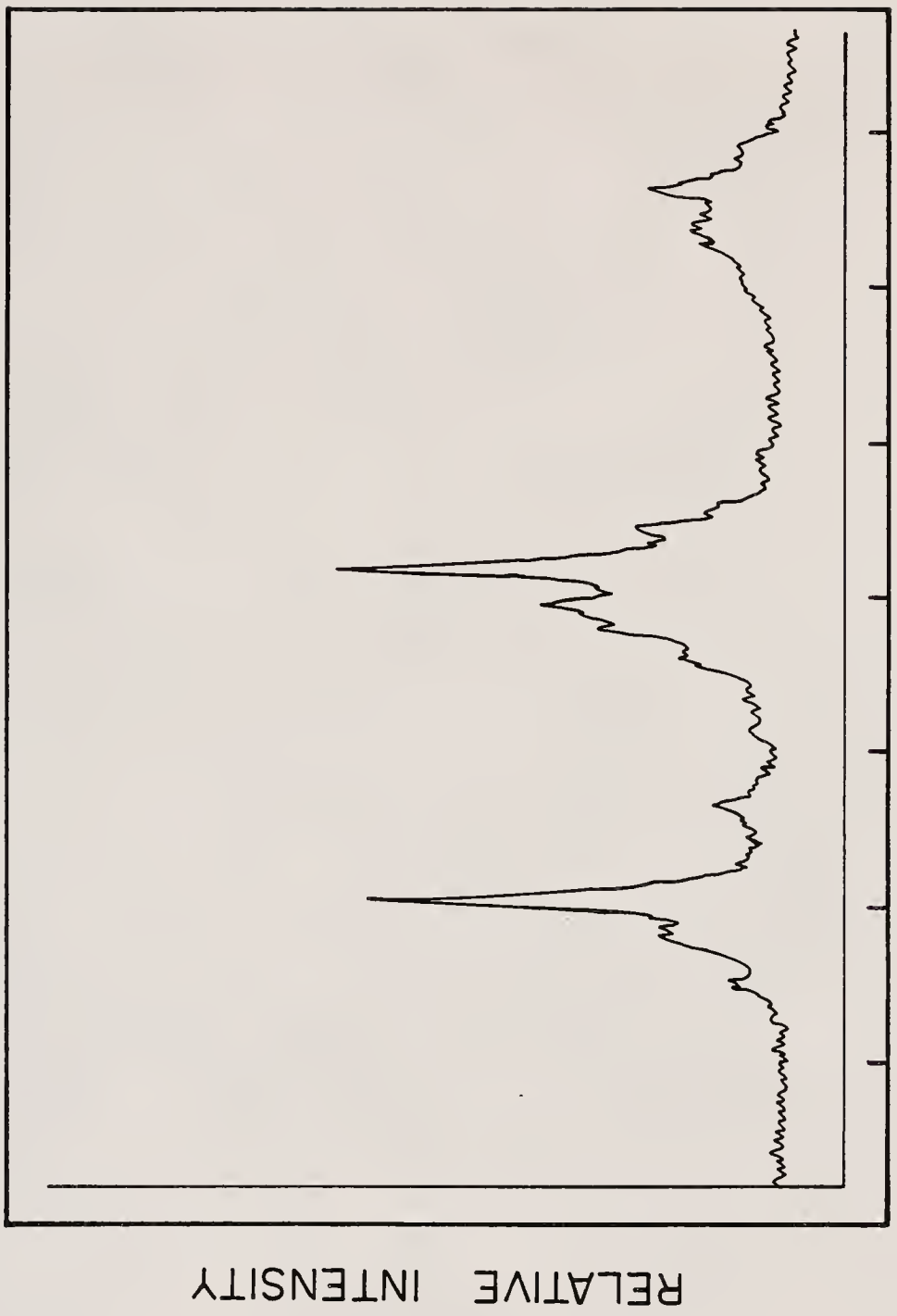
RELATIVE INTENSITY
370
380
390
400
410
420
430
EMISSION WAVELENGTH (NM)

solution of anthracene in n-heptane. Figure 48 is the low temperature fluorescence emission spectrum for this solution. The peaks from 375 to 390 nm, 390 to 415 nm, and 415 to 435 nm correspond to vibrational transitions 0-0, 0-1, and 0-2, respectively. Figure 49 is the LTCESF spectrum of this solution obtained for a $\Delta\bar{\upsilon}$ of a 1.4 kK. If a $\Delta\bar{\upsilon}$ of 2.8 kK, or two vibrational units, is selected, three sets of peaks are expected. They correspond to excitation/emission transitions of 0-2/0-0, 0-1/0-1, and 0-0/0-2. Figure 50 is the LTCESF spectrum of the anthracene solution with a $\Delta\bar{\upsilon}$ of 2.8 kK. Note the remarkable similarity between Figures 48, 49, and 50. Most of the peaks appear at the same wavelength with differences only in relative intensity.

Figures 51-53 again demonstrate these relationships for a solution of 2,3-benzofluorence in n-heptane. Similar spectra can be obtained from two entirely different scan paths. Several advantages of this characteristic were studied to determine its analytical potential. A mathematical model was sought to explain this feature.

A simple model was developed to describe the expectant LTCESF spectra. Many of the terms have been borrowed from Kohler (98). For this model, the following terms are defined: $\bar{\upsilon}_{0\text{-}0}$ is the excitation-emission 0-0 energy for the resonant transition, $\bar{\upsilon}_{0\text{-}v}$ is the vibrational transition energy relative to $\bar{\upsilon}_{0\text{-}0}$, and $S(\bar{\upsilon}_m\text{-}\bar{\upsilon}_{0\text{-}v})$ describes the distribution of transitions within a single vibrational unit. $S(\bar{\upsilon}_m\text{-}\bar{\upsilon}_{0\text{-}v})$ is the basic vibrational substructure relative to the vibrational transition energy, $\bar{\upsilon}_{0\text{-}v}$. It is assumed that this substructure is repetitive, an experimentally justified approximation for PAHs. $D(\bar{\upsilon}_{0\text{-}0}\text{-}\bar{\upsilon}_{0\text{-}v})$ is a distribution function giving the probability, and corresponding luminescence intensity, that a molecule will have a

Figure 51. Low temperature fluorescence emission spectrum of 2,3-benzofluorene in n-heptane. λ_{ex} = 319.0 nm.

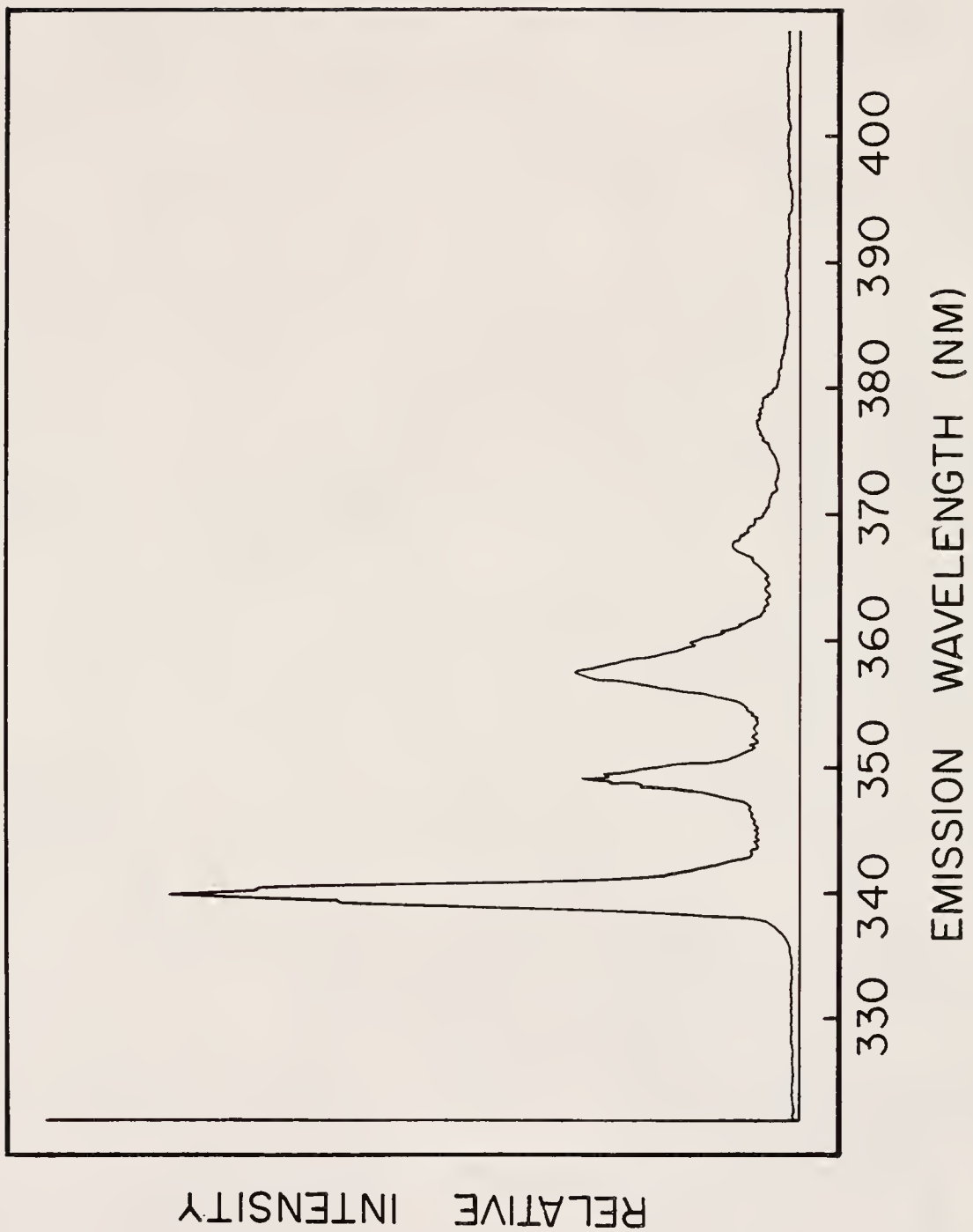
RELATIVE INTENSITY
330 340 350 360 370 380 390 400
EMISSION WAVELENGTH (NM)

Figure 52. LTCESF spectrum of 2,3-benzofluorene in n-heptane. $\Delta\bar{\upsilon}$ = 1.4 kK.

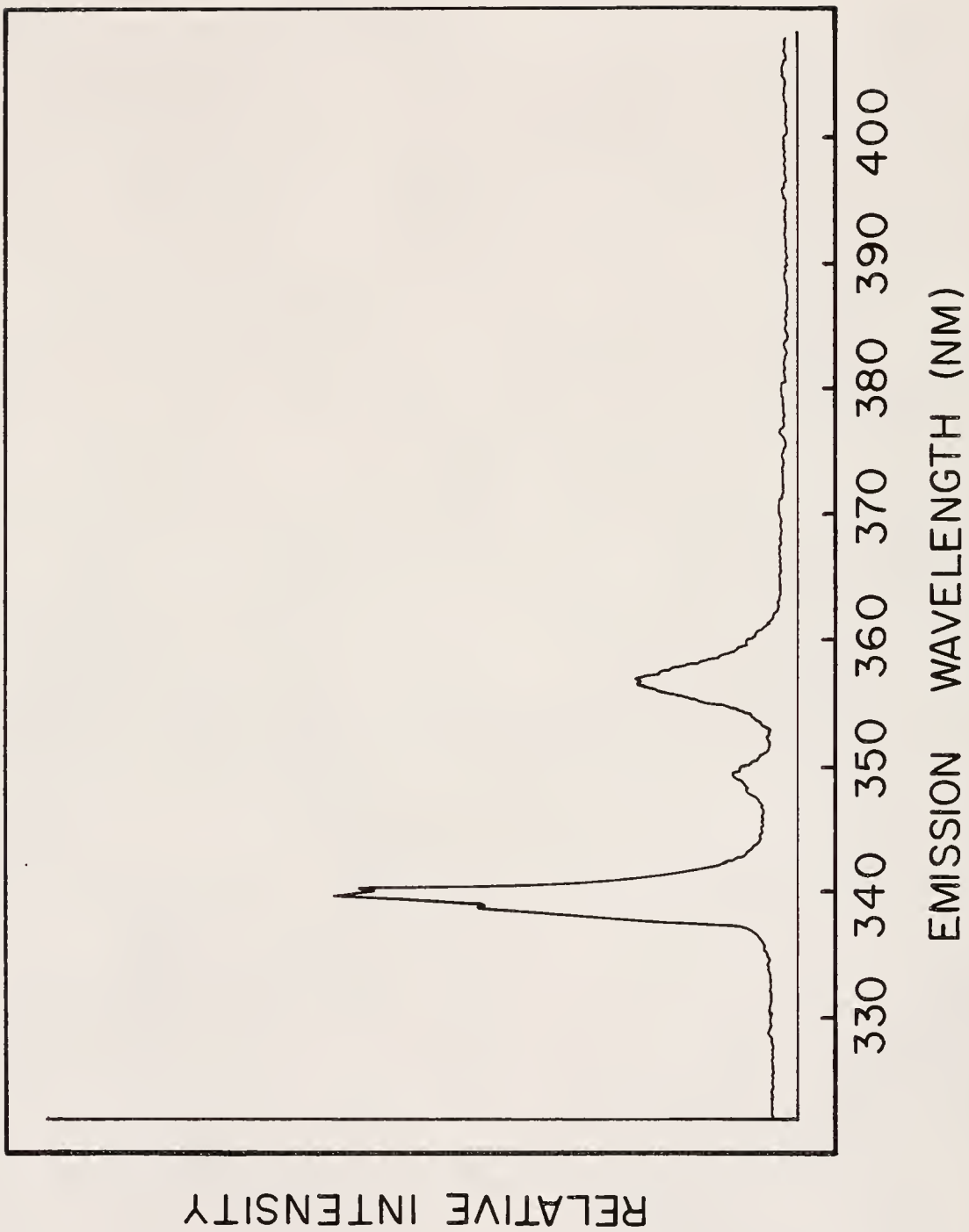
RELATIVE INTENSITY
330 340 350 360 370 380 390 400
EMISSION WAVELENGTH (NM)

Figure 53. LTCESF spectrum of 2,3-benzofluorene in n-heptane.
$\Delta\bar{\upsilon}$ = 2.8 kK.

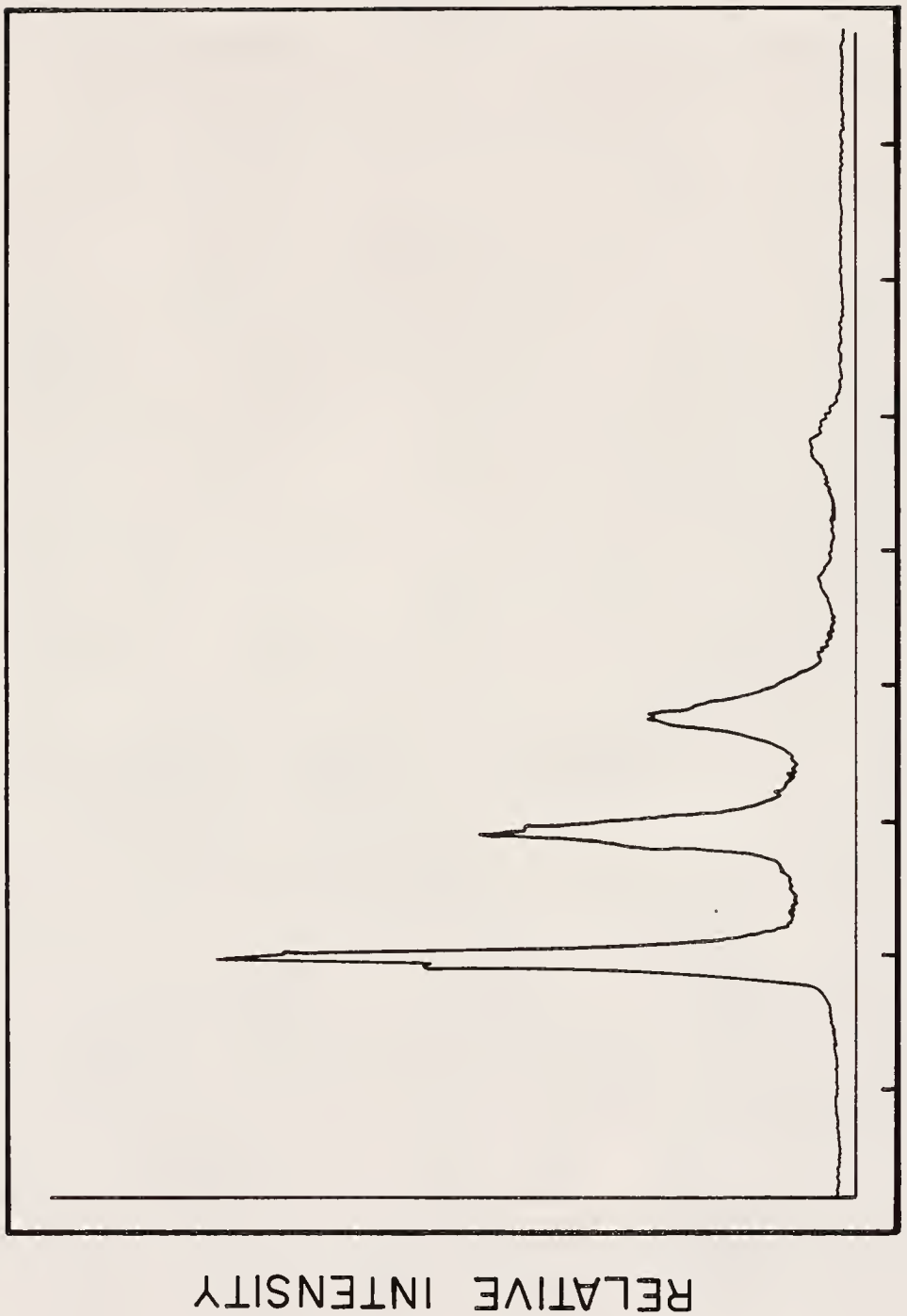
RELATIVE INTENSITY
330 340 350 360 370 380 390 400
EMISSION WAVELENGTH (NM)

vibrational transition energy, $\bar{\upsilon}_{0\text{-}v}$. If $Y(\bar{\upsilon}'_m)$ is the fluorescence intensity at $\bar{\upsilon}'_m$, then the entire emission spectrum, $\underline{Y}$, is described as

$$\underline{Y} = D(\bar{\upsilon}_{0\text{-}0}-\bar{\upsilon}_{0\text{-}v})S(\bar{\upsilon}'_m-\bar{\upsilon}_{0\text{-}v}) \tag{26}$$

A similar relationship can be described for the excitation spectrum. For a simple case, two assumptions are made. First, the absorption vibrational substructure is similar to that of the emission. While this is certainly not observed in all low temperature PAH spectra, it is approximately true for many. Also, the mirror image intensity distribution between the excitation and emission vibrational energies is assumed. Therefore,

$$D(\bar{\upsilon}_{0\text{-}0}-\bar{\upsilon}_{0\text{-}i}) = D(\bar{\upsilon}_{0\text{-}0}-\bar{\upsilon}_{0\text{-}j}) \tag{27}$$

for i equal to j, with i the excitation vibrational transition energy index and j the emission vibrational transition energy index. If $X(\bar{\upsilon}'_x)$ is the fluorescence excitation intensity at $\bar{\upsilon}'_x$, then the entire excitation spectrum, $\underline{X}$, is described

$$\underline{X} = D(\bar{\upsilon}_{0\text{-}0}-\bar{\upsilon}_{0\text{-}v})S(\bar{\upsilon}'_x-\bar{\upsilon}_{0\text{-}v}) \tag{28}$$

Substituting these relationships into Equation (9), the LTCESF spectrum is described as

$$\underline{M} = \alpha D(\bar{\upsilon}_{0\text{-}0}-\bar{\upsilon}_{0\text{-}i})S(\bar{\upsilon}'_x-\bar{\upsilon}_{0\text{-}i})D(\bar{\upsilon}_{0\text{-}0}-\bar{\upsilon}_{0\text{-}j})S(\bar{\upsilon}'_m-\bar{\upsilon}_{0\text{-}j}) \tag{29}$$

The distribution within a single vibrational substructure depends on two types of processes: those resulting in an approximately identical frequency distribution in both the excitation and emission spectra, and those that describe a mirror image relationship in the substructures. Each of these is of theoretical significance, as well as each has a major effect on synchronous spectra. If $\Delta\bar{\upsilon}$ in LTCESF is selected as multiple of 1.4 kK ($\bar{\upsilon}_{0\text{-}v}$), the positions of $\bar{\upsilon}_{0\text{-}i}$ and $\bar{\upsilon}_{0\text{-}j}$ approximately coincide, matching the largest intensities from each spectrum. The

distribution of frequencies within the vibrational substructures determines the ultimate limitation of LTCESF. For those features that are identical in both the excitation and emission substructures, complete overlap occurs and the features appear in the LTCESF spectrum. For those features that follow a mirror image relationship, overlap occurs only because of band broadening and those features will not appear in the ideal, infinitely narrow-line spectrum. The intensity distribution is much more complicated and will not be considered further.

Pyrene was selected for investigation because of its lack of a strong S_1 0-0 or 0-1 excitation transition and its complex fluorescence emission spectrum, shown in Figure 54. A LTCESF scan of a solution of pyrene in n-heptane with $\Delta\bar{\upsilon}$ of 1.4 kK yielded no peaks through its general emission range as expected. A $\Delta\bar{\upsilon}$ of 2.8 kK used in Figure 55 exhibits one set of peaks corresponding to 0-2/0-0 excitation/emission transitions. Figure 56 is the spectrum obtained with a $\Delta\bar{\upsilon}$ of 4.2 kK. Note that the positions of the peaks in LTCESF are essentially the same as in the conventional fluorescence emission spectrum. The relative intensities are different because the intensity is a function of the relative emission intensity, as well as, the relative excitation intensity in LTCESF, whereas, in conventional fluorescence emission, relative spectral intensities are functions of only the emission intensities in that the excitation wavelength is held constant. The pyrene spectra illustrate the reduction in spectral complexity by this technique.

In actuality, the pyrene example is much more complex than the simplified discussion given here. While the S_1 0-2 excitation

Figure 54. Low temperature fluorescence emission spectrum of pyrene in n-heptane. λ_{ex} = 337.0 nm.

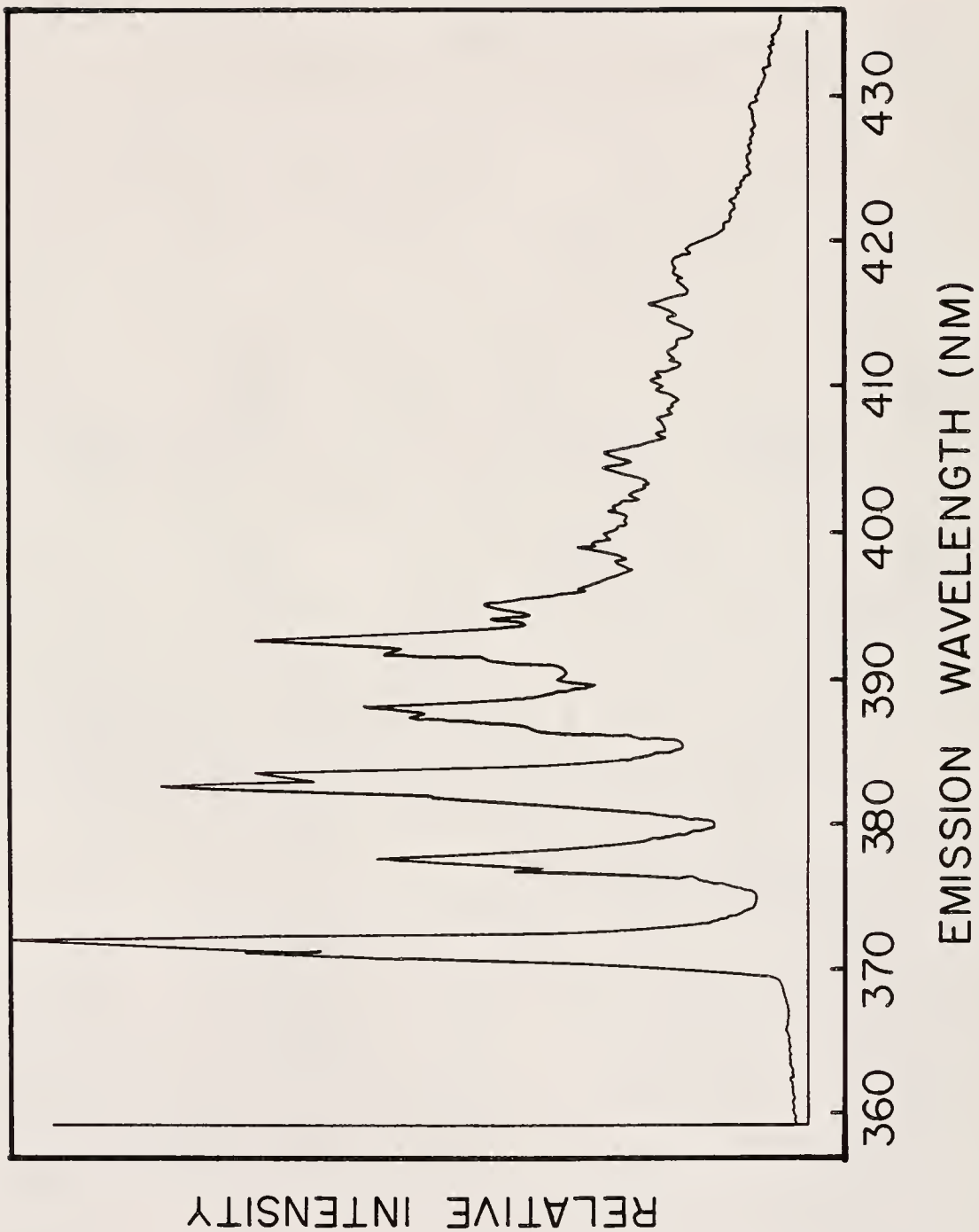
RELATIVE INTENSITY
360
370
380
390
400
410
420
430
EMISSION WAVELENGTH (NM)

Figure 55. LTCESF spectrum of pyrene in n-heptane. $\Delta\bar{\upsilon}$ = 2.8 kK.

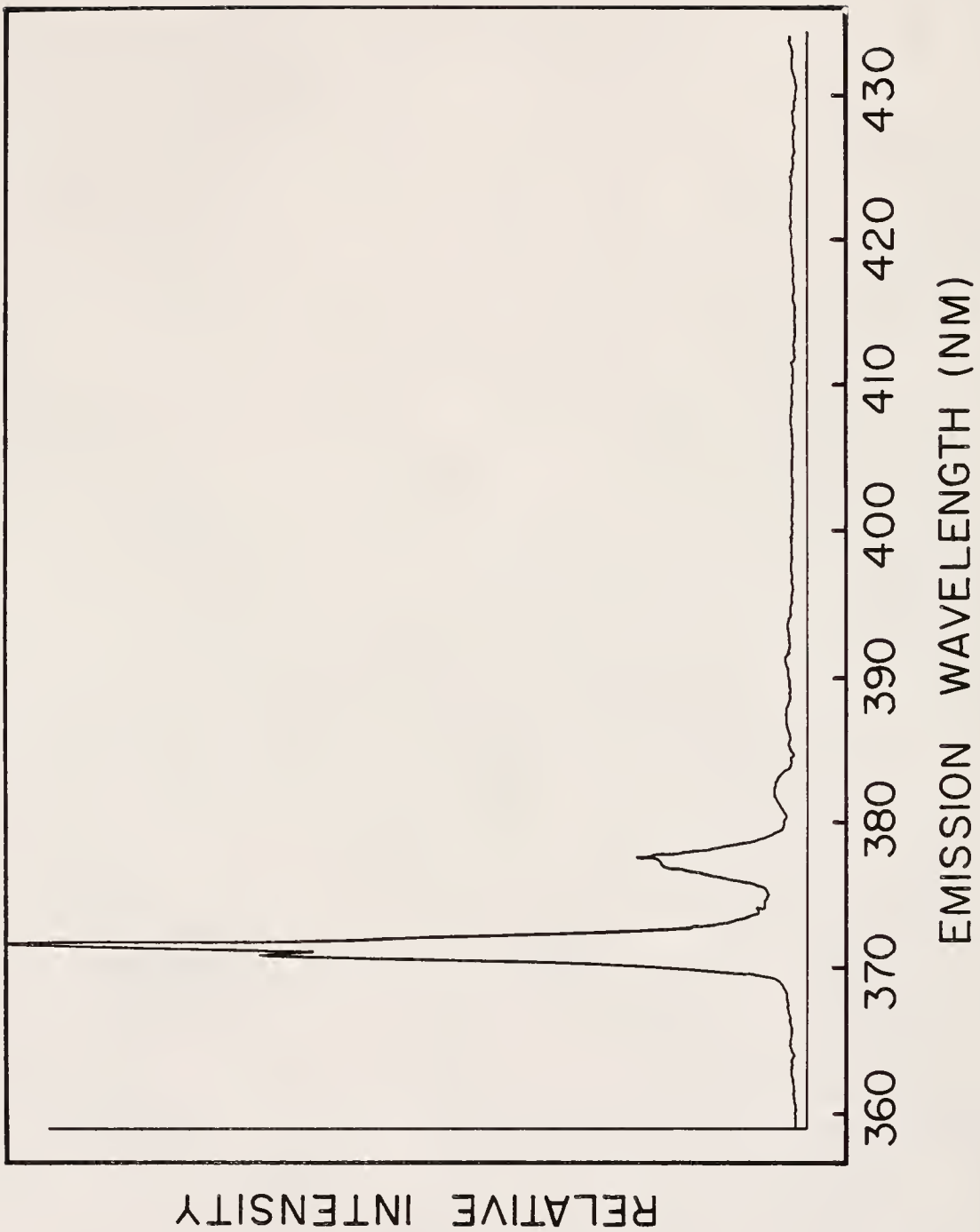
RELATIVE INTENSITY
360
370
380
390
400
410
420
430
EMISSION WAVELENGTH (NM)

Figure 56. LTCESF spectrum of pyrene in n-heptane. $\Delta\bar{\upsilon}$ = 4.2 kK.

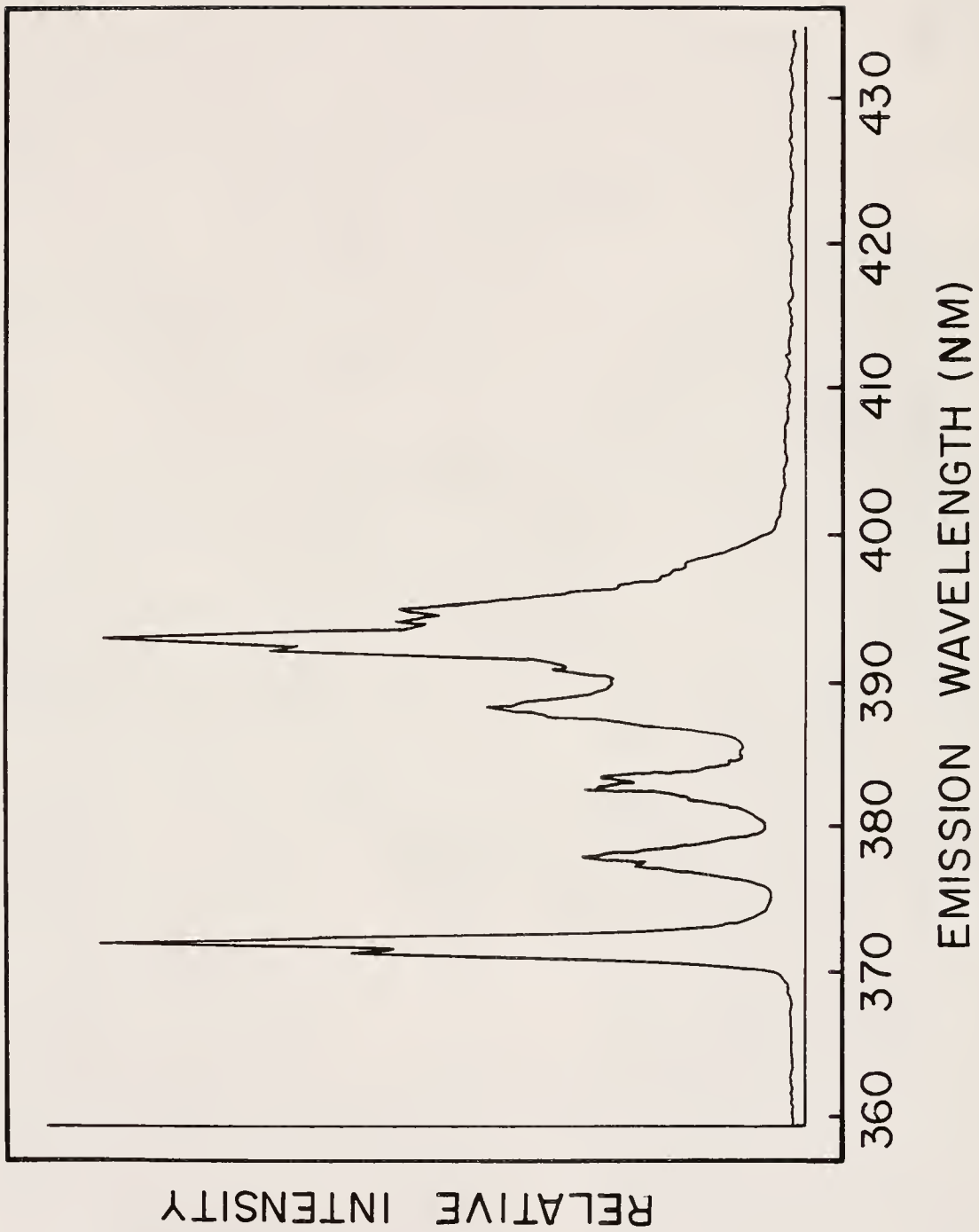
RELATIVE INTENSITY
360
370
380
390
400
410
420
430
EMISSION WAVELENGTH (NM)

transition is explainable by the Frank-Condon model, pyrene is known to have a low energy S_2 electronic state with its corresponding vibrational structure, overlapping the vibrational levels of the S_1 state. However, pyrene still supports the LTCESF model due to Herzberg - Teller vibrational coupling between vibrational levels of the S_1 and S_2 states. For a more complete discussion, see References 101 and 102.

While a vast array of peaks is interesting for physical studies, the analytical chemist usually does not need and cannot use all the information available. This has been stated by one synchronous spectroscopist that

> for the spectroscopist involved in fundamental research, the detailed structure of the entire emission spectrum is of crucial importance since it reflects directly the physical properties in which he is interested. For the analytical chemist, however, the details of the whole spectrum might not be of vital importance: usually he selects only one or several bands useful for his analysis, provided these spectrometric data are suitable for his needs (for example, direct correlation with the amount of analytes). Most of the other spectroscopic details are generally not considered and their presence serves only to confuse the total spectrum by interfering with the emission of other components in the mixture. (63)

Selection of $\Delta\bar{\upsilon}$ determines the complexity of the resultant spectrum. For pyrene, this is clearly demonstrated. By using LTCESF, the spectral range spanned by each compound is reduced, decreasing the probability of spectral overlap.

Many of the advantages of using energy relationships instead of wavelength relationships in SLS, as shown at room temperature, are even more important at low temperature. The $\Delta\bar{\upsilon}$ selected is characteristic of a group of compounds and is not unique for a single component thought to be present in the sample of interest. Also the $\Delta\bar{\upsilon}$ selected

is independent of the spectral region, whether working from 300 to 400 nm or 500 to 600 nm, unlike $\Delta\lambda$ selection in CWSF.

To demonstrate the potential utility of this technique in multi-component analysis, a seven-component PAH mixture was prepared in n-heptane. The compounds and their concentrations were: acenaphthene, 0.39 µg/mL; 2,3-benzofluorene, 0.20 µg/mL; pyrene, 0.40 µg/mL; 3,4-benzopyrene, 0.40 µg/mL; anthanthrene, 0.55 µg/mL; perylene, 0.90 µg/mL; and naphthacene, 0.90 µg/mL. These seven were selected to cover a large spectral range. Using selective excitation, several spectra would be required if all compounds were known before analysis. With no prior knowledge of the compounds present, even more excitation wavelengths are needed. Figures 57-60 show the spectra for the mixture and standard solutions of each component by LTCESF using a $\Delta\bar{\upsilon}$ of 1.4 kK and 2.8 kK. Six of the seven compounds are identified from the 1.4 kK scan. Pyrene, as described earlier, required the 2.8 kK scan. Thus, only two scans are required to characterize all seven components.

For mixtures of unknown composition, the LTCESF scan can be used as an aid to selective excitation techniques. This technique lacks many of the unique identification capabilities of the high resolution laser-excited techniques. However, when used properly, its potential appears widespread. The examples used have been limited to liquid nitrogen conditions. If liquid helium is used, additional narrowing is anticipated. A temperature of 0 K represents the ideal case for laser-excited techniques, approaching the homogeneous broadening limitations in fluorescence bandwidths.

The effort towards continuously reducing the experimentally achievable temperature for analysis is widespread in analytical

Figure 57. LTCESF spectrum of each component in the seven-component PAH mixture. $\Delta\bar{\upsilon}$ = 1.4 kK.

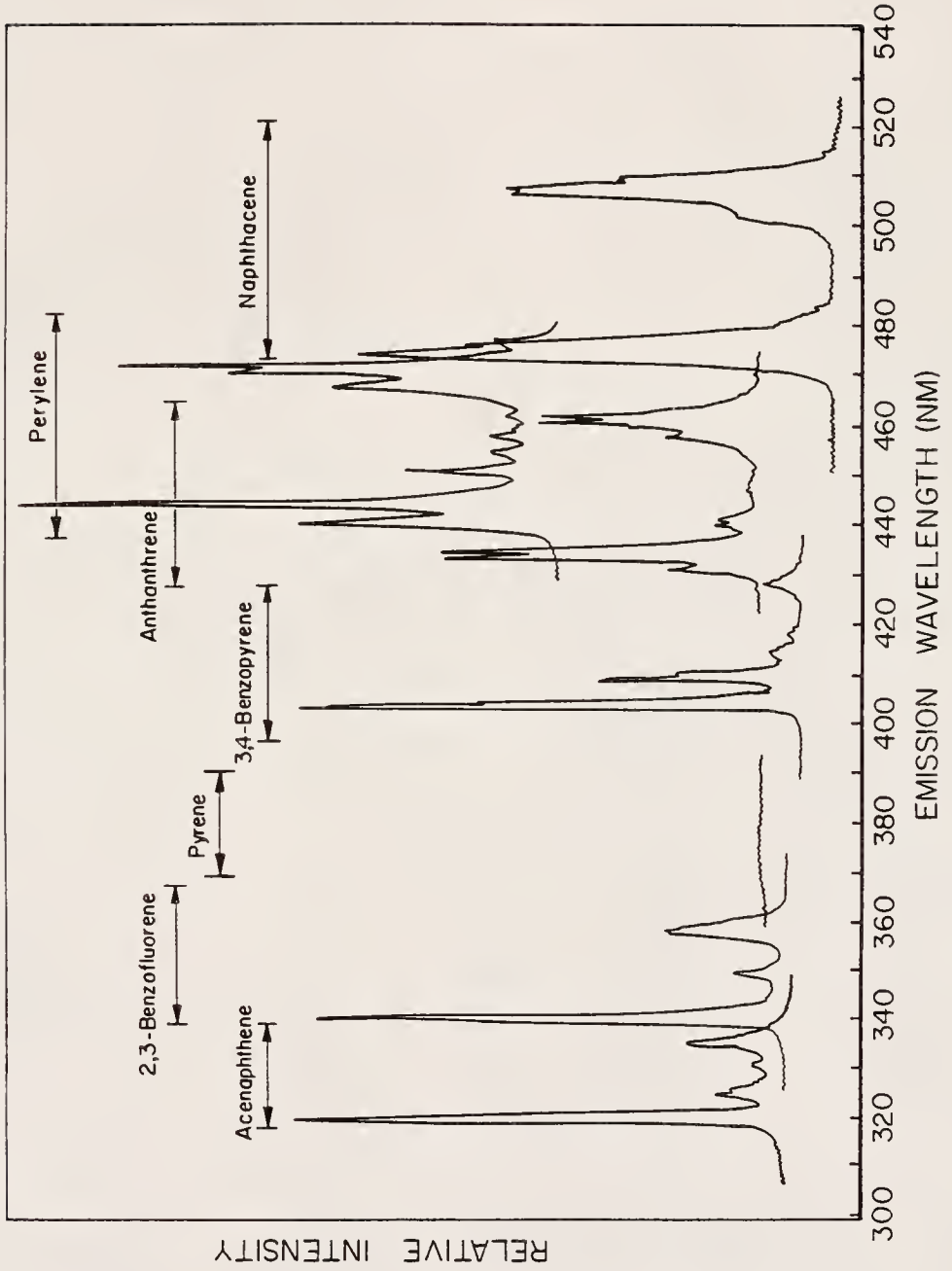
Perylene
Naphthacene
Anthanthrene
3,4-Benzopyrene
Pyrene
2,3-Benzofluorene
Acenaphthene
RELATIVE INTENSITY
300
320
340
360
380
400
420
440
460
480
500
520
540
EMISSION WAVELENGTH (NM)

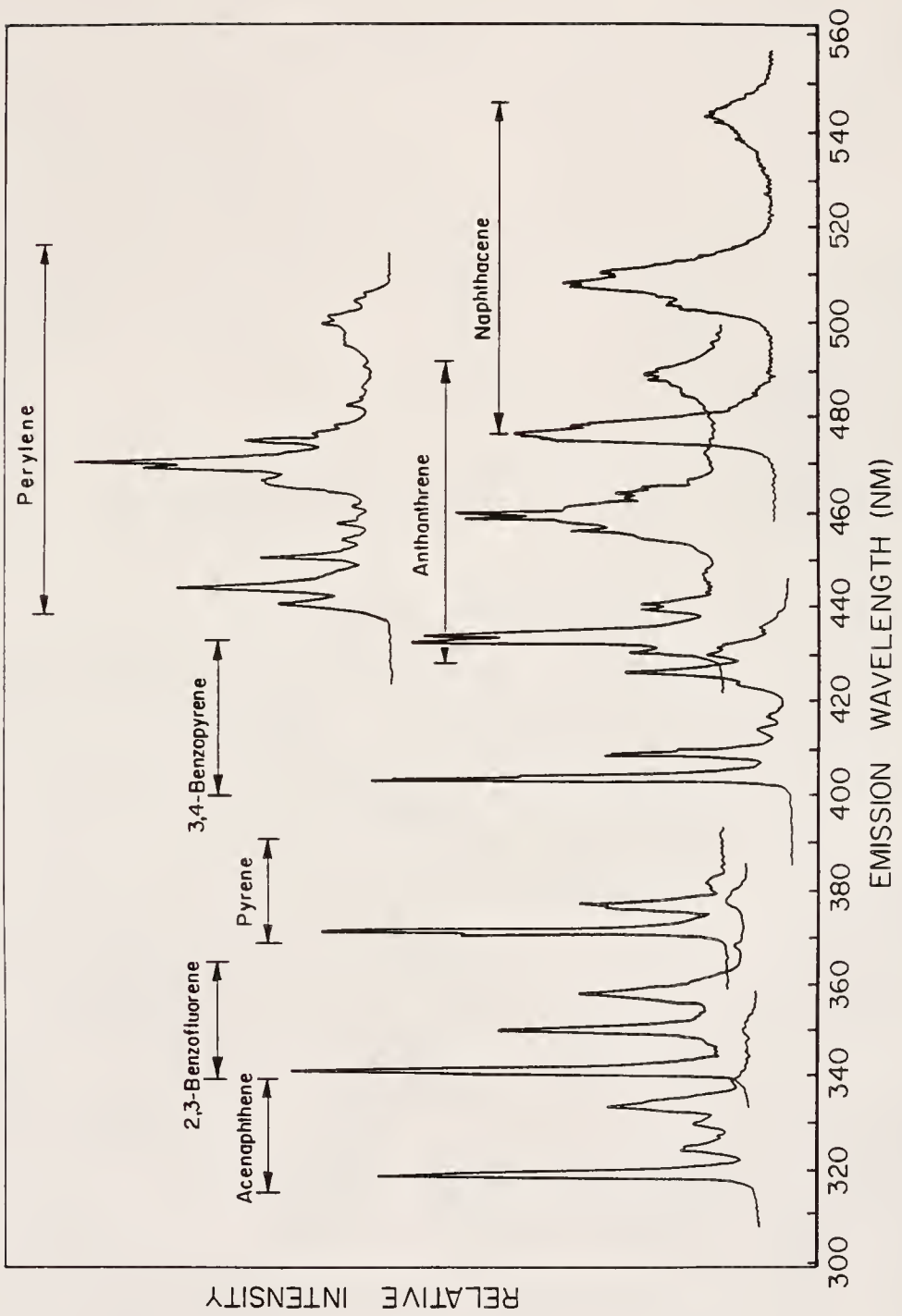
Perylene
3,4-Benzopyrene
Pyrene
2,3-Benzofluorene
Acenaphthene
Anthanthrene
Naphthacene
RELATIVE INTENSITY
300
320
340
360
380
400
420
440
460
480
500
520
540
560
EMISSION WAVELENGTH (NM)

Figure 59. LTCESF spectrum of seven-component PAH mixture. $\Delta\bar{\upsilon}$ = 1.4 kK.

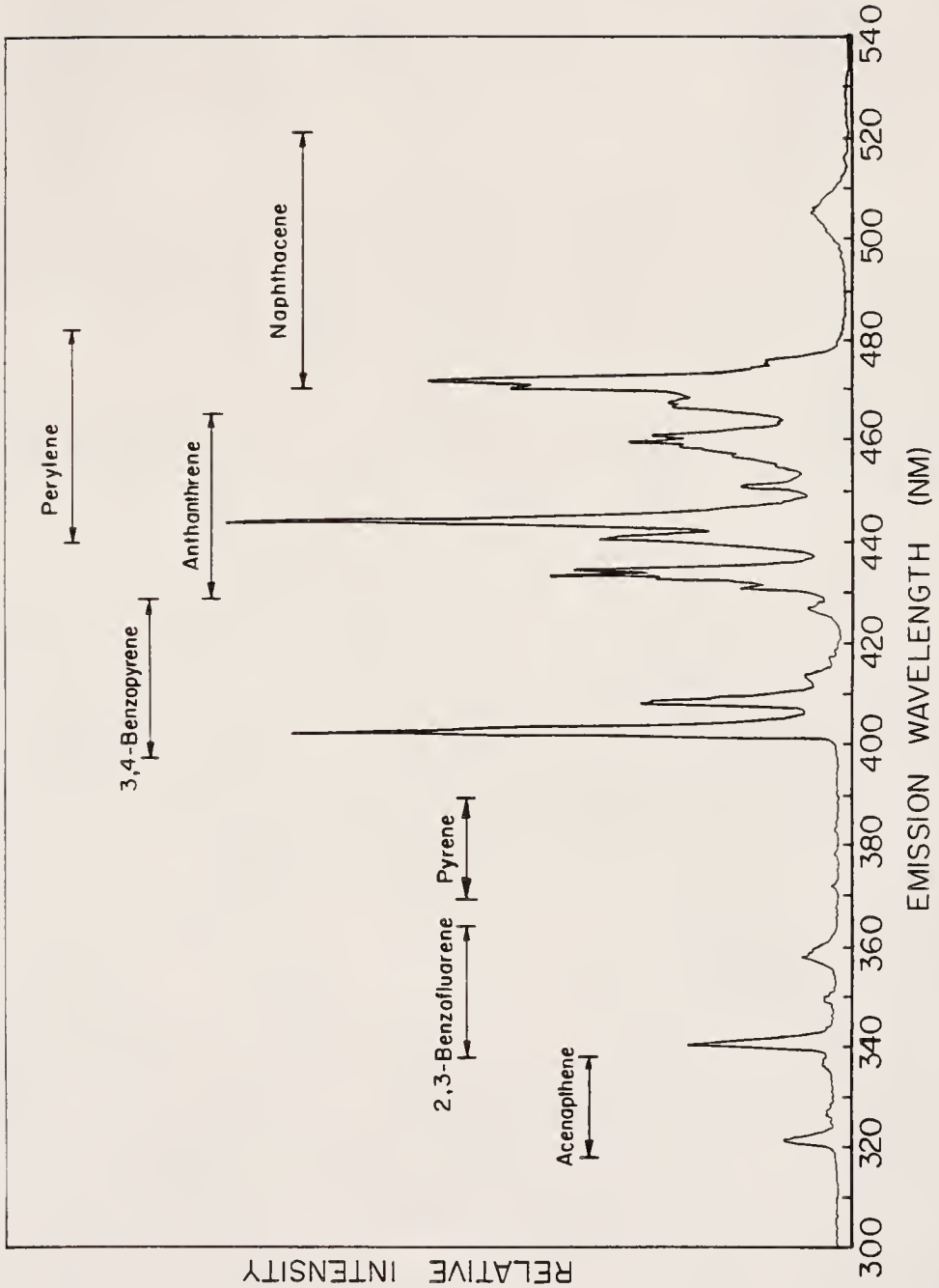
Perylene
3,4-Benzopyrene
Anthanthrene
Naphthacene
Pyrene
2,3-Benzofluarene
Acenapthene
RELATIVE INTENSITY
300
320
340
360
380
400
420
440
460
480
500
520
540
EMISSION WAVELENGTH (NM)

Figure 60. LTCESF spectrum of seven-component PAH mixture. $\Delta\bar{\upsilon}$ = 2.8 kK.

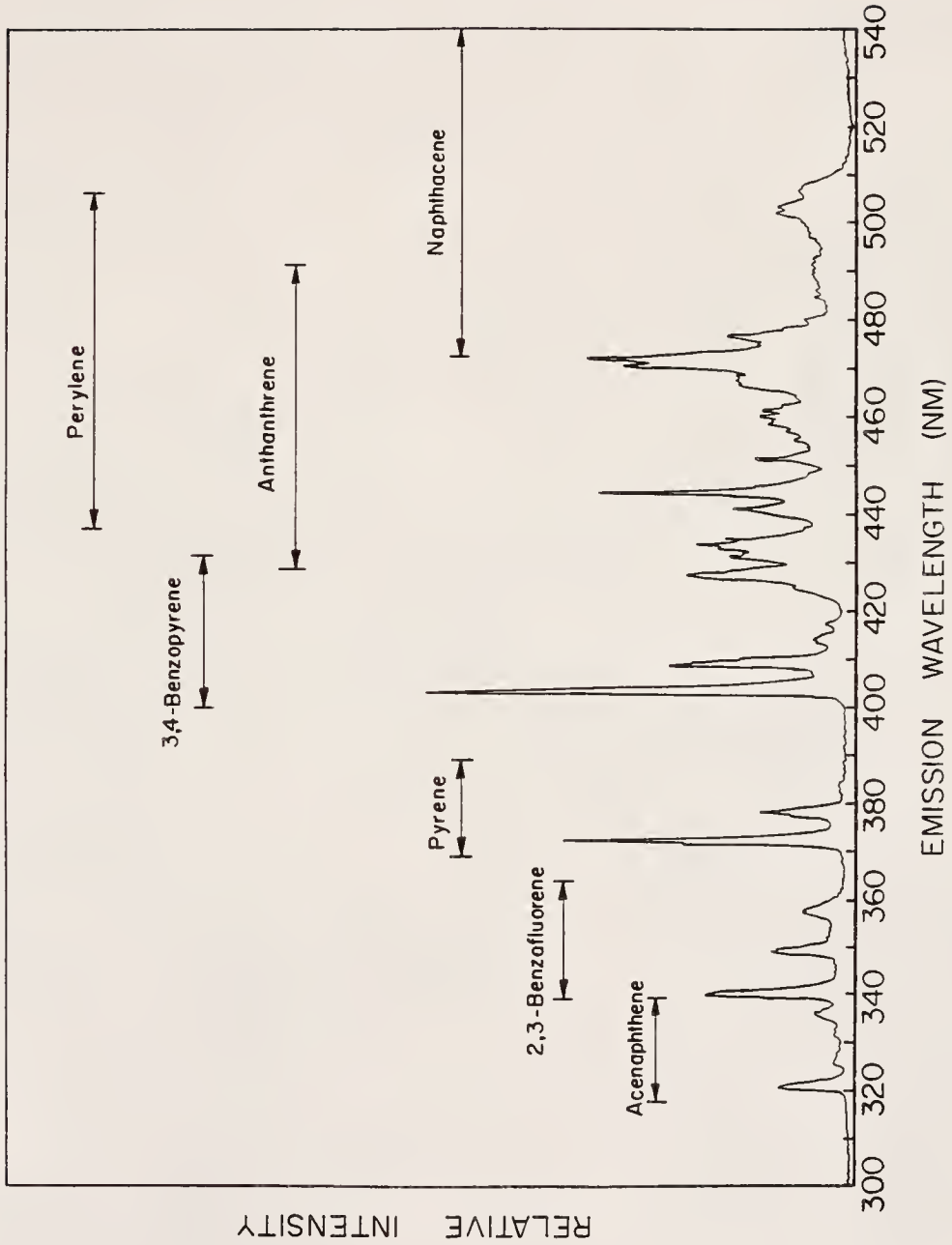
Perylene
3,4-Benzopyrene
Anthanthrene
Naphthacene
Pyrene
2,3-Benzofluorene
Acenaphthene
RELATIVE INTENSITY
300
320
340
360
380
400
420
440
460
480
500
520
540
EMISSION WAVELENGTH (NM)

chemistry. But the conclusion from this work is that below a temperature limit, LTCESF seriously breaks down for many reasons. The $\Delta\bar{\upsilon}$ approximation of 1.4 kK for PAHs is just that, an approximation. Band broadening, to some extent, is a major reason for the success of CESF. Many of the vibrational energy spacings and the assumed independence from solvent and temperature effects are also approximations. For infinitely narrow-line spectra, a $\Delta\bar{\upsilon}$ must be selected for each compound of interest. While this suggests a powerful selectivity advantage, it becomes a complicated form of selective excitation. Also the practicality of low temperature spectroscopy seems questionable (103) until technological advancements make major improvements in present instrumentation.

From the conclusions drawn from this work, one can speculate on the effect the availability of an easily tunable laser excitation source, scannable over a wide range of wavelengths, would have on low temperature SLS techniques. One consideration is the site selection capabilities of a narrow-band excitation source. As pointed out, the presence of multiple sites for molecular orientation within the solvent matrix is distinguishable within LTF spectra. Essentially, the distribution of vibrational levels for each site is identical, with a difference in electronic transition energy only. Because of this, it is expected that if a narrow-line laser is used as the excitation source and is synchronously scanned, the multiplet of sites would appear in the LTCESF spectrum. Thus site selection is not possible in SLS. Combined with liquid helium temperatures, narrow-line excitation may produce spectra that are difficult to interpret because of the approximations on which the assumptions are based. This is an area for future investigation.

Spectral features that are observable in laser-excited fluorescence spectra obtained at 4 K are often called phonon sidebands or phonon wings. These phonon sidebands appear as low intensity, broad bands next to the sharp, intense lines characterisitic of LTF spectra. They appear to the lower energy side of emission lines and to the higher energy side of excitation lines. Effectively, they appear as mirror images and extend out about 0.100 kK. Using LTCESF, these phonon sidebands should not appear, a definite selectivity advantage in that these phonon sidebands provide little analytical information.

The high resolution capabilities of laser excitation will continue to make techniques such as Matrix Isolation Spectroscopy and Fluorescence Line Narrowing Spectroscopy areas of considerable interest. But synchronous techniques combined with LTF give additional flexibility, with practical advantages for routine analysis. Its applicability must be evaluated for the specific needs of the analysis.

Phosphorescence Spectroscopy

Low Temperature Phosphorescence Spectroscopy (LTP) is another luminescence technique of interest in PAH analysis. Many PAHs phosphoresce intensely, adding another selectivity capability (104). An LTP system has been described that is red region sensitive, specifically designed for the phosphorescence of PAHs (105). Although extensive research has been done on the phosphorescence analysis of PAHs, it is not used routinely. This is perhaps due to a lack of sensitivity compared to fluorescence techniques.

While the use of synchronous techniques in phosphorescence spectroscopy has been extensively discussed by Vo-Dinh for room temperature conditions (68,106-108), LTP has only recently been

combined with SLS (109). In an effort to apply SLS methods to LTP, an underlying goal was sought, analogous to this development for RTF. That is, a technique that can be traced directly to phosphorescence theory was the objective. It appeared that this development could parallel the previous work for RTF and LTF. This would make LTP an extension of the SLS theory developed throughout this work.

The phosphorescence spectra for PAHs show many spectral features that are similar to fluorescence spectra. Vibrational spacing in phosphorescence emission spectra are approximately the same as in fluorescence spectra. To illustrate, phosphorescence data were used from previous work (104). Using a conventional low-resolution fluorimeter with a phosphoroscope attachment, the peak wavelengths were obtained from a number of PAHs. The vibrational spacings in the phosphorescence emission spectra for several PAHs are listed in Table 12. The estimated error for each wavelength is about 1 nm. These energy differences agree fairly well with the 1.4 kK energy differences observed in fluorescence spectra.

To evaluate the use of constant energy synchronous concepts in LTP, the potential energy diagram in Chapter 1 must be considered. Phosphorescence generally occurs from the lowest vibrational state of the first excited triplet. Phosphorescence emission occurs at longer wavelengths than fluorescence emission because the lowest vibrational level of the first excited triplet state is lower in energy than the lowest vibrational level of the first excited singlet state. This difference is referred to as the singlet-triplet energy difference, Δ_{ST}.

To apply CESF to LTP, the $\Delta\bar{\upsilon}$ must be selected to match the energy characteristics of the analyte. From the above discussion, $\Delta\bar{\upsilon}$ is

Table 12. Phosphorescence Emission Vibrational Spacing for Several PAHs

Compound	Peak Wavelength (nm)	Energy Difference (kK ± 0.2 kK)
Acenaphthene	478, 513, 556	1.4, 1.5
1,2-Benzofluorene	500, 540	1.5
2,3-Benzofluorene	500, 540	1.5
1,12-Benzoperylene	616, 673	1.4
1,2-Benzopyrene	540, 590, 652	1.6, 1.6
3,4-Benzopyrene	685, 751 698, 766	1.3 1.3
Chrysene	499, 540	1.5
1,2:3,4-Dibenz-anthracene	566, 618, 678	1.5, 1.4
1,2:5,6-Dibenz-anthracene	556, 603	1.4
Fluoranthene	545, 592, 646 564, 613	1.5, 1.4 1.4
Fluorene	420, 450	1.6
9-Methylanthracene	414, 444, 480	1.6, 1.7
Phenanthrene	462, 498, 534	1.6, 1.4

selected as

$$\Delta\bar{\upsilon} = \Delta_{ST} + nv \qquad (30)$$

where v is the vibrational energy spacing and n is an integer. The value of n is usually between 0 and 2. Spectral detail increases with larger values of n, similar to LTCESF. While a value of 0 for v is experimentally impractical for fluorescence (S_0, S_1 transitions), it can be used for LTCESP because Rayleigh scatter is no longer a problem.

Vo-Dinh and Gammage (110) recognized the selectivity potential of Δ_{ST} in SLS. They described the use of the singlet-triplet energy difference to optimize $\Delta\lambda$ in CWSL, using room temperature phosphorescence. The value of Δ_{ST} is specific for each PAH in the mixture, with $\Delta\lambda$ calculated as an approximation to this energy difference. It was found that for multicomponent analysis, a series of $\Delta\lambda$ can be selected, with analysis beginning with the smallest $\Delta\lambda$. The value of Δ_{ST} depends on the chemical nature of the phosphorescent compound with molecules that have similar structures having similar singlet-triplet energy differences.

Further investigation of energy relationships in LTP spectra indicated that these concepts are correct, but no further significant characterization resulted. Another related physical process is the excitation of a molecule into a singlet electronic state other than the first excited singlet. Because emission occurs from the first excited singlet or triplet, this corresponds to an excess of energy in the excitation process over the emission process. Two equations similar to Equation (30) can be written to include this situation. For fluorescence, this becomes

$$\Delta\bar{\upsilon} = \Delta_{S_n - S_1} + nv \qquad (31)$$

and for phosphorescence

$$\Delta\bar{\upsilon} = \Delta_{S_n-S_1} + \Delta_{ST} + nv \qquad (32)$$

where $\Delta_{S_n-S_1}$ is the energy difference between the lowest vibrational states of the nth excited singlet state and the first excited singlet state.

At this point, a question of considerable importance is the extension of the concepts of LTCESL to other groups of compounds. For example, polynuclear aromatic compounds with a heteroatom of nitrogen or oxygen are present in oil samples, where they contribute to the luminescence of the sample. Carbonyl compounds often exhibit vibrational structure at the carbonyl frequency of 1.750 kK, while the Raman frequency of 1.45 kK can be seen in compounds with nitro groups (111). A complementary study to this work involves an analysis of low temperature infrared and Raman spectra and the potential optimization of $\Delta\bar{\upsilon}$ selection (93,112). This would be especially useful for quinolines, quinones, and N-heterocyclics.

Synchronous Profiles

The concept of synchronous profiles, introduced in Chapter 3, can be extended to LTCESL, as demonstrated for a solution of 1,2-benzopyrene. The conventional excitation and emission spectra are shown in Figures 61A and 61B with wavelength and energy units, respectively, using the TLS instrument with 2 nm bandpasses. The emission from 370 to 475 nm corresponds to fluorescence, while phosphorescence is observed beyond 530 nm. The synchronous profiles for this solution are shown in Figures 62A and 62B. The profile in energy units is similar to the RTF profile (Figure 45) with the phosphorescence effect clearly visible. The 1.4 kK peak separation is maintained throughout this profile.

Figure 61. Low temperature luminescence excitation and emission spectra of 1,2-benzopyrene in n-heptane plotted in:

A. wavelength units

B. energy units

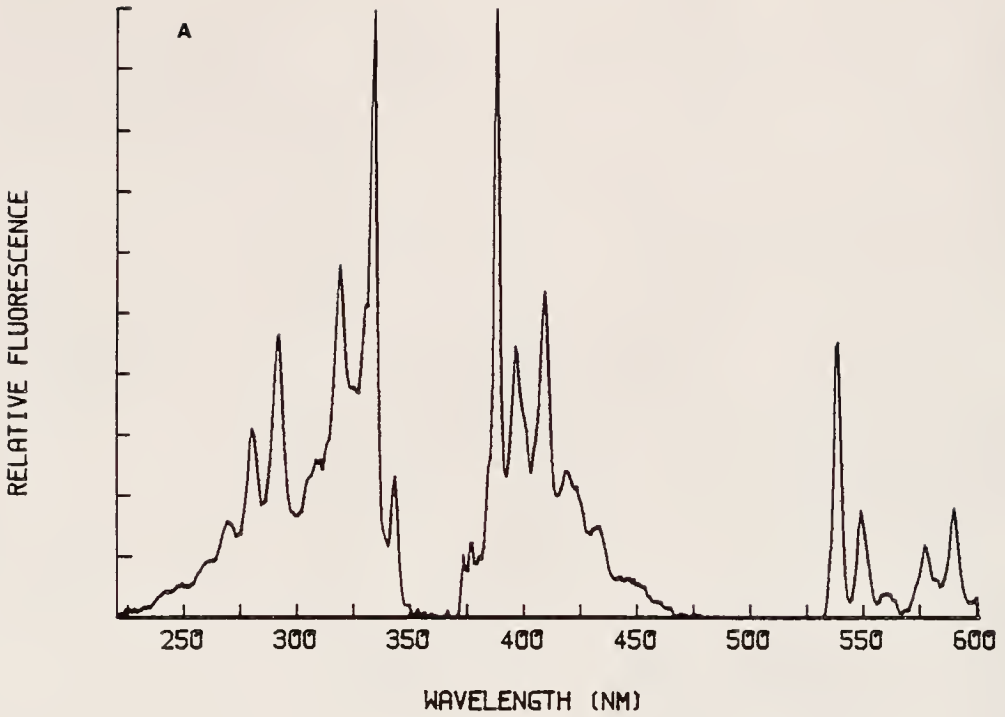
A
RELATIVE FLUORESCENCE
250
300
350
400
450
500
550
600
WAVELENGTH (NM)

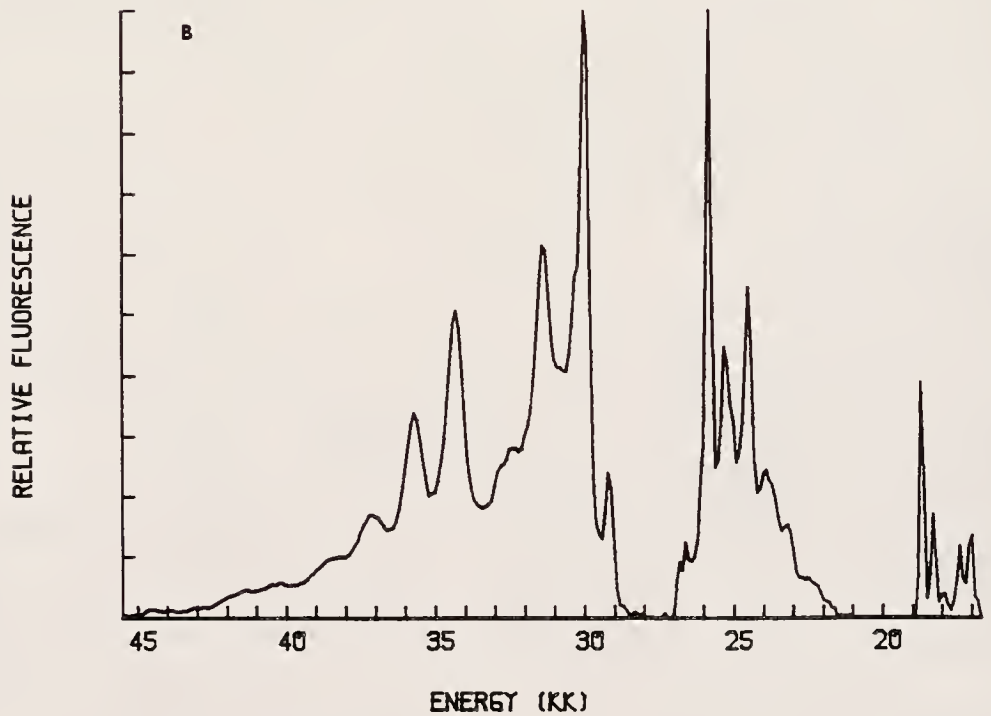
B
RELATIVE FLUORESCENCE
45
40
35
30
25
20
ENERGY (KK)

Figure 62. A. LTCWSL profile for 1,2-benzopyrene in n-heptane.

B. LTCESL profile for 1,2-benzopyrene in n-heptane.

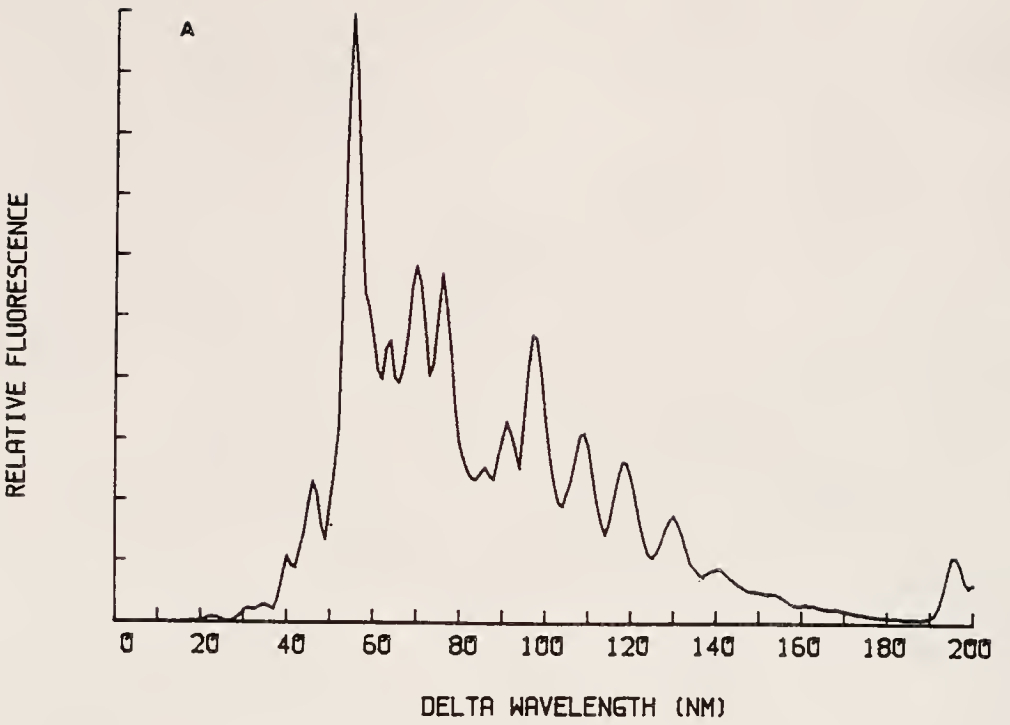
A
RELATIVE FLUORESCENCE
0
20
40
60
80
100
120
140
160
180
200
DELTA WAVELENGTH (NM)

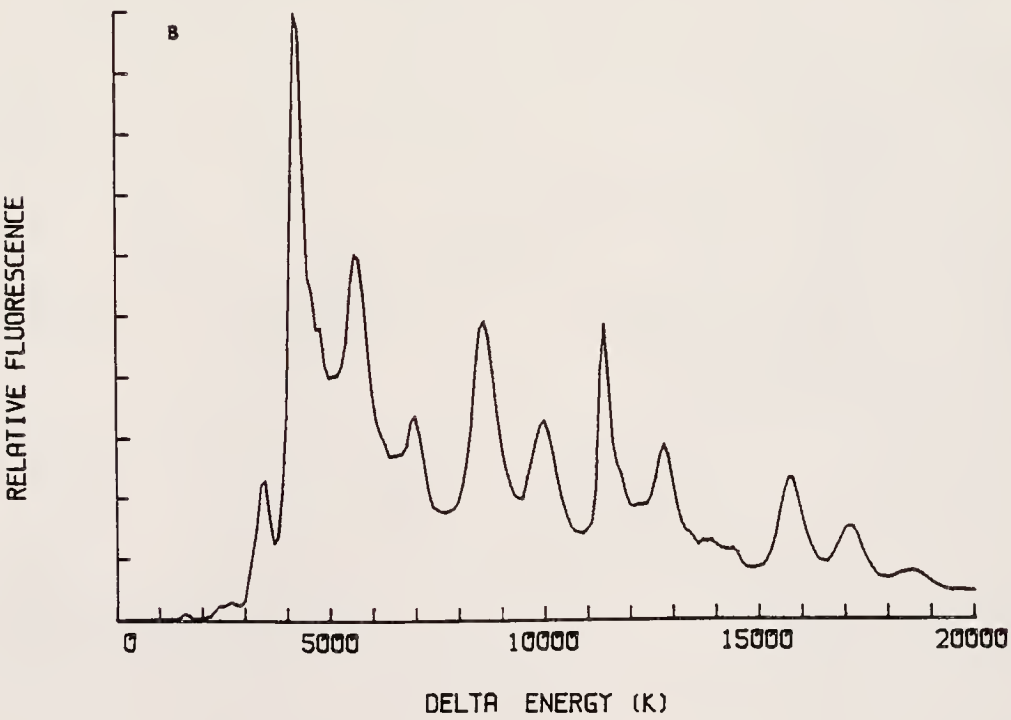
B
RELATIVE FLUORESCENCE
0
5000
10000
15000
20000
DELTA ENERGY (K)

Conclusions

Low temperature spectroscopy demonstrates increasing selectivity advantages by the reduction of spectral bandwidths, offering fingerprint spectra with potential in complex mixture analysis. The use of synchronous techniques at low temperature can provide an effective screening method for PAH analysis especially as a complement to laser-excited techniques. By tracing parameter selection to low temperature luminescence theory, the abundance of information available in LTF and LTP spectra can be more effectively used for analyte identification and quantitation.

CHAPTER 5
MATHEMATICAL AND STATISTICAL METHODS

Introduction

The matrix format of TLS data files suggests a wide variety of mathematical and statistical methods for computer recognition of information relating the data to chemically significant characteristics. The principles of linear algebra are presently experiencing extensive application in several analytical areas, especially in the analysis of mass spectroscopic data. Techniques such as factor analysis, rank annihilation, and multiple linear regression make use of the entire TLS data set. These are especially powerful for data that represent considerable spectral overlap. For many cases where instrumental resolution is inadequate, selectivity can be enhanced by use of these methods.

The research efforts of spectroscopists at the University of Washington have produced a considerable list of articles discussing the merits of several statistical methods of TLS data evaluation. Their contribution represents a combined effort of a large number of researchers and would require a number of years to duplicate. But because their work encompasses many principles that are important for a complete understanding of this research, it was decided to attempt a preliminary investigation of this area with no intention of completing a comprehensive study. From this investigation, several projects were completed and will be discussed briefly.

This chapter will be presented in six parts. Initially, the basic principles of linear algebra as they apply to TLS data will be discussed. Then these principles will be used to explain the data smoothing routines that were written for the TLS system in Chapter 2. Multiple linear regression, as used in Chapter 3, will be briefly outlined. Factor analysis is then used to determine the number of fluorescing components in a mixture. In contrast to the sophistication of these statistical methods, a simple spectral ratioing method is described for analyte identification. Finally, the application of correlation methods to TLS data files will be presented.

Software development of the statistical programs for the TLS system has depended heavily upon the Scientific Subroutine Package that was obtained from DEC to be used with the PDP 11/34 system. Table 13 summarizes the software development for the work presented in this chapter. A more complete description of each program is included in the appropriate section.

Basic Matrix Principles

Using a calibrated detection system, one generally needs to obtain k measurement values to quantitate a k-component mixture under ideal conditions. For example, in spectrophotometry, a series of absorbance measurements can be made at selected wavelengths, sufficient to characterize the absorption properties of each component in the mixture, for a series of solutions containing varying concentrations of the same components. If all measurements are made under noise-free conditions, the concentrations of all the components in all the solutions can be obtained algebraically. However, for real measurements, various noises are present and can significantly affect these calculations. If the

Table 13. Statistical Programs and Subroutines Used in TLS Data Evaluation

CROSS	Main program to perform cross-correlation calculations
CORREL[a]	Assembly language routine to perform cross-correlation calculations
FFT[a]	Assembly language routine to perform fast Fourier transformation calculations
FACTO	Main program to perform factor analysis
CORRE[b]	FORTRAN routine to create correlation matrix from TLS data file
EIGEN[b]	FORTRAN routine to compute eigenvalues and eigenvectors of a real symmetrical matrix
TRACE[b]	FORTRAN routine to compute cumulative percentage of eigenvalues
LOAD[b]	FORTRAN routine to compute a factor matrix (loading) from eigenvalues and eigenvectors
VARMX[b]	FORTRAN routine to perform orthogonal rotations of a factor matrix
SIMULT	Main program to perform multiple linear regression calculations
GDATA[b]	FORTRAN routine to generate independent variables and correlation matrix
ORDER[b]	FORTRAN routine to construct a matrix of intercorrelations
MINV[b]	FORTRAN routine to invert a matrix
MULTR[b]	FORTRAN routine to perform multiple linear regression analysis

[a]Used as provided by DEC

[b]Modified version of DEC routine

noise on these measurements is random in nature, greater confidence can be placed on the results if more measurements are made. For k-component mixtures, measurements are made at p wavelengths for q solutions, where p and q are greater than or equal to k. Mathematically, this is stated as

$$A_{qp} = \sum_{i=1}^{k} c_{qi}\varepsilon_{ip} \tag{33}$$

where A_{qp} is the absorbance at wavelength λ_p for solution q, c_{qi} is the concentration of the ith component in solution q, and ε_{ip} is the molar absorptivity of the ith component at wavelength λ_p.

The matrix $\underline{A}$ is a vector space spanned by the column vectors $\{\underline{C}_q\}$ and by the row vectors $\{\underline{\varepsilon}_p\}$ (113). A basis set of row vectors and column vectors can be found that span this vector space where each vector is linearly independent. A linearly independent vector is an element within the vector space that cannot be obtained by a linear combination of the other vectors within the basis set. The basis set of row vectors will contain k elements, with $k \leq q$, and the basic set of column vectors will contain k elements, with $k \leq p$. The rank of the vector space is equal to k, the minimum number of linearly independent vectors spanning the vector space.

These concepts can be translated directly to the TLS data relationship defined in Equation (9). The rank of the matrix $\underline{M}$ is r, with the set $\{\underline{X}_r\}$ representing the luminescence excitation spectra for the r components, and the set $\{\underline{Y}_r\}$ representing the luminescence spectra for the r components. If the TLS data matrix can be reduced to a set of row vectors and a set of column vectors that correspond to luminescence characteristics of the components in a mixture, these vectors can be compared to a standard set of known vectors for proper

identification of each component. Theoretically, the number of components that can be resolved can be increased by expanding the dimensions of the data matrix M.

Data Smoothing

The original TLS matrices of raw data are noisy due to lamp fluctuation and noise sources within the detection system. Because of the rapid scan rates used to acquire TLS data, the time constant of the gain amplifier is shorter than in conventional luminescence measurement systems, increasing high frequency noise. If the time constant is increased, noise is reduced, but detector response will lag behind the actual photophysical process. To reduce the random noise in the raw data set, a digital smoothing routine was developed.

A k-nearest neighbor smooth is commonly used in analytical data systems (114). The basic principle of k-nearest neighbor smoothing is that the nearest data points in the data matrix most closely resemble the characteristics of the data point of interest. An approximation is made that the difference in value between two points of close proximity is due mainly to random noise in the measurement system, if the sampling frequency is large enough. This is valid if the data collection process is rapid enough that small parameter changes are made during the time interval between the collection of two data points. To implement this method, each point is replaced by the weighted average of its k nearest neighbors. In the Videofluorometer system, pixel summing is performed for groups of 2X2 pixels, reducing the number of data points by 75%. Polynomial smoothing algorithms, such as the Savitsky-Golay smooth (115), are available using a variable number of neighboring points. These perform similarly to a low pass filter and cause some spectral distortion (116).

A smoothing routine was desired that would make use of the principles of linear algebra for single component TLS spectra. The rank of each matrix is one, suggesting that each row is formed from the product of a basis row vector and an intensity scalar, and each column is formed from a corresponding basis column vector and intensity scalar. Therefore, each row and column can be regenerated from the basis vectors and intensity scalars. In actuality, the intensity scalars are also contained in the basis vectors. The problem reduces to acquiring representative basis vectors. A solution to this problem resembles the smoothing ability of time averaging or repetitive scanning. To produce the row vector, the values in each column of the raw data matrix are summed and divided by the number of rows. Each row in the TLS data file is replaced by a row generated by summing the points in each row, dividing by the summed basis row, and multiplying the quotient by the basis row vector. The approximate noise reduction is proportional to the square root of the product of the number of rows and columns used for the smoothing process.

Multiple Linear Regression

Multiple linear regression calculations are especially useful for determining the concentrations of a series of components whose contribution to a measurement array is numerically predictable. It is this procedure that was used in Table 10 of Chapter 3. Briefly, the mixture data row corresponds to the solution array, equivalent to a matrix $\underline{B}$ of coefficients multiplied by a concentration array. The columns of $\underline{B}$ are reference arrays for the individual components that are potentially represented in the mixture array. For quantitation, the concentration array is obtained by solving the augmented matrix

that is described as

$$\underline{Bc} = \underline{d} \tag{34}$$

$$\underline{c} = \underline{B}^{-1}\underline{d} \tag{35}$$

Although the mathematical details of this method are well-known (117), its application to analytical data reduction is only beginning to become popular (118-120). This description is included here because of its ability to quantitate mixtures with extensive overlap, making use of the entire available data set. Ideally, the reference spectra can be selected from a library of spectra measured under identical conditions.

A multiple linear regression program was written and evaluated to determine its utility in quantitating synchronous spectra exhibiting extensive overlap. Its performance has been demonstrated by the simulation studies in Chapter 3. To evaluate this procedure for raw data and to determine the effect of noise and instrumental drift, a challenging mixture was analyzed. A five-component mixture was prepared that was composed of 9,10-dimethylanthracene, 0.42 μg/mL; anthracene, 0.40 μg/mL; 2-methylanthracene, 0.41 μg/mL; 9-methylanthracene, 0.43 μg/mL; and 9,10-diphenylanthracene, 0.36 μg/mL in n-heptane. The CESF spectra for the reference solutions of these five compounds are shown in Figure 63 with a $\Delta\bar{\upsilon}$ of 1.6 kK. The reference solutions were prepared at the same concentrations as in the mixture. The spectra show considerable noise, purposely included for this evaluation. The similarity of these spectra makes manual quantitation difficult, evidenced by the mixture spectrum in Figure 64.

The coefficient matrix, $\underline{B}$, was generated from the digitized spectra, selecting 151 points for each column, spanning from 350 to 500 nm in 1 nm increments, with the solution array, $\underline{d}$, generated from the

Figure 63. CESF spectra using a $\Delta\bar{\upsilon}$ of 1.6 kK of:

——— 9-methylanthracene
---- 9,10-diphenylanthracene
-.-. 2-methylanthracene
°°°° 9,10-dimethylanthracene
.... anthracene

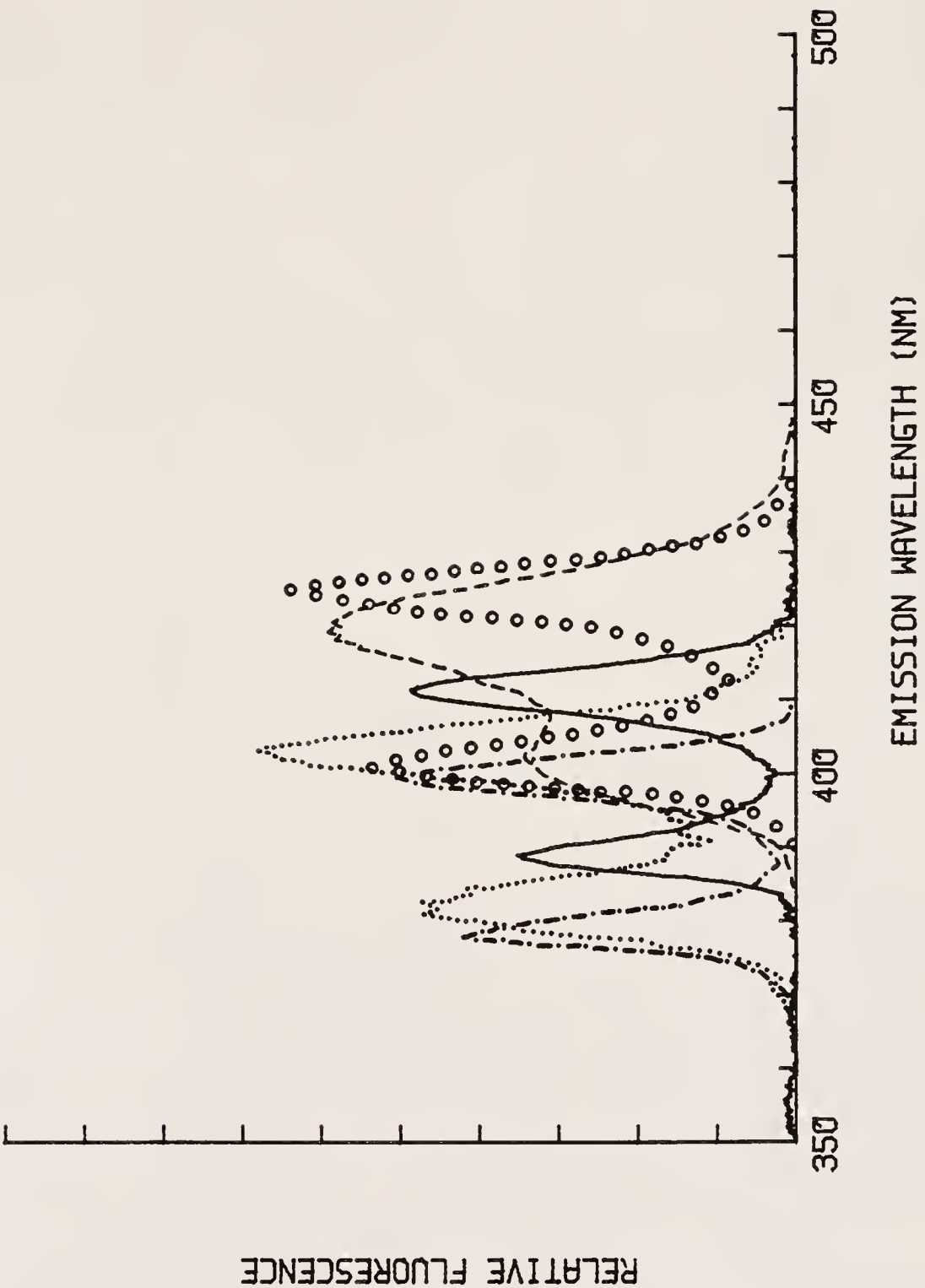
RELATIVE FLUORESCENCE
350
400
450
500
EMISSION WAVELENGTH (NM)

Figure 64. CESF spectrum of five-component PAH mixture using a $\Delta\bar{\upsilon}$ of 1.6 kK.

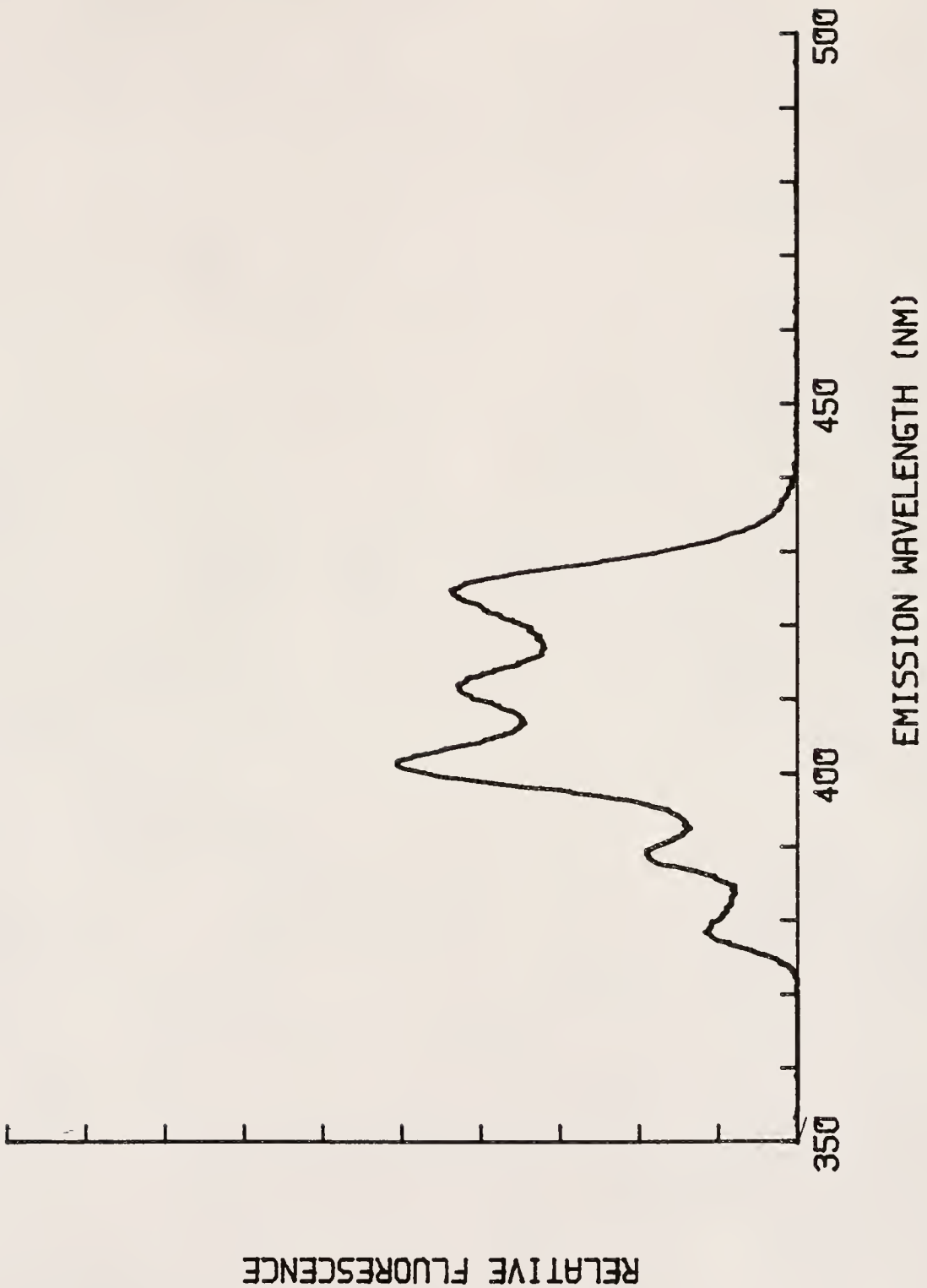
RELATIVE FLUORESCENCE
350
400
450
500
EMISSION WAVELENGTH (NM)

mixture spectrum. The calculated concentrations resulted in an average relative error of 7.1%. The major reason for this error is due to instrumental drift, as about 30 minutes were required for all spectra to be collected. This clearly demonstrates the need for rapid signal collection instrumentation.

Factor Analysis

Factor analysis is a multivariate statistical technique. The principles of factor analysis provide several possible techniques for TLS data evaluation. Qualitative and quantitative information can be extracted from the data matrix using eigenanalysis and rank annihilation. Warner et al. (121) and Ho et al. (23,122,123) have presented the details of these techniques. A rudimentary discussion will be given because of the direct applicability to the TLS data format and to suggest an area for extensive future research. The concepts of factor analysis have not been limited to luminescence data, but have widespread analytical utility, especially in mass spectroscopy (124-129).

Factor analysis provides information describing the number of components and their luminescence excitation and emission spectra for a mixture of unknown composition. As opposed to multilinear regression techniques, the components of the sample need not be known before analysis. Several relationships are important for eigenanalysis and rank annihilation. The rank of the correlation matrices $\underline{M}\,\underline{M}^T$ and $\underline{M}^T\,\underline{M}$ is equivalent to the rank of the matrix $\underline{M}$, but the correlation matrix is symmetrical and more commonly used. The objective is to find two sets of linearly independent vectors, $\{\underline{U}_r\}$ and $\{V_r\}$, that span the vector space $\underline{M}$, so that

$$\underline{M} = \sum_{k=1}^{r} \xi_k \underline{U}_k \underline{V}_k \tag{36}$$

where

$$\underline{M}\,\underline{V}_k^T = \xi_k \underline{U}_k \tag{37}$$

$$\underline{M}^T \underline{U}_k = \xi_k \underline{V}_k \tag{38}$$

In the absence of noise, all non-zero eigenvalues, ξ_k, are significant and indicate the relative importance of the contribution of the kth vectors to $\underline{M}$. Because of noise, the number of eigenvalues is equal to the dimensionality of $\underline{M}^T \underline{M}$. For practical use, the eigenvalues are ordered, $\xi_1 \geq \xi_2 \geq \xi_3 \ldots$, with a threshold value set so that only the first r eigenvalues are selected, the rank of $\underline{M}$.

In the method of rank annihilation (130), a certain amount, β, of the standard matrix $\underline{N}$, corresponding to the reference spectrum of a known component in the mixture is subtracted from the original matrix. The resultant matrix now has a rank of r-1. The eigenvalue corresponding to this component goes to zero, within the noise limitation. This procedure is repeated until all eigenvalues fall below the established threshold.

Another way of representing the relationship in Equation (9) is by

$$\underline{M} = \sum_{k=1}^{r} c_k \underline{M}_k \tag{39}$$

where c_k is the concentration of the kth component divided by the concentration of the reference solution of single component k used to generate matrix $\underline{M}$. If the qualitative composition of the solution is known and the reference spectra for all r components are available, this relationship can be used to quantitate the components in the solution. The concentration array can be solved using matrix operations, or by using a least squares approach. The least squares procedure

generates a matrix of residuals, $\underline{E}$, where

$$\underline{E} = \underline{M} - \sum_{k=1}^{r} c_k \underline{M}_k \qquad (40)$$

The calculated set of concentrations includes those values that minimize $\underline{E}$ (131). As in all least squares calculations, meaningless results are obtained if one of the components is unknown and not included in the reference spectra matrices. The details of this approach have been outlined (132).

While these methods contain a variety of linear algebra concepts, their application to multicomponent samples has been quite limited, usually to a two- or three-component mixture. Without performing a comprehensive study, a factor analysis program was developed as an introduction to these methods. Using the reference TLS data files, two-, three-, and four-component mixture analyses were attempted, with the goal of only trying to determine the number of components present. The two-component mixture included anthracene and perylene with a data matrix created from 220 to 420 nm for the excitation range and 350 to 550 nm for the emission range, with a point selected every 5 nm. This produced a 41X41 matrix. The resultant eigenvalues calculated were 24.17, 13.52, and 0.29. These were the only values greater than 0.1. The first two eigenvalues represent 91.91% of the sum of all eigenvalues for this matrix. A three-component mixture of anthracene, perylene, and naphthacene was eigenanalyzed under the same conditions. The five largest eigenvalues were 21.45, 11.60, 7.61, 0.29, and 0.02, indicating the presence of three compounds. Selection of the three largest eigenvalues represents 99.18% of the sum of all eigenvalues. Finally, a four-component mixture was simulated. The largest eigenvalues obtained were 19.29, 12.98, 7.41, and 1.30, with no other

eigenvalues greater than 0.01. These four represent 99.96% of the sum of all eigenvalues. For each mixture, the correct number of components was calculated. This is a significant capability. For this study, identification of individual components was not attempted.

A major limitation in analyte identification using factor analysis is the difficulty in obtaining excitation and emission spectra from the calculated eigenvectors. This involves rotation of the orthogonal eigenvectors to non-negative vectors, a process that generally does not yield a unique solution. While mathematical results are obtainable, often these do not correspond to experimentally meaningful spectra.

These methods need considerable improvement before they will be practical for routine analysis. Noise evaluation is a major consideration and must be well-characterized for the specific measurement system. These methods will not be applicable to real samples, such as oil samples, where the number of luminescing compounds approaches or exceeds the dimensionality of the data matrix. Although the calculations involved in these methods appear staggering, improvements in computation speed may make this an area of interest in the future. At present, however, data reduction requires on the order of 30 minutes to an hour on common minicomputer systems for a complete analysis.

Spectral Ratioing

A concept that was originally described by Hirschfeld in infrared spectroscopy (133) and more recently by Fogarty and Warner for TLS (134), spectral ratioing holds analytical potential for many spectroscopic techniques. This method involves taking the ratio of two spectra for similar samples where the sample has been preferentially

modified. For example, Hirschfeld measured the infrared spectrum of the original sample and then heated the sample. After some evaporation, the sample was analyzed again. The spectrum of the original sample can be described as

$$M_1(\upsilon) = \sum_{k=1}^{r} \alpha_k f_k(\upsilon) \tag{41}$$

where $f_k(\upsilon)$ is the spectrum of a single component. After sample modification, the new spectrum becomes

$$M_2(\upsilon) = \sum_{k=1}^{r} \beta_k f_k(\upsilon) \tag{42}$$

By ratioing,

$$R(\upsilon) = M_2(\upsilon)/M_1(\upsilon) = \sum_{k=1}^{r} \beta_k f_k(\upsilon) / \sum_{k=1}^{r} \alpha_k f_k(\upsilon) \tag{43}$$

where $R(\upsilon)$ is the ratio distribution. The value of $R(\upsilon)$ is most significant in the region of the spectrum unique to a single component. In this region, k is equal to one and

$$R(\upsilon) = \beta_k/\alpha_k = \text{constant} \tag{44}$$

When plotted, $R(\upsilon)$ forms a plateau, identifying that fingerprint region. For those regions that are not unique, $R(\upsilon)$ is curved. A plateau occurs in any spectral region dominated by one compound, with the number of plateau heights a minimum for the number of components in the mixture. This concept can be extended to TLS spectra analogously.

Two major criteria must be met for this method to be applicable. A preferential sample modification method must be available. For volatile organic molecules, partial evaporation provides this condition. Fluorescence quenching by heavy atom addition is applicable to fluorescence, as well as phosphorescence spectroscopy. The second requirement is that a unique spectral region must exist for each component. For RTF, this may be a problem due to spectral overlap.

For spectral regions with low S/N, interpretation is difficult. To avoid this problem, a threshold can be set for computer discrimination. As the number of components increases, the probability of meeting this criterion decreases. Occasionally, the plateau heights for multiple components are closely spaced. For this, multiple sample modification steps are required.

This ratioing method shows some potential in SLS, especially for LTCESF. Unique spectral regions are clearly identifiable. An interesting feature of this method is that it is effective over the entire spectrum, not just at peak maxima or shoulders in the spectrum. Information is obtained from regions that may otherwise be featureless.

A mathematically similar technique for unique spectral region identification is the ratioing of the original spectrum by a reference spectrum of the desired component. Equation (43) becomes

$$R(\upsilon) = \beta_1 f_1(\upsilon) / \sum_{k=1}^{r} \alpha_k f_k(\upsilon) \tag{45}$$

In the unique spectral regions for component 1, the value of $R(\upsilon)$ reaches a maximum for

$$R(\upsilon) = \beta_1/\alpha_1 = \text{maximum} \tag{46}$$

Each component must be known and determined individually. If plateau regions are obtained, spectral stripping can be employed.

The Hirschfeld ratioing method is substantially simpler than the other statistical techniques described. It demonstrates analytical potential in several spectroscopic techniques. However, in this context, its greatest significance is the identification of fingerprint spectral regions, more efficiently using all data available for identification and quantitation. There is room for a more thorough

evaluation of the practical utility of this method for specific analytical problems.

Correlation Methods

Introduction

Correlation methods in spectroscopy are powerful analytical tools for extracting information from experimental data (135). Correlation offers the ability to detect a desired signal buried in noise and to recognize a specific pattern in spectral data (136). It is inherent in many data handling devices routinely used in the laboratory, such as the lock-in amplifier. Several reports have described electronic developments utilizing correlation principles (137,138). The major improvements afforded by these devices have been in sensitivity enhancement.

Correlation techniques yield information relating the similarity between two waveforms. Thus, the ability to recognize patterns within spectral data allows one to use more of the data generated for analyte identification and quantitation. Ng and Horlick (139) have used cross-correlation masks to effectively reduce spectral interferences in atomic emission spectroscopy. The raw spectral dataare cross-correlated with a noise-free mask of the desired pattern. In this way, pattern recognition can be automated for more efficient use of spectral data.

Synchronous Luminescence Spectroscopy (SLS) is a technique relating two waveforms, the luminescence excitation and emission spectra. Because of this inherent relationship to cross-correlation methods, many concepts can be utilized to optimize the information obtainable by SLS and to improve parameter selection. An evaluation was performed on luminescence spectra, cross-correlating excitation and emission

spectra, relating the results back to luminescence theory and SLS optimization. The results for model compounds under room temperature fluorimetric, low temperature fluorimetric, and low temperature phosphorimetric conditions are discussed.

Experimental

RTF spectra were obtained using the TLS system described in Chapter 2. LTF and LTP spectra were obtained using the LTCESL system described in Chapter 4. All cross-correlation calculations were performed using fast Fourier transform routines similar to those discussed in the literature (140). The details of Fourier transformation for data analysis have been reviewed recently (141). The PDP 11/34 minicomputer was used for all calculations.

The correlation and fast Fourier transform routines were obtained from DEC, with a FORTRAN-callable assembly language format. The wavelength ranges used in each spectrum were required to fulfill the requirement of including 2^n data points. For most calculations, 512, 1024, or 2048 data points were used, with the cross-correlation calculations requiring about 3 to 10 s.

Background

The correlation procedure is mathematically defined as

$$C_{1,2}(\tau) = 1/2T \int_{-T}^{T} f_1(t) f_2(t-\tau) d\tau \qquad (47)$$

where $C_{1,2}(\tau)$ is the correlation between two functions, f_1 and f_2, t is time, τ is the time delay between the two functions, and T is the period of each function. If functions f_1 and f_2 are the same, an auto-correlation is obtained. It is best envisioned as the integrated product between two waveforms as one is shifted in time. Examples of this procedure on common waveforms can be found in the literature (142).

In CESL, a restriction is placed on the data set so that a constant energy difference is maintained between the wavelengths. Equation (7) then becomes

$$M_{ij} = \alpha x(\bar{\upsilon}_i)y(\bar{\upsilon}_i - \Delta\bar{\upsilon}) \qquad (48)$$

The similarities between Equations (47) and (48) become clear if several assumptions are made. In CESL, waveforms are expressed in terms of energy instead of time, similar to the correlation mask concept. Therefore τ becomes equivalent to $\Delta\bar{\upsilon}$. Each spectrum described in Equation (48) represents one point in Equation (47), integrated over the spectral range. A cross-correlation plot indicates the total luminescence collected for each value of $\Delta\bar{\upsilon}$ in CESL. For the study here, $\Delta\bar{\upsilon}$ must be greater than or equal to zero. So correlation for τ less than zero will not be included.

This investigation was another attempt to understand further CESL spectra by using the data in an entire TLS spectrum. The results obtained will be compared with the conclusions drawn from the more instrumental approach described in Chapter 3. Finally, the concept of correlation masks will be discussed.

Results and Discussion

A room temperature fluorescence analysis of a solution of anthracene in n-heptane illustrates the information obtained from the correlation procedure. Figure 65A is the conventional fluorescence spectra of anthracene. The cross-correlation of the spectral region from 300 to 500 nm is plotted in Figure 65B. This plot resembles the profile plots for anthracene in Chapter 2, with a loss in resolution of the 1.4 kK vibrational spacing. The broadness of the spectra at room temperature limits the conclusions that can be drawn. It does indicate that

Figure 65. A. RTF excitation and emission spectra of anthracene in n-heptane.

B. Cross-correlation of the anthracene RTF excitation and emission spectra.

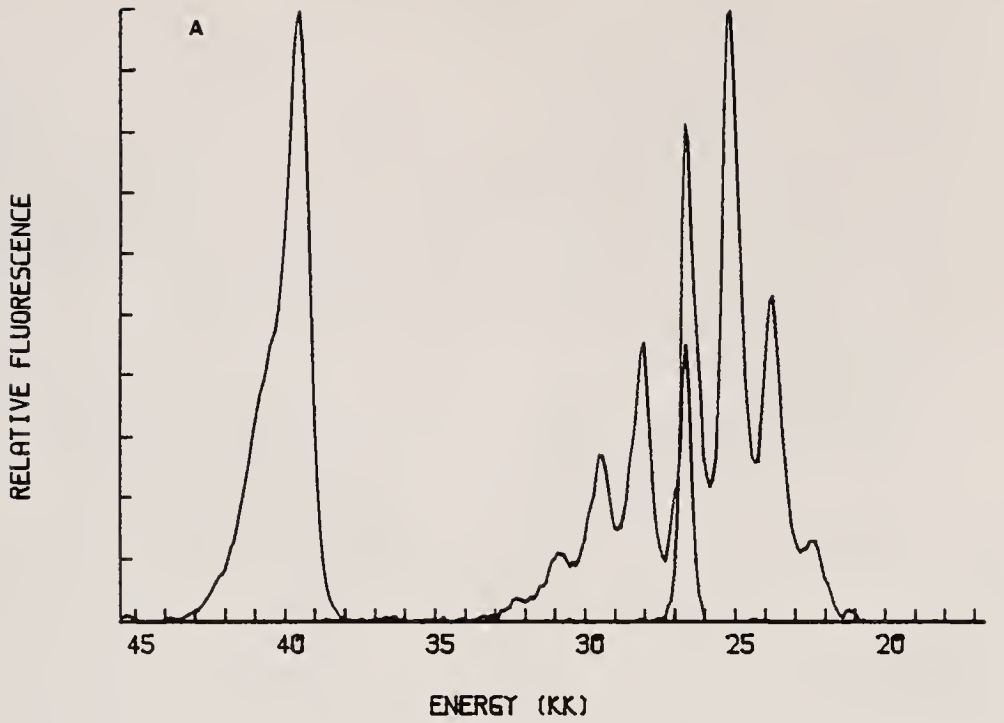
A
RELATIVE FLUORESCENCE
45
40
35
30
25
20
ENERGY (KK)

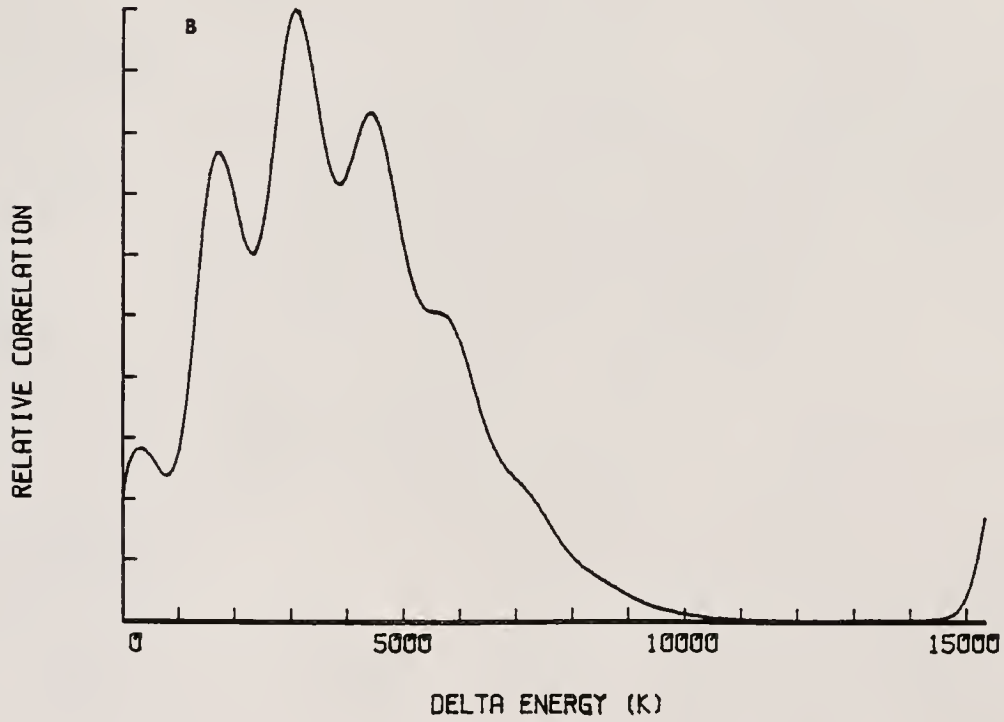
B
RELATIVE CORRELATION
0
5000
10000
15000
DELTA ENERGY (K)

selection of a $\Delta\bar{\upsilon}$ value is not critical to obtain a spectrum of sufficient intensity. Another example, 3,4-benzopyrene, is given in Figure 66.

With this background, the analysis was then extended to low temperature spectra. Figure 67 is the LTF spectra obtained from the anthracene solution using the LTCESF system with a 0.2 nm bandpass on each monochromator. An auto-correlation was first performed on the excitation and emission spectra. These are plotted in Figure 68. This confirms the similarity between the excitation and emission vibrational level distributions. Also, the smoothing feature of the correlation calculation is noticeable. With such a large number of spectral features available, the probability of overlapping bands is increased.

The cross-correlation for these two spectra is plotted in Figure 69. The values for $\Delta\bar{\upsilon}$ that would produce sufficient intensity are evident. However, much of the fine structure is lost in the vibrational substructure. This agrees with the LTF model assumption that within the 1.4 kK vibrational unit, spectral features appear that are identical in both the excitation and emission spectra, and other features appear as mirror images. Those features that are mirror images cause broadening in the cross-correlation pattern, suggesting again that an exact value for $\Delta\bar{\upsilon}$ is not required.

Anthracene LTF spectral features are still fairly broad compared to what is attainable by this system. For a more complex, narrow-line spectrum, a solution of coronene in n-heptane was analyzed. The spectra are shown in Figure 70. The excitation spectrum is found from 250 to 400 nm, with the fluorescence from 400 to 500 nm, and the phosphorescence from 500 to 600 nm. Each spectrum has been

Figure 66. A. RTF excitation and emission spectra of 3,4-benzopyrene in n-heptane.

B. Cross-correlation of the 3,4-benzopyrene excitation and emission spectra.

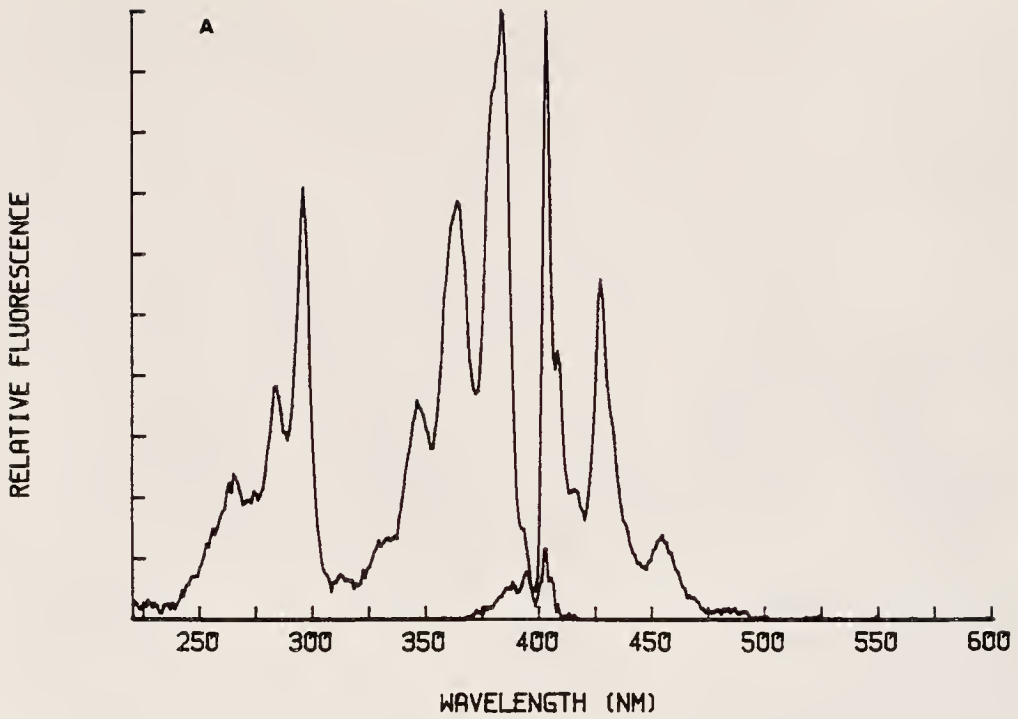
A
RELATIVE FLUORESCENCE
250
300
350
400
450
500
550
600
WAVELENGTH (NM)

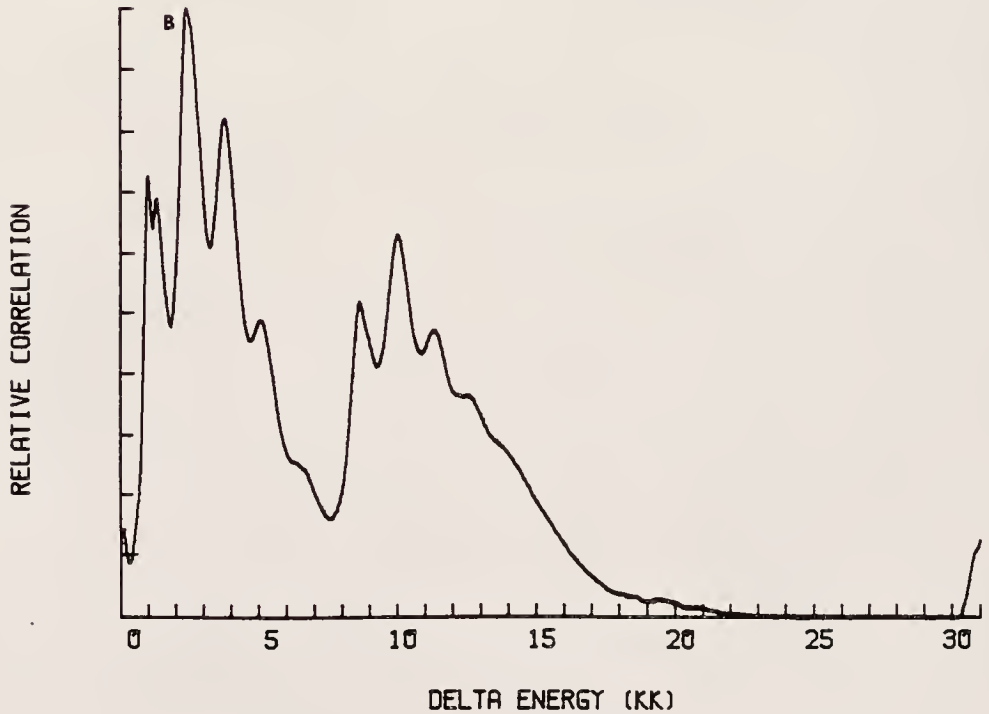
B
RELATIVE CORRELATION
0
5
10
15
20
25
30
DELTA ENERGY (KK)

Figure 67. LTF excitation and emission spectra of anthracene in n-heptane.

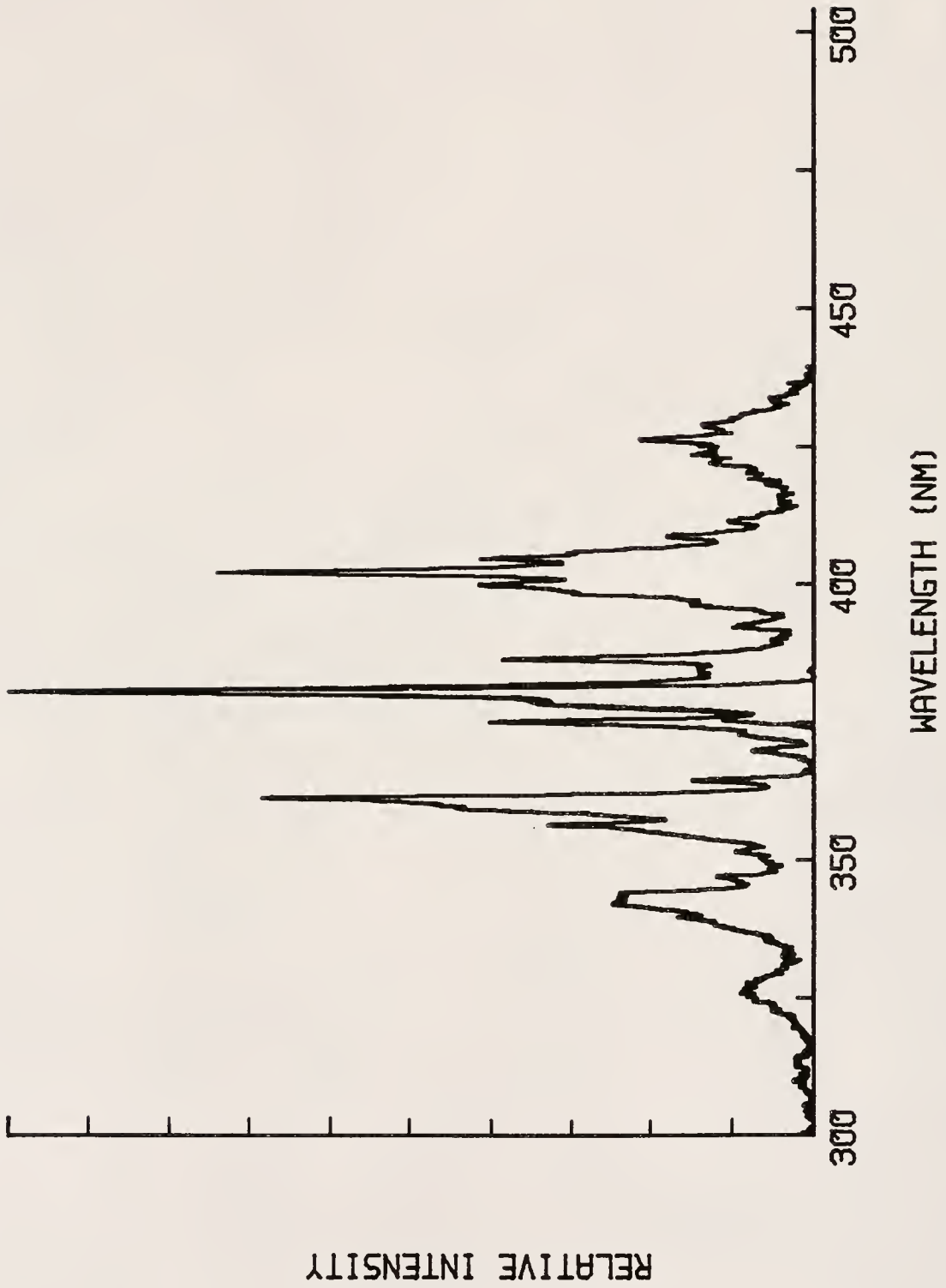
RELATIVE INTENSITY
300
350
400
450
500
WAVELENGTH (NM)

Figure 68. Auto-correlation for the: a. excitation spectrum, and b. emission spectrum of anthracene in n-heptane at 77 K.

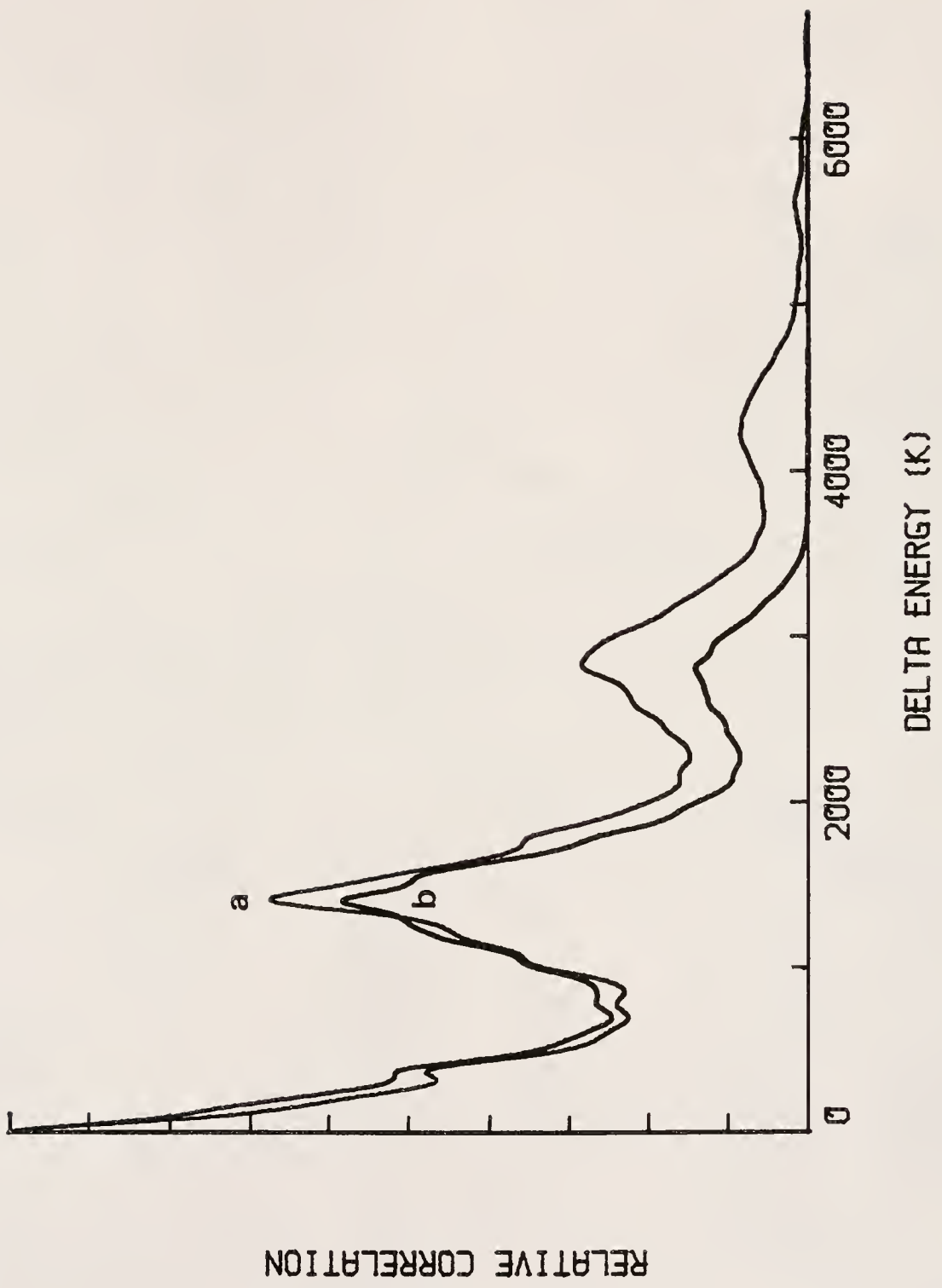
RELATIVE CORRELATION
a
b
0
2000
4000
6000
DELTA ENERGY (K)

Figure 69. Cross-correlation for the LTF excitation, emission spectra of anthracene in n-heptane.

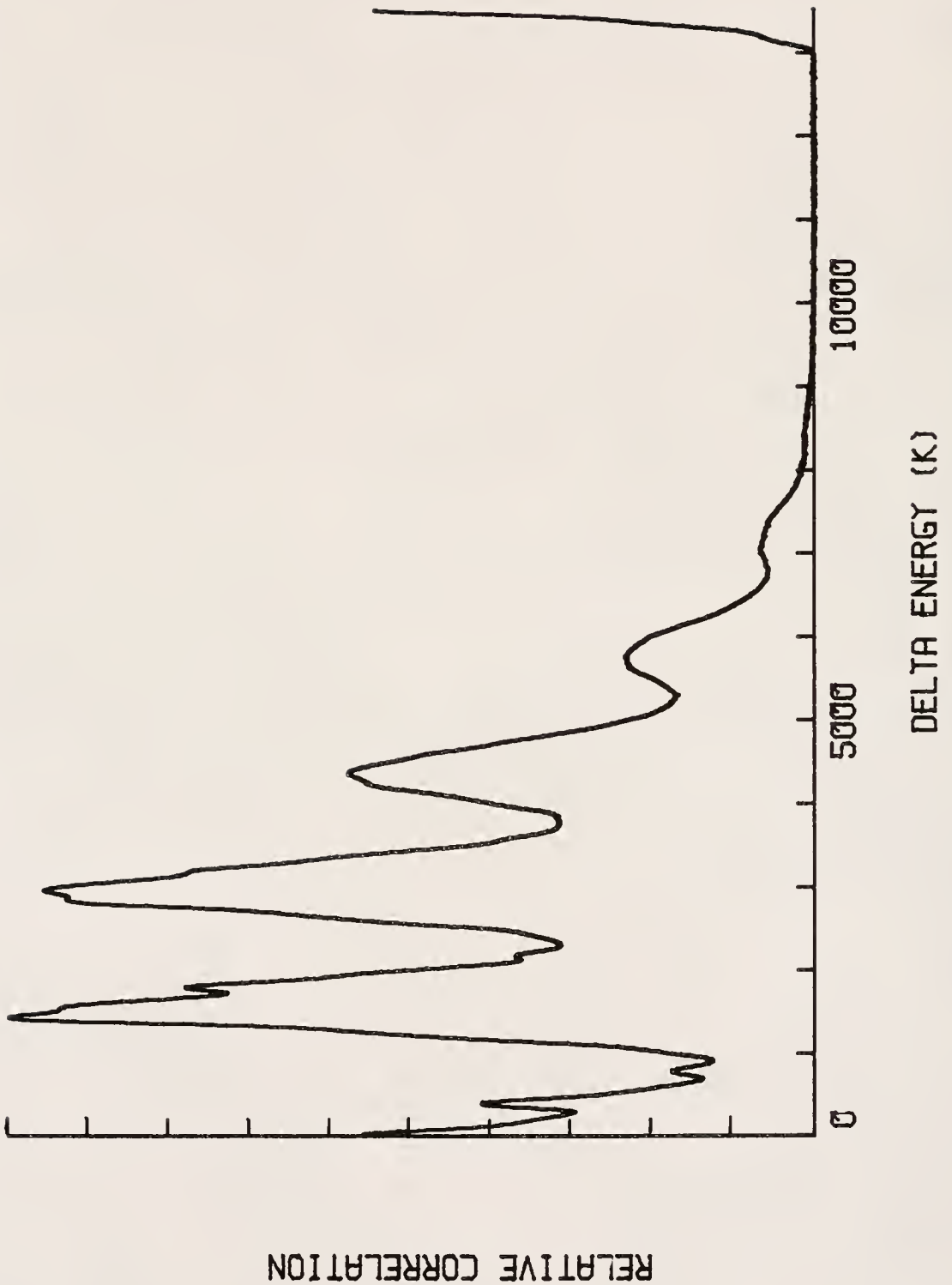
RELATIVE CORRELATION
0
5000
10000
DELTA ENERGY (K)

Figure 70. Low temperature spectra of coronene in n-heptane.
A. Fluorescence excitation spectrum;
F. Fluorescence emission spectrum;
P. Phosphorescence emission spectra.

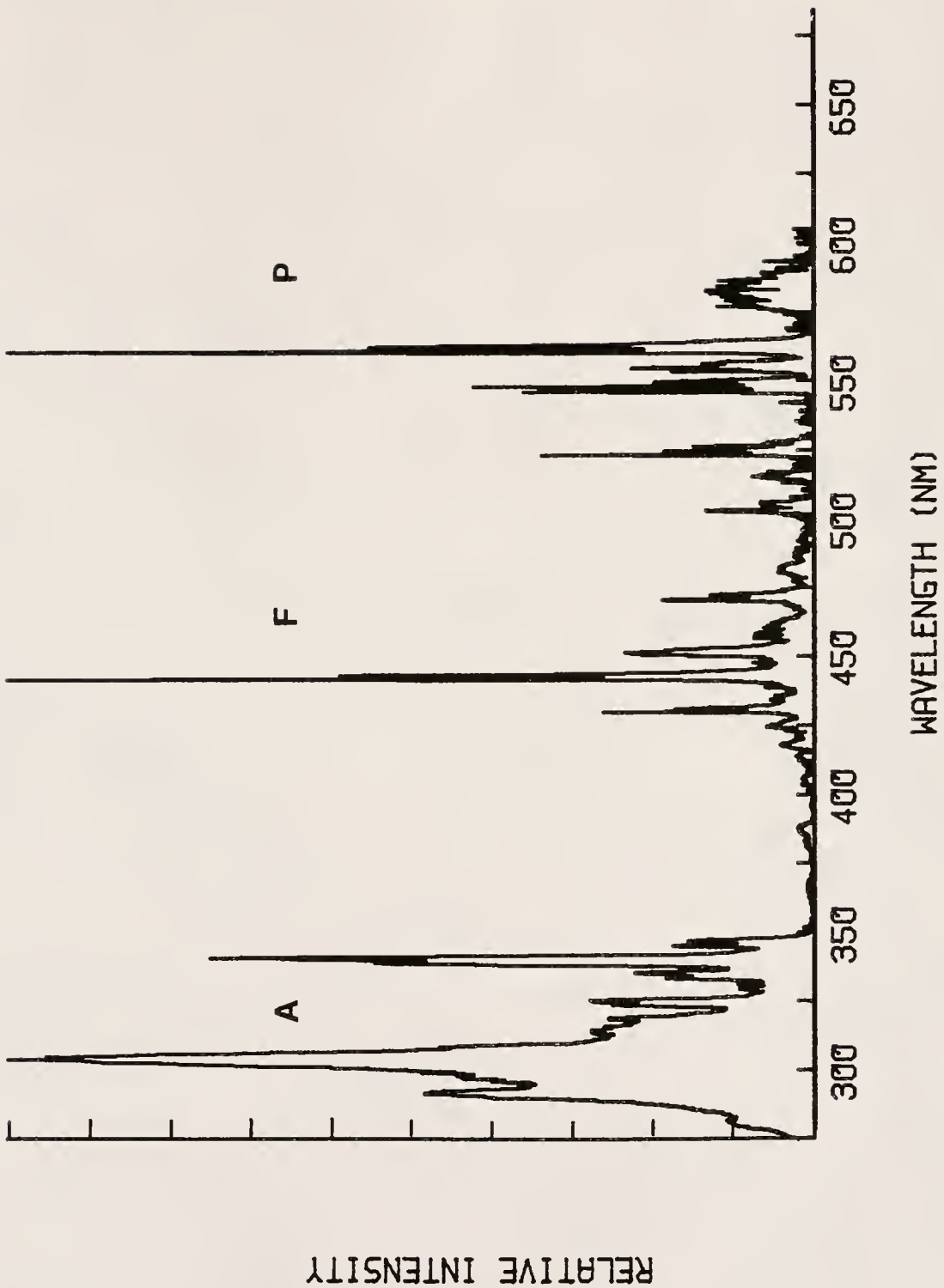
RELATIVE INTENSITY
A
F
P
300
350
400
450
500
550
600
650
WAVELENGTH (NM)

individually scaled to full-scale. It is difficult to visually establish a pattern within the data. The excitation bands are much broader than those from either emission processes.

The cross-correlation plots are shown in Figure 71 with the fluorescence-excitation correlation on the left and the phosphorescence-excitation correlation on the right. Note the similarity between the two. Also a similarity can be seen between the correlation plots and the excitation spectrum. The correlation plot resembles the mirror image of the excitation spectrum.

After further investigation of LTF spectra demonstrating various degrees of bandwidths, several observations and conclusions can be drawn, complementary to those drawn from LTCESF data. The correlation plot feature sharpness is limited by the sharpness of the broader of the excitation or emission spectra. In Chapter 3, it was concluded that the feature sharpness within a single spectrum is determined by the spectrum with the sharpest features. This has major instrumental significance for LTCESF. If one of the two spectra is broad, $\Delta\bar{\upsilon}$ selection can be an approximation. For the seven-component PAH mixture, the 1.4 kK and 2.8 kK approximations for $\Delta\bar{\upsilon}$ were sufficient, as demonstrated. The experimental conditions forced each PAH into the broad excitation spectrum case by using a large bandpass on the excitation monochromator. As was shown, the emission resolution was not degraded. This also suggests another possibility. For polynuclear aromatic compounds with a nitrogen or oxygen heteroatom, high resolution LTCESF spectra can be obtained even if the $\Delta\bar{\upsilon}$ used does not exactly match the vibrational level spacing for these molecules. The selectivity of $\Delta\bar{\upsilon}$ can be varied by changing the excitation monochromator bandpass.

Figure 71. Low temperature cross-correlation functions of the coronene in n-heptane spectra, a. Excitation - fluorescence emission; b. Excitation - phosphorescence emission.

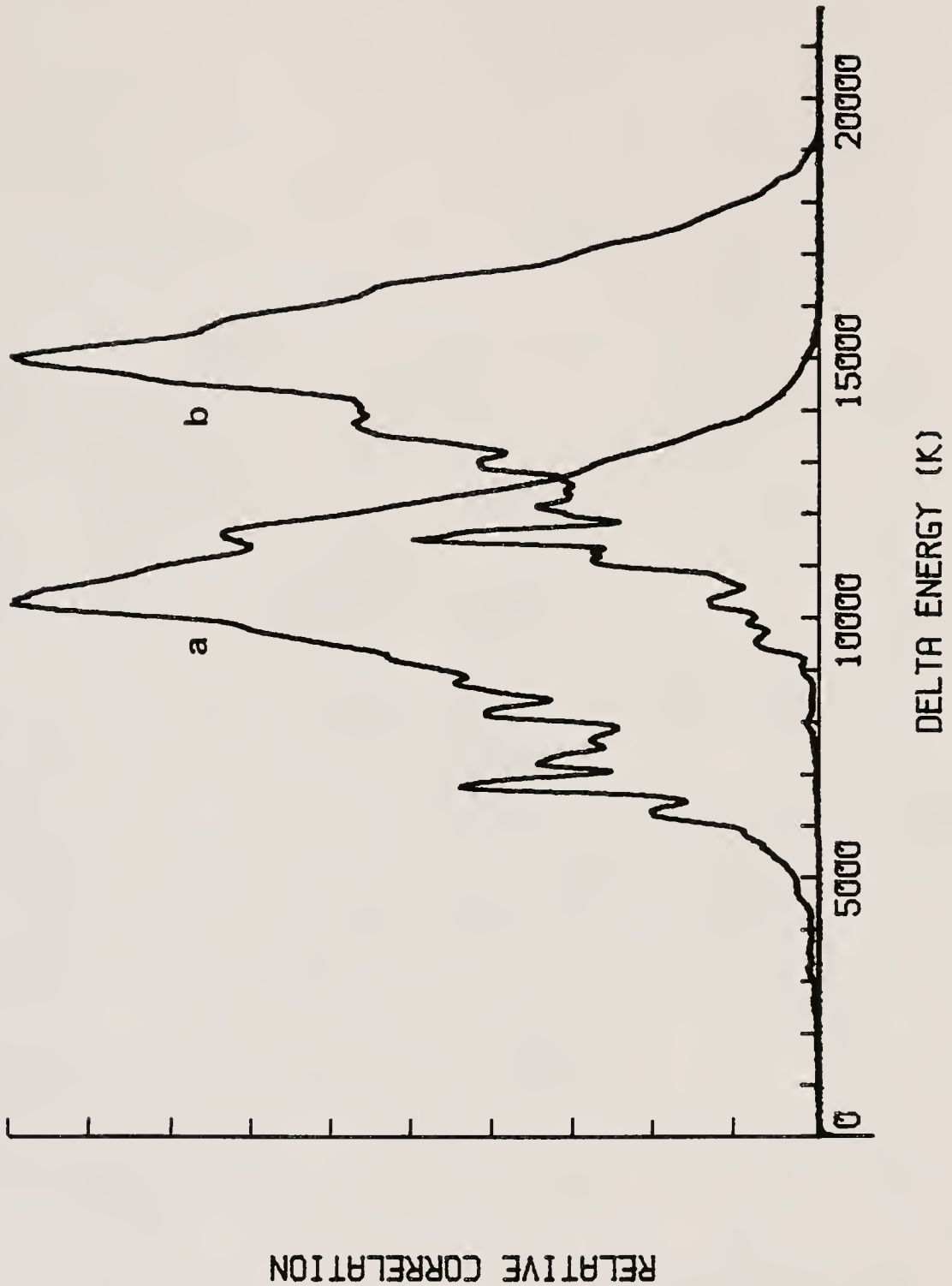
RELATIVE CORRELATION
0
5000
10000
15000
20000
DELTA ENERGY (K)
a
b

This evaluation was also performed on LTF spectra using wavelength units. For narrow-band spectra, the correlation plots were consistently rather broad and featureless. This confirms the conclusions made for CWSF at low temperatures. While low temperatures reduce bandwidths, the number of bands can be enormous. The correlation pattern appears almost random, suggesting that almost any $\Delta\lambda$ can be selected to obtain a CWSF spectrum. However, the interpretation of this spectrum may be impossible.

Correlation masks have two areas of potential utility in TLS. By determining key spectral positions that are characteristic of groups of compounds, instrumentation can be developed that is selectively optimized for the group of compounds with special interest. An example of this is given in Chapter 6. Another use for correlation masks in TLS is the generation of digital masks based on the spectra in the generated database. The desired waveform can be calculated easily and used to identify important spectral features. Digital correlation should have more applicability than the electronic equivalent due to its versatility over a wide range of analyses.

Conclusions

While several observations have been made from this investigation, it appears that this combination is worthy of further study. Of particular interest would be the evaluation of high resolution spectra obtained at 4 K. Also the correlation of emission spectra from different compounds may be useful in computer search routines to link specific patterns to families of compounds. Correlation techniques in analytical chemistry continue to demonstrate vast potential.

CHAPTER 6
APPLICATIONS IN OIL ANALYSIS

Introduction

The development of TLS and SLS can be traced back to applications in oil sample analysis. To place these techniques in proper perspective, an investigation was completed on the empirical development of luminescence spectroscopy for oil identification. This is included for completeness, to introduce the type of problems for which these techniques appear most suited. Clear characterization of this analytical problem suggests future projects, summarized in the next chapter.

The aromatic content of various crude oils can range from 10 to 30% (143). Because of the intense luminescence that is characteristic of many aromatic compounds, the analytical chemist is faced with a unique situation. While this represents a rather complex mixture, the sensitivity in oil analysis is generally not the limiting factor in technique selection. Selectivity becomes the major concern in oil analysis. But oil analysis also requires somewhat different information than many luminescence applications. The concentration of specific components is usually not required, but rather, the characterization of groups of compounds provides sufficient information necessary to trace oil samples to their sources and to allow for the screening of selected properties.

With the problem outlined in this manner, an extensive evaluation of current luminescence techniques was begun as a joint effort by the U. S. Energy Research and Development Administration and Baird, with projects

created in the early 1970's (144). This specific research was directed towards U. S. Coast Guard oil spill tracing and formed the basis for the commercially available TLS instrument sold through Baird, described in Chapter 2. TLS was especially important in this early research. On-site and remote-sensing applications make luminescence spectroscopy an invaluable technique for oil-in-water characterization.

The overall analytical approach to oil analysis has been reviewed by Bentz (145). The measurement step is often fairly routine when compared to the difficulties of representative sampling and weathering effects. The determination of oil sample elemental composition has also been a major research area for spectroscopists. However, for this consideration, molecular analysis is the focus.

Total Luminescence Spectroscopy

TLS spectra of petroleum products are characterized by broad features, with extensive spectral overlap (146). The fingerprint spectra are difficult to interpret and thus forms a considerable challenge for the techniques described in this study. Several experimental analyses were performed to demonstrate the complexity of this problem. For this investigation, three representative oil samples were obtained from Oak Ridge National Laboratories. These were identified as shale-derived crude oil #4101.10, coal-derived crude oil #1701.18, and petroleum-derived crude oil #5301.01.

The major emphasis of published work on oil analysis has been in sample preparation for luminescence analysis. For example, crude oil must be diluted by several orders of magnitude before spectroscopy can be utilized. The most recommended solvents for PAH analysis include n-heptane, cyclohexane, and methylcyclohexane. Cyclohexane dissolves

the oils more completely, but methylcyclohexane demonstrates the best spectroscopic characteristics at low temperatures, forming a glass rather than a snow. To keep concentration effects low, concentrations usually employed range from 10 μg/mL to 100 μg/mL of the original sample diluted with solvent. For many PAHs, this dilution causes the concentrations of individual compounds to be below their detection limits.

Figures 72-77 are the TLS spectra for the three types of oil samples at room temperature. Each spectrum was obtained from a 10 to 20 μg/mL solution of the original stock oil diluted with n-heptane. Spectra obtained from cyclohexane dilutions closely resemble these. While each spectrum is rather broad, there is sufficient pattern development to distinguish among the three. Obviously, specific compounds are not identifiable, although spectral regions have been catalogued for specific families of compounds, such as the emission region from 340 to 350 nm is due to substituted naphthalenes, while the emission region from 400 to 450 nm is characteristic of chrysenes (48). TLS spectra for a variety of fuel oils and petroleum products are available in the literature (147). No further research was attempted in oil classification or sample discrimination.

Synchronous Luminescence Spectroscopy

The original application of SLS techniques was in oil analysis. Since 1971, Lloyd has evaluated SLS techniques for the analysis of engine oils (59-61), rubber materials (148), and petroleum products (73) from the perspective of a forensic scientist. From this research, he has catalogued those spectral features that have the most utility for identification and discrimination purposes (149). Feature selection was based on statistical tabulations of a large database of samples from

Figure 72. TLS spectrum of shale-derived crude oil diluted to 20 μg/mL with n-heptane.

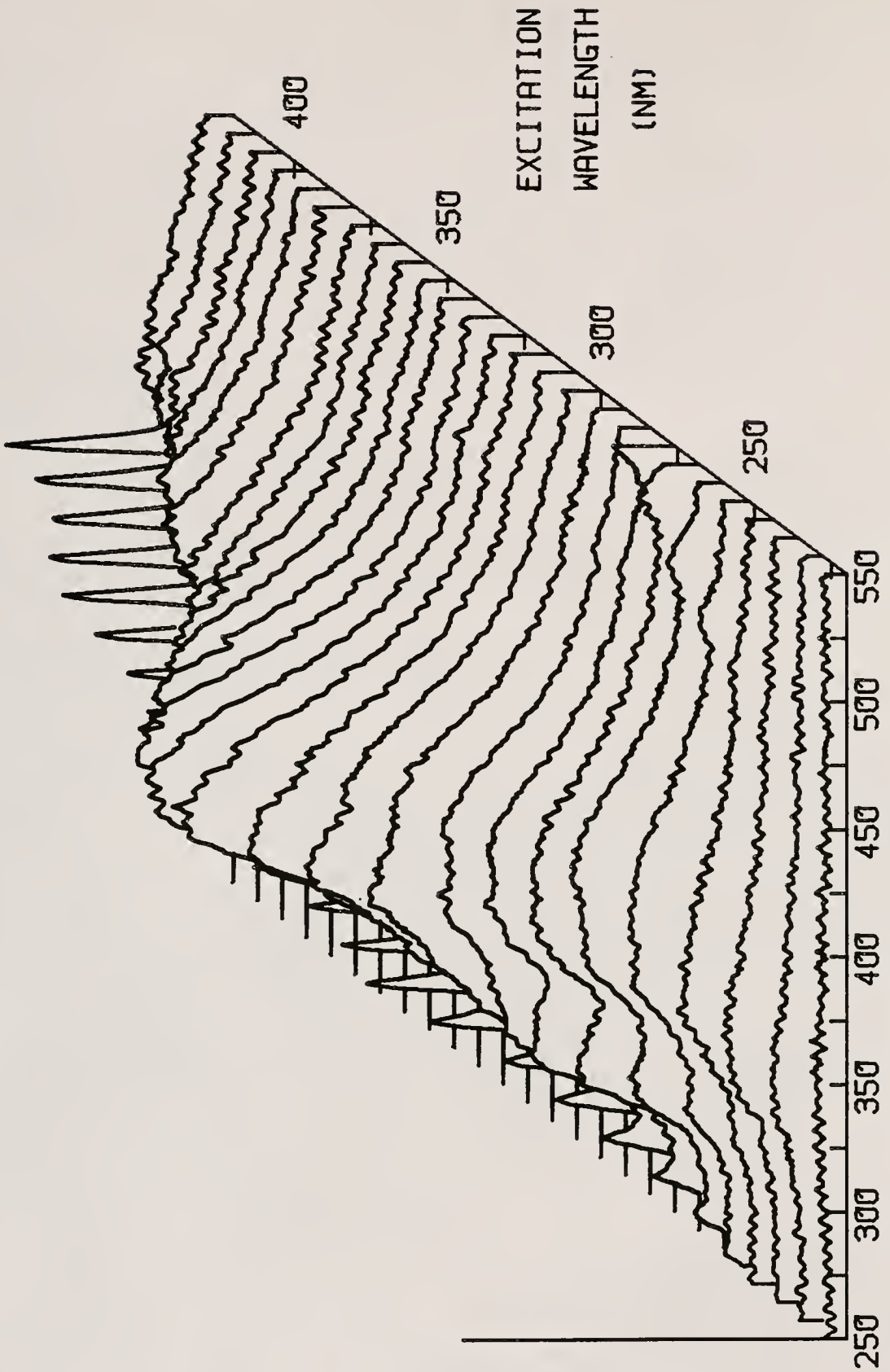
EXCITATION
WAVELENGTH
(NM)
400
350
300
250
250
300
350
400
450
500
550
EMISSION WAVELENGTH (NM)

Figure 73. TLS contour plot of shale-derived crude oil diluted to 20 μg/mL with n-heptane.

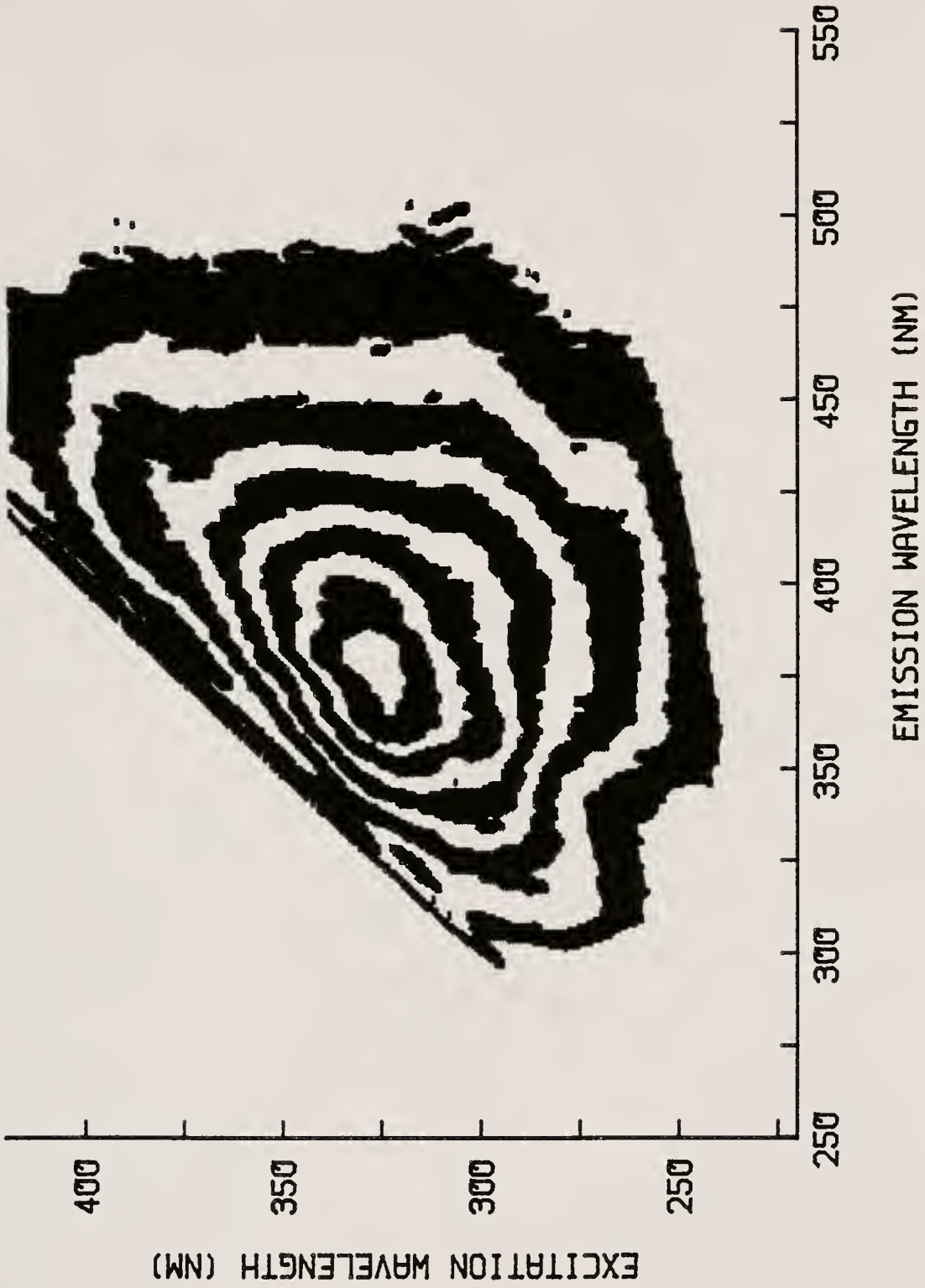
EXCITATION WAVELENGTH (NM)
400
350
300
250
250
300
350
400
450
500
550
EMISSION WAVELENGTH (NM)

Figure 74. TLS spectrum of coal-derived crude oil diluted to 20 μg/mL with n-heptane.

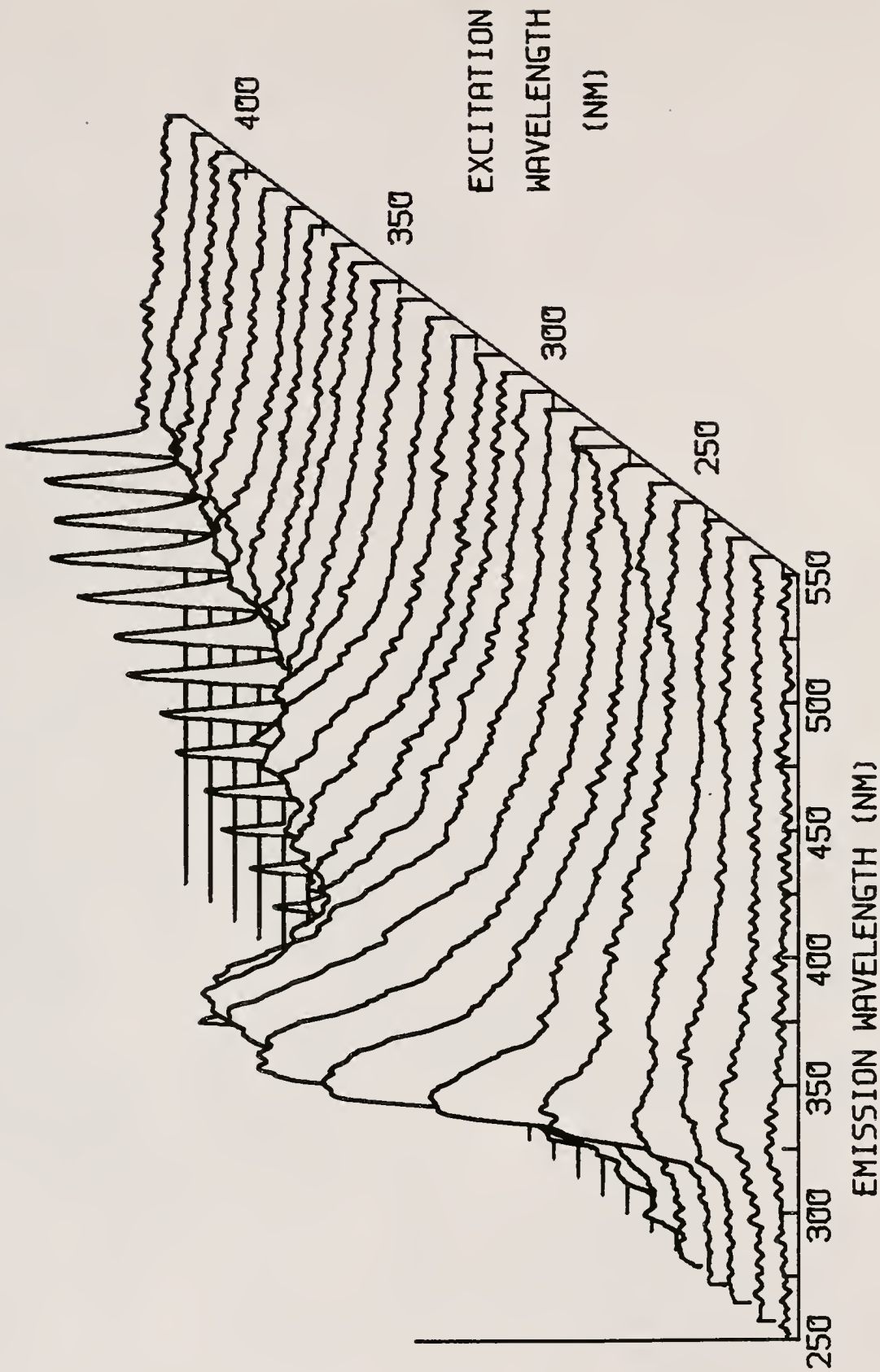
EXCITATION
WAVELENGTH
(NM)
400
350
300
250
250
300
350
400
450
500
550
EMISSION WAVELENGTH (NM)

Figure 75. TLS contour plot of coal-derived crude oil diluted to 20 µg/mL with n-heptane.

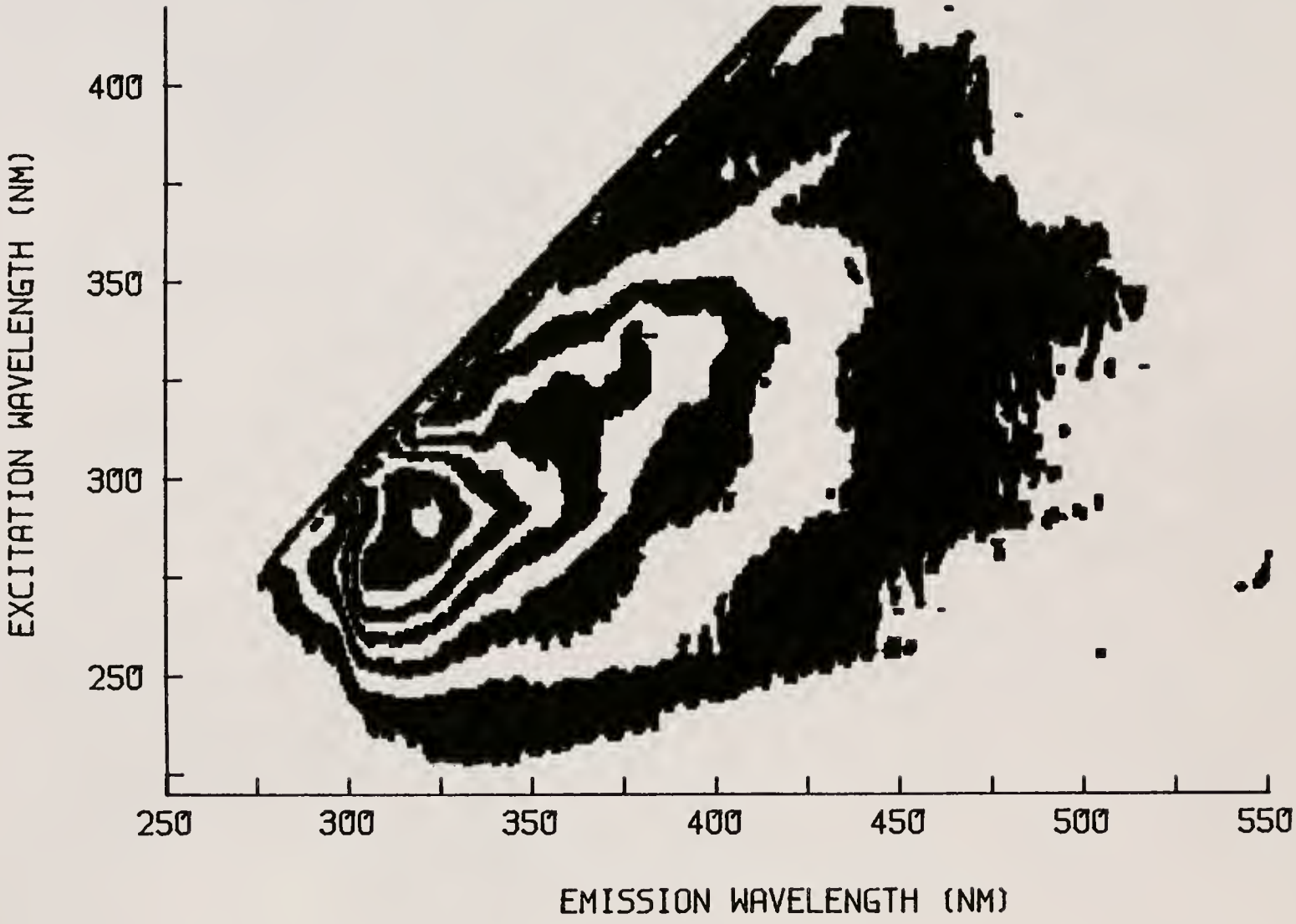
EXCITATION WAVELENGTH (NM)
400
350
300
250
250
300
350
400
450
500
550
EMISSION WAVELENGTH (NM)

Figure 76. TLS spectrum of petroleum crude oil diluted to 20 µg/mL with n-heptane.

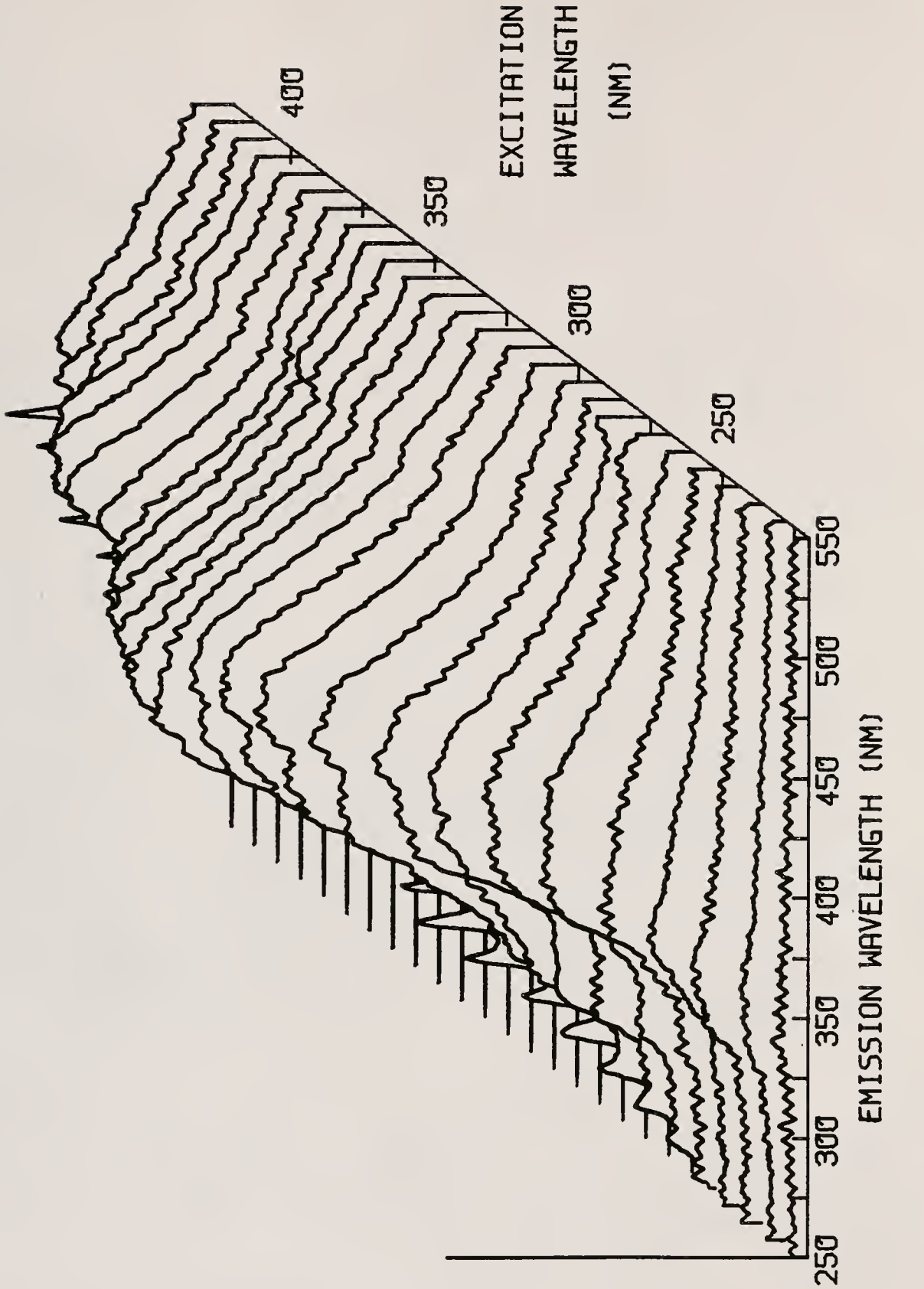
EXCITATION
WAVELENGTH
(NM)
400
350
300
250
EMISSION WAVELENGTH (NM)
250
300
350
400
450
500
550

Figure 77. TLS contour plot of petroleum crude oil diluted to 20 μg/mL with n-heptane.

EXCITATION WAVELENGTH (NM)
400
350
300
250
EMISSION WAVELENGTH (NM)
250
300
350
400
450
500
550

a variety of sources. Using his results, many unknown substances have been identified.

John and Soutar (150) have presented a comprehensive evaluation of the parameters influencing SLS analysis of crude oils. This evaluation included solvent, $\Delta\lambda$ selection, concentration, temperature, and monochromator bandpass. Their results verified the work of Lloyd, concluding that this technique offers excellent potential for crude oil identification. A similar report by Wakeham (151) compared conventional fluorescence techniques to SLS for the aromatic fraction from oils separated by liquid-solid chromatography.

A shipboard oil-in-water monitoring fluorimeter has been developed, implementing a synchronous scan mode with the use of spatial masks that are placed at the exit plane of the excitation and emission polychromators (143). The polychromators are positioned so that a predetermined wavelength difference is maintained while large regions of the spectrum are summed. Each slit has an effective bandpass of about 20 nm and a number of slits are used, centered about 30 nm apart. Optimization of mask selection was empirically determined. This instrument provides excellent sensitivity because of the large spectral regions observed, but provides little selectivity.

Several SLS experiments were performed on the three oil samples described. The quality of spectra obtained matched those in literature. Because of the complexity of these spectra, optimization is difficult even with sufficient theoretical background. The analytical potential of the CESL methods described throughout this work was not ascertainable because of the limited variety of samples available.

Low Temperature Fluorescence Spectroscopy

The application of low temperature fluorescence spectroscopy has been mainly limited to the laser-excited techniques described in Chapter 4. Two reports (72,146) have discussed the use of low temperature techniques for oil analysis. Several experiments were completed with the LTCESF system, reproducing the data that were obtained in these papers. A reduction in temperature increased the number of spectral features observable, with a considerable increase in measured luminescence beyond 450 nm as phosphorescence emission is enhanced. While low temperatures show a definite improvement, the limitations of liquid nitrogen temperatures prevent complete characterization of oil constituents.

Phosphorescence Spectroscopy

A recent report (109) describes the potential of low temperature phosphorescence spectroscopy for oil analysis, including the use of synchronous scanning and total phosphorescence plotting. Total phosphorescence spectra resemble room temperature TLS spectra for oil samples in that they are broad and relatively featureless. The heavy atom effect can be used for phosphorescence and is an area for future consideration. By proper selection of heavy atom concentrations, selectivity can be effectively enhanced. Using synchronous phosphorescence spectroscopy, little is gained over conventional techniques, with $\Delta\lambda$ selection of little significance. Selectivity is limited by the basic phosphorescence measurement process and this technique provides little to enhance spectra interpretation without prior sample pretreatment.

Vo-Dinh and Martinez (106) have applied synchronous methods to room temperature phosphorescence spectroscopy (RTP) and to the analysis

of coal liquefaction products. Selectivity is enhanced by the limitation that only a few compounds phosphoresce on solid substrates at room temperature. Quantitation was achieved using a standard addition method, with a tabulation of the comparative results for these samples using other techniques. Synchronous techniques combined with RTP analysis have been suggested as a screening method for synthetic fuels (107).

Conclusions

The complexity of oil samples makes luminescence analysis difficult if no separation step is included, although many components within the samples exhibit intense luminescence individually. A more suitable compromise is the combination of high performance liquid chromatography (HPLC) and fluorescence detection. Several reports have demonstrated the potential of this combination, optimizing the separation step while utilizing a sensitive detection system that provides additional information for analyte identification (152,153). This combination has found extensive use for oil analysis. For remote-sensing or situations where a separation is not feasible, luminescence techniques will continue to be a major consideration. To increase the effectiveness of automated data interpretation, more sophisticated pattern recognition techniques are being developed (154). At present, considerable research must be done on this challenging analytical problem.

CHAPTER 7
CONCLUSIONS AND FUTURE WORK

Throughout this research, an attempt was made to not only develop analytical instrumentation backed by luminescence theory, but to apply this instrumentation to multicomponent samples and to evaluate the position this work holds in the field of analytical chemistry to enhance selectivity. The goal was to develop methods to optimize the extraction of analytically useful information from measured spectral data. The available information source was the Total Luminescence Spectroscopy data matrix, data that are routinely obtainable with state-of-the-art instrumentation. It is the interpretation of these data that completes the analytical process.

Synchronous Luminescence Spectroscopy has been evaluated as a subset of Total Luminescence Spectroscopy, with several suggestions to enhance selectivity in multicomponent analysis. But the principles of Constant Energy Synchronous Luminescence Spectroscopy do not hold a unique relationship to TLS. Instead, CESL represents a concept that encompasses a variety of potential luminescence developments. CESL, conceivably, does have analytical utility when applied to problems requiring a measurement system with the characteristics matching those outlined in this work. But these concepts can be applied to other situations.

The results from the oil analysis in Chapter 6 demonstrate the need for separation methods prior to luminescence detection. Past separation methods using spectroscopic detectors have been limited to

spectrophotometric detection at 254 nm. The emphasis has been on sensitivity, with the ideal detector providing universal application. But with analytical problems becoming continuously more complex, selectivity is a major concern. As a result, variable wavelength spectrophotometric and fluorimetric detection are increasing in popularity.

Fluorimetric HPLC detection offers enhanced selectivity potential (155). But exploiting this potential fully is a considerable problem. An idea that was pioneered by the work of Ogan et al. (156,157) has found utility in PAH mixture analysis. At predetermined times during a separation, the excitation and emission wavelengths of the fluorescence detector are adjusted to match the fluorescence characteristics of each compound as it elutes from the column. On a reversed-phase column, larger PAHs have longer retention times than smaller PAHs. A similar fluorescence feature is known that larger PAHs fluoresce more towards the red region of the spectrum than smaller PAHs (63). By optimizing the detector for each eluant, an approximate SLS concept is used. Synchronization includes not only the wavelengths, but the retention times of each compound. This is another area for continued research.

TLS principles can be directly utilized in HPLC detection. The application of the Videofluorometer to HPLC detection illustrates the need for substantial improvements before routine utility can be realized. Using the system described by Ho, Warner, and Fogarty (53), data storage is a significant problem. Nineteen TLS spectra can be obtained in a run, with individual spectra collected every 30 s. Each matrix consists of 50X50, or 2500 data points. A more extensive

discussion of the application of the Videofluorometer to HPLC detection includes several more major concerns for the analyst (158). Using this system, a 60X60 data matrix is collected and stored in about 10 s. The long data collection times can be traced back to the insensitivity that is characteristic of present-day imaging detectors. The sensitivity is much worse than a fixed wavelength fluorimeter and is approximately equivalent to an absorption detector if quantitation involves summing the entire data matrix.

The main advantage of a system using a fingerprinting detection system following a separation step is the information available for analyte identification (159). However, the HPLC-Videofluorometer has been restricted in its selectivity advantage. Because of the long integration times required, separation by the HPLC is degraded. The reports describing these systems indicate a serious problem, one whose solution has been the major objective of this research. Once the instrumental difficulties of rapid data collection are reduced, as will, no doubt, occur, effective interpretation of the TLS data is necessary. Reference 158 demonstrates the need for considerable more research towards this end. Identification and quantitation using this system have been achieved by plotting the measured fluorescence signal at a preselected pixel, optimized for the separation at hand. This same analysis can be performed using a conventional scannable fluorimeter with much more sensitivity.

A recent report (160) represents an extension of the mathematical techniques developed for static TLS data to HPLC-Videofluorometer applications. A three-dimensional matrix with dimensions of excitation wavelength, emission wavelength, and elution time can be solved using

the algorithms developed for two-dimensional matrices. Again, a least squares approach was used to resolve simulated data matrices. Each matrix was 30X30X10, with the eluting peaks modeled as Gaussian functions.

To the mathematician, this extension to three-dimensional matrices is appealing because it is based on a wealth of linear algebra principles and allows for extensive data manipulation. However, its practical utility is seriously questioned. First, a matrix of sufficient size to represent adequately the separation would be enormous. The resultant mathematical manipulations required are difficult to imagine. Perhaps of even more concern is the treatment of the separation step. The resolution by optimizing the HPLC would be substantially degraded by reducing the sampling rate to make the data manageable. Therefore, the problems demonstrated for two-dimensional matrix analysis are even more pronounced for the three-dimensional case.

The computer system developed in this research can be used to study the sensitivity-selectivity trade-off in HPLC detection. Using the database that has been generated along with the bandpass degradation routines, wavelength selection can be optimized for simulated mixtures. Computer modeling can be effectively used to reduce method development time.

Another area of consideration is the development of TLS spectral masks. If fingerprint regions are well characterized, masks can be produced to match these regions. In principle, this resembles the Hadamard concept (161). However, digital masks are easier to implement than instrumental masks. Again, effective utilization of the information content of TLS data is the ultimate goal.

Finally, there are many areas of luminescence theory that need to be evaluated relative to synchronous luminescence concepts. While this is oriented more towards theory and less towards real sample analysis, a wealth of analytical development is possible. The low temperature results in Chapter 4 indicate several potential research projects. The application of Fourier Transform Infrared Spectroscopy (FTIR) and Raman Spectroscopy to molecular samples at 10 K or below demonstrates the selectivity that is available in resolved vibrational frequencies. The correlation of these data with LTF and LTP spectra provides considerable fingerprinting capabilities. The high resolution low temperature luminescence spectra that are available in the literature (162,163) provide a wealth of analytical information. As techniques are developed that optimize the extraction of analytically useful information from complex data systems, multicomponent analysis becomes practical.

APPENDIX 1
CHEMICALS AND THEIR SOURCES USED IN THIS RESEARCH

Compound	Source
1,2-Benzofluorene 2,3-Benzofluorene 1,12-Benzoperylene 1,2-Benzopyrene 3,4-Benzopyrene Carbazole 1,2:3,4-Dibenzanthracene 9,10-Dimethylanthracene 9,10-Diphenylanthracene 2-Methylanthracene Perylene	Aldrich Chemical Co. Milwaukee, WI 53233
Doubly-deionized water	Barnstead Sybron Corp. Boston, MA 02132
Fluoranthene	Chem Service, Inc. West Chester, PA 19386
Tripelennamine hydrochloride Terbutaline sulfate	CIBA-GEIGY Summit, NJ 07901
Acenaphthene Anthracene 1,2-Benzanthracene Chrysene 1,2:5,6-Dibenzanthracene Fluorene 9-Methylanthracene Naphthacene Naphthalene Phenanthrene Pyrene	Eastman Kodak Rochester, NY 14650
Coronene	Fluka AG Buchs, Switzerland
Anthanthrene 1-Methylpyrene	K & K Laboratories, Inc. Plainview, NY 11803

Compound	Source
n-Hexane n-Heptane Cyclohexane	Matheson, Coleman & Bell Norwood, OH 45212
Quinine sulfate	Nutritional Biochemicals Corp. Cleveland, OH 44128
Ethanol	U. S. Industrial Chemicals New York, NY 10016

APPENDIX 2
BANDWIDTH REDUCTION AND PEAK LOCATION IN CESL

Geometric Model for Bandwidth Reduction

An expression can be obtained that relates the effective CESL bandwidth to the bandwidths of the excitation and emission peaks. For a general TLS peak, the line corresponding to an equivalent intensity contour forms an ellipse. For these calculations, an ellipse can be drawn that defines the contour equivalent to half the maximum intensity. The bandwidth in a conventional spectrum is defined as the full-width-half-maximum (FWHM) value. Figure 78A is a plot of the FWHM contour with its corresponding coordinate system. The following terms will be used:

$\delta\lambda_m = 2a$ = luminescence emission bandwidth (nm)

$\delta\lambda_x = 2b$ = luminescence excitation bandwidth (nm)

$\delta\lambda_s = 2x$ = CESL effective bandwidth (nm)

The dashed line in Figure 78A represents the CESL scan path. It is assumed that this scan path passes directly through the peak maximum, (0,0). The equation of the ellipse is

$$x^2/a^2 + y^2/b^2 = 1 \tag{49}$$

By definition, the CESL scan path requires that x and y are equal. Substituting,

$$x^2/a^2 + x^2/b^2 = 1 \tag{50}$$

$$x^2 = a^2b^2/(a^2+b^2) \tag{51}$$

$$x = \pm ab/(a^2+b^2)^{1/2} \tag{52}$$

Figure 78. Geometric model for CESL.

A. Elliptical contour defining the FWHM values for a Gaussian peak shape. The dashed line defines the CESL scan path.

B. Relative vibrational band locations for CESL scans of $\Delta\bar{\upsilon}_1$, $\Delta\bar{\upsilon}_2$, and $\Delta\bar{\upsilon}_3$ assuming symmetrical peaks.

C. Relative vibrational band locations for CESL scans of $\Delta\bar{\upsilon}_1$, $\Delta\bar{\upsilon}_2$, and $\Delta\bar{\upsilon}_3$ assuming non-symmetrical peaks.

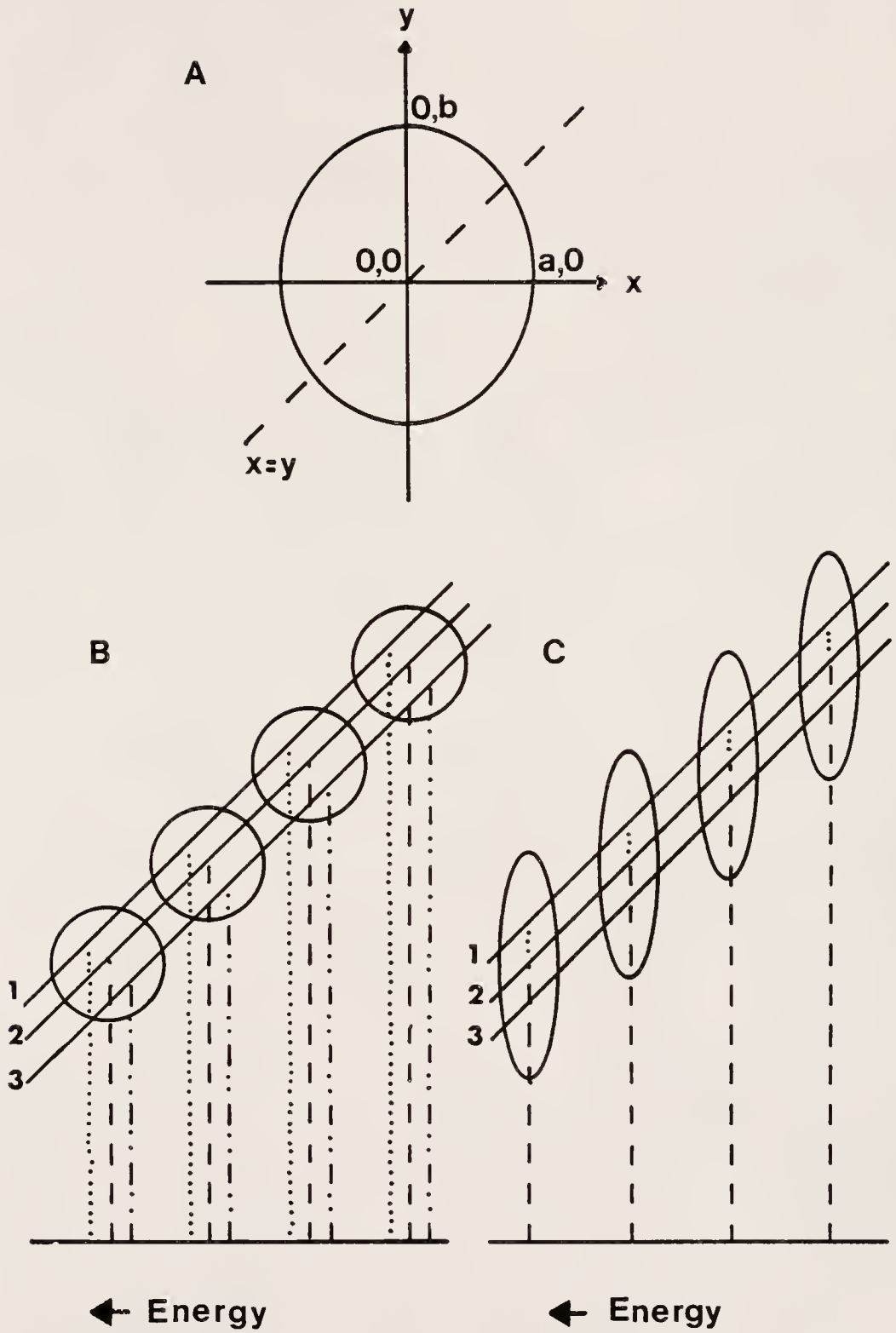
A
y
0,b
0,0
a,0
x
x=y
B
1
2
3
Energy
C
1
2
3
Energy

From the above definitions,

$$\delta\lambda_s = \delta\lambda_x\delta\lambda_m/(\delta\lambda_x^2+\delta\lambda_m^2)^{1/2} \tag{53}$$

This forms the basic bandwidth relationship. There are three cases that are of special interest. The first case represents a symmetrical peak where a and b are equivalent, reducing the model to a circle. Equation (53) reduces to

$$\delta\lambda_s = \delta\lambda_x/\sqrt{2} = \delta\lambda_m/\sqrt{2} \tag{54}$$

The second case is the limit a >> b, yielding

$$\delta\lambda_s = \delta\lambda_x \tag{55}$$

A final case is the limit a << b, yielding

$$\delta\lambda_s = \delta\lambda_m \tag{56}$$

If energy units are used instead and λ_x and λ_m are approximately the same, then the CESL effective bandwidth, $\delta\bar{\upsilon}_s$, is expressed as

$$\delta\bar{\upsilon}_s = \delta\bar{\upsilon}_x\delta\bar{\upsilon}_m/(\delta\bar{\upsilon}_x^2+\delta\bar{\upsilon}_m^2)^{1/2} \tag{57}$$

where $\delta\bar{\upsilon}_x$ and $\delta\bar{\upsilon}_m$ are the bandwidths corresponding to $\delta\lambda_x$ and $\delta\lambda_m$, respectively, expressed in K. The exact relation between $\delta\bar{\upsilon}$ and $\delta\lambda$ is expressed as

$$\lambda\bar{\upsilon} = 10^7 \tag{58}$$

$$\delta\lambda = (-10^7/\bar{\upsilon}^2)\delta\bar{\upsilon} \tag{59}$$

$$\delta\bar{\upsilon} = (-10^7/\lambda^2)\delta\lambda \tag{60}$$

Because luminescence bands are more appropriately described in energy terms, energy relationships are used for the remainder of this discussion, with wavelength relationships obtainable by substitution of Equations (58-60). As $\delta\bar{\upsilon}$ and the difference between λ_i and λ_j increase, wavelength approximations introduce more error.

Algebraic Model for Bandwidth Reduction

The surface defined by M_{ij} where

$$M_{ij} = \alpha x_i y_j \tag{61}$$

and M_{ij} is assumed to be the product of two Gaussian functions defined as

$$x_i = x_{i_o} \exp(-(\bar{\upsilon}_i - \bar{\upsilon}_{i_o})^2/2\sigma_i^2) \tag{62}$$

and

$$y_j = y_{j_o} \exp(-(\bar{\upsilon}_j - \bar{\upsilon}_{j_o})^2/2\sigma_j^2) \tag{63}$$

where:

x_{i_o} = relative intensity at peak excitation wavelength λ_{i_o}

y_{j_o} = relative intensity at peak emission wavelength λ_{j_o}

$\bar{\upsilon}_i$ = energy equivalent to wavelength λ_i, (K)

$\bar{\upsilon}_j$ = energy equivalent to wavelength λ_j, (K)

$\bar{\upsilon}_{i_o}$ = energy equivalent to peak wavelength λ_{i_o}, (K)

$\bar{\upsilon}_{j_o}$ = energy equivalent to peak wavelength λ_{j_o}, (K)

σ_i = standard deviation of excitation Gaussian function, (K)

σ_j = standard deviation of emission Gaussian function, (K)

Substitution into Equation (61) yields

$$M_{ij} = \alpha x_{i_o} y_{j_o} \exp(-(\bar{\upsilon}_i - \bar{\upsilon}_{i_o})^2/2\sigma_i^2)\exp(-(\bar{\upsilon}_j - \bar{\upsilon}_{j_o})^2/2\sigma_j^2) \tag{64}$$

Combining the exponential expressions

$$M_{ij} = \alpha x_{i_o} y_{j_o} \exp(-(\bar{\upsilon}_i - \bar{\upsilon}_{i_o})^2/2\sigma_i^2 - (\bar{\upsilon}_j - \bar{\upsilon}_{j_o})^2/2\sigma_j^2) \tag{65}$$

Because the assumption was made that the scan path passes directly through the peak maximum, the limitation

$$\bar{\upsilon}_i - \bar{\upsilon}_{i_o} = \bar{\upsilon}_j - \bar{\upsilon}_{j_o} \tag{66}$$

is placed on the system. Substitution and simplification results in

$$M_{ij} = \alpha x_{i_o} y_{j_o} \exp(-(\bar{\upsilon}_i - \bar{\upsilon}_{i_o})^2/(2(\sigma_i^2\sigma_j^2/(\sigma_i^2+\sigma_j^2)))) \tag{67}$$

By definition of the Gaussian function,

$$\sigma_s = \sigma_i\sigma_j/(\sigma_i^2+\sigma_j^2)^{1/2} \tag{68}$$

This agrees with Equation (57), with $\delta\bar{\upsilon}_s$ proportional to σ_s. The

relationship between σ_i and $\delta\lambda_i$ is given by

$$\sigma_i = ((1+(\delta\lambda_i/\lambda_{i_o})^2)^{1/2}-1)(\delta\lambda_x(2\ln 2)^{1/2})^{-1} \quad (69)$$

If Equations (58) and (59) are substituted into Equation (69), then

$$\sigma_i = ((1+(\delta\bar{\upsilon}_x/\bar{\upsilon}_{i_o})^2)^{1/2}-1)((10^7 * \bar{\upsilon}_x/\bar{\upsilon}_{i_o}^2)(2\ln 2)^{1/2})^{-1} \quad (70)$$

Both terms are used here because of their common usage in the literature for the respective expressions.

Peak Location for the General CESL Scan

A more general problem occurs when the CESL line does not pass through the center of the peak. This calculation predicts the emission wavelength for the maximum in the CESL spectrum of a single peak.

Starting with the ellipse model,

$$x^2b^2 + y^2a^2 = a^2b^2 \quad (71)$$

The maxima are assumed to fall on a line that runs through (0,0) in Figure 78A. A second point can be determined by finding the two points on the ellipse where the tangential line forms a 45° angle relative to the x axis. From this,

$$dy/dx = 1 \quad (72)$$

Differentiating Equation (71),

$$2xb^2+2ya^2 = 0 \quad (73)$$

$$y = -(b^2/a^2)x \quad (74)$$

This is the equation for the line of maxima. The real luminescence peak represents an offset from the (0,0) point. For this condition,

$$x = (\bar{\upsilon}_j-\bar{\upsilon}_{j_o}) \quad (75)$$

$$y = (\bar{\upsilon}_i-\bar{\upsilon}_{i_o}) \quad (76)$$

$$\Delta\bar{\upsilon} = (\bar{\upsilon}_i-\bar{\upsilon}_j) \quad (77)$$

where $\Delta\bar{\upsilon}$ is the energy difference used in the CESL scan. When these are substituted into Equation (74),

$$\bar{\upsilon}_i - \bar{\upsilon}_{i_o} = (-b^2/a^2)(\bar{\upsilon}_j - \bar{\upsilon}_{j_o}) \tag{78}$$

$$\bar{\upsilon}_i = (-b^2/a^2)\bar{\upsilon}_j + (b^2/a^2)\bar{\upsilon}_{j_o} + \bar{\upsilon}_{i_o} \tag{79}$$

$$\bar{\upsilon}_i = \bar{\upsilon}_j + \Delta\bar{\upsilon} \tag{80}$$

$$\bar{\upsilon}_j + \Delta\bar{\upsilon} = (-b^2/a^2)\bar{\upsilon}_j + (b^2/a^2)\bar{\upsilon}_{j_o} + \bar{\upsilon}_{i_o} \tag{81}$$

$$\bar{\upsilon}_{j_{max}} = ((b^2/a^2)\bar{\upsilon}_{j_o} + \bar{\upsilon}_{i_o} - \Delta\bar{\upsilon})/(1+b^2/a^2) \tag{82}$$

$$\bar{\upsilon}_{j_{max}} = ((\delta\bar{\upsilon}_x^2/\delta\bar{\upsilon}_m^2)\bar{\upsilon}_{j_o} + \bar{\upsilon}_{i_o} - \Delta\bar{\upsilon})/(1+\delta\bar{\upsilon}_x^2/\delta\bar{\upsilon}_m^2) \tag{83}$$

Returning to the algebraic model, CESL maximum location is determined by locating the maximum in the Gaussian function defined by Equation (65) by differentiating M_{ij} with respect to $\bar{\upsilon}_j$ and setting this equal to 0. This gives

$$dM_{ij}/d\bar{\upsilon}_j = \alpha x_{i_o} y_{j_o} (\exp(-(\bar{\upsilon}_j + \Delta\bar{\upsilon} - \bar{\upsilon}_{i_o})^2/2\sigma_i^2 - ((\bar{\upsilon}_j - \bar{\upsilon}_{j_o})^2/2\sigma_j^2))) * ((-2(\bar{\upsilon}_j + \Delta\bar{\upsilon} - \bar{\upsilon}_{i_o})/2\sigma_i^2) - (2(\bar{\upsilon}_j - \bar{\upsilon}_{j_o})/2\sigma_j^2)) = 0 \tag{84}$$

$$-(\bar{\upsilon}_j + \Delta\bar{\upsilon} - \bar{\upsilon}_{i_o})/\sigma_i^2 = (\bar{\upsilon}_j - \bar{\upsilon}_{j_o})/\sigma_j^2 \tag{85}$$

Simplifying,

$$\bar{\upsilon}_{j_{max}} = ((\sigma_i^2/\sigma_j^2)\bar{\upsilon}_{j_o} + \bar{\upsilon}_{i_o} - \Delta\bar{\upsilon})/(1+\sigma_i^2/\sigma_j^2) \tag{86}$$

Again, agreement is found in maximum location in both models, indicating that either model can be used.

Three cases are of special interest in peak maximum location. For a symmetrical peak, where a and b are equivalent, Equation (86) reduces to

$$\bar{\upsilon}_{j_{max}} = (\bar{\upsilon}_{j_o} + \bar{\upsilon}_{i_o} - \Delta\bar{\upsilon})/2 \tag{87}$$

If $\Delta\bar{\upsilon}$ is selected to match $\bar{\upsilon}_{i_o} - \bar{\upsilon}_{j_o}$, the CESL scan passes over the center of the peak, and $\bar{\upsilon}_{j_{max}} = \bar{\upsilon}_{j_o}$. This is the special case on

which the original models were based. To illustrate the spectral effect of Equation (87), schematic CESL scans and resultant spectra are shown in Figure 78B for this case. While the selection of $\Delta\bar{\upsilon}$ may shift the absolute positions of the CESL peaks, the relative spectral positions of vibrational bands are unchanged, with only the intensities varying. This case represents typical CESL applications in RTF. The LTCESL method is an example of the second case, where b >> a. The maximum now becomes $\bar{\upsilon}_{j_{max}} = \bar{\upsilon}_{j_o}$ if $\Delta\bar{\upsilon}$ is selected to match approximately $\bar{\upsilon}_{i_o} - \bar{\upsilon}_{j_o}$. This is schematically shown in Figure 78C. Under the conditions described in Chapter 4, $\Delta\bar{\upsilon}$ need not be exact to produce similar spectra. The case where a >> b can be treated similarly, but appears to have little analytical significance.

Bandwidth Reduction for the General CESL Scan

The original bandwidth reduction model assumed a scan path that passed through the peak maximum. A more general equation can be derived for other CESL scan paths that expresses the relationship between the effective synchronous bandwidth and the excitation and emission maxima, the energy difference of the synchronous scan, and the bandwidths. Using the ellipse equation and substituting Equations (75), (76), and (77),

$$\bar{\upsilon}_j^2(a^2+b^2)+\bar{\upsilon}_j(2\Delta\bar{\upsilon}a^2-2\bar{\upsilon}_{j_o}b^2-2\bar{\upsilon}_{i_o}a^2)+\bar{\upsilon}_{j_o}^2b^2+\Delta\bar{\upsilon}^2a^2-2\Delta\bar{\upsilon}\bar{\upsilon}_{i_o}a^2+\bar{\upsilon}_{i_o}a^2-a^2b^2 = 0 \qquad (88)$$

This equation defines the intersection of the ellipse and the scan path, two points. Solving for $\bar{\upsilon}_j$,

$$\bar{\upsilon}_j = ((b^2/a^2)\bar{\upsilon}_{j_o}+\bar{\upsilon}_{i_o}-\Delta\bar{\upsilon})/(1+b^2/a^2) \pm (ab/(a^2+b^2)^{1/2})* (a^2+b^2-(\bar{\upsilon}_{j_o}+\Delta\bar{\upsilon}-\bar{\upsilon}_{i_o})^2)^{1/2} \qquad (89)$$

The first term is the peak maximum, as in Equation (86). The CESL bandwidth, $\delta\bar{\upsilon}_s$, is finally described by

$$\delta\bar{\upsilon}_s = (\delta\bar{\upsilon}_x \delta\bar{\upsilon}_m / (\delta\bar{\upsilon}_x^{-2} + \delta\bar{\upsilon}_m^{-2})^{1/2})(\delta\bar{\upsilon}_x^{-2} + \delta\bar{\upsilon}_m^{-2} - (\bar{\upsilon}_{j_o} - \Delta\bar{\upsilon} - \bar{\upsilon}_{i_o})^2)^{1/2} \qquad (90)$$

If the original scan condition is applied, Equation (57) is obtained.

APPENDIX 3
SOFTWARE FOR LTCESL

Memory Allocation

Address Hex	Address Decimal	Description
00 ED	237	Temporary delay storage
00 EE	238	Index for look up table address low byte
00 EF	239	Index for look up table address high byte
75 30	30 000	Look up table beginning
94 70	38 000	Look up table end
94 7A	38 010	CONVERT-subroutine to store ADC data
94 D4	38 100	Excitation length high byte
94 D5	38 101	
94 D6	38 102	Excitation monochromator ON mask
94 D7	38 103	Excitation monochromator OFF mask
94 D8	38 104	Emission length high byte
94 D9	38 105	Emission length low byte
94 DA	38 106	Emission monochromator ON mask
94 DB	38 107	Emission monochromator OFF mask
94 DC	38 108	Total steps high byte
94 DD	38 109	Total steps low byte
95 06	38 150	SCANNER-subroutine to scan monochromators
95 9C	38 300	PULSE-subroutine to initialize PIA 2
95 C0	38 336	ASTART-subroutine to initialize PIA 1
C0 D2	49 362	PIA 1 A data register
C0 DA	49 370	PIA 2 A data register

BASIC Program -- ENERGY

```
 5  D$=CHR$(4):  REM CNTR-D
10  PRINT D$; "BLOAD ASTART"
12  PRINT D$; "BLOAD PULSE"
14  PRINT D$; "BLOAD SCANNER"
16  PRINT D$; "BLOAD CONVERT"
18  REM LOWER HIMEM FROM 38400 TO 30000
20  POKE 116,117
30  POKE 115,48
50  REM INITIALIZE PIA 1 FOR ADC
```

```
 60  PRINT D$; "BRUN ASTART"
 70  REM INITIALIZE PIA 2 TO SCAN MONOCHROMATORS
 80  PRINT D$; "BRUN PULSE"
 90  DIM A(4001)
100  PRINT "EMISSION WAVELENGTH START (NM)"
110  INPUT M1
120  PRINT "EMISSION WAVELENGTH STOP (NM)"
130  INPUT M2
140  PRINT "INCREMENT"
150  INPUT M3
160  PRINT "DELTA"
170  INPUT D
172  PRINT "SCAN RATE (A/S)"
174  INPUT R1
176  Y1=6000/R1
180  L2=Y1*M3
190  K3=INT(L2/256)
200  K4=L2-K3*256
210  Q1=2
220  Q2=0
230  Q3=1
240  Q4=0
242  POKE 38102, Q1
244  POKE 38103, Q2
250  POKE 38104, K3
260  POKE 38105, K4
270  POKE 38106, Q3
280  POKE 38107, Q4
290  K=(M2-M1)/M3
300  REM GENERATE LOOK UP TABLE
310  X1=1.E7/(1.E7/M1+D)
312  X1=INT(X1*100)/100
315  PRINT "EXCI. MONO. @",X1
316  REM DELAY PROMPT
317  INPUT B$
320  S1=30000
330  FOR I=1 TO K
340  X2=1.E7/((1.E7/(M1+I*M3))+D)
344  X2=INT(X2*100)/100
350  X3=X2-X1
360  L1=Y1*X3
370  K1=INT(L1/256)
380  K2=INT(L1-K1*256)
390  POKE S1,K1
400  POKE S1+1,K2
410  S1=S1+2
415  X1=X1+(K1*256+K2)/Y1
420  NEXT I
430  Z1=INT(K/256)
435  Z2=K-Z1*256
440  POKE 38108,Z1
445  POKE 38109,Z2
450  PRINT D$; "BRUN SCANNER"
```

```
500  PRINT "DATA DISPLAY"
510  INPUT DT$
520  IF DT$<>"Y" GO TO 990
525  S1=30000
530  FOR I=1 TO K
540  X=PEEK(S1+2*(I-1))
550  Y=PEEK(S1+2*(I-1)+1)
560  A(I)=INT(X*16+Y/16)
570  NEXT I
575  PRINT D$; "PR#1"
580  FOR I=1 TO K STEP 10
590  PRINT A(I);A(I+1);A(I+2);A(I+3);A(I+4);A(I+5);
          A(I+6);A(I+7);A(I+8);A(I+9)
600  NEXT I
610  PRINT D$; "PR#0"
990  END
```

Assembly Routines

CONVERT

```
947A        A9 A1          LDA #$A1
947C        8D D2 C0       STA $C0D2
947F        A9 01          LDA #$01
9481        8D D3 C0       STA $C0D3
9484        A9 00          LDA #$00

9486        8D D3 C0       STA $C0D3
9489        A9 A0          LDA #$A0
948B        8D D2 C0       STA $C0D2
948E        A9 01          LDA #$01
9490        8D D3 C0       STA $C0D3

9493        A9 00          LDA #$00
9495        8D D3 C0       STA $C0D3
9498        8D D0 C0       STA $C0D0
949B        8D D2 C0       STA $C0D2
949E        A9 04          LDA #$04

94A0        8D D0 C0       STA $C0D0
94A3        A9 08          LDA #$08
94A5        8D D3 C0       STA $C0D3
94A8        88             DEY
94A9        AD D2 C0       LDA $C0D2

94AC        91 EE          STA ($EE),Y
94AE        C8             INY
94AF        A9 04          LDA #$04
94B1        8D D3 C0       STA $C0D3
94B4        AD D2 C0       LDA $C0D2
```

```
94B7        91 EE          STA ($EE),Y
94B9        A9 00          LDA #$00
94BB        8D D3 C0       STA $C0D3
94BE        8D D0 C0       STA $C0D0
94C1        A9 FF          LDA #$FF

94C3        8D D2 C0       STA $C0D2
94C6        A9 04          LDA #$04
94C8        8D D0 C0       STA $C0D0
94CB        C8             INY
94CC        60             RTS


SCANNER

9506        A0 00          LDY #$00
9508        A9 75          LDA #$75
950A        85 EF          STA $EF
950C        A9 30          LDA #$30
950E        85 EE          STA $EE

9510        B1 EE          LDA ($EE),Y
9512        8D D4 94       STA $94D4
9515        C8             INY
9516        B1 EE          LDA ($EE),Y
9518        AA             TAX

9519        AD D6 94       LDA $94D6
951C        8D DA C0       STA $C0DA
951F        A9 50          LDA #$50
9521        38             SEC
9522        E9 01          SBC #$01

9524        B0 FC          BCS $9522
9526        AD D7 94       LDA $94D7
9529        8D DA C0       STA $C0DA
952C        A9 50          LDA #$50
952E        38             SEC

952F        E9 01          SBC #$01
9531        B0 FC          BCS $952F
9533        CA             DEX
9534        E0 00          CPX #$00
9536        D0 E1          BNE $9519

9538        AD D4 94       LDA $94D4
953B        C9 00          CMP #$00
953D        F0 06          BEQ $9545
953F        CE D4 94       DEC $94D4
9542        38             SEC

9543        B0 D4          BCS $9519
9545        AE D9 94       LDX $94D9
```

```
9548        AD D8 94        LDA $94D8
954B        8D DF 94        STA $94DF
954E        AD DA 94        LDA $94DA

9551        8D DA C0        STA $C0DA
9554        A9 50           LDA #$50
9556        38              SEC
9557        E9 01           SBC #$01
9559        B0 FC           BCS $9557

955B        AD DB 94        LDA $94DB
955E        8D DA C0        STA $C0DA
9561        A9 50           LDA #$50
9563        38              SEC
9564        E9 01           SBC #$01

9566        B0 FC           BCS $9564
9568        CA              DEX
9569        E0 00           CPX #$00
956B        D0 E1           BNE $954E
956D        AD DF 94        LDA $94DF

9570        C9 00           CMP #$00
9572        F0 06           BEQ $957A
9574        CE DF 94        DEC $94DF
9577        38              SEC
9578        B0 D4           BCS $954E

957A        20 7A 94        JSR $947A
957D        C0 00           CPY #$00
957F        D0 02           BNE $9583
9581        E6 EF           INC $EF
9583        CE DD 94        DEC $94DD

9586        AD DD 94        LDA $94DD
9589        C9 00           CMP #$00
958B        D0 83           BNE $9510
958D        AD DC 94        LDA $94DC
9590        C9 00           CMP #$00

9592        F0 06           BEQ $959A
9594        CE DC 94        DEC $94DC
9597        4C 10 95        JMP $9510
959A        60              RTS


PULSE

959C        A9 00           LDA #$00
959E        8D D8 C0        STA $C0D8
95A1        A9 FF           LDA #$FF
95A3        8D DA C0        STA $C0DA
95A6        A9 04           LDA #$04
```

```
95A8        8D D8 C0        STA $C0D8
95AB        A9 00           LDA #$00
95AD        8D D9 C0        STA $C0D9
95B0        A9 FF           LDA #$FF
95B2        8D DB C0        STA $C0DB

95B5        A9 34           LDA #$34
95B7        8D D9 C0        STA $C0D9
95BA        60              RTS


ASTART

95C0        A9 00           LDA #$00
95C2        8D D0 C0        STA $C0D0
95C5        A9 FF           LDA #$FF
95C7        8D D2 C0        STA $C0D2
95CA        A9 04           LDA #$04

95CC        8D D0 C0        STA $C0D0
95CF        A9 00           LDA #$00
95D1        8D D1 00        STA $C0D1
95D4        A9 FF           LDA #$FF
95D6        8D D3 C0        STA $C0D3

95D9        A9 34           LDA #$34
95DB        8D D1 C0        STA $C0D1
95DE        A9 00           LDA #$00
95E0        8D D3 C0        STA $C0D3
95E3        A9 A0           LDA #$A0

95E5        8D D2 C0        STA $C0D2
95E8        A9 01           LDA #$01
95EA        8D D3 C0        STA $C0D3
95ED        A9 00           LDA #$00
95EF        8D D3 C0        STA $C0D3

95F2        60              RTS
```

REFERENCES

1. R. Schoental and E. J. Y. Scott, J. Chem. Soc., 1949, 1683.

2. C. A. Parker, "Photoluminescence of Solutions," American Elsevier, New York, 1968.

3. E. Sawicki, Talanta, 1969, 16, 1231.

4. R. S. Becker, "Theory and Interpretation of Fluorescence and Phosphorescence," Wiley-Interscience, New York, 1969.

5. J. D. Winefordner, S. G. Schulman, and T. C. O'Haver, "Luminescence Spectroscopy in Analytical Chemistry," John Wiley and Sons, New York, 1972.

6. J. B. Birks, "Photophysics of Aromatic Molecules," John Wiley and Sons, London, 1970.

7. G. G. Guilbault, "Practical Fluorescence: Theory, Methods, and Techniques," Marcel Dekker, New York, 1973.

8. I. B. Berlman, "Handbook of Fluorescence Spectra of Aromatic Molecules," Academic Press, New York, 1971.

9. S. G. Schulman, "Fluorescence and Phosphorescence Spectroscopy: Physicochemical Principles and Practice," Pergamon Press, New York, 1976.

10. J. U. White, Anal. Chem., 1976, 48, 2089.

11. J. H. Richardson, in "Modern Fluorescence Spectroscopy," E. L. Wehry, Ed., Plenum Publishing, New York, Volume 4, 1981.

12. K. Miyaishi, M. Kunitake, T. Imasaka, T. Ogawa, and N. Ishibashi, Anal. Chim. Acta, 1981, 125, 161.

13. A. Jurgensen, E. L. Inman, Jr., and J. D. Winefordner, Anal. Chim. Acta, 1981, 131, 187.

14. J. D. Winefordner and M. S. Epstein, in preparation.

15. J. D. Winefordner, in "New Applications of Lasers to Chemistry," G. M. Hieftje, Ed., American Chemical Society, Washington, D. C., 1978.

16. T. F. VanGeel and J. D. Winefordner, Anal. Chem., 1976, 48, 335.

17. E. S. Yeung and M. J. Sepaniak, Anal. Chem., 1980, 52, 1465A.

18. G. J. Diebold, N. Karny, and R. N. Zare, Anal. Chem., 1979, 51, 67.

19. N. Strojny and J. A. F. deSilva, Anal. Chem., 1980, 52, 1554.

20. J. H. Richardson and M. E. Ando, Anal. Chem., 1977, 49, 955.

21. E. Voigtman, A. Jurgensen, and J. D. Winefordner, Anal. Chem., 1981, 53, 1921.

22. E. Voigtman, A. Jurgensen, and J. D. Winefordner, Analyst, in press.

23. C.-N. Ho, G. D. Christian, and E. R. Davidson, Anal. Chem., 1980, 52, 1071.

24. J. H. Rho, Anal. Biochem., 1980, 105, 414.

25. D. W. Johnson, J. B. Callis, and G. D. Christian, in "Multichannel Image Detectors," Y. Talmi, Ed., American Chemical Society, Washington, D. C., 1979.

26. G. Weber, Nature, 1961, 190, 27.

27. J. H. Rho and J. L. Stuart, Anal. Chem., 1978, 50, 620.

28. G. R. Haugen, B. A. Raby, and L. P. Rigdon, Chem. Inst., 1975, 6, 205.

29. T. C. O'Haver, G. L. Green, and B. R. Keppler, Chem. Inst., 1973, 4, 197.

30. R. N. Wightman, R. L. Scott, C. N. Reilley, R. W. Murray, and J. N. Burnett, Anal. Chem., 1974, 46, 1492.

31. I. M. Warner, J. B. Callis, E. R. Davidson, and G. D. Christian, Clin. Chem., 1976, 22, 1483.

32. D. W. Johnson, J. B. Callis, and G. D. Christian, Anal. Chem., 1977, 49, 747A.

33. I. M. Warner, J. B. Callis, E. R. Davidson, M. Gouterman, and G. D. Christian, Anal. Lett., 1975, 8, 665.

34. D. W. Johnson, J. A. Gladden, J. B. Callis, and G. D. Christian, Rev. Sci. Instrum., 1979, 50, 118.

35. G. D. Christian, J. B. Callis, and E. R. Davidson, in "Modern Fluorescence Spectroscopy," E. L. Wehry, Ed., Plenum Publishing, New York, Volume 4, 1981.

36. I. M. Warner, M. P. Fogerty, and D. C. Shelley, Anal. Chim. Acta, 1979, 109, 361.

37. D. C. Shelley, J. M. Quarles, and I. M. Warner, Clin. Chem., 1980, 26, 1127.

38. M. P. Fogarty and I. M. Warner, Appl. Spectrosc., 1980, 34, 438.

39. Y. Talmi, Anal. Chem., 1975, 47, 658A.

40. Y. Talmi, Anal. Chem., 1975, 47, 699A.

41. Y. Talmi, in "Multichannel Image Detectors," Y. Talmi, Ed., American Chemical Society, Washington, D. C., 1979.

42. Y. Talmi, D. C. Baker, J. R. Jadamec, and W. A. Saner, Anal. Chem., 1978, 50, 936A.

43. L. P. Giering, Ind. Res. Dev., 1978, 20(9), 134.

44. T. C. O'Haver and J. D. Winefordner, J. Chem. Ed., 1969, 46, 241.

45. C. E. White and R. J. Argauer, "Fluorescence Analysis: A Practical Approach," Marcel Dekker, New York, 1970.

46. R. K. Kostuk, Appl. Opt., 1981, 20, 2181.

47. J. C. Wright, in "Lasers in Chemical Analysis," G. M. Hieftje, J. C. Travis, and F. E. Lytle, Eds., The Humana Press, Clifton, NJ, 1981.

48. L. P. Giering and A. W. Hornig, Amer. Lab., 1977, 9(11), 113.

49. A. Pebler and J. M. Zomp, Appl. Opt., 1981, 20, 4059.

50. J. B. F. Lloyd, Analyst, 1974, 99, 729.

51. W. K. Giloi, "Interactive Computer Graphics," Prentice-Hall, Englewood Cliffs, NJ, 1978.

52. W. M. Newman and R. F. Sproull, "Principles of Interactive Computer Graphics," McGraw-Hill, New York, 1979.

53. C.-N. Ho, I. M. Warner, and M. P. Fogarty, Ind. Res. Dev., 1981, 23(4), 118.

54. R. J. Anderegg, Anal. Chem., 1981, 53, 2169.

55. T. Vo-Dinh, in "Modern Fluorescence Spectroscopy," E. L. Wehry, Ed., Plenum Publishing, New York, Volume 4, 1981.

56. J. C. Andre, Ph. Baudot, and M. Niclause, Clin. Chim. Acta, 1977, 76, 55.

57. J. B. F. Lloyd and I. W. Evett, Anal. Chem., 1977, 49, 1710.

58. J. B. F. Lloyd, Nature Phys. Sci., 1971, 231, 64.

59. J. B. F. Lloyd, J. Forensic Sci. Soc., 1971, 11, 83.

60. J. B. F. Lloyd, J. Forensic Sci. Soc., 1971, 11, 153.

61. J. B. F. Lloyd, J. Forensic Sci. Soc., 1971, 11, 235.

62. J. C. Andre, M. Bouchy, and M. Niclause, Anal. Chim. Acta, 1977, 92, 369.

63. T. Vo-Dinh, Anal. Chem., 1978, 50, 396.

64. H. W. Latz, A. H. Ullman, and J. D. Winefordner, Anal. Chem., 1978, 50, 2148.

65. H. W. Latz, A. H. Ullman, and J. D. Winefordner, Anal. Chem., 1980, 52, 191.

66. J. B. F. Lloyd, Anal. Chem., 1980, 52, 189.

67. R. B. Gammage, T. Vo-Dinh, A. R. Hawthorne, J. H. Thorngate, and W. W. Parkinson, in "Analytical Chemistry of Liquid Fuel Sources, Tar Sands, Oil Shale, Coal, and Petroleum," P. C. Uden, S. Siggia, and H. B. Jensen, Eds., American Chemical Society, Washington, D. C., 1978.

68. T. Vo-Dinh, R. B. Gammage, and P. R. Martinez, Anal. Chem., 1981, 53, 253.

69. E. R. Weiner, Anal. Chem., 1978, 50, 1583.

70. J. C. Andre, M. Bouchy, and M. L. Viriot, Anal. Chim. Acta, 1979, 105, 297.

71. J. B. F. Lloyd, Analyst, 1977, 102, 782.

72. S. H. Fortier and D. Eastwood, Anal. Chem., 1978, 50, 334.

73. J. B. F. Lloyd, I. W. Evett, and J. M. Duberty, J. Forensic Sci. Soc., 1980, 25, 589.

74. A. Colmsjo and U. Stenberg, Chem. Scr., 1976, 9, 227.

75. E. L. Wehry and G. Mamantov, in "Modern Fluorescence Spectroscopy," E. L. Wehry, Ed., Plenum Publishing, New York, Volume 4, 1981.

76. E. P. Lai, E. L. Inman, Jr., and J. D. Winefordner, Talanta, in press.

77. A. Colmsjo and U. Stenberg, Chem. Scr., 1977, 11, 220.

78. Y. Yang, A. P. D'Silva, V. A. Fassel, and M. Iles, Anal. Chem., 1980, 52, 1350.

79. Y. Yang, A. P. D'Silva, and V. A. Fassel, Anal. Chem., 1981, 53, 2107.

80. J. C. Brown, J. A. Duncanson, Jr., and G. J. Small, Anal. Chem., 1980, 52, 1711.

81. R. C. Stroupe, P. Tokousbalides, R. B. Dickinson, Jr., E. L. Wehry, and G. Mamantov, Anal. Chem., 1977, 49, 701.

82. J. R. Maple and E. L. Wehry, Anal. Chem., 1981, 53, 1244.

83. L. A. Bykovskaya, R. I. Personov, and Yu. V. Romanovskii, Anal. Chim. Acta, 1981, 125, 1.

84. Y. Yang, A. P. D'Silva, and V. A. Fassel, Anal. Chem., 1981, 53, 894.

85. A. Colmsjo and U. Stenberg, Anal. Chem., 1979, 51, 145.

86. B. S. Causey, G. F. Kirkbright, and C. G. deLima, Analyst, 1976, 101, 376.

87. A. Colmsjo and U. Stenberg, in "Polynuclear Aromatic Hydrocarbons," P. W. Jones and P. Leber, Eds., Ann Arbor Science, Ann Arbor, MI, 1979.

88. G. F. Kirkbright and C. G. deLima, Analyst, 1974, 99, 338.

89. J. R. Maple, E. L. Wehry, and G. Mamantov, Anal. Chem., 1980, 52, 920.

90. R. B. Dickinson, Jr. and E. L. Wehry, Anal. Chem., 1979, 51, 778.

91. E. L. Wehry and G. Mamantov, Anal. Chem., 1979, 51, 643A.

92. J. C. Brown, M. C. Edelson, and G. J. Small, Anal. Chem., 1978, 50, 1394.

93. J. R. Maple and E. L. Wehry, Anal. Chem., 1981, 53, 266.

94. W. C. McColgin, A. P. Marchetti, and J. H. Eberly, J. Am. Chem. Soc., 1978, 100, 5622.

95. P. Tokousbalides, E. R. Hinton, Jr., R. B. Dickinson, Jr., P. V. Bilotta, E. L. Wehry, and G. Mamantov, Anal. Chem., 1978, 50, 1189.

96. G. Mamantov, E. L. Wehry, R. R. Kemmerer, and E. R. Hinton, Anal. Chem., 1977, 49, 86.

97. D. M. Hembree, A. A. Garrison, R. A. Crocombe, R. A. Yokley, E. L. Wehry, and G. Mamantov, Anal. Chem., 1981, 53, 1783.

98. B. E. Kohler, in "Chemical and Biochemical Applications of Lasers," C. B. Moore, Ed., Academic Press, New York, Volume 4, 1979.

99. J. J. Dekkers, G. Ph. Hoornweg, G. Visser, C. Maclean, and N. H. Velthorst, Chem. Phys. Lett., 1977, 47, 357.

100. R. Farooq and G. F. Kirkbright, Analyst, 1976, 101, 566.

101. A. Bree and V. V. B. Vilkos, Spectrochim. Acta, 1971, 27A, 2333.

102. P. A. Geldof, R. P. H. Rettschnick, and G. J. Hoytink, Chem. Phys. Lett., 1971, 10, 549.

103. R. J. Lukasiewicz and J. D. Winefordner, Talanta, 1972, 19, 381.

104. E. L. Inman, Jr., A. Jurgensen, and J. D. Winefordner, Analyst, submitted.

105. E. L. Inman, Jr., A. Jurgensen, and J. D. Winefordner, Talanta, in press.

106. T. Vo-Dinh and P. R. Martinez, Anal. Chim. Acta, 1981, 125, 13.

107. T. Vo-Dinh, R. B. Gammage, and P. R. Martinez, Anal. Chim. Acta, 1980, 118, 313.

108. T. Vo-Dinh, R. B. Gammage, A. R. Hawthorne, and J. H. Thorngate, Environ. Sci. Technol., 1978, 12, 1297.

109. M. M. Corfield, H. L. Hawkins, P. John, and I. Soutar, Analyst, 1981, 106, 188.

110. T. Vo-Dinh and R. B. Gammage, Anal. Chem., 1978, 50, 2054.

111. M. Zander, "Phosphorimetry," Academic Press, New York, 1968.

112. D. M. Hembree, E. R. Hinton, Jr., R. R. Kemmerer, G. Mamantov, and E. L. Wehry, Appl. Spectrosc., 1979, 33, 477.

113. S. Isaak and M. N. Manougian, "Basic Concepts of Linear Algebra," W. W. Norton & Co., New York, 1976.

114. W. A. Byers and S. P. Perone, Anal. Chem., 1980, 52, 2173.

115. A. Savitsky and M. J. E. Golay, Anal. Chem., 1964, 36, 1627.

116. C. G. Enke and T. A. Nieman, Anal. Chem., 1976, 48, 705A.

117. J. C. Sternberg, H. S. Stillo, and R. H. Schwendeman, Anal. Chem., 1960, 32, 84.

118. J. P. Gourlia and J. Bordet, J. Chromatogr. Sci., 1981, 19, 35.

119. J. T. Lundeen and R. S. Juvet, Jr., Anal. Chem., 1981, 53, 1369.

120. B. Goldberg, J. Chromatogr. Sci., 1971, 9, 287.

121. I. M. Warner, G. D. Christian, E. R. Davidson, and J. B. Callis, Anal. Chem., 1977, 49, 564.

122. C.-N. Ho, G. D. Christian, and E. R. Davidson, Anal. Chem., 1981, 53, 92.

123. C.-N. Ho, G. D. Christian, and E. R. Davidson, Anal. Chem., 1978, 50, 1108.

124. G. L. Ritter, S. R. Lowry, T. L. Isenhour, and C. L. Wilkins, Anal. Chem., 1976, 48, 591.

125. H. B. Woodruff, P. C. Tway, and L. J. Cline Love, Anal. Chem., 1981, 53, 81.

126. E. R. Malinowski and D. G. Howery, "Factor Analysis in Chemistry," Wiley-Interscience, New York, 1980.

127. M. A. Sharaf and B. R. Kowalski, Anal. Chem., 1981, 53, 518.

128. R. N. Cochran and F. H. Horne, Anal. Chem., 1977, 49, 846.

129. G. T. Rasmussen, T. L. Isenhour, S. R. Lowry, and G. L. Ritter, Anal. Chim. Acta, 1978, 103, 213.

130. D. Katakis, Anal. Chem., 1965, 37, 876.

131. D. J. Leggett, Anal. Chem., 1977, 49, 276.

132. I. M. Warner, E. R. Davidson, and G. D. Christian, Anal. Chem., 1977, 49, 2155.

133. T. Hirschfeld, Anal. Chem., 1976, 48, 721.

134. M. P. Fogarty and I. M. Warner, Anal. Chem., 1981, 53, 259.

135. R. C. L. Ng and G. Horlick, Spectrochim. Acta, 1981, 36B, 529.

136. G. Horlick, Anal. Chem., 1973, 45, 319.

137. K. R. Betty and G. Horlick, Appl. Spectrosc., 1978, 32, 31.

138. G. Horlick, Anal. Chem., 1972, 44, 943.

139. R. C. L. Ng and G. Horlick, Spectrochim. Acta, 1981, 36B, 543.

140. G. Horlick, Anal. Chem., 1971, 43, 61A.

141. R. B. Lam, R. C. Wieboldt, and T. L. Isenhour, Anal. Chem., 1981, 53, 889A.

142. G. M. Hieftje and G. Horlick, Amer. Lab., 1981, 13(3), 76.

143. A. W. Hornig, J. T. Brownrigg, B. R. Chisholm, L. P. Giering, and R. L. Skewes, "Development of an Oil in Water Content Monitor," presented at 1977 Oil Spill Conference, New Orleans, March, 1977.

144. B. R. Chisholm, H. G. Eldering, L. P. Giering, and A. W. Hornig, "Total Luminescence Contour Spectra of Six Topped Crude Oils," Report BERC/R1-76/16, Nov., 1976.

145. A. P. Bentz, Anal. Chem., 1976, 48, 454A.

146. D. Eastwood, S. H. Fortier, and M. S. Hendrick, Amer. Lab., 1978, 10(3), 45.

147. D. Eastwood, in "Modern Fluorescence Spectroscopy," E. L. Wehry, Ed., Plenum Publishing, New York, Volume 4, 1981.

148. J. B. F. Lloyd, Analyst, 1975, 100, 82.

149. J. B. F. Lloyd, Analyst, 1980, 105, 97.

150. P. John and I. Soutar, Anal. Chem., 1976, 48, 520.

151. S. G. Wakeham, Environ. Sci. Technol., 1977, 11, 272.

152. M. L. Lee, M. V. Novotny, and K. D. Bartle, "Analytical Chemistry of Polycyclic Aromatic Compounds," Academic Press, New York, 1981.

153. K. D. Bartle, M. L. Lee, and S. A. Wise, Chem. Soc. Rev., 1981, 10, 113.

154. T. J. Killeen, D. Eastwood, and M. S. Hendrick, Talanta, 1981, 28, 1.

155. J. R. Jademac, W. A. Saner, and Y. Talmi, Anal. Chem., 1977, 49, 1316.

156. K. Ogan, E. Katz, and W. Slavin, Anal. Chem., 1979, 51, 1315.

157. K. Ogan, E. Katz, and T. J. Porro, J. Chromatogr. Sci., 1979, 17, 597.

158. L. W. Hershberger, J. B. Callis, and G. D. Christian, Anal. Chem., 1981, 53, 971.

159. T. Hirschfeld, Anal. Chem., 1976, 48, 16A.

160. C. J. Appellof and E. R. Davidson, Anal. Chem., 1981, 53, 2053.

161. M. G. Moran and B. R. Kowalski, Anal. Chem., 1979, 51, 776A.

162. T. Vo-Dinh, Ph.D. Dissertation, Swiss Federal Institute of Technology, Zurich, Switzerland, 1975.

163. R. N. Capps, Ph.D. Dissertation, Univeristy of Florida, Gainesville, FL, 1979.

BIOGRAPHICAL SKETCH

Eugene Lee Inman, Jr., was born April 26, 1956, in Kankakee, Illinois. After attending public schools in Illinois and Michigan, he completed his high school education in Seminole, Florida. He spent the next four years at Grace College in Winona Lake, Indiana, graduating with a Bachelor of Arts degree in chemistry and mathematics in May, 1978. Since September, 1978, Eugene has attended the University of Florida, working towards the Doctor of Philosophy degree.

While attending high school, Eugene met Wanda Jo Mason. On June 26, 1976, he married his high school sweetheart. Joshua Eugene was born to Eugene and Wanda on January 8, 1981,in Gainesville, Florida.

I certify that I have read this study and that in my opinion it conforms to acceptable standards of scholarly presentation and is fully adequate, in scope and quality, as a dissertation for the degree of Doctor of Philosophy.

James D. Winefordner, Chairman
Professor of Chemistry

I certify that I have read this study and that in my opinion it conforms to acceptable standards of scholarly presentation and is fully adequate, in scope and quality, as a dissertation for the degree of Doctor of Philosophy.

Richard A. Yost
Assistant Professor of Chemistry

I certify that I have read this study and that in my opinion it conforms to acceptable standards of scholarly presentation and is fully adequate, in scope and quality, as a dissertation for the degree of Doctor of Philosophy.

John G. Dorsey
Assistant Professor of Chemistry

I certify that I have read this study and that in my opinion it conforms to acceptable standards of scholarly presentation and is fully adequate, in scope and quality, as a dissertation for the degree of Doctor of Philosophy.

Shamkant B. Navathe
Associate Professor of Computer and
Information Sciences

I certify that I have read this study and that in my opinion it conforms to acceptable standards of scholarly presentation and is fully adequate, in scope and quality, as a dissertation for the degree of Doctor of Philosophy.

Leslie H. Oliver
Associate Professor of Computer and Information Sciences

This dissertation was submitted to the Graduate Faculty of the Department of Chemistry in the College of Liberal Arts and Sciences and to the Graduate Council, and was accepted as partial fulfillment of the requirements for the degree of Doctor of Philosophy.

May, 1982

Francis G. Stehli
Dean for Graduate Studies and Research

UNIVERSITY OF FLORIDA
3 1262 08554 0820